Control and energy management of a hybrid active wing generator including energy storage system with super-capacitors and hydrogen technologies for microgrid application

Tao Zhou

N° d'ordre : *103*

ECOLE CENTRALE DE LILLE

THESE

présentée en vue
d'obtenir le grade de

DOCTEUR

en

Spécialité : Génie Electrique

par

Tao ZHOU

DOCTORAT DELIVRE PAR L'ECOLE CENTRALE DE LILLE

Titre de la thèse:

Commande et Supervision Energétique d'un Générateur Hybride Actif Eolien incluant du Stockage sous forme d'Hydrogène et des Super-Condensateurs pour l'Intégration dans le Système Electrique d'un Micro Réseau

Soutenue le 30 Juin 2009 devant le jury d'examen :

Président	*Geneviève DAUPHIN-TANGUY, professeur, Ecole Centrale de Lille, LAGIS*
Rapporteur	*Bernard DAVAT, Professeur, ENSEM de Nancy, GREEN*
Rapporteur	*Daniel HISSEL, Professeur, Université de Franche-Comté, FEMTO-FCLAB*
Membre	*Yongdong LI, Professeur, Université de Tsinghua, Beijing, Chine*
Membre	*Stéphane LECOEUCHE, Professeur, Ecole des Mines de Douai*
Membre	*Gille NOTTON, Maître de Conférences (HDR), Université de Corse, LSPE*
Membre	*Frédéric COLAS Docteur-Ingénieur de recherche, ENSAM ParisTech, L2EP*
Directeur de thèse	*Bruno FRANCOIS, Maître de Conférences (HDR) Ecole Centrale de Lille, L2EP*

Thèse préparée dans le Laboratoire L2EP à l'Ecole Centrale de Lille

Ecole Doctorale SPI 072

Control and Energy Management of a Hybrid Active Wind Generator including Energy Storage System with Super-capacitors and Hydrogen technologies for Microgrid Application

Tao ZHOU

Ph.D dissertation

Laboratoire d'Electrotechnique et d'Electronique de Puissance de Lille (L2EP)
ECOLE CENTRALE DE LILLE, FRANCE

June 30th 2009

Preface

Preface

The PhD work, which is presented in this thesis, has been done at the "Laboratoire d'Electrotechnique et d'Electronique de Puissance de Lille" (L2EP), from September 2006 to July 2009. This work has been carried out as a part of a research project "ANR–SUPERENER", at Ecole Centrale de Lille with the support of the French National Research Agency (ANR) and the China Scholarship Council (CSC).

Acknowledgements

This dissertation is not only a result of my own dedication and perseverance, but is largely a credit to the patient and helpful people that I have worked with and to the supporting and understanding people that I have lived with over these past three years. I would like to take this opportunity to express my gratitude to everyone who contributed to this work.

My sincere thanks go to my supervisor, Dr. Bruno FRANCOIS, for his confidence in me throughout this project and for his valuable guidance during the study.

I would like to thank members of the jury, Prof. Bernard DAVAT, Prof. Daniel HISSEL, Prof. Yongdong LI, Prof. Geneviève DAUPHIN-TANGUY, Prof. Stéphane LECOEUCHE, Gille NOTTON and Frédéric COLAS, for their valuable discussions and insightful comments during the writing of the manuscript.

I am equally indebted to Prof. Stephane LECOEUCHE and his colleagues (Mohamed el hadi LEBBAL, Didier JUGE-HUBERT and Gabriel HOUSSAYE) in the Department of Informatics and Control Systems of the Ecole des Mines de Douai for their generous cooperation and helpful discussion when I worked on the electrolyzer system in their laboratory. Working with them during that period has been a very enriching experience.

I am also very grateful to Prof. Alain BOUSCAYROL and his colleagues (Anne-Laure ALLEGRE, CHEN Keyu, Walter LHOMME and Christian DEMIAN) in the control team of the L2EP for their constructive suggestions and continuous help during my work on the fuel cell system in their laboratory.

Many thanks go also to Xavier CIMETIERE, Simon THOMY, Christophe RYMEK and Hicham FAKHAM for their enormous help on implementation of the experimental test bench.

I would like also to thank my colleagues in the Grid Network Team (Omar BOUHALI, LI Peng, LU Di, PENG Ling, Gauthier DELILLE, ZHANG He, Amir AHMIDI) and my colleagues in the L2EP (TRAN Tuan Vu, Arnaud VIDET, Jean LEBESNERAIS, Fouzia MOUSSOUNI, David MARIN, Francois GRUSON, Souleymane BERTHE, Xavier MARGUERON, Guillaume PARENT) for their infinite friendship and encouraging supports.

Finally, I am infinitely grateful to all my friends and my families for their moral support, to my parents for their continuous encouragement, and especially to my wife LU Yao for being supportive and understanding during these three years, which are also the most difficult period for her study.

Explore everything around you,
penetrate to the furthest limits of human knowledge,
and always you will come up with something inexplicable in the end.

It is called life.

Albert Schweitzer

Contents

List of Figures

List of Tables

Nomenclature of Symbols

x	Variable
$\hat{x}$	Measured value of the variable x
$\tilde{x}$	Estimated value of the variable x
x_{ref}	Reference value of the variable x
$PI(x_{ref}-\hat{x})$	Proportional-Integral controller of the variable x

Introduction

Introduction

More and more decentralized generation systems are integrated into electrical network, as result, new structures of the electrical system should be considered. The microgrid is one of the solutions. The advantages of the microgrids consist of

- the association of the local generators and local loads in order to minimize the energy losses in the electricity transport;
- the possibility of electricity and heat cogeneration in order to increase the energy generation efficiency;
- the ease of using communication means in order to optimise the total electricity generation and to increase the quality and the reliability of the power system.

Nowadays, it is preferred to integrate renewable energies in the microgrid in order to reduce the CO_2 emission and the fossil fuel consumption. But the renewable energy sources are usually very intermittent and fluctuant. Moreover the renewable energy production is generally difficult to predict. The power balance between the production and the consumption becomes very difficult. In order to increase the development of renewable energy generators in the electrical network, we must imagine new renewable energy generators, which are more flexible and more controllable for the grid operation.

The topic of this thesis is the transformation of a renewable energy generator into an active generator by using energy storage systems. A hybrid power system is studied in the thesis. It consists of a wind generator (as primary energy source), super-capacitors (as fast-dynamic storage system), fuel cells and electrolyzers (as long-term storage system in the form of hydrogen). They are all connected to a common DC bus and an inverter is used for the connection of the whole system to the grid.

The objective of this thesis is to design the control system, including the power balancing and energy management strategies for all embedded sources. The proposed active wind generator is able to supply controllable powers as most conventional power plants. As result, it is able to provide ancillary services to the electrical system of the microgrid [Appendix H].

The context of the thesis is introduced in the first chapter. And then the thesis work is presented in four chapters.

In Chapter II, a wind energy conversion system is studied. The system modelling and the control design are detailed. In order to overcome the fluctuation problems of the wind power, a super-capacitor based fast-dynamic storage system is added. Power balancing strategies are proposed for their coordination in this hybrid power system. The delivered power to the grid is well smooth, but the operation can not be ensured for a long time. Hence a hydrogen based long-term storage system (including the fuel cells and the electrolyzers) is considered in the following chapters.

In Chapter III and in Chapter IV, the studies of a fuel cell system and of an electrolyzer system are presented. The system modelling and the control design are studied and validated

by some experimental tests on the commercial systems (1200W Ballard Nexa fuel cell system and 500W CETH GENHY electrolyzer system). In order to set up a flexible experimental platform, some real-time emulators are built for the fuel cell and the electrolyzer by using validated models. These emulators can provide the same electrical behaviours as the fuel cell and the electrolyzer. This allows us to test the power balancing strategies in the active wind generator, which is presented in the following chapter.

In Chapter V, the study of the active wind generator is presented. The modeling and control of the entire system are detailed. The power balancing strategies are proposed according to the characteristics of each energy source. They are experimentally implemented in the digital control board (DSpace 1103), and their performances are compared with respect to the DC-bus voltage regulation and the grid power control. The energy management strategies are implemented in order to ensure the good energy availability. They are performed with different operating modes to adjust the required energy storage levels.

The conclusion and the perspectives of this thesis are finally presented in Chapter VI.

The main scientific contributions of this thesis are the followings:

- the use and the adaptation of the graphical tools for the modeling of complex systems and their control design;
- the design and the experimental implementation of real-time emulators in order to reduce the time and the cost of an experimental test bench;
- The proposition and the validation of two power balancing strategies for the active wind generator to regulate the DC-bus voltage and to control the grid power;
- The proposition of different energy management strategies with the definition of the operating modes for the active wind generator to ensure the energy availibility.

These contributions can be adapted and extended for other hybrid power systems, which consist of a renewable energy source, a fast-dynamic energy storage system and a long-term energy storage system.

Chapter I

Context and Methodologies

Chapter I Context and Methodologies

In the last decades, Renewable Energy Sources (RES) and Distributed Generation (DG) have attracted special attention in Europe and all over the world, in order to reach two goals:

- Increasing the security of energy supply by reducing the dependency on imported fossil fuels such as oil, natural gas and coal;
- Reducing the emission of greenhouse gases, specifically carbon dioxide, from the burning of fossil fuels.

In the mean time, new concepts and technologies are being developed in the Transmission and Distribution Networks (like *Smartgrid*) and in the management and control concepts (like *Microgrid*), in order to improve the grid integration and the local consumption of these distributed renewable energy generators. Controllable and reliable generators are necessary in order to make all these concepts above feasible and flexible. In this PhD thesis we propose the association of a wind generator, super-capacitors and hydrogen technologies to assess an active generator for a microgrid application.

So before presenting this generator, this chapter recalls some concepts about renewable energy sources, distributed generators, smart grids and microgrids. Then in a second part, characteristics and opportunities of hydrogen as alternative energy carrier to electricity is presented. Hence, the context, which is related with microgrid and active generators, is explained as well as the structure of the active generator. Finally, the objectives of the research work and the followed methodologies are presented.

I.1 Renewable energy sources and distributed generation

I.1.1 Renewable energy sources

Renewable Energy Sources (RESs) refer to the sustainable natural energy sources, such as the sun and the wind. Renewable energy systems convert these natural energy sources into consumable energy forms (electricity and heat), which are easy to transport and to use. According to the European directive on RES for production of electricity [Dir 01], RESs include:

- Wind;
- Solar (photovoltaic, thermal electric);
- Geothermal;
- Wave and tidal energy;
- Biodegradable waste;
- Biomass (solids, biofuels, landfill gas, sewage treatment plant gas and biogas).

Nowadays, hydropower and wind power are technically and economically the best renewable energy utilizations. In countries with hydropower potential, small hydro turbines are used at distribution level to sustain the utility network in dispersed or remote locations. In many countries, the wind power potential has led to a fast development of wind turbine technologies in the last decade [Ewe 05]. A total amount of nearly 120GW wind power has been installed in the world by the end of 2008 (Fig.I-1a). Another renewable energy based sustainable power supply is the photovoltaic (PV) technology [Iea 05]. The number of PV

installations increases exponentially and the worldwide PV cells production reaches 3.7GW (Fig.I-1b), mainly thanks to the governments and utility companies that support programs focusing on grid-connected PV systems.

The main advantage of renewable energy systems is the low impact on the environmental pollution as no fossil fuels are involved. An additional advantage is the insensitivity to fuel prices since they are free natural resources. This decreases the operational cost of renewable energy systems and reduces economic operation risks.

The major drawback is the initial investment in renewable energy systems. It is often more expensive to build renewable energy systems than non-renewable energy systems, since the environmental deterioration has not yet been taken into account for the cost calculation. However, this investment cost will be reduced with the fast developing technologies (just like the development of computer industry in the last three decays). Other disadvantages of RES are the specific requirements of the site and the unpredictability of the generated power. ***The intermittent availability of the RES means a higher cost for balancing the electricity and for maintaining reserve capacity, for example in the event that the wind drops below or increases above the operating area of wind turbines.*** These quality and security problems have already been encountered in areas with a high penetration of wind turbines, such as in Germany and in Denmark.

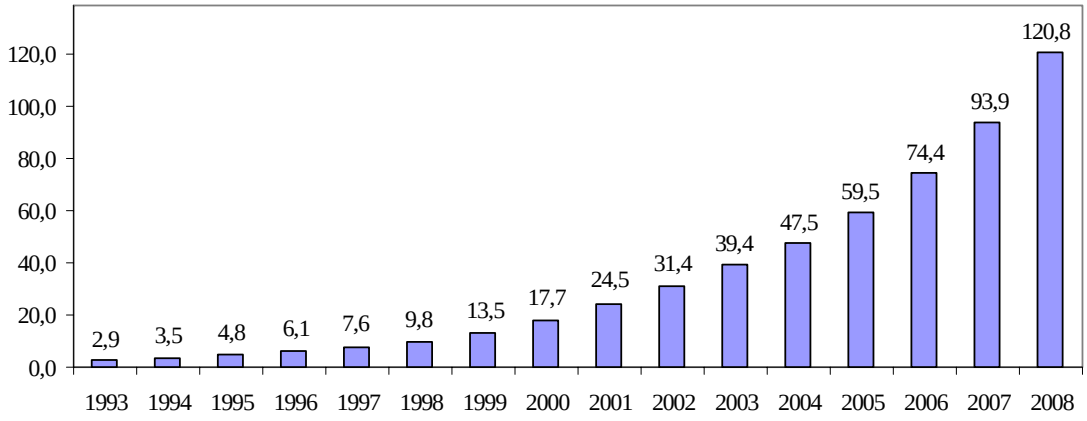

(a) Total wind power installed in the world since 1993 (in GW)

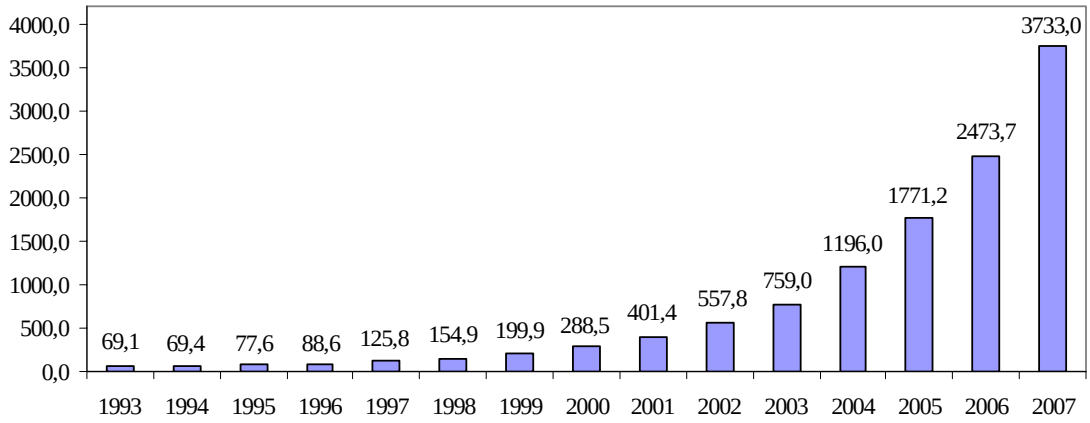

(b) Total photovoltaic cell production in the world since 1993 (in MW)

Figure I-1: Evolution of installed wind power and photovoltaic cell production in the world [Eur 09].

I.1.2 Distributed generation

Distributed Generation (DG) refers to distributed energy generation and energy storage (like electricity and heat, near to or at the load center). Generally, a part of the electricity is used locally and the remainder is delivered to the grid. The heat, on the other hand, is always used locally, as heat transport is costly and involves relatively large losses. In this dissertation, we focus on the generation of electricity. DGs are usually smaller than 50 MW and are connected to the distribution network, which has a low or medium operating voltage level (240/400 up to 110kV). Fig.I-2 gives an overview of DG systems and their typical uses.

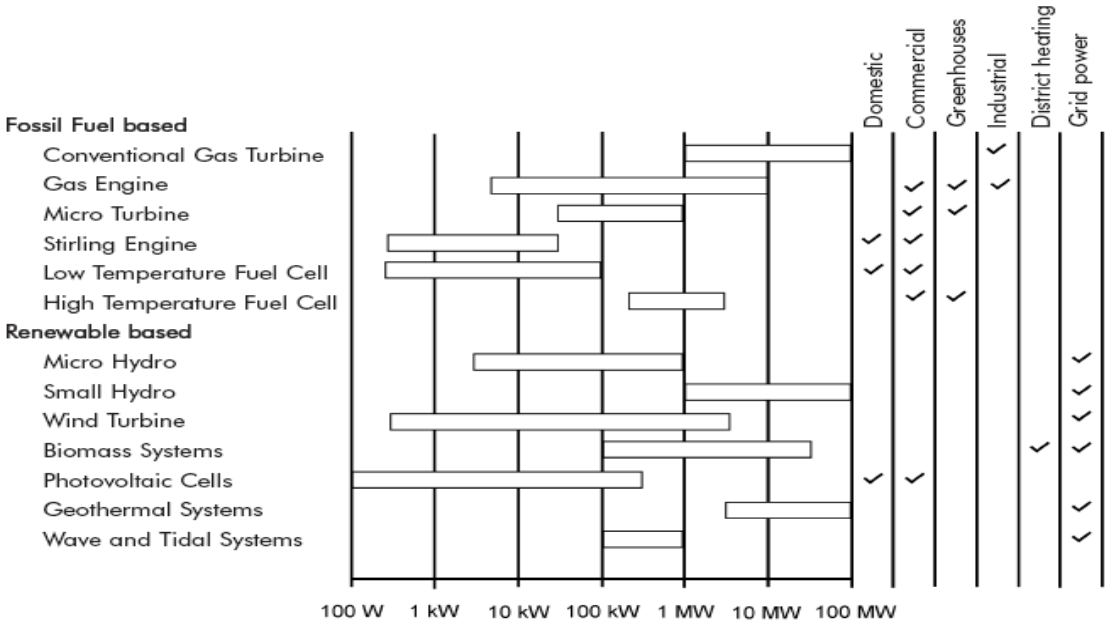

Figure I-2: Overview of distributed generation (based on [Ack 01] [Van 05] and of typical uses)

Today, central electricity production still dominates electricity production because of many issues, like economy of scale, efficiency, fuel capability and lifetime [Wil 00]. However, the advantage of the central production's economy of scale is decreasing, because fossil fuels, which are economically suitable for central production, are not abundant enough for the next century (without steady supply or stable price). Recently, the world has shown its great interest and ambition of integrating RES and DG into the Transmission and Distribution Network (electrical grid) because of many advantages. These advantages include additional energy-related benefits (improved security of supply, avoidance of overcapacity, peak load reduction, reduction of grid losses) and network-related benefits (transmission network infrastructure cost, power quality support, reliability improvement) [Sch 03]. Moreover, DG can increase the overall fuel efficiency of the plant considerably, as the heat can be used locally. Appendix A outlines the ongoing research, development and demonstration (RD&D) efforts currently in progress in Europe, the United States, Japan and Canada.

Except for large-scale hydro, offshore wind farms and co-combustion of biomass in conventional (fossil fuelled) power plants, most renewable energy systems are small DG systems. In the last decades, electric power systems undertook several modifications toward a more decentralized energy system paradigm, allowing the increase of DG integration. With the fast development of distributed renewable energies, many efforts should be done in the following domains:

- Modernization of the *Transmission and Distribution (T&D) networks* (like SmartGrid), for distributed renewable energies' grid integration;
- Innovation of the local system's *Management and Control Concepts* (like Microgrid), for distributed renewable energies' local demand and supply optimization;
- Implementation of *Controllable and Reliable Generation* (like Active Generators), to overcome the intermittent and fluctuant availability of renewable energies and to supply ancillary services to the electrical network.

In this context, we propose solutions to transform a wind generator into a controllable production unit.

I.1.3 Smart grid

Today's electrical grid has to take the challenges to match the modern digital economy and information age, which requires higher load demands, uninterruptible power supplies, and other high-quality, high-value services. Especially, the integration of more and more DGs based on intermittent and fluctuant RES will lead to reliability problems of ancillary service, power quality disturbances, brownouts, and blackouts. The original power grid technology has its control systems embedded in the generating plants. The utilities attempt to meet the demand and succeed or fail with varying degrees (brownout, rolling blackout, uncontrolled blackout). The total amount of power loaded by the users can have a very wide probability distribution, which requires a lot of spare generating plants in standby mode to respond to the rapidly changing power usage. Thus, the clusters' generating capacity should usually be oversized, so it is very expensive for the power producers, and the resulted brownouts and outages can be also very costly for consumers.

As new electricity transmission and distribution network is required for integrating the newly emerging distributed renewable energies. Smart Grid is a modernized "grid" that uses robust two-way communications, advanced sensors and distributed computers to improve the efficiency, reliability and safety of power delivery and use. With the application of communication and information technologies to the electric grid, many smart digital meters can be integrated in the modernized grid to replace analog mechanical meters. The Smart Grid System Operator (SGSO) is able [Maz 03]:

- to control the electrical powers down to the residential level, small-scale DGs and storage devices;
- to communicate information on operating status and needs and to collect information on prices and grid conditions;
- to transform the grid under central control into a collaborative network.

Moreover, the Demand Response (DR) will be the next step for the smart grid development. This can be very simple like timers to switch off electric water heaters during peak-demand periods, but such systems are unable to respond to contingencies. The full Smart Grid allows generators and loads to interact in real time, by using modern communication and information technology. So the demand managements can eliminate the cost of generators, can cut the wear and extend the life of equipment and allow users to get more value from the system by putting their most important needs first.

A comparison of a future's Smart Grid with the today's grid is summarized in Table I-1.

Table I-1: Comparison of future's Smart Grid with today's grid [Glo 05]

20th Century Grid	**21st Century Smart Grid**
Electromechanical	Digital
One-way communications (if any)	Two-way communications
Built for centralized generation	Accommodates distributed generation
Radial topology	Network topology
Few sensors	Monitors and sensors throughout
"Blind"	Self-monitoring
Manual restoration	Semi-automated restoration and, eventually, self-healing
Prone to failures and blackouts	Adaptive protection and islanding
Check equipment manually	Monitor equipment remotely
Emergency decisions by committee and phone	Decision support systems, predictive reliability
Limited control over power flows	Pervasive control systems
Limited price information	Full price information
Few customer choices	Many customer choices

I.1.4 Microgrid

With a large number of widely dispersed distributed generators, the real-time communication and control are difficult to perform for the whole power system, especially with extremely large amounts of information and long transmission distance. Therefore, the optimized real-time control and management of distributed generators and loads should be implemented within local power systems. The necessary information should be firstly gathered and then be exchanged with the Grid System Operator (GSO) for the whole power grid's control and optimization. As a new control and management concept of organizing the distributed renewable energies and local loads, microgrids have attracted great attention all over the world. An example of organizing all distributed generators and loads by means of smart grid and microgrids in a hierarchical structure is shown as in Fig.I-3.

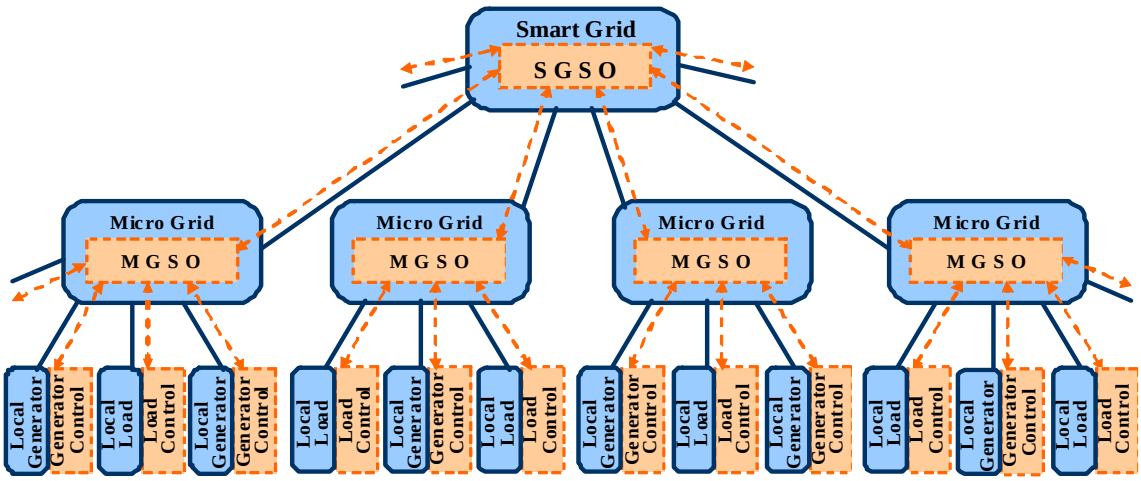

Figure I-3: Example for organizing distributed generators and loads by means of Smart grid and Microgrid

The power connections are presented by the bold lines, which symbolize the infrastructure network. The Smart Grid interfaces many microgrids and each microgrid combines locally the dispersed generators and load, which are totally or partially controllable. The information connections are presented by the dotted lines, which symbolize the advanced communication technologies connecting Smart Grid System Operator (SGSO), MicroGrid System Operator (MGSO) and the controllers of distributed generators and loads

Microgrids comprise dispersed energy resources (like wind turbines, photovoltaic panels, fuel cells, micro gas turbines…), storage devices (like flywheels, super-capacitors and batteries) and controllable loads in order to offer considerable control capabilities to the local network operation. These systems are interconnected to the low-voltage distribution network, but they can also be operated in islanding mode in case of faults in the upstream network. From the customer's point of view, microgrids provide both thermal and electricity supplies, and in addition enhance local reliability, reduce emissions, improve power quality by supporting voltage and reducing voltage dips, and potentially reduce costs of energy supply. A series of microgrid symposiums have started in California, on 17 June 2005, and then have been organized in Montreal on 23 June 2006, in Nagoya on 6 April 2007 and recently in Kythnos on 2 June 2008. The main researches include control philosophies, energy management, local generator and load issues and analysis tools…

Islanded operation is expected to happen very few times in a year and it is obvious that the main concern is to "keep the lights on" in such periods. In interconnected operation, MicroGrid System Operator (MGSO) should ensure the maximization of renewable energy generation and the optimization of the microgrid's operation. Controller functions have to be considered in order to achieve optimal operation of the microgrid in interconnected mode. The MGSO might use load forecasts (electric and possibly heat) and production capacity forecasts (from local generators). It uses the market prices of electricity, the gas costs, the local production capability, the local load demands, the grid security concerns and the distribution network's requests to determine the amount of power that the microgrid should draw from its owned distributed generators and another amount of power that should be exchanged with the upstream grid network. The defined optimized operating profile can be achieved by controlling the local generators and the local loads in the microgrid by sending control signals to their controllers. In this framework, non-critical, controllable loads can be cut off, when necessary. Furthermore, it is necessary to monitor the actual active and reactive power balancing. These techniques can be considered equivalent to the secondary control of the interconnected grid [Tsi 05].

Many technical challenges are associated with the operation and the control of microgrids. Energy management is very important for the achievement of good energy efficiencies by optimizing production and consumption of heat, gas and electricity. With various conflicting requirements and limited communication techniques among a large number of distributed energy sources, the management of instantaneous active and reactive power balancing is a key challenge of microgrids. Another key challenge of microgrids is to ensure stable operation during faults and various network disturbances. Transitions from interconnected operation to islanding operation are likely to cause large mismatches between generations and loads, and to cause severe frequency and voltage control problems. Maintaining stability and power quality in the islanding mode of operation requires the development of sophisticated control strategies.

In this context, we propose to design a local control interface of a wind generator based hybrid power system in order to make it available for the microgrid management.

I.1.5 Hybrid power system

Because of the intermittent and fluctuant availability of the renewable energy sources, Hybrid Power Systems (HPS) provide a high level of energy security through the mix of various generation systems and often incorporate energy storage systems to ensure maximum reliability of power supply. Several kinds of hybridization of power sources are presented as follows:

- ***Hybridization of renewable energy sources and backup power units***: Because of the intermittent availability of renewable energy sources, backup power units are usually integrated for a high level of local energy security. For example, diesel generator, micro gas turbine and fuel cells are usually used as for uninterrupted power supplies [Che 03].
- ***Hybridization of renewable primary sources***: Two or more renewable primary sources can be associated for complementary advantages. For example, the PV-Wind system are often proposed, because the PV panels provide powers only in the day time and wind generators produce usually more powers with stronger wind in the night. [Ahm 06].
- ***Hybridization of renewable energy sources and energy storage devices***: The association of energy storage devices with renewable energy sources can ensure reliability and security of the distributed power generation system while maximizing the benefit from renewable energies. For these systems, the excess and deficit of energy production can be optimally adjusted by the energy storage units to increase the energy efficiency [Abb 05].
- ***Hybridization of different kinds of energy storage devices***: In this PhD thesis, we have classified energy storage devices into two categories: fast-dynamic storage devices and long-term storage devices. We propose an association of these two kinds of device to bring their complementary advantages to the renewable energy based generator for improvement of the power supply [Zho 07].

In this PhD thesis, a hybrid power system is proposed to assess an active wind generator in order to provide some ancillary services to microgrid.

I.2 Hydrogen as alternative energy carrier to electricity

I.2.1 Hydrogen market

Because of the effects of carbon emissions into the atmosphere on global climate change, a carbon-constrained world is coming and alternative energy sources will be required to supplement the carbon-intensive sources that currently power the utility network and the transport vehicles. One promising solution to this problem is the direct use of hydrogen. Hydrogen, is not a primary energy source like coal and oil, but is an energy carrier like electricity. Ideally, 1kg of hydrogen at 25°C and 1bar corresponds to 39kWh of electricity. But unlike electricity, hydrogen can be stored quite easily.

Hydrogen can be manufactured or extracted from hydrogen-rich materials such as coal, natural gas, biomass or water. Currently, the primary means of manufacturing hydrogen is to strip it from natural gas via steam methane reforming. The technologies to produce hydrogen

from non-fossil sources are also available, such as biomass, wind, and solar. As advantages, the hydrogen production cycle from non-fossil sources can produce less greenhouse gases than from fossil sources.

The current market for hydrogen is divided into two segments: captive users, who produce the hydrogen at the location where it is to be used; and merchant users, who have their hydrogen delivered to the point of use. In the worldwide, the captive market is larger, and includes chemical producers, refineries, fat and oil hydrogenation and metal production. The merchant market is smaller and serves industries such as electronics manufacturers, float gas producers and public utilities for generator cooling in nuclear plants [Sur 04].The future market for hydrogen is even much larger, if hydrogen is to be used as fuel for vehicles.

I.2.2 Hydrogen-electric economy

Hydrogen economy refers to a society that can use hydrogen as an energy carrier because of the following advantages:

- hydrogen can be produced from a clean energy sources;
- hydrogen can be distributed and stored in a variety of ways;
- hydrogen can replace fossil fuels to provide electricity and transportation fuels;
- domestic resources can be used for hydrogen production to lead to energy independence.

Such an idea is not new and it dates back up to 1874 "…Water will one day be employed as fuel, that hydrogen and oxygen of which the water is constituted will be used, simultaneously or in isolation, to furnish an inexhaustible source of heat and light"[Ver 01].

As in France, the all-electric economy relies on inexpensive nuclear electricity [Gre 72]. Additional means are required to modulate the electricity production with fast response time. Classically they are pumped-storage hydro and coal or oil based thermal generators. Both additional power-regulation means have their own drawbacks as the site-specific application, the increasing price of the fossil fuel and environmental pollution.

The use of hydrogen to replace fossil fuels and as an alternative to the *all-electric economy* is examined. The term hydrogen-electric economy was also developed [Lot 74] to describe the possibilities of combining production, transmission and sales of both energy carriers. Like electricity, hydrogen can be centrally produced and then be distributed to the point of use. It can also be produced locally (decentralized hydrogen production) (Fig.I-4).

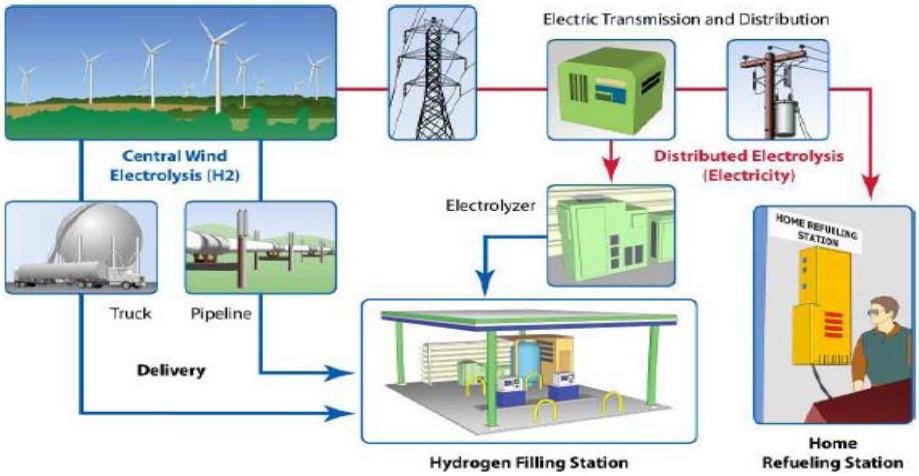

Figure I-4: Examples of wind electrolysis [Kot 08]

If hydrogen can be produced economically, hydrogen-based internal combustion engines (IECs) and fuel cells could be used to provide electrical power in distributed energy applications. If the loads can also use the heat from the distributed generators, a combined heat and power (CHP) application can increase the overall efficiency of the packaged system. Moreover, new technological advantages may be developed:

- the electrolyzers can be used during off-peak times in order to increase the efficiency of the electrical power system by allowing it to run close to its rated capacity [Fer 74];
- the hydrogen, which is produced on site, can be used for generator cooling with its high thermal capacity and low density[Gre 73];
- For wind electrolysis, the wind tower may even be used as hydrogen storage tank [Kot 03].

I.2.3 Hydrogen as storage for electricity

a) Hydrogen production from electricity

Hydrogen can be produced from a variety of sources. Currently, hydrogen is mainly produced by reforming natural gas and dissociating hydrocarbons and a smaller amount is produced by electrolysis. Reforming natural gas is currently the least expensive way to produce large quantities of hydrogen. However, some drawbacks exist:

- the process is based on a non-renewable fossil-fuel source;
- the reactions produce also carbon dioxide;
- the produced hydrogen gas can have high impurities.

As another way, electrolysis uses direct current electricity to split water into its basic elements of hydrogen and oxygen. For large-scale energy storage, the hydrogen should be further compressed before stored. Since the electrolysis process uses only water and electricity, it can produce pure hydrogen and oxygen (99.9995%).

In the actual hydrogen market, electrolyzers are still used in places where low electricity prices are available or for high hydrogen purity requirements. As the price of natural gas increases, electrolysis becomes a viable option for competition in the hydrogen market and electric utilities are well placed to provide the electricity for hydrogen production by water electrolysis.

b) Electricity generation from hydrogen

Hydrogen can also be used to generate electricity in different ways. Hydrogen can be used as fuel to supply the combustion engine for electricity generation by rotating machine. Hydrogen can also be directly used through electro-chemical reactor (eg. fuel cells) to generate electricity. For high power levels, the most efficient conversion from hydrogen to electricity can be achieved in combined heat and power (CHP) plant, where the thermal energy can also be used. For lower power levels, fuel cells alone can be applied.

c) Round-trip evaluation

Fuel cells require very high hydrogen purity, so electrolyzers are very suitable for the application. Both components use direct electro-chemical conversion and higher round-trip efficiency can be expected (in the range of 35-40%) than using “steam methane reforming” (for hydrogen production) and “hydrogen combustion” (for electricity generation).

I.3 Integration of renewable energy based generators into a microgrid

I.3.1 General framework of the microgrid operation

In our study we consider a microgrid, which is powered by a gas micro-turbine (Fig.I-5). At first sight the use of Renewable Energy System can decrease the environmental impact. So we want to evaluate the integration of a wind generator into the operation and the management of the studied microgrid.

The microgrid can operate both in connected mode with a distribution network and in islanding mode. The MicroGrid System Operator (MGSO) controls the microgrid's operation through the local generator controllers (Fig.I-3).

In connected operation, a timing power planning is established between the DSO and the MGSO. The MGSO adapts the power reference of the gas micro-turbine in order to fulfill this contract.

In islanding operation, the microgrid should ensure the local electricity supply and energy security. To perform the power balance between the production and consumption, the MGSO should predict the local production capacity and the local consumption needs for the next period. If the production is more than the consumption, the power production of the gas micro-turbine must be reduced and during this transient state the excess power is dissipated in dummy resistor loads in case of overvoltage. If the production is less than the consumption, two solutions exist. The micro gas turbine will be prepared to supply the deficit power or a part of loads will be disconnected from the microgrid (if necessary).

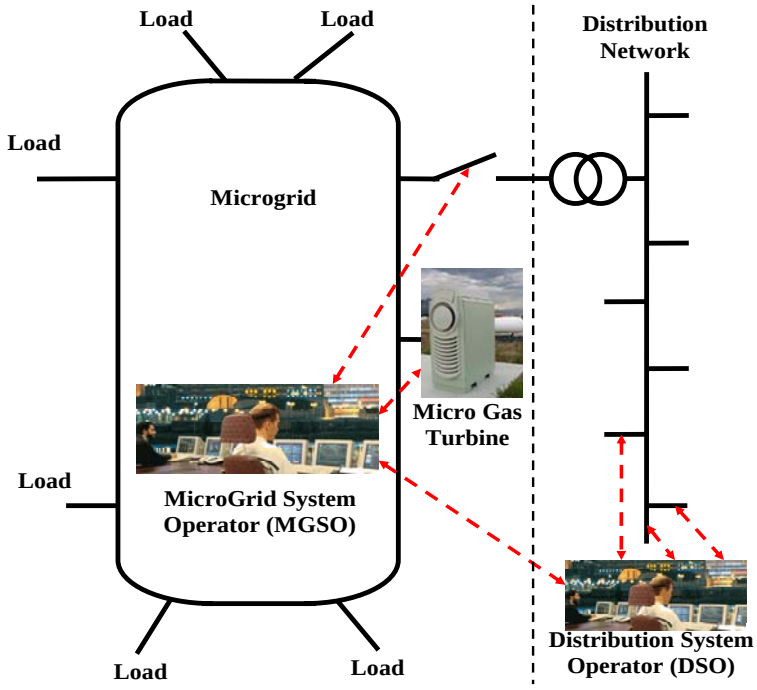

Figure I-5: Example of a microgrid

I.3.2 Problems of renewable energy sources

Actual wind generators are not dispatched by a microgrid system operator because their output active and reactive powers are not controllable. In an isolated microgrid if a wind

generator is used the electrical production may exceed the consumed load power. This event may occur during the night when the loads are very low. This is a typical problem, which is a barrier for the integration of wind generator in grids. So research efforts must be done to transform this wind generator into a classical generator.

As example one desirable control action is to be able to reduce the wind power production when it is not useful for the microgrid operation. In order to increase the value of renewable energy, it is interesting to store locally the non-used electrical power. Another advantage of having load storage capability is to make able the supply of more power (as the wind turbine can) if the microgrid operator asks it.

Moreover the generated wind power is very fluctuant. So the gas micro-turbine has to perform a real time compensation of power transients and it implies abnormal stresses. Important collateral effects may decrease expected economic and environmental benefits. So a great improvement is to erase the wind-caused power variations by using a local storage unit with fast dynamic abilities. It should smooth the produced power. A local control system must manage the storage to supply or absorb the power difference between the generated wind power and the power reference set by the MGSO.

In connected mode, it is very important to have a constant power exchange with the grid during each period (15 or 30 minutes) between the microgrid and the distribution grid. If renewable energy based generators are connected, the MGSO must estimate the production capacity with the climate forecasts as well as the local consumption demands for the next period τ_n. To have a great benefit of "clean" electricity production we must imagine a possible scenario. The MGSO should send to the DSO the average power, which will be exported during the period τ_n . Hence the DSO has enough time in advance to gather and to send set points to coordinate the power production for his interest. At the same time, the MGSO assigns the power references to each local generator for the period τ_n according to the climate condition. Then each active generator should respect its power reference during the period τ_n, against the possible large fluctuations of the weather condition.

These problems and possible solutions show the necessity to get a wind generator, which is capable of exchanging information with the MGSO and of supplying the power requirements of the microgrid.

I.3.3 Concept of active generator

The task of an active generator is to supply the electrical power references, which has been previously set by the MGSO for a given period by taking into account all the local factors and the distributed network's requirements.

Conventional power plants are usually active generators because they are controllable and can supply necessary powers to satisfy the grid requirements. Moreover, they can usually provide some ancillary services to the grid, basically like frequency regulation by active power control, voltage regulation by reactive power control, etc… They are mostly fossil and nuclear fuelled and rely on the abundant fuel supply like coal, oil, natural gas or nuclear fuels. Most of the time, they can work at any power level below its nominal power (Fig.I-6a) by controlling the fuel supply.

Renewable energy generators are usually considered as passive generators because they can not participate to the grid management, because they are dependent on the availability of the primary renewable source. Most of the time, they work far below their nominal capacity (Fig.I-6b). Moreover, the reliability and efficiency of the power system can not be ensured.

Therefore, they can not provide ancillary services to the grid, like power balance between the production and the consumption.

Energy storage devices can serve as backup power plants. They can work at any power level between two nominal powers, for storing and releasing energies (Fig.I-6c). So they can be used to support the operation of sources, transmission, distribution, and loads. When they serve as source devices, they can help to solve the problems of renewable energies' intermittent availabilities and fast transients.

For each unit, the classified power domain can be achieved by a proper control (Fig.I-6).

Thus, a hybrid power system combining a renewable energy based generator and energy storage devices can be a good solution to make an active generator. Such an active generator corresponds to both the needs of clean energy generation and high power quality for the future's electrical network. For this objective, two major innovative improvements should be made:

- ***Energy Storage Systems*** should be well chosen and associated with renewable energy generators to compensate or to absorb the power difference between the actual renewable energy production and the required grid consumption;
- ***Energy Management Strategies*** should be properly designed and adapted to control the power flows among the renewable energy generator, the energy storage systems and the grid. Various additional control functions have to be implemented to provide ancillary services for the grid [Appendix H].

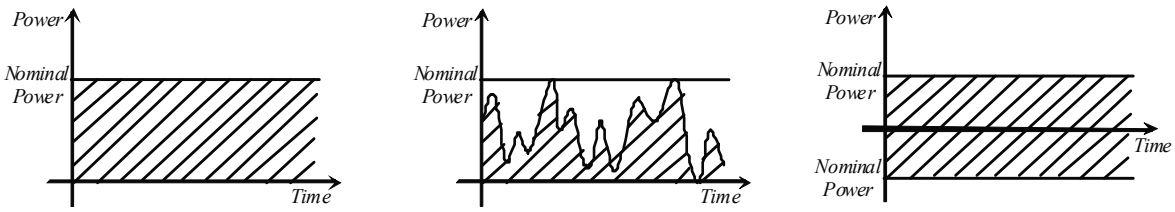

(a) Conventional plant (b) Renewable energy source (c) Energy storage system

Figure I-6: Characteristic of different kinds of energy sources

With proper power control and energy management strategies, active generators must perform local optimization of the active and reactive power production and fast load tracking.

I.4 Presentation of the studied active generator

I.4.1 Technologies of wind generators

Among the different renewable energy generators, the wind generator is technically and economically the most developed one. In general, wind generators can be classified into three categories [Bla 06].

Wind generator without power electronic converters: Most of these topologies are based on a squirrel-cage induction machine (SCIM), which is directly connected to the grid. A soft starter is usually used to reduce the inrush current during start up. Moreover, a capacitor bank is necessary for the reactive power compensation (Fig.I-7a).

By adding power electronic converters into the wind generator, a variable-speed wind generator can be achieved. Although the system complexity and the solution cost are

increased, a better control of the converted primary power and of the grid connection can be obtained. For example, maximum power can be extracted for a large variation of wind speed. The use of power electronic converters in the wind generator can be further divided into two categories: systems using partial-scale power electronic converters and systems using full-scale power electronic converters.

Wind generator using partial-scale power electronic converters: A particular structure is based on a wounded-rotor induction machine. An extra resistor controlled by power electronic converters is added in the rotor and gives a variable speed range of 2% to 4%. The power converter for the rotor resistor control is for low voltage but high currents. This solution also needs a soft starter and a reactive power compensator. Another solution is to use a back to back power electronic converter with the wounded rotor induction machine, as shown in Fig.I-7b. In this case, a power converter connected to the rotor through slip rings controls the rotor currents. If the generator is running super-synchronously, the electrical power is delivered through both the rotor and stator. If the generator is running sub-synchronously, the electrical power is only delivered into the rotor from the grid. A speed variation of 60% around synchronous speed may be obtained by the use of a power converter of 30% of the nominal power.

Wind generator using full-scale power electronic converters: By implementing a full-scale power converter between the electrical machine and the utility grid, additional technical performances of the wind generator can be achieved. Normally, as shown in Fig.I-7c, a squirrel-cage induction machine (SCIM) or a synchronous machine (SM) is used in this configuration. By using a multi-pole wound rotor (or permanent-magnet) synchronous machine (MPSM), the gearbox can be eliminated (Fig.I-7d).

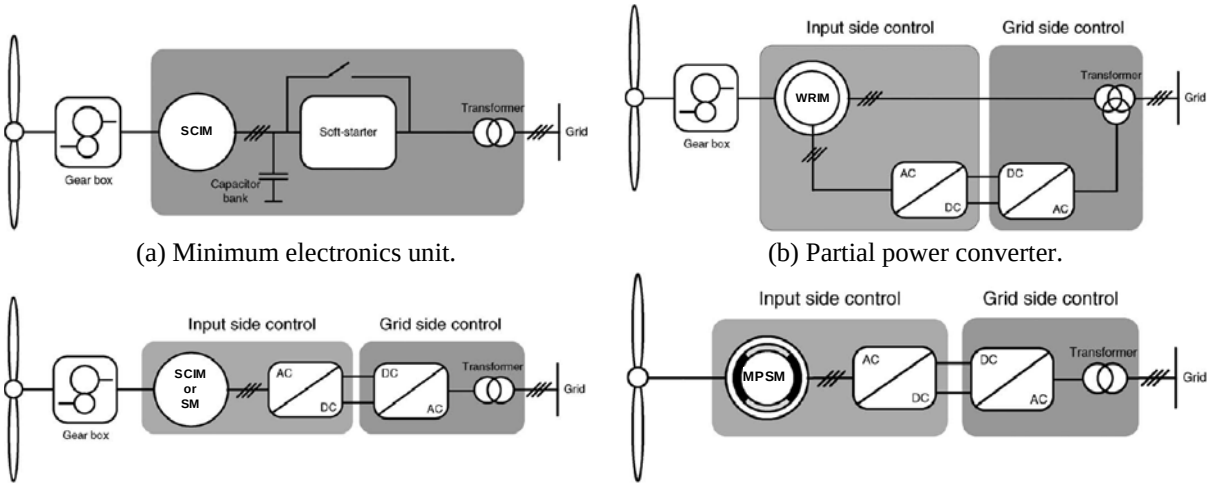

(a) Minimum electronics unit.

(b) Partial power converter.

(c) Full-scale power converter with gearbox.

(d) Full-scale power converter without gearbox.

Figure I-7: Wind generator with power electronics

In our study, a variable-speed wind generator as shown in Fig.I-7c is considered for extracting the maximum available wind power. Such kind of wind generator supplies continuously varying powers, which depend on the intermittent and fluctuant wind velocity. When a large scale of wind generators is connected to the grid, stability problems will occur due to the dependence of the power production on the wind condition. It is very important for the future's power grid to transform wind generators into active generators. So we choose wind generators as the renewable energy source in our studied system.

I.4.2 Classification of energy storage systems

Energy storage systems can be classified in accordance with the storage of electrical, magnetic, thermal, chemical, kinetic and gravitational potential energy. From the system view, more attentions should be paid to the access time, application and control of the storage units, as illustrated in Fig.I-8. According to this Ragone Chart, they can be classified into two categories:

- ***Fast-dynamic storage systems*** ("power sources"), which usually can deliver high specific power with fast dynamics. They can not store much energy for a long-term operation but can provide fast and high power variations, such as flywheels, super-capacitors, super-conducting magnetic energy storage (SMES);
- ***Long-term storage systems*** ("energy sources"), which usually have slow dynamic and high specific energy. They can not provide fast varying power but can store much energy for long-term operation, such as diesel generator, micro gas turbine, batteries, fuel cells with electrolyzers and hydrogen bottles.

Therefore, long-term storage systems are suitable to overcome the uncertainty of energy availability of the renewable energy generators. Fast-dynamic storage systems can be used to compensate the power difference between the fast power variations of loads and the fluctuant power supply of the renewable energy generation. In order to make the wind energy conversion system work like a conventional power generator, energy storage systems will be used to store or to compensate the power difference between the continuously varying production and consumption.

An ideal energy storage device, which can work as an excellent long-term energy source and as a perfect high-dynamic power source, does not exist. The batteries are the "trade-off" product, which are usually used to provide medium performances in both energy density and power density. In order to combine the complementary advantages of these two kinds of energy storage devices, hybrid power systems are chosen for our study and the batteries are not considered.

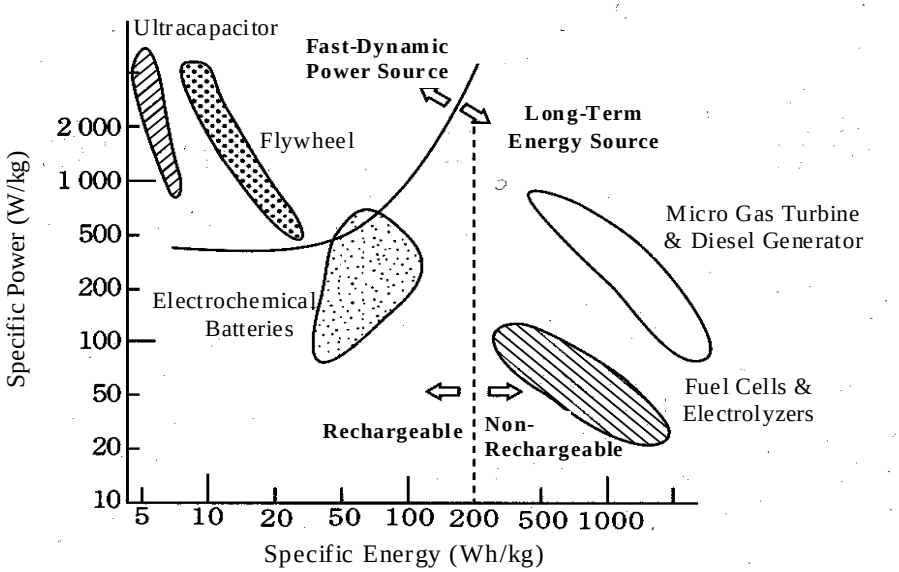

Figure I-8: Characterization of main energy backup systems

1.4.3 Long-term storage system through hydrogen technologies

Diesel generators and micro gas turbines have a good controllability, so they are good candidates for long-term backup power plants. They are often used in microgrids for the security of power supply. However, they consume fossil fuels, which should be transported from far away.

Some fuel cells consume hydrogen to generate electricity and heat and the only product is water, which has no environmental impact. There are many methods to produce hydrogen. If we can find a way to produce hydrogen by using electrical power, the electricity can be stored in the form of hydrogen. The water electrolyzer is the good candidate. The idea is to design an intelligent control system to perform a combined use of both power sources.

The excess wind power can be consumed by the electrolyzer to produce hydrogen, which is stored in a hydrogen tank and later is used to compensate the deficit wind power by fuel cells. In a system point of view, the whole hydrogen based energy storage system can be charged and discharged like traditional batteries. The power capacity can be sized by adjusting the nominal powers of the fuel cells and the electrolyzers. The energy capacity can be sized by adjusting the hydrogen tank volume. Therefore, it is easier to avoid wasting over-sizing problems with the hydrogen devices than with the batteries. So we choose hydrogen devices for long-term energy storage in our studied hybrid power system.

Regenerative fuel cells have also earned many researchers' interests. They are electrochemical reactors, which can be operated both in fuel cell mode and in electrolyzer mode. However, we can not ensure good efficiencies because different catalysts are needed for the different operations. Therefore, regenerative fuel cells have not yet been commercialized today. However, although some technical points should still be improved and the cost should be decreased, fuel cells and electrolyzers are relatively mature products and have already been commercialized. So we choose the fuel cells and the electrolyzer for our hybrid power system.

1.4.4 Fast-dynamic storage unit by super-capacitors

Thanks to their high dynamics, long lifetime and good efficiency, flywheel systems are suitable for fast-dynamic energy storage [Fra 02] [Gra 06]. A flywheel is a rotating mass, which can store energy in the form of kinetic energy through an electrical machine (working in motor or in generator). However, being a mechanical system, it is currently hampered by the danger of "explosive" shattering of the massive wheel due to overload (tensile strength because of high weight and high velocity).

Recent progress in technology makes super-capacitors the best candidates for fast-dynamic energy storage devices [Tho 05] [Abb 07]. Compared to the batteries, super-capacitors are capable of very fast charging and discharging and can achieve a very large number of cycles without degradation, even at 100% depth of discharge without "memory effect". Globally, super-capacitors have a better round-trip efficiency than batteries. For discharge peak power, super-capacitors have always a high efficiency of 95%, but batteries have only an efficiency of 50% with large thermal dissipations. Super-capacitor can be recharged in several minutes with high current magnitude, but batteries take much more time because of the limited charging current. Moreover, super-capacitors are less sensitive in

operating temperature than batteries and have no mechanical security problems that the flywheel has. So we choose super-capacitors for fast-dynamic energy storage in our hybrid power system.

I.4.5 Structure of the studied hybrid power system

The structures of Hybrid Power System (HPS) can be classified into two categories: AC-coupled and DC-coupled.

In an ***AC-coupled HPS***, all sources are connected to a main AC-bus before being connected to the grid (Fig.I-9a) [Bas 06] [Li 08a]. In AC-coupled structure, different sources can be located anywhere in the microgrid with a long distance from each other. However, the voltage and the frequency of the main AC bus should be well controlled in order to ensure the stability of the DG and the compatibility with the utility network.

In a ***DC-coupled HPS***, all sources are connected to a main DC-bus before being connected to the grid through a main inverter (Fig.I-9b) [Yu 04] [Fra 04]. In a DC-coupled structure, the voltage and the frequency of the grid are independent from those of each source.

However, not all HPSs can be classified into AC or DC-coupled system, since it is possible to have both coupling methods (Fig.I-9c) [Ona 06], then a Mixed HPS is obtained. In this case, some advantages can be taken from both structures.

In our study, we use the DC-coupled structure as shown in Fig.I-9b. The DC-coupled structure is flexible and expandable since the number and the type of the energy sources may be freely chosen. Even more, the grid frequency is independent from the sources through the use of the DC bus. The grid voltage is also independent from the DC-bus voltage and each source's voltage through the use of different power converters. So even if both the control structure and the power management are developed properly for a specified hybrid power system, the number and the type of the power sources do not alter the global control structure of the HPS and the main idea of the power management.

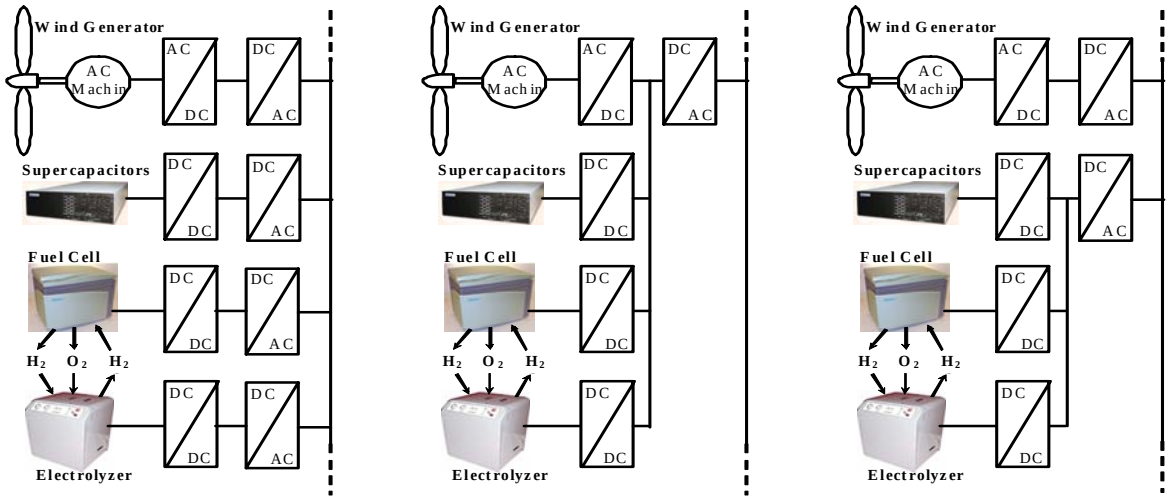

(a) AC-coupled structure (b)DC-coupled structure (c)Mixed structure

Figure I-9: Structures of hybrid power systems for distributed generation

I.5 Objectives and methodologies of the PhD thesis

I.5.1 Objectives

The global goal of the thesis is to theoretically propose and to practically validate efficient energy management strategies to implement an active generator. These strategies must control the power flows among the different energy sources in the studied hybrid power system (Fig.I-9b), in order to supply the active and reactive power required by the microgrid system operator during a certain period. In our laboratory, the system modeling and the control design for wind generators have already been studied. The following objectives have been formulated:

1. In order to build the proposed multi-source hybrid power system, power balancing strategies should be studied to control the power flows among the different sources. These power balancing strategies should firstly be tested in a wind/super-capacitor based hybrid power system. Technical limitations must be highlighted.
2. In order to integrate the hydrogen based long-term energy storage system, the modeling of the fuel cells and the electrolyzers should be studied and experimentally validated. Then proper control strategies should be proposed by taking into account the low dynamic of the auxiliary systems. The performances of the fuel cells and the electrolyzers should be tested before we integrate them in the hybrid power system.
3. With integrated long-term energy storage system, the whole hybrid power system should be modeled and the control system should be adapted. Moreover, efficient power balancing and energy management strategies should be proposed to decide the operating mode of the hybrid power system and to control the power flows among the different sources.

I.5.2 Tools

a) Equivalent average modeling

Different power converters are used in our system. The power electronic converters are discrete-event systems [Hau 99] [Lab 98], whereas the generator and the AC grid are continuous systems. For the analysis of the dynamical behavior of the generators and for the design of the different controllers, it is very useful to define firstly an equivalent average model of the global system including power converters [Rob 01] [Rob 02].

Equivalent average models of power electronic converters take into account only the useful components of modulated currents and voltages in our system (Appendix B). Hence they allow the simulation of the global dynamical behavior of the power system and are sufficient for the analysis and control of the power flow. Moreover, the numerical simulation time is reduced because the integration step is smaller than the switching period of power electronic converters. Even more, the models of other complementary elements, which are connected to the DC bus, can be easily added in.

However, it must be noted that the equivalent model is not able to calculate the voltage and current harmonics because the switching frequency is not taken into account.

b) Graphical tools for system modeling and control design

The studied hybrid power system is a very complex system and a large number of physical quantities are involved. For the system modeling and control design, graphical tools can help the understanding and the analysis of the global system. In our study, we will refer to the following graphical representation tools:

Causal Ordering Graph (COG) has been introduced in 1996 [Hau 96] [Hau 04] to describe power electronics and electrical machines for developing their control systems. This graphical description exclusively uses integral causality [Iwa 94] [Rub 97] on the contrary as the well-known Bond Graph, which allows the derivative causality [Pay 61]. The inversion of this graph yields the control structure of the system with sensors and controllers [Gui 00] [Gui 03]. More details are presented in Appendix D.

Energetic Macroscopic Representation (EMR) has been introduced in 2000 for research development in complex electromechanical drives especially multi-drives [Bou 00]. It is based on action-reaction principle, which organises the system as interconnected subsystems according to the integral causality as for the COG. Inversion of the graphical description by using specific rules leads to a Maximal Control Structure of the system [Bar 06] for which we assume that all variables are measurable. This methodology has been successfully applied to fault-tolerant supplies [Del 03], railway traction systems [Bou 06a], wind energy conversion systems [Bou 05a], hybrid electric vehicles using super-capacitors [Lho 05a] and energy storage system using compressed air [Bos 07]. More details are presented in Appendix E.

Multi-Level Representation (MLR) has been recently proposed for a synthetic and dynamic description of the electromechanical conversion systems [Li 08b]. The MLR has the same advantages as the EMR. Moreover, it integrates power modelling levels (“power calculation” and “power flow”) as well as the corresponding control levels (“power control” and “power sharing”) , in order to design the power supervision for microgrid application. It has been successfully used for the power management of a PV unit and a standalone super-capacitor unit and a gas micro-turbine [Li 09]. More details are presented in Appendix F.

In our study, all generation systems and power conversion systems are physically causal systems. In order to model the process and to design the control, the COG is adapted to make appear the causality among the different quantities. However, the hybrid power system is a very complex multi-physic system, including electro-mechanic fields (wind generator), electrochemical fields (fuel cells and electrolyzer), etc. In order to give a synthetic description, EMR is adapted to organise the different subsystems together. For our microgrid application, power flow control is an important task for the energy management and system supervision. MLR will be properly used to make appear the power flows and to design the different power control strategies.

c) Real-time emulator for flexible experimental assessment

Real-time emulators by Hardware-In-the-Loop (HIL) simulations are more and more used for first validation tests before implementation on the entire real process [Rab 02] [Lu 07]. HIL simulation uses one or several real devices for experimental tests, the other parts of the process are simulated in real time on a control board or parallel computers. Such a methodology has been used in aeronautics and automotive industry since a long time [Han 96] [Mac 97]. Traction applications are nowadays more and more developed by using HIL simulation [Ter 99] [Ath 04] [Bou 06b]. HIL simulations of wind energy conversion systems

have also been developed during the last decade [Koj 04][Bou 05b] [Ste 06]. Different HIL simulation concepts for electric drives are presented in Appendix G [Bou 08].

In our study, we need to build an experimental test bench of the hybrid power system in order to test the power balancing and energy management strategies. In order to make the experimental test bench more flexible, we have decided to implement some real-time emulators to replace the real components because of the following advantages:

- ***Equivalent performances***: HIL simulator can provide the same electrical behavior (with the same current-voltage characteristic) as the real component. It is accurate enough to test the power balancing and energy management strategies of the hybrid power system, which is the main objective of the PhD work.
- ***Flexible control***: The commercialized systems (fuel cells or electrolyzers) are usually closed systems and the users have no access to modify the control algorithms for better performances. With HIL simulation, advanced control strategies can be implemented according to the wished functions.
- ***Simple implementation***: It takes less time to implement an HIL simulation, thus time and money are saved during the development of the experimental test bench in laboratory, without unnecessary constraints (with reduced system sizing, without security concerns, etc);
- ***Updating capacity***: With HIL simulation, the system characteristic can always be updated with mathematic modeling and this implies a very long lifetime and a good immunity to the fast developing market. Moreover, it can be used to compare different technologies and products with the static and dynamic characteristics, which are provided by the manufacturers.

I.5.3 Methods

We recall that the objective is to test the control functions and the energy management of a hybrid active wind generator. Specifically in our experimental test bench, real-time emulators by HIL simulation are used to replace the wind generator, the fuel cell and the electrolyzer, in order to avoid sizing constraints and security worries for laboratory implementation. The following steps have been followed (Fig.I-10):

1) Firstly a real system is studied to obtain the system model with mathematical equations and modeling tools in order to make appear necessary and useful properties.
2) A real-time emulator of certain parts of the system is constructed with corresponding modeling equations in order to make a fast assessment of the experimental platform for cost and risk reasons.
3) The emulators are validated by comparing the obtained performances with the behaviors of the studied real systems in the same conditions.
4) The system modeling is also used to design the control algorithms for certain wished performances of the system.
5) The control system can be firstly implemented on the experimental platform with real-time emulators to test the performances. This can be considered as the demonstration of the control performances because normally the same control performance can also be obtained when the control system is implemented on the real system.

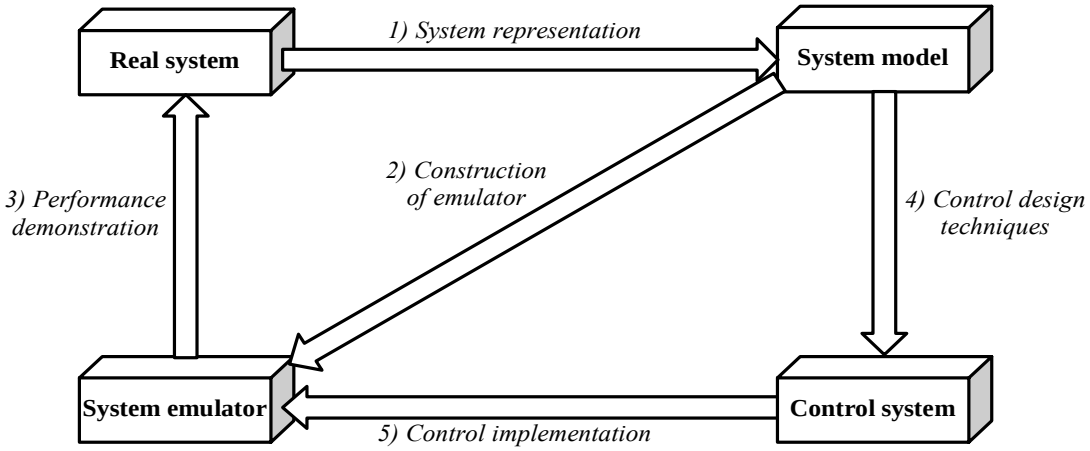

Figure I-10: Methodologies of the PhD work

I.5.4 Thesis layout

According to the existing problems and the formulated objectives, the following parts of the dissertation are organized as follows.

In Chapter 2, the wind/super-capacitor based hybrid power system is studied, including the system modeling, the control design. Two power balancing strategies are proposed and tested for the power flow control among the different sources.

In Chapter 3, a detailed study of fuel cells is presented. An analytical model is chosen for the study and is experimentally validated with a commercial fuel cell system. A control method is proposed to regulate the fuel cell power flow and is validated with a fuel cell emulator.

In Chapter 4, a detailed study of electrolyzers is presented. An analytical model is chosen and is experimentally validated with a commercial electrolyzer system. A control method is proposed to regulate the electrolyzer power flow and is validated with an electrolyzer emulator.

In Chapter 5, we present the hybrid power system, consisting of a wind energy conversion system, super-capacitors based fast-dynamic storage system and hydrogen based long-term storage system (fuel cells and electrolyzers). The system modeling and control design are presented. Different power balancing and energy management strategies are proposed to implement the active wind generator. Finally, the experimental test bench of the hybrid wind generator is presented.

Finally, some conclusions are driven from the studies on the implementation of this active wind generator.

Chapter II

Basic and Advanced Wind Energy Conversion System with Super-capacitors

Chapter II Wind Energy Conversion System

As introduced in the previous chapter, hybrid power systems can be a good solution for the integration of distributed renewable energies in a microgrid. Before presenting the proposed active wind generator (in Chap.V), a classical wind energy conversion system is firstly studied in this chapter, including the system modeling by EMR (Appendix E), the control design and the power balancing strategies. This energy conversion system enables to extract the maximum wind power by adjusting the wind turbine's rotational speed. The obtained electrical power must be adapted (sinusoidal wave form at 50 Hz, phasing) before being sent to the grid. A "grid following" power balancing strategy must be used, while the wind generator works in Maximum Power Point Tracking (MPPT) strategy. Then the DC-bus voltage is regulated with the grid power.

Then, in order to reduce wind power variations, super-capacitors are used to build a first hybrid power system. The system modeling, the control design and the power balancing strategies are presented. The "grid following" strategy and the "power dispatching" strategy can both be used for the power balancing. In the "power dispatching" strategy, the DC-bus voltage is regulated with the powers from the wind generator and the super-capacitors. The performances of these two power balancing strategies are compared in the end of the chapter.

II.1 Study of a wind energy conversion system

II.1.1 Presentation

A classical wind energy conversion system consists of a 3-blade turbine, a gearbox, an electrical machine, a three-phase rectifier, a DC-bus capacitor, a three-phase inverter, line filters which are connected to the grid through a grid transformer (Fig.II-1).

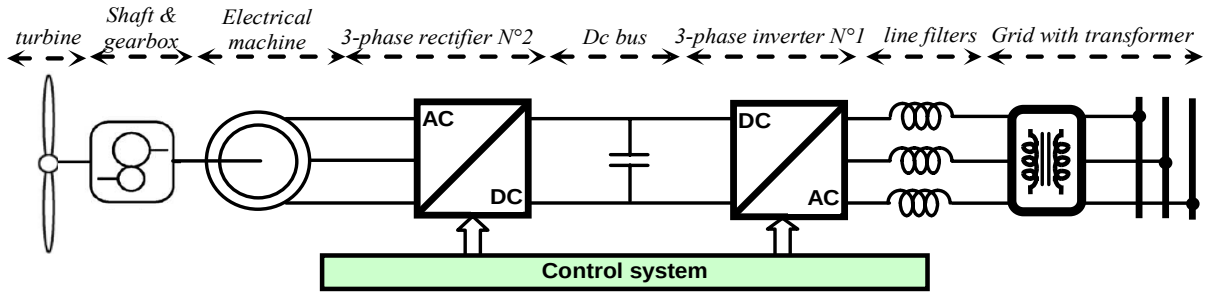

Figure II-1: A classical variable-speed wind energy conversion system

When the wind energy conversion system works in MPPT strategy, the power, which is delivered to the grid, is very fluctuant. We are going to use a wind speed profile, which has been recorded in a wind farm in the north of the France (Fig.II-2) [Lec 04] [Bou 07].

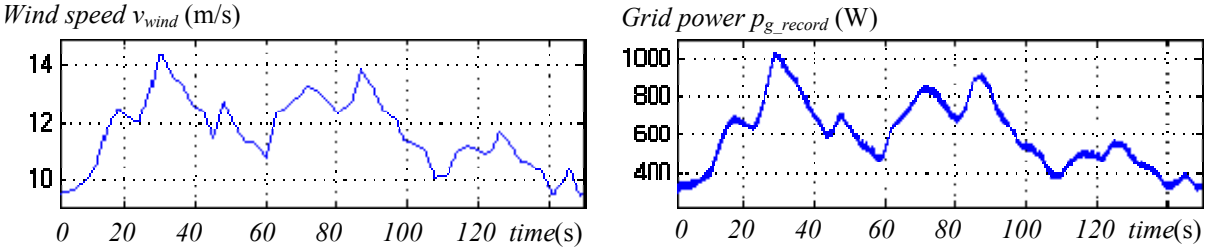

Figure II-2: Experimentally recorded wind speed and wind power [Lec 04][Bou 07]

II.1.2 Modeling of the wind energy conversion system

a) Average modeling of the electrical conversion chain

By using equivalent average models of power electronic converters (Appendix B), the average modeling of the electrical power conversion chain is obtained for the wind energy conversion system (Fig.II-3). The grid with transformer is considered as three-phase voltage sources and the electrical machine is considered as three-phase current sources. The two back-to-back voltage source converters introduce control inputs for the power control. As the DC bus has a relatively slow dynamic, it's shown that we can have three different subsystems with their inner dynamic and control tasks: the wind generator, the grid connection system and the DC bus.

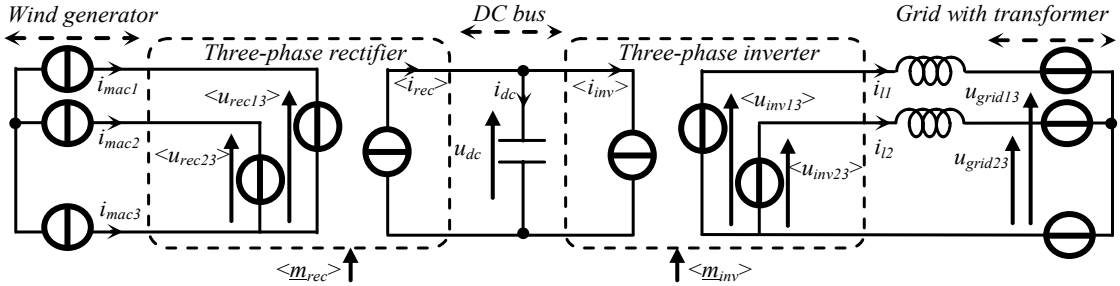

Figure II-3: Equivalent average modeling of the power electronic converters

Three-phase rectifier: The equivalent average model is used with average modulation functions It yields the average values ($<\underline{u}_{rec}>=[(<u_{rec13}> <u_{rec23}>]^T$) of the modulated voltages from the dc-bus capacitor voltage (u_{dc}) and the average value ($<i_{rec}>$) of the modulated current from the machine currents ($\underline{i}_{mac}=[i_{mac1} \ i_{mac2}]^T$) :

$$\begin{cases} <\underline{u}_{rec}> = <\underline{m}_{rec}> u_{dc} \\ <i_{rec}> = <\underline{m}_{rec}^T> \underline{i}_{mac} \end{cases} . \qquad \text{(II-1)}$$

where $\underline{m}_{rec}$ is the vector of modulation functions of the grid inverter.

Three-phase inverter: The three-phase inverter is modeled in the same way. The average value of the modulated voltages ($<\underline{u}_{inv}>=[(<u_{inv13}> <u_{inv23}>]^T$) is calculated from the DC-bus voltage (u_{dc}) and the average value ($<i_{inv}>$) of the modulated current from the line currents ($\underline{i}_l=[i_{l1} \ i_{l2}]^T$):

$$\begin{cases} <\underline{u}_{inv}> = <\underline{m}_{inv}> u_{dc} \\ <i_{inv}> = <\underline{m}_{inv}^T> \underline{i}_l \end{cases} , \qquad \text{(II-2)}$$

where $\underline{m}_{inv}$ is the vector of modulation functions of the grid inverter.

b) Modeling of the wind generator

The modeling of the wind energy generation system is presented in detail with the help of the EMR as below (Fig.II-4).

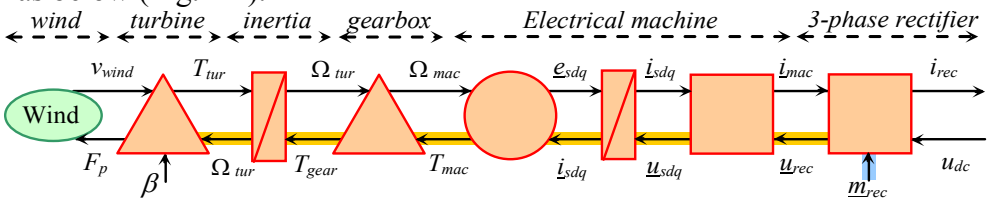

Figure II-4: EMR of the considered wind energy generation system

Wind: The wind is modeled by a mechanical source (oval pictogram), which sets the wind velocity (v_{wind}) to the blades.

Turbine: The turbine is modeled as a mechanical converter (triangular pictogram). The torque (T_{tur}), which is produced by the turbine, depends on the wind velocity (v_{wind}) and on the blade pitch angle (β):

$$T_{tur} = \frac{1}{2} C_T(\lambda, \beta) \rho S_b R_b v_{wind}^2 \tag{II-3}$$

with S_b: the area, which is swept by the blades;
R_b: the blade length;
ρ: the air density;
C_T: the torque coefficient, a non-linear function of the tip-slip ratio (λ) (Fig.II-5);
λ: the tip-slip ratio depending on the wind velocity and the rotational speed (Ω_{tur}).

$$\lambda = \frac{R_b \Omega_{tur}}{v_{wind}} \tag{II-4}$$

For the study, we will consider a normal turbine operating with a constant pitch angle.

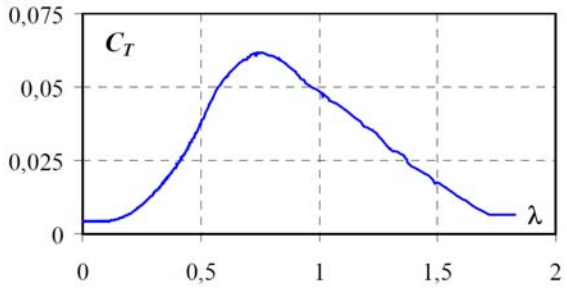

Figure II-5: Blade characteristic: C_T versus λ for a fixed blade angle

Inertia: The shaft is an element with energy accumulation (rectangular pictogram), which imposes the rotational speed (Ω_{tur}) with the torque difference between the blade torque (T_{tur}) and the gear torque (T_{gear}),

$$J_{shaft} \frac{d\Omega_{tur}}{dt} = T_{tur} - T_{gear} - f_{shaft} \Omega_{tur} \tag{II-5}$$

with J_{shaft}: the equivalent inertia moment of the shaft;
f_{shaft}: the friction coefficient of the equivalent shaft.

Gearbox: The gearbox is a mechanical converter (triangular pictogram) and adapts the low speed of the turbine with the high speed of the electrical machine. It yields the rotational speed (Ω_{mac}) and the torque (T_{gear}) through the gear ratio (m_{gear}):

$$\begin{cases} \Omega_{mac} = m_{gear} \Omega_{tur} \\ T_{gear} = m_{gear} T_{mac} \end{cases} \tag{II-6}$$

Electrical machine: The electrical machine can be globally modeled as an electromechanical converter (circular pictogram) with the rectifier voltages (u_{rec}=[u_{rec13}, u_{rec23}]^T) and the gear speed (Ω_{mac}) as the inputs. The stator currents (i_{mac}=[i_{mac1}, i_{mac2}]^T) and the machine torque (T_{mac}) are the outputs. It can be divided into three sub-blocks.

The first block corresponds to mathematical transformations (square pictogram) from phase-to-phase voltages ($\underline{u}_{rec}$) to machine line voltages and then into a rotating d-q frame

($\underline{u}_{sdq}$). This Park transformation expresses stator voltages and currents in a d-q rotational frame:

$$\begin{cases} \underline{u}_{sdq} = [T(\theta_{sdq})]\underline{u}_{rec} \\ \underline{i}_{mac} = [T(\theta_{sdq})]^{-1}\underline{i}_{sdq} \end{cases}, \tag{II-7}$$

where θ_{sdq} is the angle of the rotating d-q frame with respect to the stator stationary frame.

The second block is an element with energy accumulation (rectangular pictogram). In the d-q frame, the equivalent stator windings set the stator currents ($\underline{i}_{sdq}=[i_{sd},\ i_{sq}]^{T}$) as state variables, which are calculated with the stator voltages ($\underline{u}_{sdq}=[u_{sd},\ u_{sq}]^{T}$) and the e.m.f. ($\underline{e}_{sdq}=[e_{sd},\ e_{sq}]^{T}$),

$$\begin{cases} L_s \dfrac{di_{sd}}{dt} = u_{sd} - e_{sd} - R_s i_{sd} \\ L_s \dfrac{di_{sq}}{dt} = u_{sq} - e_{sq} - R_s i_{sq} \end{cases}, \tag{II-8}$$

with R_s: the resistor of the stator winding;

L_s: the cyclic inductor of the stator winding.

The third block is an electromechanical converter (circular pictogram), which leads to the machine torque (T_{mac}) and the e.m.f. ($\underline{e}_{sdq}$) from the stator currents and the rotor's electrical angular speed (Ω_{mac}).

$$T_{mac} = \rho\phi_{rd} i_{sq}, \tag{II-9}$$

$$\begin{cases} e_{sd} = L_s \Omega_{mac} i_{sq} \\ e_{sq} = L_s \Omega_{mac} i_{sd} \end{cases}. \tag{II-10}$$

with ρ: number of pole-pairs;

ϕ_{rd}: constant rotor flux of the permanent magnet.

c) Modeling of the grid connection

The modeling of the grid connection system is presented in detail with the help of the EMR as below (Fig.II-6).

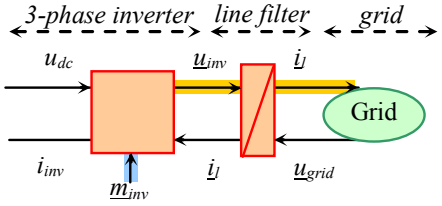

Figure II-6: EMR of the grid connection system

Grid filter: The line currents ($\underline{i}_l$) are calculated from dynamic equations of the filter with the inverter phase-to-phase voltages ($\underline{u}_{inv}$) and the phase-to-phase grid voltages ($\underline{u}_{grid}$):

$$L_{line}\frac{d\underline{i}_l}{dt} = \frac{1}{3}\begin{bmatrix} 2 & -1 \\ -1 & 2 \end{bmatrix}\left(\underline{u}_{inv} - \underline{u}_{grid}\right) - r_{line}\underline{i}_l, \tag{II-11}$$

with L_{line}: the equivalent inductor of the grid filter;

r_{line}: the equivalent resistor in series of the grid filter.

Grid: The electrical network with the grid transformer is considered as ideal sinusoidal phase-to-phase voltage sources $\underline{u}_{grid}=[u_{grid13}\ \ u_{grid23}]^{T}$.

d) Modeling of the DC bus

The modeling of the DC bus is presented in detail with the help of the EMR (Fig.II-7).

Coupling: In order to control the power exchange around the DC bus, the DC coupling should be modeled in detail:

$$i_{dc} = i_{rec} - i_{inv}\,, \tag{II-12}$$

with i_{rec}: the rectifier's modulated current;
i_{inv}: the inverter's modulated current.

Capacitor: The DC-bus capacitor is an element with energy accumulation and its voltage is calculated from the dynamic equation:

$$C_{dc}\frac{du_{dc}}{dt} = i_{dc}\,, \tag{II-13}$$

with C_{dc}: the DC-bus capacitor;
u_{dc}: the DC-bus voltage.

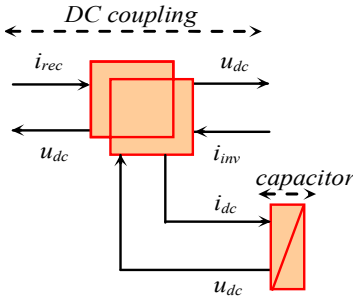

Figure II-7: EMR of the DC bus

e) Modeling of the entire wind energy conversion system

The modeling of the entire wind energy conversion system is obtained (Fig.II-8) by combining all EMR, which have been previously presented (Fig.II-4, Fig.II-6 and Fig.II-7).

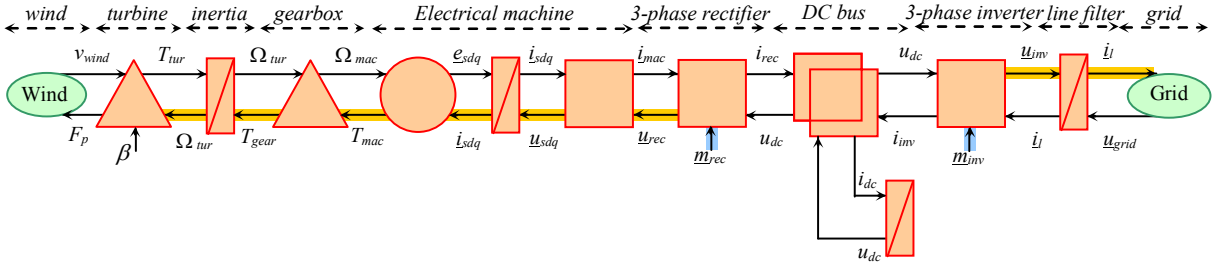

Figure II-8: EMR of the entire wind energy conversion system

II.1.3 Hierarchical control structure

The wind energy conversion system is designed to transfer powers from the wind generator to the electrical grid. Two power converters are used to regulate the power exchange. A hierarchical control structure is used to implement the control system (Appendix C). Two Switching Control Units and two Automatic Control Units are used seperately in the control system for the two power converters. A common Power Control Unit and a common

Mode Control Unit are used for the power balancing and the energy management of the entire power system (Fig.II-9).

In the SCU of each converter, the IGBT drivers and PWM techniques are used to control the commutation circuits. These control units are not the main concern of this study, so they will not be detailed here. However, the control algorithms in the ACU should be presented in order to highlight the physical quantities, which can be used for the power flow control among the different energy sources.

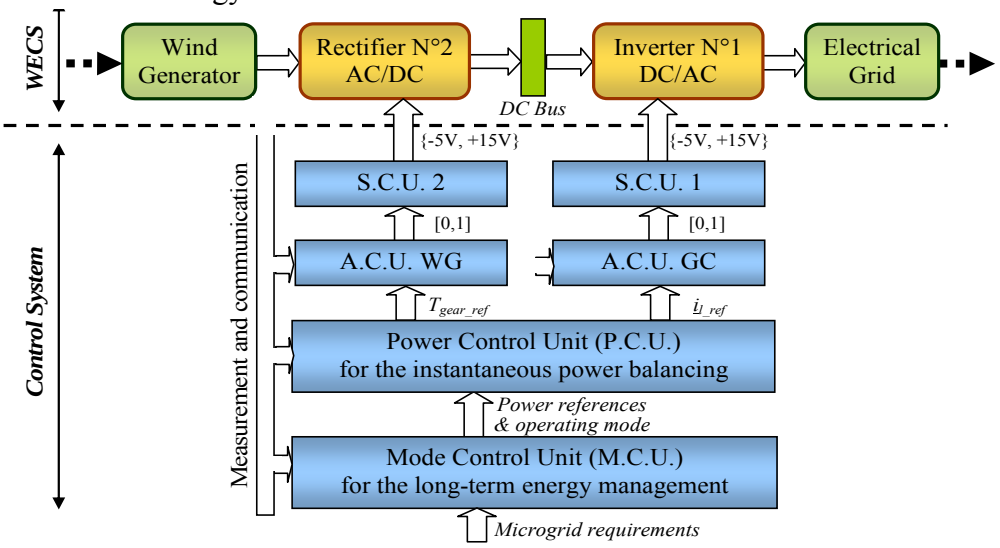

Figure II-9: Hierarchical control structure of the wind energy conversion system

The ACU is designed from the EMR of the system modeling according to inversion rules (Appendix E). The use of an average modeling of power electronic converters gives three different subsystems, whose ACUs are now respectively detailed.

II.1.4 Automatic control unit

a) Control of the wind generator

The electrical power vs. speed curves of a typical wind turbine is given in Fig.II-10. For example if the wind velocity is v_1 the output power can be raised to the maximum value at point A by setting the mechanical speed to Ω_1. If the wind speed changes to v_2 the power output jumps to point B. For this wind velocity the maximum power can be extracted by setting the speed to Ω_2 at point C. This shows that, as the wind speed changes, the generator speed should track these changes in order to extract the maximum power. This strategy is called Maximum Power Point Tracking (MPPT) strategy.

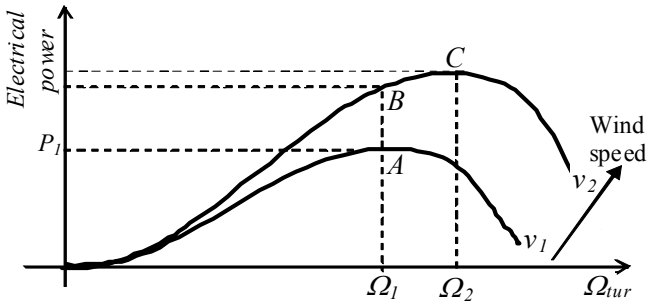

Figure II-10: Turbine power vs. speed

The EMR of the wind energy conversion system modeling (Fig.II-8) shows that the speed (Ω_{tur}) can be controlled by acting on two inputs: the aerodynamic torque (T_{tur}) and the torque of the generator (T_{gear}). As here we consider a normal operation with a constant pitch angle, the aerodynamic torque must be considered as a perturbation input (linked to the wind speed) for the system. So the turbine speed can be controlled by acting on the gearbox torque (T_{gear}) via the control input ($\underline{m}_{rec}$) of the power electronic converter.

From the EMR of the wind energy conversion system modeling, an action chain appears from the control inputs ($\underline{m}_{rec}$) of the rectifier to the gear's mechanical torque (T_{gear}) (Fig.II-8). The control scheme of the wind energy generation system is obtained by inverting this action chain (Fig.II-11). It consists to calculate the reference of the rectifier's duty ratios ($\underline{m}_{rec\_ref}$) according to a torque references (T_{gear_ref}). It is composed of a torque control, a field oriented control and a rectifier control.

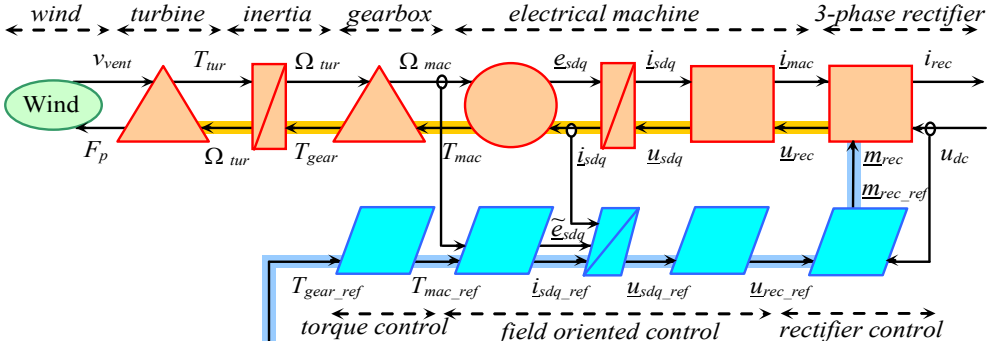

Figure II-11: Control scheme of the wind energy generation system.

Torque control: The calculated mechanical torque reference (T_{gear_ref}) from a MPPT strategy is converted into the machine torque reference (T_{mac_ref}) by inverting Eq.II-6:

$$T_{mac\_ref} = \frac{1}{m_{gear}} T_{gear\_ref} . \tag{II-14}$$

Field oriented control: A standard field oriented control is used to control the electrical machine (Fig.II-12) [Bou 02]. The inversion of Eq.II-9 leads to the current references ($\underline{i}_{sdq\_ref}=[i_{sd\_ref}\ \ i_{sq\_ref}]^T$), i_{sq_ref} is obtained from the torque reference (T_{mac_ref}) with the constant rotor flux (ϕ_{rd}) of the permanent magnet and i_{sd_ref} is set to zero with a properly chosen frame orientation:

$$\begin{cases} i_{sq\_ref} = \dfrac{1}{\rho \phi_{rd}} T_{mac\_ref} \\ i_{sd\_ref} = 0 \end{cases} . \tag{II-15}$$

As the stator windings are accumulation elements, closed-loop controllers are needed to invert Eq.II-8:

$$\underline{u}_{sdq\_ref} = PI\left(\underline{i}_{sdq\_ref} - \underline{\hat{i}}_{sdq}\right) + \underline{\tilde{e}}_{sdq} . \tag{II-16}$$

where $PI(x_{ref}-x)$ is the controller of the variable x. In practice, the e.m.f. ($\underline{e}_{sdq}$) can not be measured, but it can be estimated through the sensed rotor's rotational speed (Ω_{mac}) by using Eq.II-10:

$$\begin{cases} \tilde{e}_{sd} = L_s \Omega_{mac} \hat{i}_{sq} \\ \tilde{e}_{sq} = L_s \Omega_{mac} \hat{i}_{sd} \end{cases} . \quad \text{(II-17)}$$

Finally by inverting Eq.II-7, the inverse Park transformation ($[T(\theta_{sdq})]^{-1}$) leads to the references of the rectifier voltages ($\underline{u}_{rec\_ref}$):

$$\underline{u}_{rec\_ref} = [T(\theta_{sdq})]^{-1} \underline{u}_{sdq\_ref} . \quad \text{(II-18)}$$

Rectifier control: The reference modulation functions $\underline{m}_{rec\_ref}$ are obtained by inversion of Eq.II-1 through the measurement of the DC-bus voltage u_{dc}:

$$\underline{m}_{rec\_ref} = \frac{1}{\hat{u}_{dc}} \underline{u}_{rec\_ref} . \quad \text{(II-19)}$$

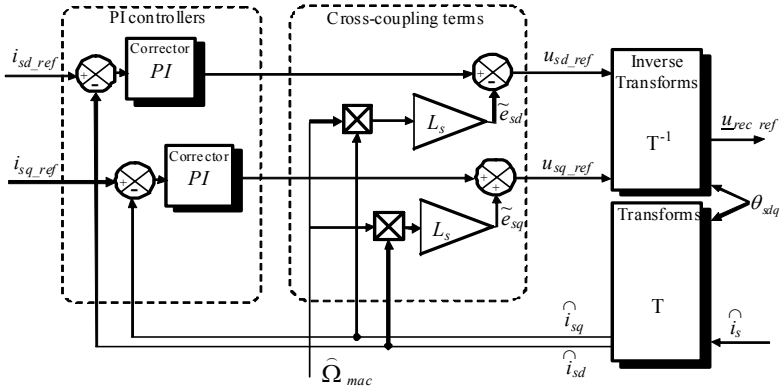

Figure II-12: Block diagram of the oriented field control of the electrical machine.

b) Control of the grid connection

The EMR of the grid connection system modeling makes appear a path from the control inputs ($\underline{m}_{inv}$) of the inverter to the line currents ($\underline{i}_l$) in Fig.II-6. The control scheme of the grid connection system is obtained by inverting this path (Fig.II-13). It consists to calculate the reference of the inverter's duty ratios ($\underline{m}_{inv\_ref}$) according to the line currents' references ($\underline{i}_{l\_ref}$).

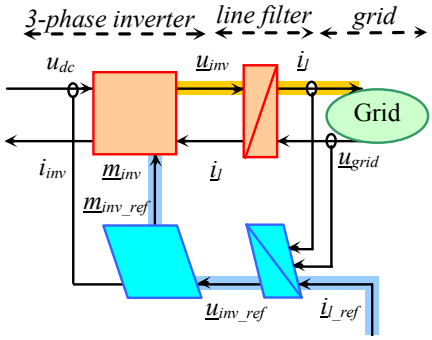

Figure II-13: Control scheme of the grid connection system.

Line current control: The grid is a voltage source ($\underline{u}_{grid}$), so the line current should be controlled in order to regulate the exchanged power with the grid. In order to control this current, a current controller is needed with a Park transformation (T) and an inverse Park transformation (T^{-1}) as shown in Fig.II-14:

$$\underline{u}_{inv\_ref} = [T(\theta_{dq})]^{-1}\underline{u}_{inv\_dq\_ref}$$
$$\begin{cases} u_{inv\_d\_ref} = PI\left(i_{l\_d\_ref} - i_{l\_d}\right) + \hat{u}_{grid\_d} - \tilde{e}_{lq} \\ u_{inv\_q\_ref} = PI\left(i_{l\_q\_ref} - \underline{i}_{l\_q}\right) + \hat{u}_{grid\_q} + \tilde{e}_{ld} \end{cases} \quad \text{(II-20)}$$

with $\underline{i}_{l\_dq\_ref} = \left[T(\theta_{dq})\right]\underline{i}_{l\_ref}$, $\hat{\underline{i}}_{l\_dq} = \left[T(\theta_{dq})\right]\hat{\underline{i}}_{l}$, $\hat{\underline{u}}_{grid\_dq} = \left[T(\theta_{dq})\right]\hat{\underline{u}}_{grid}$, $\tilde{e}_{lq} = 2\pi f L_{line}\hat{i}_{l\_q}$ and $\tilde{e}_{ld} = 2\pi f L_{line}\hat{i}_{l\_d}$, where f is the frequency of the grid voltage.

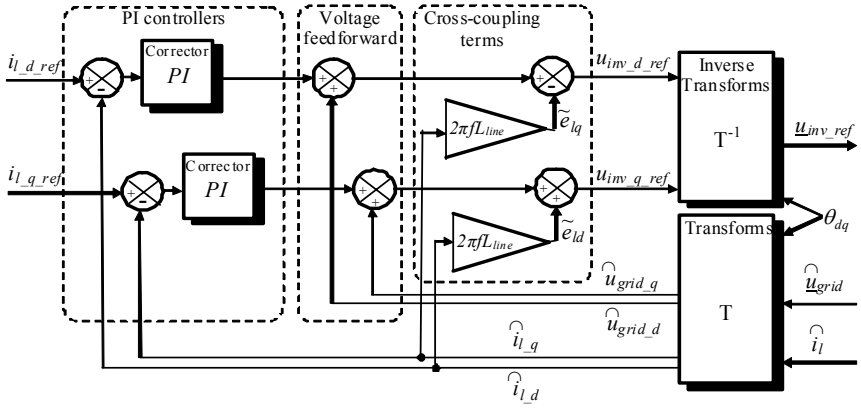

Figure II-14: Block diagram of the line current control in the grid connection system.

Inverter control: The modulation functions of the inverter are obtained by inverting Eq.II-2:

$$\underline{m}_{inv\_ref} = \frac{1}{\hat{u}_{dc}}\underline{u}_{inv\_ref}. \quad \text{(II-21)}$$

c) Control of the DC bus

The wind energy conversion system can be decomposed into three independent subsystems if the DC-bus voltage is constant. The control scheme of the DC bus is obtained by inverting the EMR of the system modeling. The DC-bus voltage should be well regulated for the stability of the grid connection because it is used in a division operator in the converter control algorithms (Eq.II-19 and Eq.II-21). So a voltage controller is needed (Fig.II-15):

$$i_{dc\_ref} = PI(u_{dc\_ref} - \hat{u}_{dc}). \quad \text{(II-22)}$$

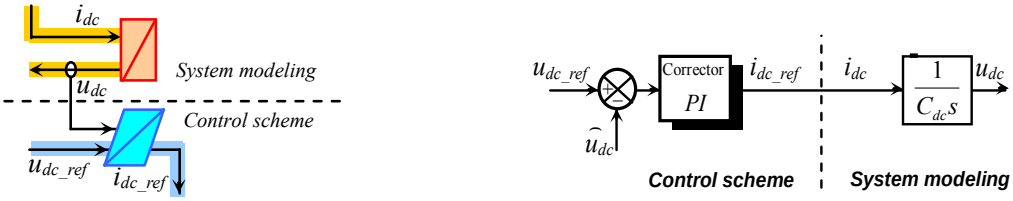

(a) Energetic macroscopic representation (b) Block diagram

Figure II-15: Control scheme of the DC bus.

d) Control of the entire wind energy conversion system

The control scheme of the entire wind energy conversion system is obtained by combining all the control schemes presented above (Fig.II-16). And the corresponding bloc diagram is shown in Fig.II-17.

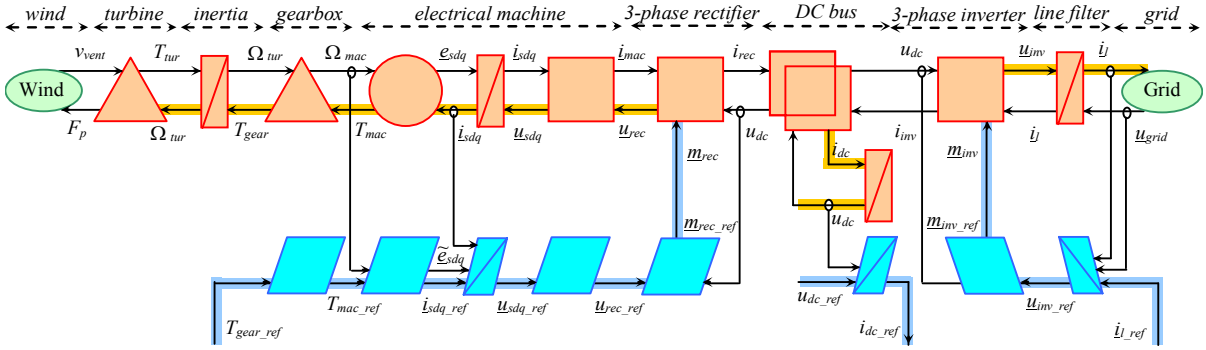

Figure II-16: Control scheme of the entire wind energy conversion system.

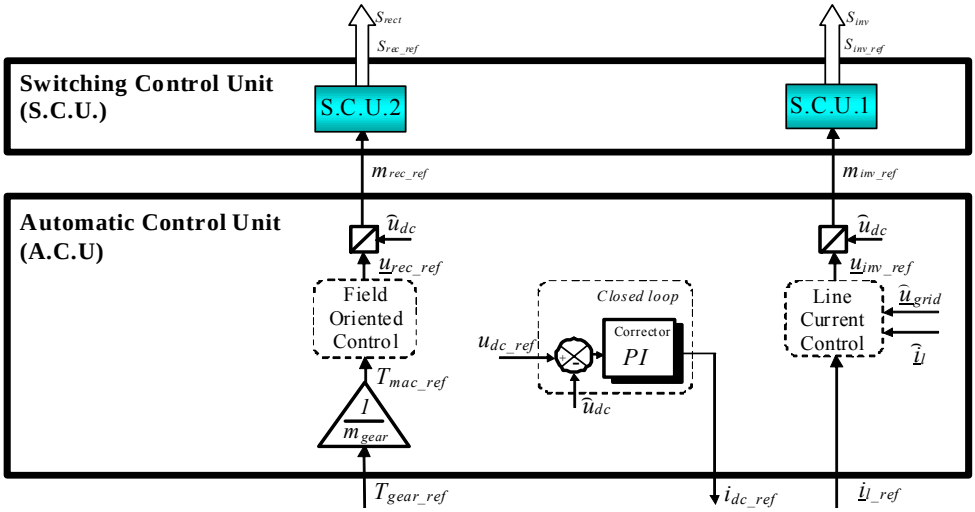

Figure II-17: Block diagram of the automatic control units for the wind energy conversion system.

II.1.5 Power control unit

In the studied wind energy conversion system, all power exchanges are performed via the DC-bus (Fig.II-18) and have an impact on the DC-bus voltage:

$$\frac{dE_{dc}}{dt} = C_{dc} u_{dc} \frac{du_{dc}}{dt} = u_{dc} i_{dc} = p_{dc} = p_{wg} - p_{gc} . \qquad \text{(II-23)}$$

with E_{dc}: the stored energy in the DC-bus capacitor;
p_{dc}: the exchanged power with the DC-bus capacitor;
p_{wg}: the power, which is injected into the DC bus from the wind generator;
p_{gc}: the power, which is extracted from the DC bus into the grid;

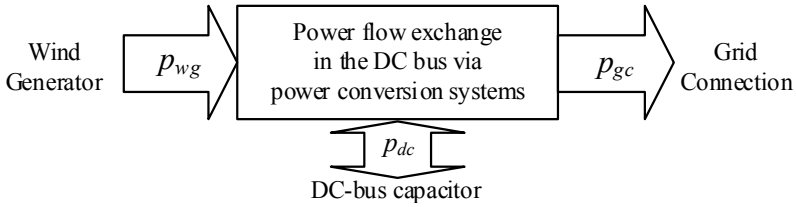

Figure II-18: Power flow exchanges around the DC bus

a) Layout

The Power Control Unit (PCU) can be divided into two levels: the Power Control Level (PCL) and the Power Sharing Level (PSL). The power control level consists to calculate the

reference of the related quantities (T_{gear_ref}, $\underline{i}_{dc\_ref}$, $\underline{i}_{l\_ref}$) from the power references (p_{wg_ref}, p_{dc_ref}, p_{g_ref}, q_{g_ref}). The power sharing level coordinates the power flow exchanges among the different energy sources.

b) Power control level

Each controlled quantities implies a power, which is calculated in Table II-1.

For the wind generator, a MPPT strategy is used to extract the maximum power. The power reference (p_{wg_ref}) can be set by calculating the corresponding torque reference (T_{gear_ref}) with the sensed value of the rotational speed (Ω_{tur}) according to the inverse equation (***Int2c***).

The powers, which are exchanged with the grid, can be calculated through the "two-wattmeter" method with the equation (***Int1***) and the line current references are calculated by the inverse equations (***Int1c***).

The output of the DC-bus voltage control loop is the reference of the required dc current (i_{dc_ref}) and its product with the measured DC-bus voltage (u_{dc}) gives the necessary power reference (p_{dc_ref}) for the DC-bus voltage regulation according to the equation (***Int0e***).

Table II-1: Power calculation and control algorithms for the wind energy conversion system.

Energy source	Power calculation	Power control
DC-bus capacitor	***Int0***: $p_{dc} = u_{dc} i_{dc}$	***Int0e***: $p_{dc\_ref} = \hat{u}_{dc} i_{dc\_ref}$
Grid connection	***Int1***: $\begin{cases} p_g = u_{13} i_1 + u_{23} i_2 \\ q_g = \sqrt{3}(u_{13} i_1 - u_{23} i_2) \end{cases}$	***Int1c***: $\begin{cases} i_{l1\_ref} = \dfrac{(2\hat{u}_{13} - \hat{u}_{23}) p_{g\_ref} + \sqrt{3}\hat{u}_{23} q_{g\_ref}}{2\hat{u}_{13}^2 - 2\hat{u}_{13}\hat{u}_{23} + 2\hat{u}_{23}^2} \\ i_{l2\_ref} = \dfrac{(2\hat{u}_{23} - \hat{u}_{13}) p_{g\_ref} - \sqrt{3}\hat{u}_{13} q_{g\_ref}}{2\hat{u}_{13}^2 - 2\hat{u}_{13}\hat{u}_{23} + 2\hat{u}_{23}^2} \end{cases}$
Wind generator	***Int2***: $p_{wg} = \Omega_{tur} T_{gear}$	***Int2c***: $T_{gear\_ref} = \dfrac{1}{\hat{\Omega}_{tur}} p_{wg\_ref}$

c) Power sharing level

The choke filters are sized to obtain a small voltage drop across them and their losses and reactive powers are small. Moreover, these powers will be considered as disturbances and can be attenuated by the various used closed-loop controls. So we will not discuss in detail the power estimation of losses and compensation algorithms in order to focus on the power balancing algorithms.

We can assume that the wind power (p_{wg}) is divided into two parts (Fig.II-19). One part (p_{dc}) is sent to the DC-bus capacitor. The other part is sent to the grid (p_g). The power exchange can be expressed as,

$$\textbf{Pow1}: \; p_g = p_{wg} - p_{dc}. \tag{II-24}$$

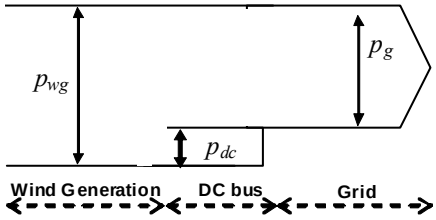

Figure II-19: Power flow exchange inside the wind energy conversion system.

The wind generator is connected to a three-phase rectifier and various control strategies can be used. For example, when the wind velocity is not too high, the wind generator can work in a Maximum Power Point Tracking (MPPT) strategy to improve the global energy efficiency. When the wind velocity becomes too high, the wind generator can work in rated power strategy by reducing the power efficiency for security reasons. In our study, we assume that the wind velocity is medium and we use a MPPT strategy in the form of a searching algorithm of the maximum power as shown in Fig.II-10. Therefore, with the fluctuant wind, the wind power is very fluctuant. This fluctuant power is rectified and sent to the DC bus. Hence a "grid following" power balancing strategy should be used (Fig.II-20) because the availability of the wind power is not ensured for the DC bus control. So the DC-bus voltage is regulated by the line current controller through the three-phase inverter. The wind power (p_{wg}) must be seen as a fluctuant disturbance. In order to regulate the DC-bus voltage, the only way is to use the grid power (p_g), as shown in the closed loop ($u_{dc\_ref} \rightarrow p_{dc\_ref} \rightarrow p_{g\_ref} \rightarrow m_{inv} \rightarrow p_g \rightarrow p_{dc} \rightarrow u_{dc}$) in Fig.II-20.

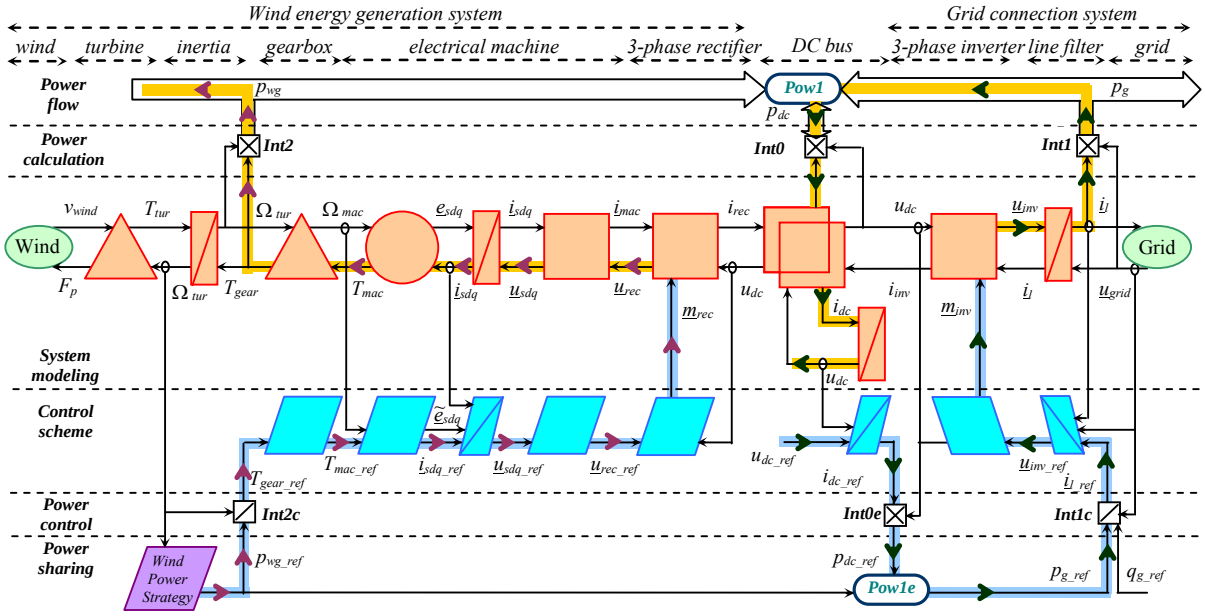

Figure II-20: Multi-Level Representation of the wind energy conversion system.

So the grid power reference (p_{g_ref}) is obtained by taking into account the DC-bus power reference (p_{dc_ref}) for the voltage regulation and the estimated wind power $\tilde{p}_{wg}$ (Fig.II-21),

$$\textbf{Pow1e:}\quad p_{g\_ref} = \tilde{p}_{wg} - p_{dc\_ref}\,. \tag{II-25}$$

In practice, we can set $\tilde{p}_{wg} = p_{wg\_ref}$.

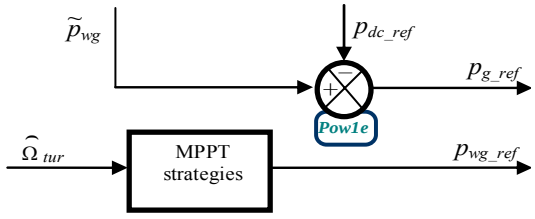

Figure II-21: Power flow balance and power sharing inside the wind energy conversion system.

All these power control and power sharing algorithms are presented with the help of the Multi-Level Representation (Appendix F) in Fig.II-20, which has been developed by Peng LI

in 2008 [Li 08]. The control system of the wind energy conversion system is then extended as shown in the block diagram (Fig.II-22).

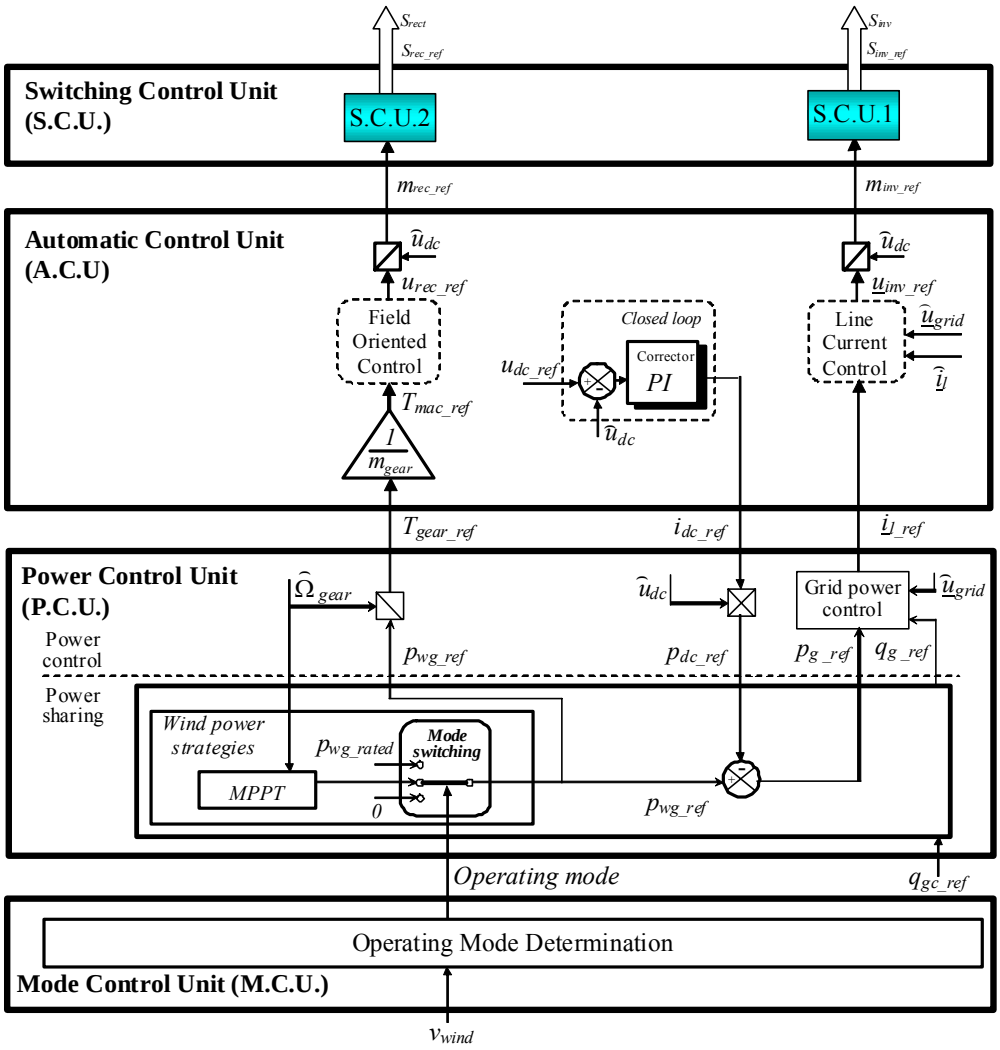

Figure II-22: Block diagram of the hierarchical control for the wind energy conversion system.

II.1.6 Mode control unit

The operating mode of the wind generator depends on the wind speed condition and the microgrid requirements (Fig.II-22). The wind generator can work normally while the microgrid capacity is large enough to receive the fluctuant wind power without much impact. If the wind speed is low or medium, the wind generator works in a MPPT strategy. Otherwise, the wind generator should be limited with the rated power value (p_{wg_rated}) with high wind speed, or even be shut down with extremely high wind speed for the security reasons.

$$p_{wg\_ref} = \begin{cases} MPPT(\Omega_{tur}) & with\ weak\ or\ medium\ wind \\ p_{wg\_rated} & with\ strong\ wind \\ 0 & with\ extremely\ strong\ wind \end{cases} . \qquad \text{(II-26)}$$

These strategies can be switched in the Power Control Unit by a signal (*Operating mode*) coming from the Mode Control Unit (Fig.II-22).

II.2 Experimental test of the grid connection control

II.2.1 Wind power emulator

Recently, wind generator emulators have been designed in the laboratory [Sau 05]. In this part, we present a simplified version because the main interest is to obtain the same power variation as from the real wind generator (Fig.II-2). In order to have a flexible and "easy-to-use" wind energy conversion system for testing control algorithms we have developed an emulator with a reduced rated power (1.2kW).

a) Hardware structure

The wind power emulator is a controllable power source, which must provide the same power profile as the wind energy generation system. So, the wind generator in Fig.II-3 is replaced experimentally by the wind power emulator as shown in the equivalent average modeling (Fig.II-23).

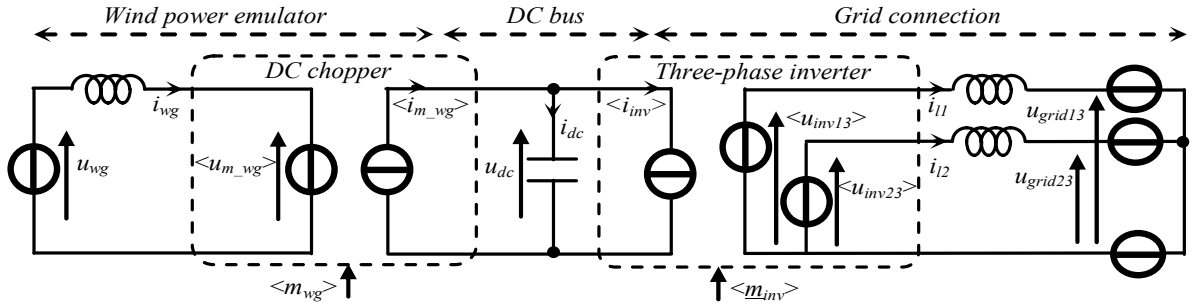

Figure II-23: Equivalent average modeling of the power conversion chain with a wind power emulator.

In this case, the average value of the modulated current from the chopper ($<i_{m\_wg}>$) in Fig.II-23 is proportional to the average value of the modulated current from the three-phase rectifier ($<i_{rec}>$) in Fig.II-3.

The power electronic stage of the wind power emulator is implemented with a step-up power conversion circuit (Fig.II-24), including a constant DC voltage source (120V), a choke filter (20mH), a DC chopper. By controlling the current (i_{wg}) of the filter inductor, the power of the emulator can be well controlled through the duty ratio (m_{wg}) as control input.

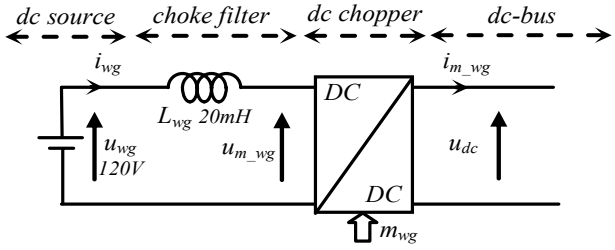

Figure II-24: Power electronic stage of the wind power emulator.

b) Software implementation

Modeling and control of the power electronic stage are presented with the help of the EMR (Fig.II-25).

The choke filter is an element with accumulation and the state variable is the current (i_{wg}):

$$L_{wg}\frac{di_{wg}}{dt}=\hat{u}_{wg}-u_{m\_wg}, \tag{II-27}$$

with L_{wg}: the inductor ;

u_{m_wg}: the modulated voltage of the chopper.

The chopper is a conversion element:

$$\begin{cases} u_{m\_wg}=m_{wg}\hat{u}_{dc} \\ i_{m\_wg}=m_{wg}\hat{i}_{wg} \end{cases}, \tag{II-28}$$

with m_{wg}: the duty ratio of the chopper

u_{dc}: the DC-bus voltage.

The EMR of the power electronic stage of the emulator shows a path between the control input (m_{wg}) and the choke current (i_{wg}) in Fig.II-25. The objective is to control this current. The control scheme of the wind power emulator is obtained by inverting this path. So a converter controller and a current controller are required.

A current controller is needed to make equal the inductor current (i_{wg}) to a reference value (i_{wg_ref}):

$$u_{m\_wg\_ref}=\hat{u}_{wg}-PI(i_{wg\_ref}-\hat{i}_{wg}). \tag{II-29}$$

A converter controller is obtained by inverting the Eq.II-28:

$$m_{wg\_ref}=\frac{1}{\hat{u}_{dc}}u_{m\_wg\_ref}. \tag{II-30}$$

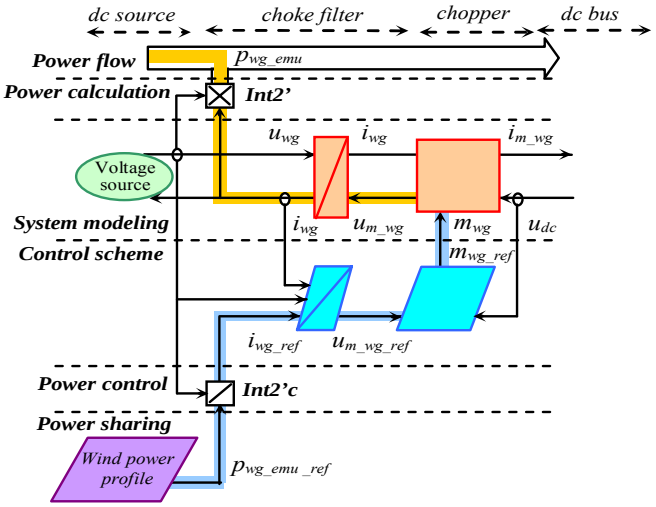

Figure II-25: Multi-Level Representation of the wind power emulator.

Modeling and control of the emulated wind power are presented with the help of the MLR. The generated power can be described as below (Fig.II-25),

$$\textbf{\textit{Int2'}}:\ p_{wg\_emu}=u_{wg}i_{wg}. \tag{II-31}$$

Then, this power reference ($p_{wg\_emu\_ref}$) for the emulator leads to a current reference (i_{wg_ref}) for the control system.

$$\textbf{\textit{Int2'c}}:\ i_{wg\_ref}=\frac{1}{\hat{u}_{wg}}p_{wg\_ref}. \tag{II-32}$$

In normal operation, the DC-bus voltage is regulated to a prescribed constant value and then from Eq.II-24 (***Pow1***), we obtain

$$p_g=p_{wg}. \tag{II-33}$$

So the objective is to make the produced power from the emulator equal to a previously recorded wind power profile (Fig.II-2),

$$p_{wg\_ref} = p_{g\_record}. \tag{II-34}$$

The "wind power profile", which is implemented in the digital control board (DSpace1103) set this power reference ($p_{wg\_emu\_ref}$) according to the recorded wind speed profile (Fig.II-2). The experimental test bench is built with a 1.2kW rated power, thus the coefficient (k_{wg}) is adapted to have a wind power profile ($p_{wg\_emu\_ref}=k_{wg}p_{wg\_ref}$) below 1.2kW.

II.2.2 Experimental implementation

The grid connection system is experimentally implemented with a wind power emulator through a DC-bus capacitor (2300uF), a three-phase inverter, three line filters (10mH) and a three-phase grid transformer.

The implementation of the wind energy conversion experimental test bench is shown in Fig.II-26. Its modeling and control is obtained by replacing the wind energy generation system by the wind power emulator. The Multi-Level Representation of the entire experimental test bench is shown in Fig.II-27 with previously presented equations. The proposed hierarchical control system (Fig.II-21) is experimentally applied and tested with the real DC bus and grid connection system by taking into account the fluctuant wind power.

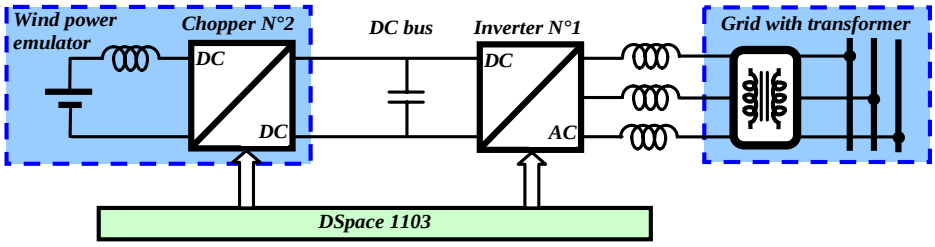

(a) Block diagram

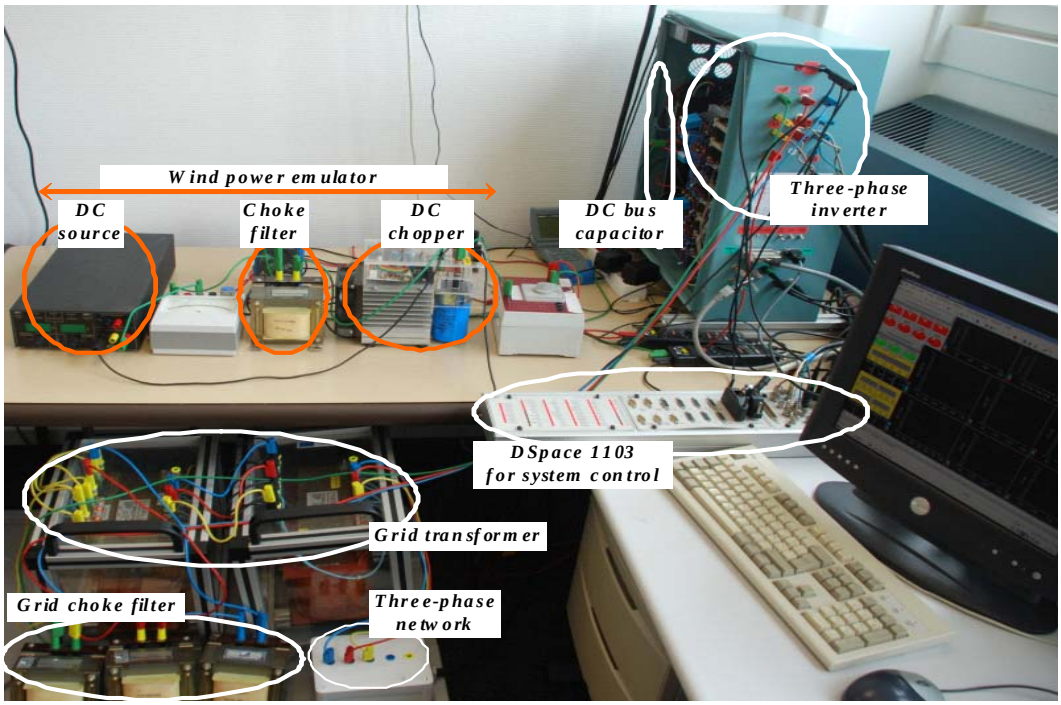

(b) Photo

Figure II-26: Implementation of the wind energy conversion experimental test bench.

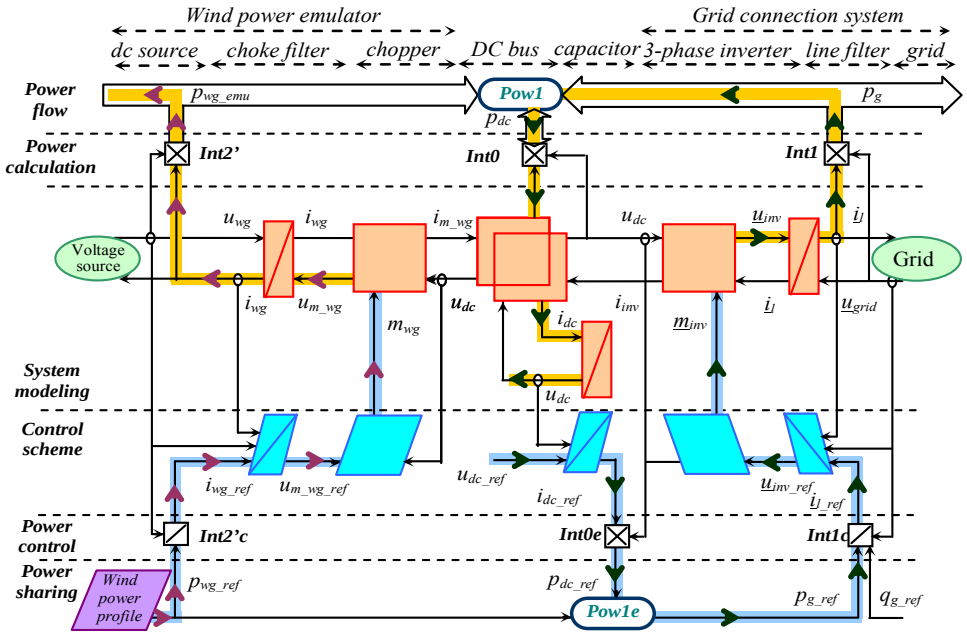

Figure II-27: Multi-Level Representation of the wind energy conversion experimental test bench.

II.2.3 Simulation and experimental results

In order to validate our mathematical modeling and control design, we have firstly simulated this academic study under the software Matlab/Simulink™. We can see that the obtained simulated active power (p_g) in Fig.II-28a is very close to the recorded grid active power (Fig.II-2).

Hence, this mathematical model gives us the same power dynamics as from a real wind generator. Moreover, we have now some knowledge about the internal physical quantities and also about the different control functions.

The grid connection test of the wind energy conversion system is performed with the same wind power profile during 150 seconds. The experimental results are compared with the previous simulation results.

We can see that the similar power profile (Fig.II-28b) can be generated as the recorded wind power profile (Fig.II-2). The DC-bus voltage is well regulated (around 400V) by the line current control loop in a "grid following" power balancing strategy. The emulated fluctuant wind power is totally delivered to the grid through the three-phase inverter.

This experimental test bench enables us to have similar power dynamics and characteristics as a real wind generator. We will use it to validate our proposed improvement in order to design a wind based active generator.

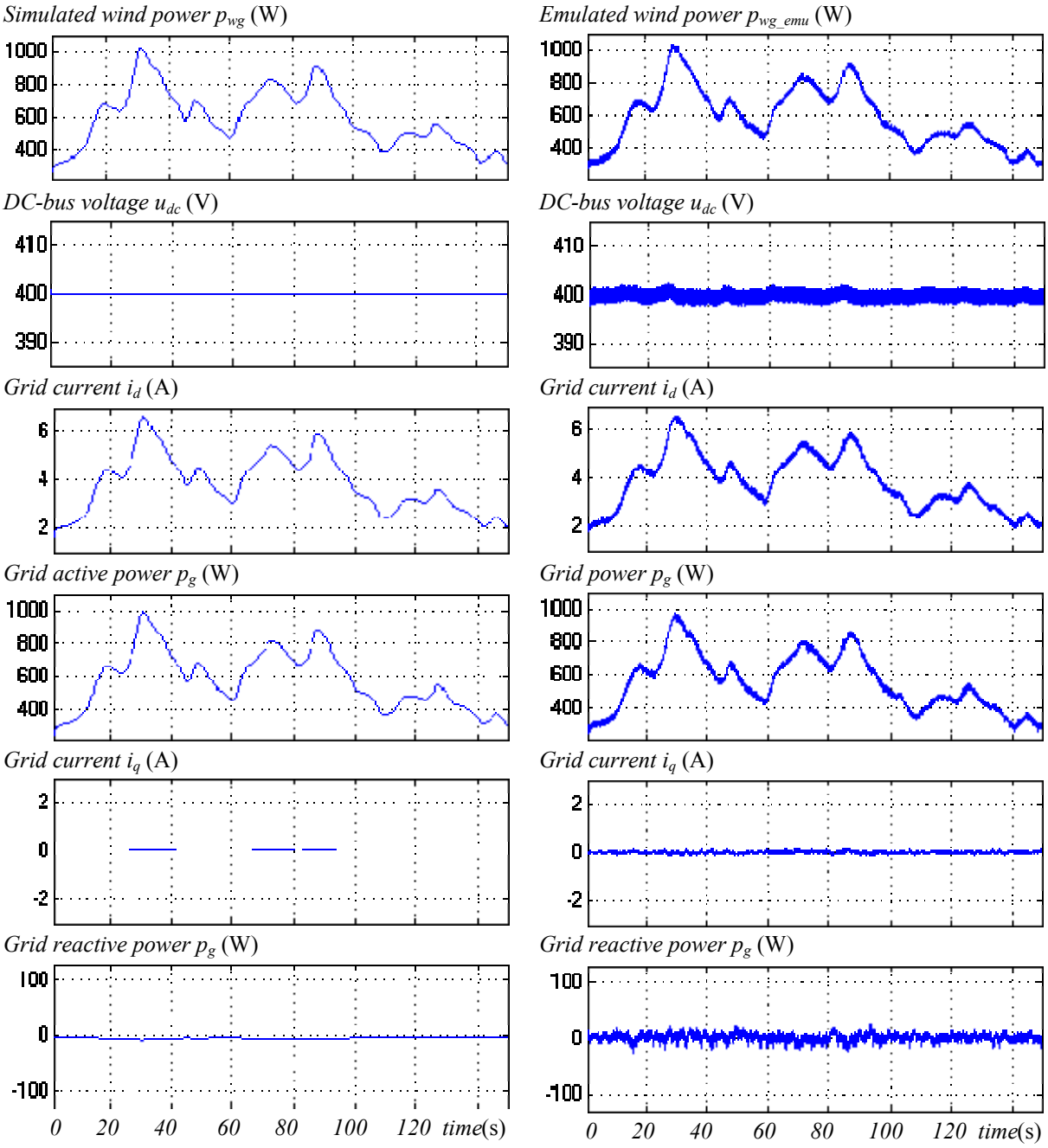

(a) Simulation results (b) Experimental results

Figure II-28: Test results of the wind energy conversion experimental test bench

II.2.6 Discussion

The fluctuant power from the wind generator depends entirely on the wind condition, but not on the microgrid's requirements. Therefore, the wind energy conversion system working in MPPT strategy behaves like a passive generator. It can not supply smooth powers to the microgrid and can not supply any ancillary services for the power system. It can only generate continuously varying powers depending on meteorological conditions. Moreover, it becomes a considerable disturbance input for the grid power quality if many wind generators are used.

Energy storage systems can help to solve the fluctuation problem of the wind power and can ensure a good energy availability. However, additional control functions should be added

to coordinate the different sources. In the following sections, a super-capacitor assisted wind energy conversion system is studied in detail.

II.3 Study of a wind/super-capacitor hybrid power generator

II.3.1 Presentation

As explained in Chap.I, a hybrid power system combining renewable energy generators and energy storage devices is a possible solution for clean energy generation and high power quality supply for the future electrical network. In this chapter, we study a hybrid power system, which consists of a wind energy conversion system and a super-capacitor based energy storage system. The purpose is to filter wind power fluctuations in order to satisfy a grid power reference from a microgrid system operator. A DC-coupled structure is considered (Fig.II-29) and the super-capacitor system is connected to the DC bus through a DC/DC power converter (N°3). This power electronic converter is used to have a control input for the load of super-capacitors.

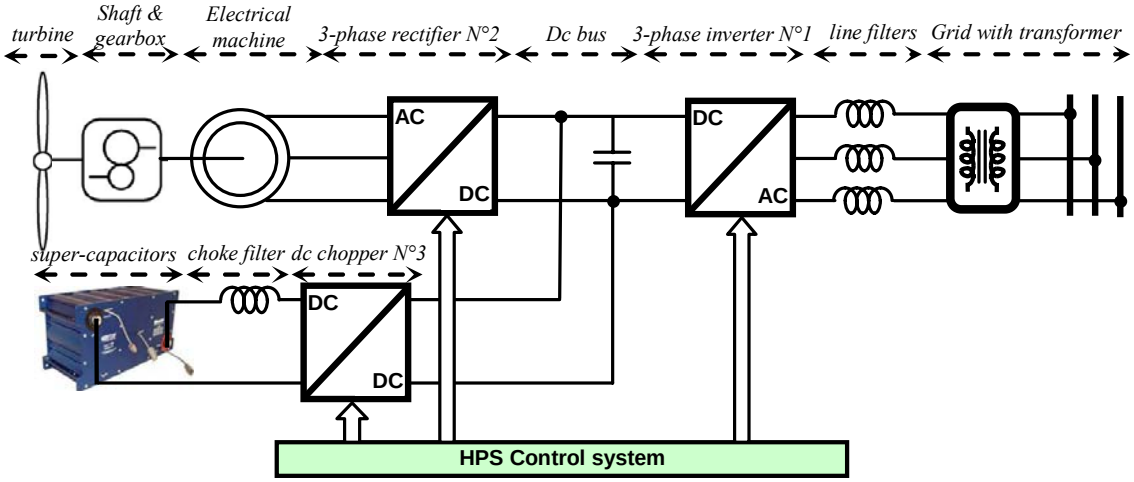

Figure II-29: A wind/super-capacitor hybrid generator.

II.3.2 Modeling of the super-capacitor storage system

A super-capacitor tank is used to enable fast-dynamic energy storage for high power dynamic requirement. A choke filter and a chopper are associated to adapt the voltage levels between the super-capacitor tank and the DC bus (Fig.II-30). As shown in the equivalent average electrical model (Fig.II-31), the chopper introduces a control input, which is the duty ratio of the chopper (m_{sc}). We will use it for the power control. The modeling of the super-capacitor storage system is presented in details with the help of the EMR (Fig.II-32).

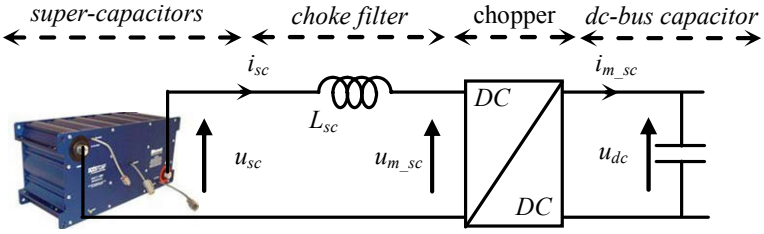

Figure II-30: Super-capacitor power conversion system

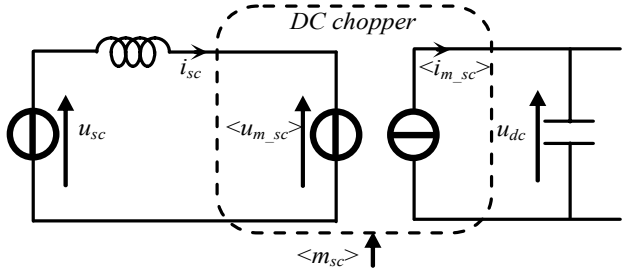

Figure II-31: Equivalent average electrical modeling of the super-capacitor power conversion system

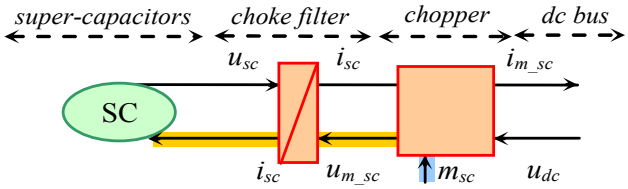

Figure II-32: EMR of the super-capacitor power conversion system modeling

Super-capacitors: For the majority of energy storage applications, the model of Zubieta and Bonert [Zub 00] can be used (Fig.II-33). This model takes into account a non-linear equivalent capacitor (C_o and C_u), a leakage resistor (R_l), a series resistor (R_s) and the relaxation phenomenon (R_1, C_1; R_2, C_2; …; R_n, C_n). Nevertheless, the load and discharge frequencies of R_1, C_1; R_2, C_2; …; R_n, C_n are weak enough in this application to neglect relaxation phenomenon. The leakage resistor R_l is also neglected due to its high value, as well as the series resistor R_s due to its small value. Finally, a series connection of super-capacitors can then be represented in the same way as an ideal capacitor [Lho 05b]. The super-capacitor tank is modeled as a voltage source (terminal element), which has the choke current i_{sc} as input and it's voltage u_{sc} as output:

$$C_{sc}\frac{du_{sc}}{dt} = -i_{sc}, \tag{II-35}$$

with C_{sc}: the equivalent capacitor of the super-capacitor tank;
u_{sc}: the voltage across the super-capacitor tank;
i_{sc}: the current applied to the super-capacitor tank.

Choke filter: The choke is an element with energy accumulation and the state variable is the current (i_{sc}):

$$L_{sc}\frac{di_{sc}}{dt} = u_{sc} - u_{m\_sc}, \tag{II-36}$$

with L_{sc}: the equivalent inductor ;
u_{m_sc}: the modulated voltage of the chopper.

Chopper: The chopper is a conversion element and the average model can be described as below:

$$\begin{cases} < u_{m\_sc} > = < m_{sc} > u_{dc} \\ < i_{m\_sc} > = < m_{sc} > i_{sc} \end{cases}, \tag{II-37}$$

with m_{sc}: the duty ratio of the dc chopper;
u_{dc}: the DC-bus voltage.

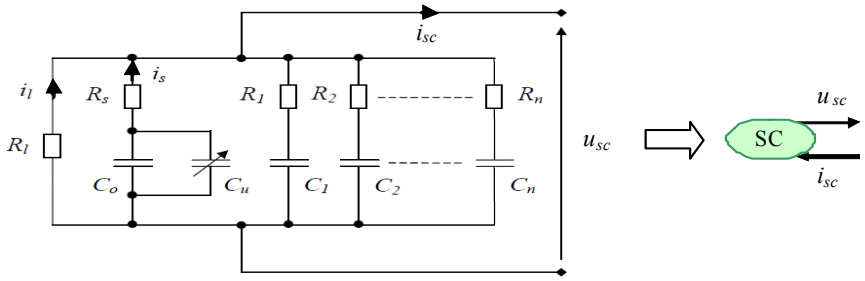

Figure II-33: Electrical model of super-capacitors

II.3.3 Modeling of the hybrid power system

a) Average modeling of the electrical conversion chains

An average modeling is sufficient for studying the power balancing and energy management strategies of the hybrid power system. Moreover, it can reduce significantly the simulation time for pre-validation. In this case, the modulated values are replaced by their average values during the modulation period. It is shown in Fig.II-34. The electrical diagram with equivalent average modeling of power electronic converters makes appear four parts corresponding to the wind generator, the grid connection, the super-capacitors and the DC bus.

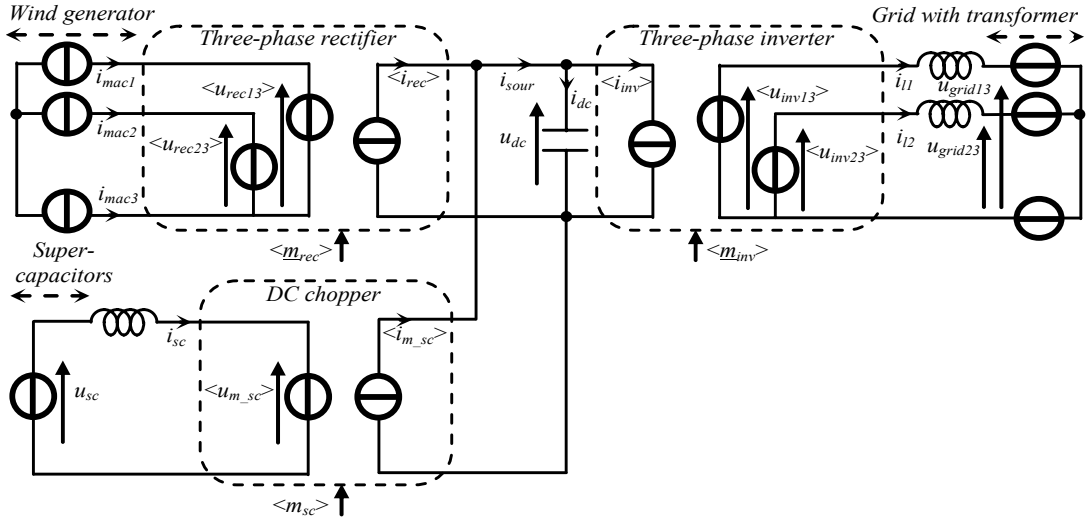

Figure II-34: Equivalent electrical diagram of the wind/super-capacitors hybrid power system

b) Modeling of the DC bus

In order to control the power flow among the three sources (the wind generator, the super-capacitors and the grid connection), the DC coupling should be modeled in detail (Fig.II-35):

$$i_{sour} = i_{rec} + i_{m\_sc} \quad \text{(II-38)}$$

$$i_{dc} = i_{sour} - i_{inv} \quad \text{(II-39)}$$

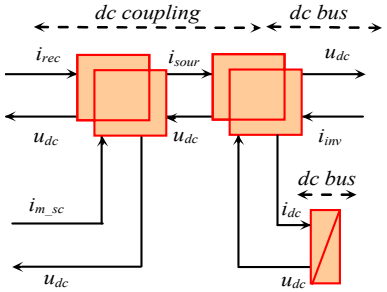

Figure II-35: EMR of the DC bus in the wind/super-capacitors hybrid power system.

And the DC-bus voltage is obtained as follows:

$$C_{dc}\frac{du_{dc}}{dt} = i_{dc}\,. \tag{II-40}$$

c) Energetic Macroscopic Representation

The EMR of the super-capacitor assisted wind energy conversion system is obtained (Fig.II-36) by combining the EMRs of the wind energy conversion system modeling (Fig.II-8), the super-capacitor power conversion system (Fig.II-32) and the DC bus modeling (Fig.II-35).

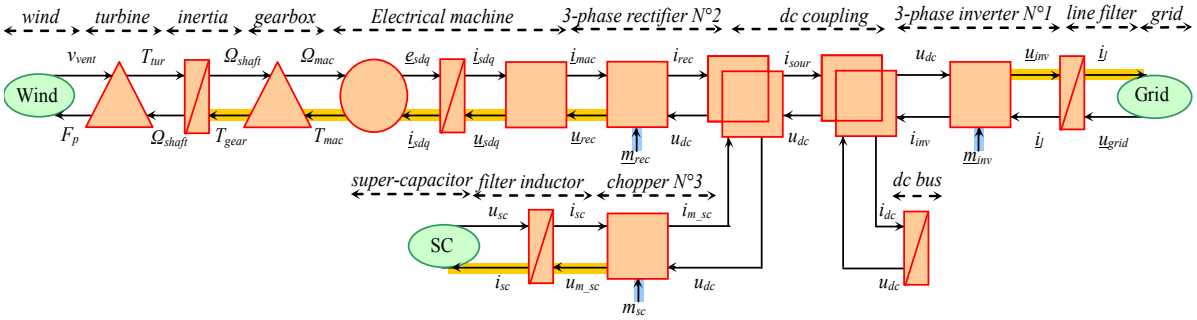

Figure II-36: EMR of the wind/super-capacitors hybrid power system.

II.3.4 Hierarchical control of the hybrid power system

a) Hierarchical control structure

We have used a hierarchical structure of the control system in order to organize the control functions (Appendix C).

In a DC-coupled hybrid power system, all energy sources are connected to the DC bus through different power converters [Zho 08]. In the super-capacitors assisted wind energy conversion system, three energy sources are considered: the wind generator (WG), the super-capacitors (SC) and the grid connection (GC). Three power converters are used to regulate the power exchanges among them (Fig.II-34). So in the control system, three SCUs and three ACUs are used to control the three energy sources, a common PCU and a common MCU are used for the power balancing and energy management of the entire system (Fig.II-37).

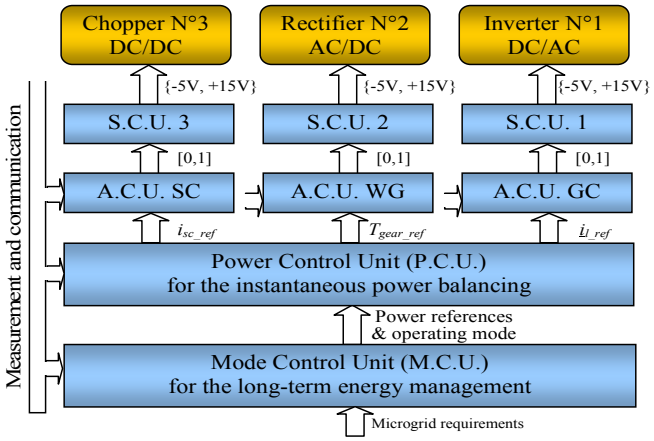

Figure II-37: Hierarchical control structure of the wind/super-capacitors hybrid power system

In the SCU of each converter, the IGBT drivers and PWM techniques are used to control the switching circuits. These units are not the main concerns of the study, so they will not be

detailed here. However, the control algorithms in the ACU should be presented in order to highlight the physical quantities, which can be used for the power flow control among the different energy sources. The control scheme in the ACU and the power balancing algorithms will be presented in the following sections.

b) Automatic control unit

For the wind generator, the DC bus and the grid connection, the control tasks are the same as previously exposed (Paragraph II.1.4). Then we retrieve the same control schemes (Fig.II-38). For the super-capacitors, the EMR (Fig.II-32) shows a path between the duty ratio m_{sc} and the choke current i_{sc}. The objective is to control this current. The control scheme of the super-capacitor power conversion system is obtained by inverting this path. So a converter control and a current control are required. (Fig.II-38).

Current control: As the super-capacitor bank is a voltage source, a current controller is needed to set its current:

$$u_{m\_sc\_ref} = u_{sc} - PI(i_{sc\_ref} - \hat{i}_{sc}) . \qquad \text{(II-41)}$$

Converter control: Then the duty radio of the dc chopper is obtained by inverting the Eq.II-37:

$$m_{sc\_ref} = \frac{1}{\hat{u}_{dc}} u_{m\_sc\_ref} . \qquad \text{(II-42)}$$

As result, four groups of physical variables (i_{dc_ref}, i_{l_ref}, T_{gear_ref}, i_{sc_ref}) appear to interface the automatic control units with the power control unit (Fig.II-39).

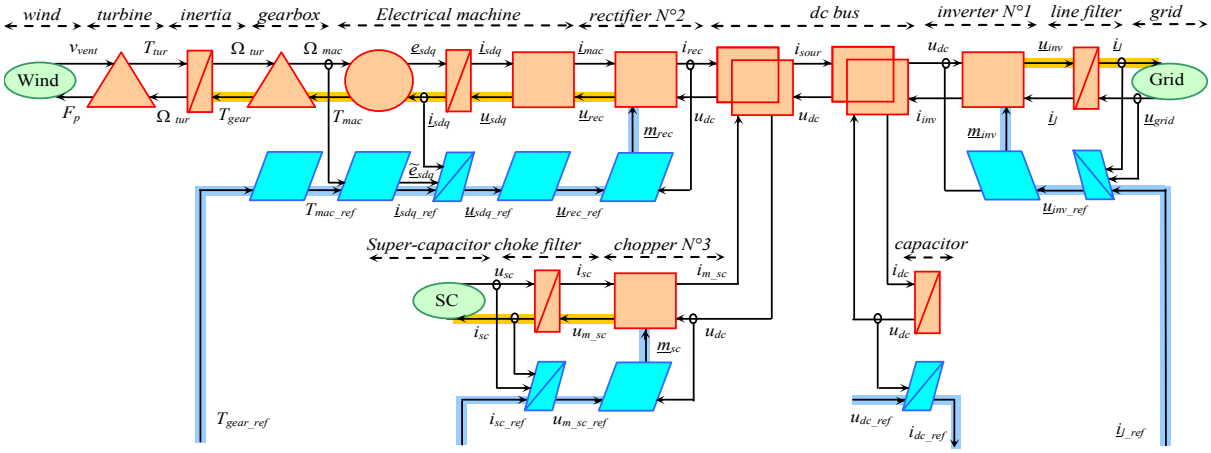

Figure II-38: Control scheme of the entire wind/super-capacitors hybrid power system.

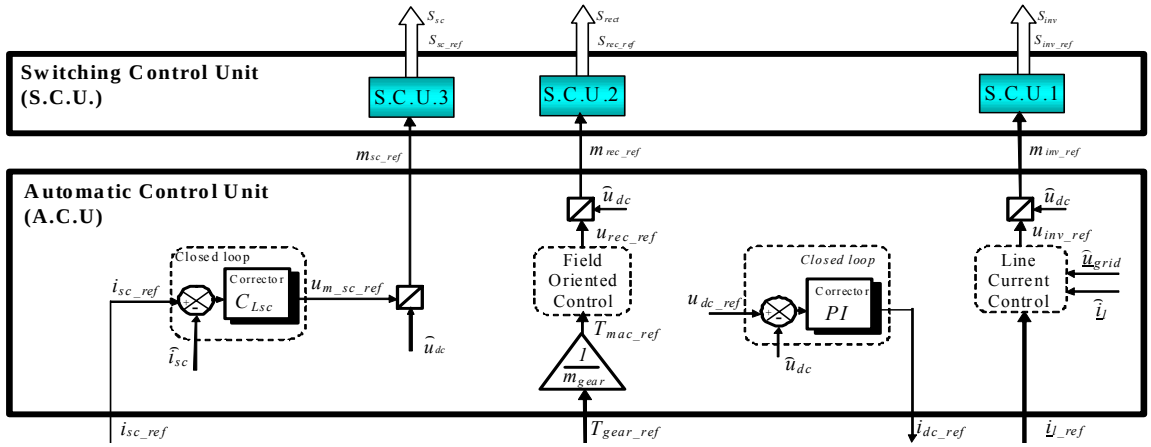

Figure II-39: Block diagram of the automatic control unit for the wind/super-capacitors hybrid power system.

c) Power control unit

The power control unit is divided in two levels: the Power Control Level (PCL) and the Power Sharing Level (PSL).

The Power Control Level (PCL) is obtained by inverting the equations calculating the different powers (Table II-2). For the super-capacitor storage system, the power (p_{sc}) is calculated by multiplying the current (i_{sc}) and the voltage (u_{sc}). The super-capacitor current reference (i_{sc_ref}) is calculated by dividing the wished super-capacitor power reference (p_{sc_ref}) with the measured voltage (u_{sc}). For the other powers, the same equations are used (as in Table II-1). As explained before (in Paragraph.II.1.5), the instantaneously exchanged reactive power with the inductors, the filter losses and the power converter losses are neglected.

The organization of the power control unit can then be presented with the help of the Multi-Level Representation (Fig.II-40). And the control system of the hybrid power system is then extended as shown in Fig.II-41.

Table II-2: Power calculation and control algorithms for the wind/super-capacitors hybrid power system.

Energy source	Power calculation	Power control
DC-bus capacitor	**Int0:** $p_{dc} = u_{dc} i_{dc}$	**Int0e:** $p_{dc\_ref} = \hat{u}_{dc} i_{dc\_ref}$
Grid connection	**Int1:** $\begin{cases} p_g = u_{13} i_1 + u_{23} i_2 \\ q_g = \sqrt{3}(u_{13} i_1 - u_{23} i_2) \end{cases}$	**Int1c:** $\begin{cases} i_{l1\_ref} = \dfrac{(2\hat{u}_{13} - \hat{u}_{23}) p_{g\_ref} + \sqrt{3}\hat{u}_{23} q_{g\_ref}}{2\hat{u}_{13}^2 - 2\hat{u}_{13}\hat{u}_{23} + 2\hat{u}_{23}^2} \\ i_{l2\_ref} = \dfrac{(2\hat{u}_{23} - \hat{u}_{13}) p_{g\_ref} - \sqrt{3}\hat{u}_{13} q_{g\_ref}}{2\hat{u}_{13}^2 - 2\hat{u}_{13}\hat{u}_{23} + 2\hat{u}_{23}^2} \end{cases}$
Wind generator	**Int2:** $p_{wg} = \Omega_{gear} T_{gear}$	**Int2c:** $T_{gear\_ref} = \dfrac{1}{\hat{\Omega}_{tur}} p_{wg\_ref}$
Super-capacitors	**Int3:** $p_{sc} = u_{sc} i_{sc}$	**Int3c:** $i_{sc\_ref} = \dfrac{1}{\hat{u}_{sc}} p_{sc\_ref}$

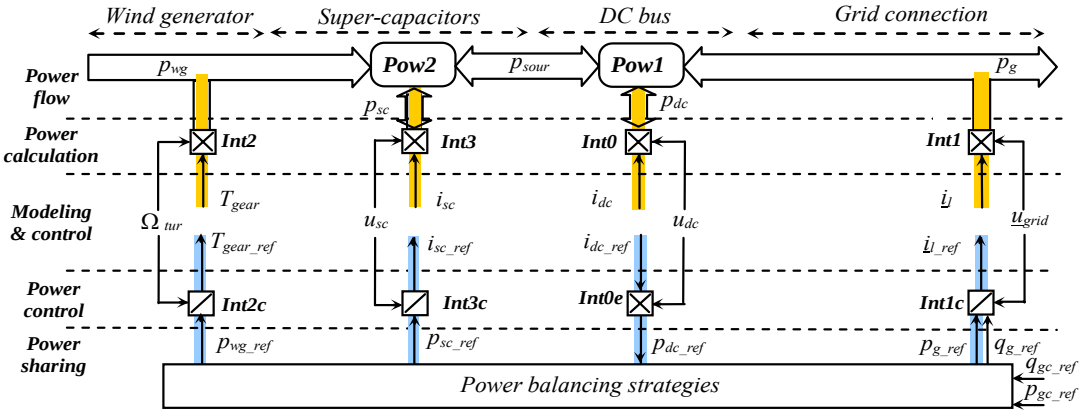

Figure II-40: Multi-Level Representation of the power modeling and control for the hybrid power system

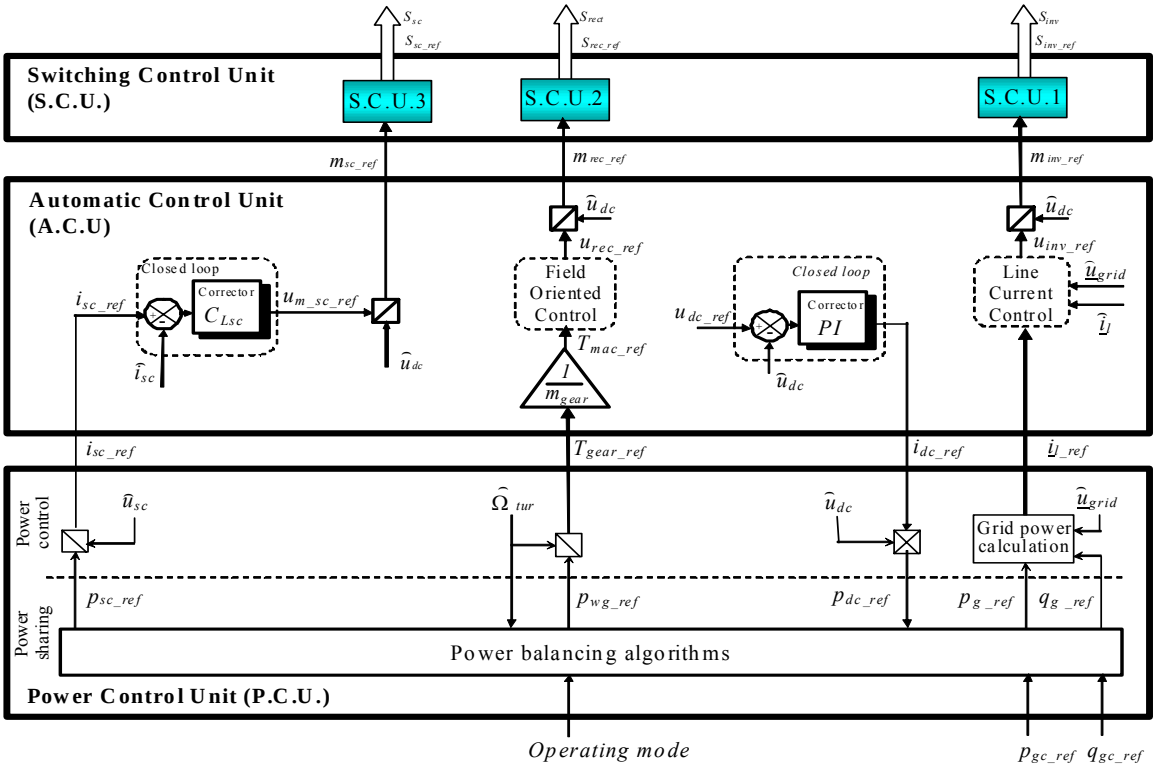

Figure II-41: Block diagram of the hierarchical control for the wind/super-capacitors hybrid power system.

The Power Sharing Level is used to implement power balancing strategies in order to coordinate the different sources in the hybrid power system. They are developed by using the power flow modeling equations. So before presenting the power balancing strategies in the next paragraph, we explain here the modeling of the power flow inside the wind/super-capacitor hybrid power system (Fig.II-42):

$$\textbf{Pow1:}\quad p_g = p_{sour} - p_{dc}\,, \tag{II-43}$$

$$\textbf{Pow2:}\quad p_{sour} = p_{wg} + p_{sc}\,, \tag{II-44}$$

with p_{dc}: the exchanged power with the DC-bus capacitor;
p_g: the power, which is delivered to the grid from the DC bus;
p_{sour}: the total power, which arrives to the DC bus from the sources.
p_{wg}: the power, which is injected into the DC bus from the wind generator;
p_{sc}: the power, which is injected into the DC bus from the super-capacitors.

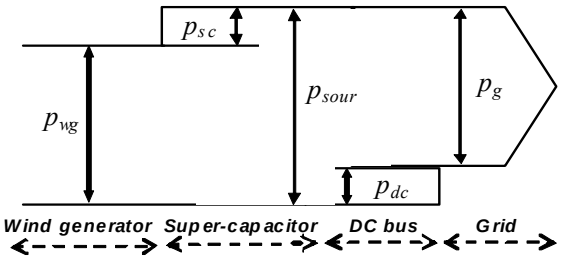

Figure II-42: Power flow balance inside the wind/super-capacitors hybrid power system.

II.3.5 Power balancing strategies of the wind/super-capacitors hybrid power system

a) Role of the power balancing

The power balancing plays a very important role in the control system of the hybrid power system. It leads directly to the stability of the hybrid power system. In the studied wind

energy conversion system, all power exchanges are performed via the DC-bus (Fig.II-43) and have an impact on the DC-bus voltage:

$$\frac{dE_{dc}}{dt} = C_{dc}u_{dc}\frac{du_{dc}}{dt} = u_{dc}i_{dc} = p_{dc} = p_{sour} - p_g = p_{wg} + p_{sc} - p_{gc}\,. \qquad \text{(II-45)}$$

with E_{dc}: the stored energy in the DC-bus capacitor;
p_{dc}: the exchanged power with the DC-bus capacitor;
p_{wg}: the power, which is injected into the DC bus from the wind generator;
p_{sc}: the power, which is injected into the DC bus from the wind generator;
p_g: the power, which is delivered to the grid from the DC bus.

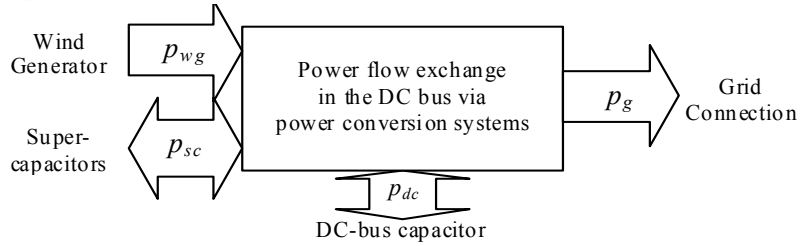

Figure II-43: Power flow exchanges around the DC bus in the wind/super-capacitors hybrid power system

The super-capacitors introduce a possibility to perform the regulation of the DC-bus voltage. The various power balancing strategies can be implemented in the Power Control Unit (PCU). In the super-capacitor assisted wind energy conversion system, the three power electronic converters can regulate the power transfer with each source. The three-phase rectifier is used to control the wind generator with a MPPT strategy. The three-phase inverter in the grid connection system and the DC chopper in the super-capacitor power conversion system can be used for the DC-bus voltage regulation and the grid power control. According to the function of the line current loop's function, two power balancing strategies can be implemented [Zho 09a]:

- ***The grid following strategy*** uses the line current loop to regulate the DC-bus voltage;
- ***The power dispatching strategy*** uses the line current loop to control the grid active power.

b) Grid following strategy

For this hybrid power system, the grid following strategy is an extension of the previous one (paragraph II.1.5) by taking into account the super-capacitor power (p_{sc}). As shown in the Multi-Level Representation (Fig.II-44), the required power for the DC-bus voltage regulation (p_{dc_ref}) is used to estimate the grid power reference (p_{g_ref}) from the equation (***Pow1***),

$$\textbf{Pow1e:}\ \ p_{g\_ref} = \widetilde{p}_{sour} - p_{dc\_ref}\,. \qquad \text{(II-46)}$$

And the sources' total power (p_{sour}) is considered as a disturbance and is estimated as below,

$$\textbf{Pow2e:}\ \ \widetilde{p}_{sour} = \widetilde{p}_{wg} + \widehat{p}_{sc}\,. \qquad \text{(II-47)}$$

While the DC-bus voltage is regulated, the exchanged power with the DC-bus capacitor (p_{dc}) is zero in average value in the equation (***Pow1***). With the presence of the super-capacitor based fast-dynamic energy storage system, the microgrid system operator can set power requirements (p_{gc_ref} and q_{gc_ref}) for the grid power (p_g). Hence we obtain

$$\textbf{Pow1c:}\ \ p_{sour\_ref} = p_{gc\_ref}\,. \qquad \text{(II-48)}$$

In order to help the wind energy conversion system to respect the active power requirement, the super-capacitor power conversion system is then controlled to supply or

absorb the difference between this power requirement p_{gc_ref} and the fluctuant wind power p_{wg} by inverting the equation (***Pow2***) in Fig.II-44:

$$\textbf{Pow2c:}\ p_{sc\_ref} = p_{sour\_ref} - \widetilde{p}_{wg}\,. \tag{II-49}$$

The block diagram of the grid following strategy for the wind/super-capacitor hybrid power system is presented in Fig.II-45.

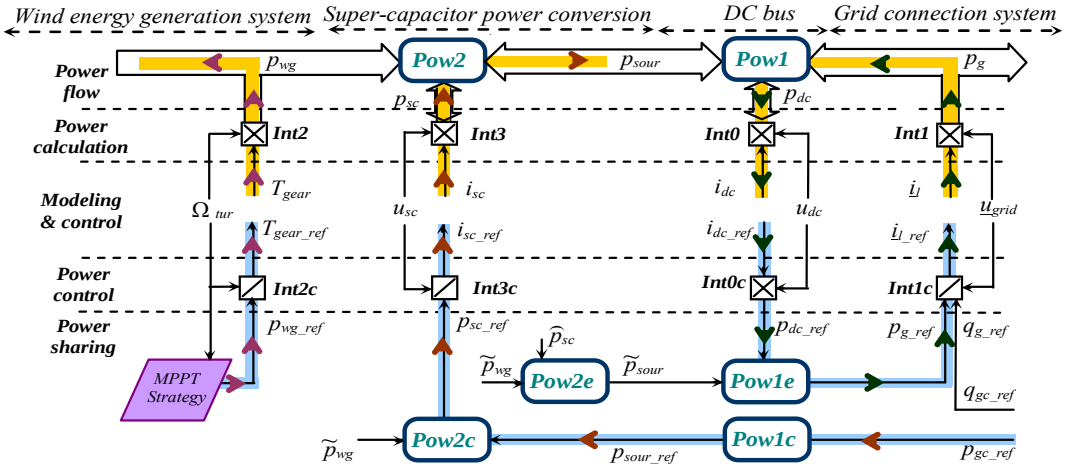

Figure II-44: Multi-Level Representation of the grid following strategy for the hybrid power system.

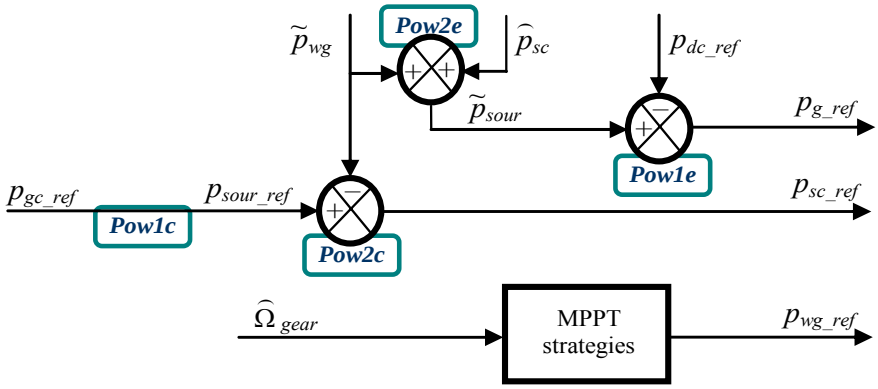

Figure II-45: Block diagram of the grid following strategy for the hybrid power system.

c) Power dispatching strategy

If the stored energy is enough, the super-capacitors can also be used to regulate the DC-bus voltage while the wind generator works in a MPPT strategy (Fig.II-46). This second strategy relies on a second power-based closed loop (p_{dc_ref} → p_{sour_ref} → p_{sc_ref} → p_{sc} → p_{sour} → p_{dc}). In this case, the necessary power from the sources (p_{sour_ref}) must be first calculated by taking into account the required power for the DC-bus voltage regulation (p_{dc_ref}) and the measured grid power (p_g) by inverting the equation (***Pow1***) in the Multi-Level Representation (Fig.II-46),

$$\textbf{Pow1c:}\ p_{sour\_ref} = p_{dc\_ref} + \widehat{p}_{g}\,, \tag{II-50}$$

Then the super-capacitor power reference (p_{sc_ref}) is deduced by taking into account the estimated fluctuant wind power (p_{wg}) in Fig.II-46,

$$\textbf{Pow2c:}\ p_{sc\_ref} = p_{sour\_ref} + \widetilde{p}_{wg}\,, \tag{II-51}$$

It is used to supply fast varying power (p_{dc}) to regulate the DC-bus voltage against the fluctuant wind power (p_{wg}).

While the DC-bus voltage (u_{dc}) is regulated, the exchanged power with the DC-bus capacitor (p_{dc}) is zero in average value. The microgrid system operator can directly set power requirements (p_{gc_ref} and q_{gc_ref}) for the grid connection system (Fig.II-46),

$$p_{g\_ref} = p_{gc\_ref} . \quad \text{(II-52)}$$

Therefore, the hybrid power system can directly supply the required powers for providing the ancillary services to the microgrid, like the regulations of the RMS grid voltage and frequency.

Moreover, if the grid power is well controlled (p_g=p_{g_ref}=p_{gc_ref}), we can modify the equation (***Pow1c***) as: p_{sour_ref}=p_{dc_ref}+p_{gc_ref}.

The block diagram of the power dispatching strategy for the wind/super-capacitor hybrid power system is presented in Fig.II-47.

As the grid power is not used to regulate the DC-bus voltage, the grid power requirements can be better satisfied. So the power dispatching strategy is preferred if the microgrid is fed by this hybrid power generator alone.

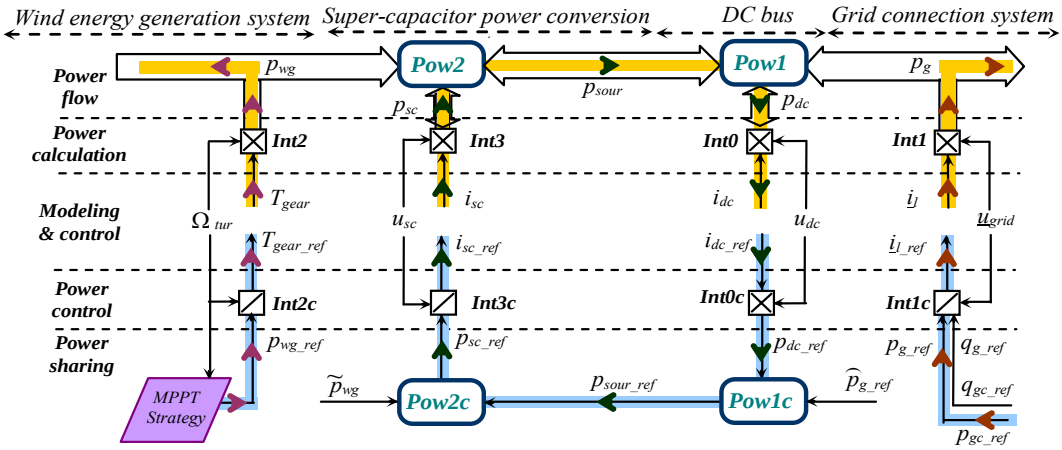

Figure II-46: Multi-Level Representation of the power dispatching strategy for the hybrid power system.

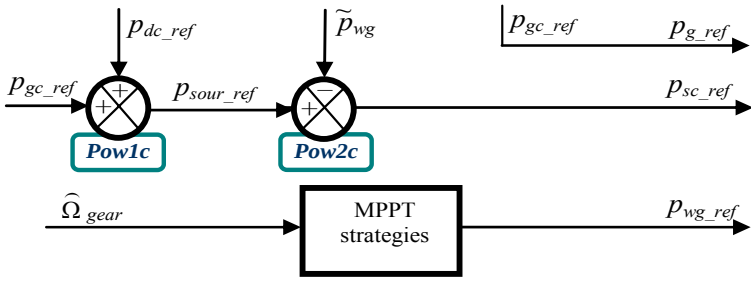

Figure II-47: Block diagram of the power dispatching strategy for the hybrid power system

II.4 Experimental test of the wind/super-capacitor hybrid power generator

II.4.1 Experimental implementation

The super-capacitor based energy storage system is added in the previously presented experimental test bench of the wind energy conversion system. Three "BOOSTCAP" super-capacitor modules (160F and 48V) are connected in series. Therefore, the equivalent capacitor of the super-capacitor bank is about 53F and the maximal voltage (u_{sc}) is about 144V. The super-capacitors are connected to the DC-bus capacitor through a step-up power conversion

system, including a choke filter (20mH) and a DC chopper (Fig.II-48). The two power balancing strategies are respectively tested and compared on this test bench.

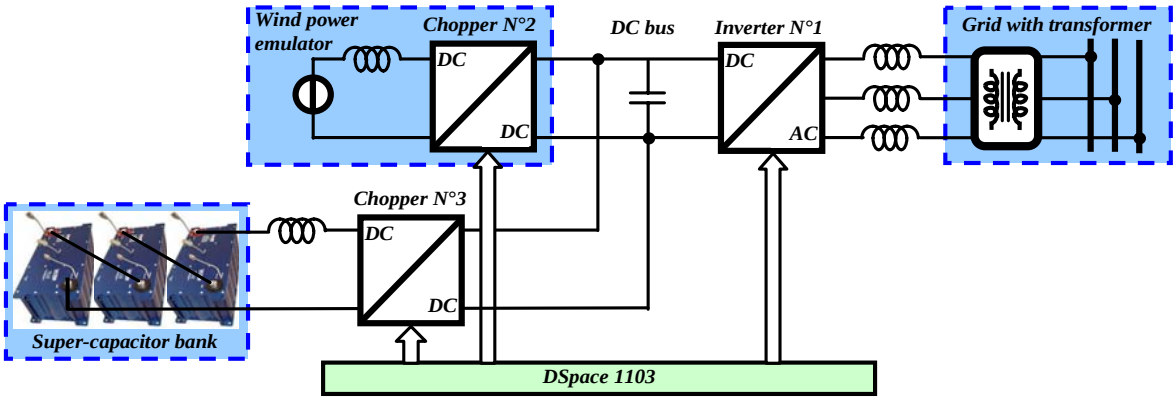

(a) Block diagram

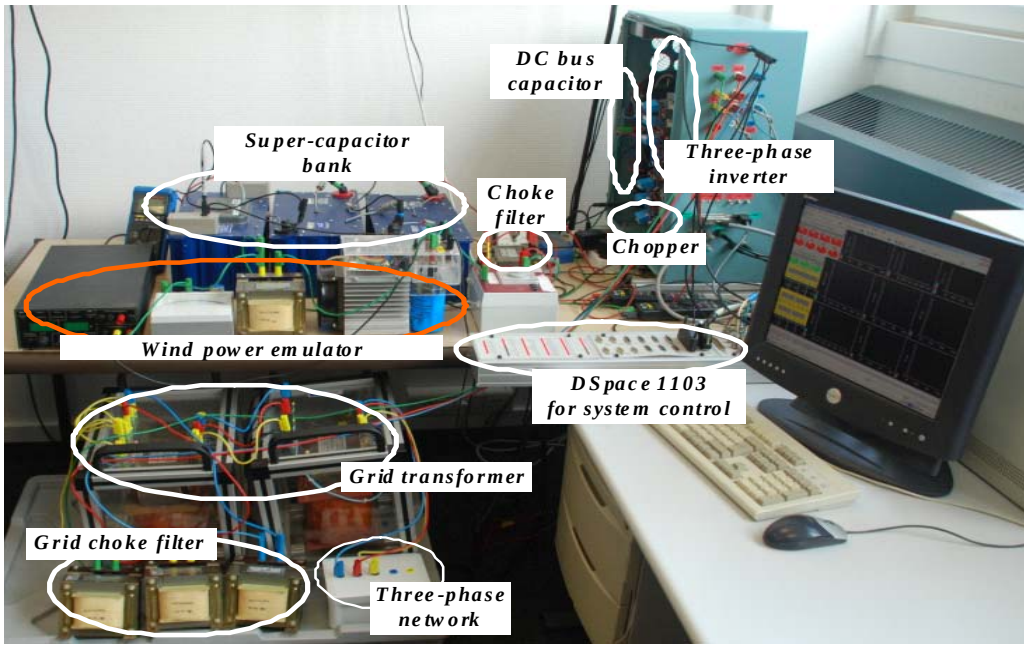

(b) Photo

Figure II-48: Implementation of the experimental test bench for the hybrid power system.

II.4.2 Test of the grid following strategy

a) Test with grid power steps from the microgrid system operator

The dynamic performance of the "grid following" strategy is tested with grid power requirement through simulation and experimental tests (Fig.II-49).

In first, the wind power is set to zero in order to highlight the performances of the super-capacitor power conversion system and the grid connection system with respect to the grid power steps. Two steps of the grid active power (p_{gc_ref}) are given from 0W to 1000W then from 0W to –1000W. Two steps of the grid reactive power (q_{gc_ref}) are given from 0VAR to 500VAR then from 0VAR to –500VAR. (Obviously, this operation is not possible with a classical power generator)

We can see that the DC-bus voltage is well regulated around 400V by the grid connection system. The reactive power requirement is well achieved dynamically. However, a small

steady-state difference appears in the grid active power between the simulation results and experimental results, because the power losses in the filters and in the power converters are not considered in the simulation. In the grid following strategy, the grid power requirement is directly sent to the primary sources and the storage systems (p_{sour_ref}=p_{gc_ref}). As the wind power is zero, the super-capacitor power is controlled to supply the same power as the grid power requirement (p_{sc_ref}=p_{gc_ref}).

In practice, the exchanged power with the grid is slightly less than the requirement (p_g<p_{gc_ref}) because of the power losses in the filters and in the power converters. The super-capacitor voltage varies differently in the experimental test in comparison with the simulation results. It drops or rises about 1V instantaneously in the experimental results during the transient because of the equivalent series resistance, which is not taken into account in the simulation.

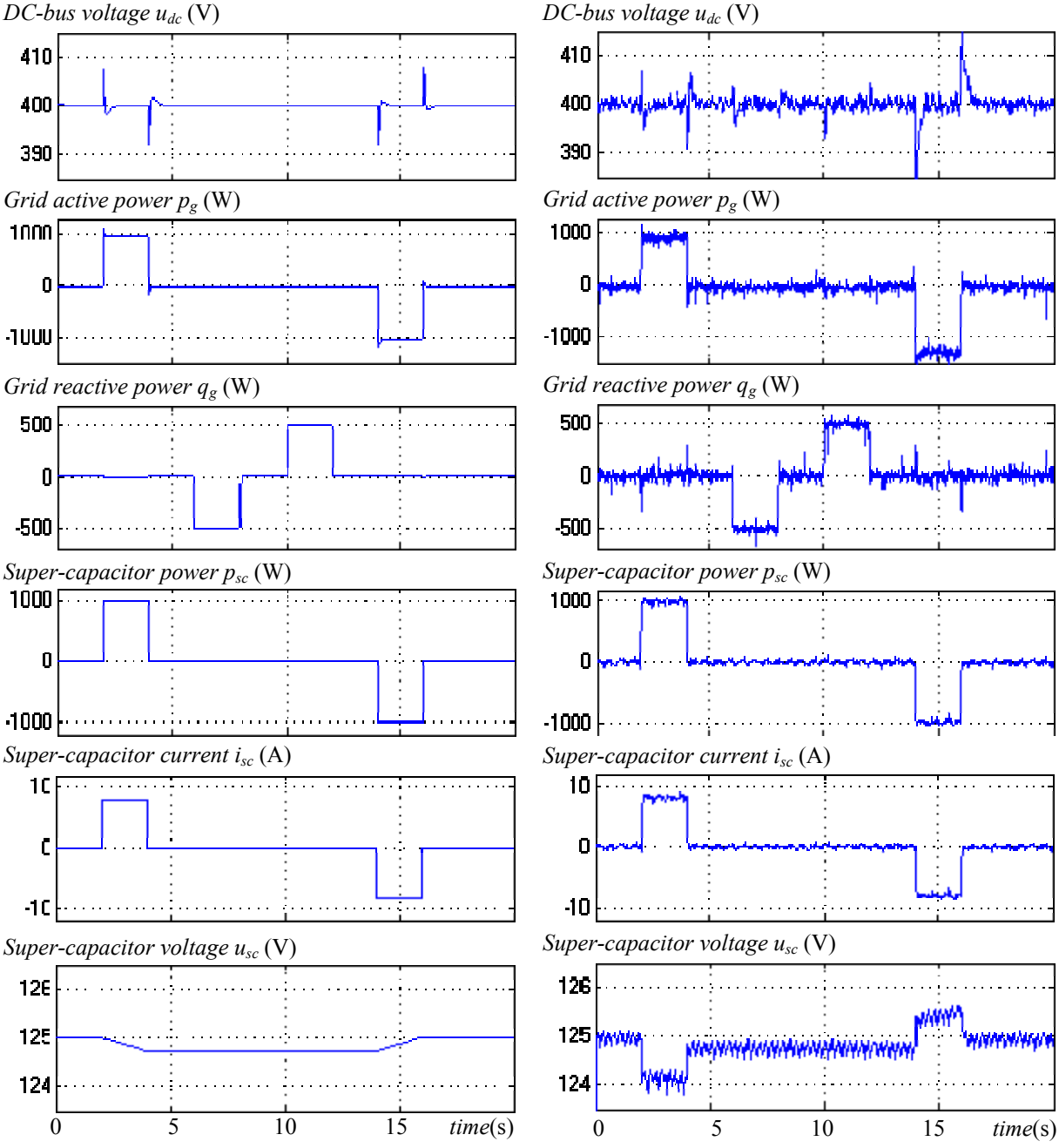

(a) simulation results (b) experimental results

Figure II-49: Dynamic test of the wind/super-capacitor hybrid generator with the grid following strategy

b) Test with wind power fluctuations

The performance of the hybrid power system in "grid following" strategy is now tested with the prescribed wind power profile (Fig.II-50). The same wind power profile, which is presented in Fig.II-2, is used here during 150s. The power requirement from the microgrid is assumed to be p_{gc_ref}=800W and q_{gc_ref}=0VAR.

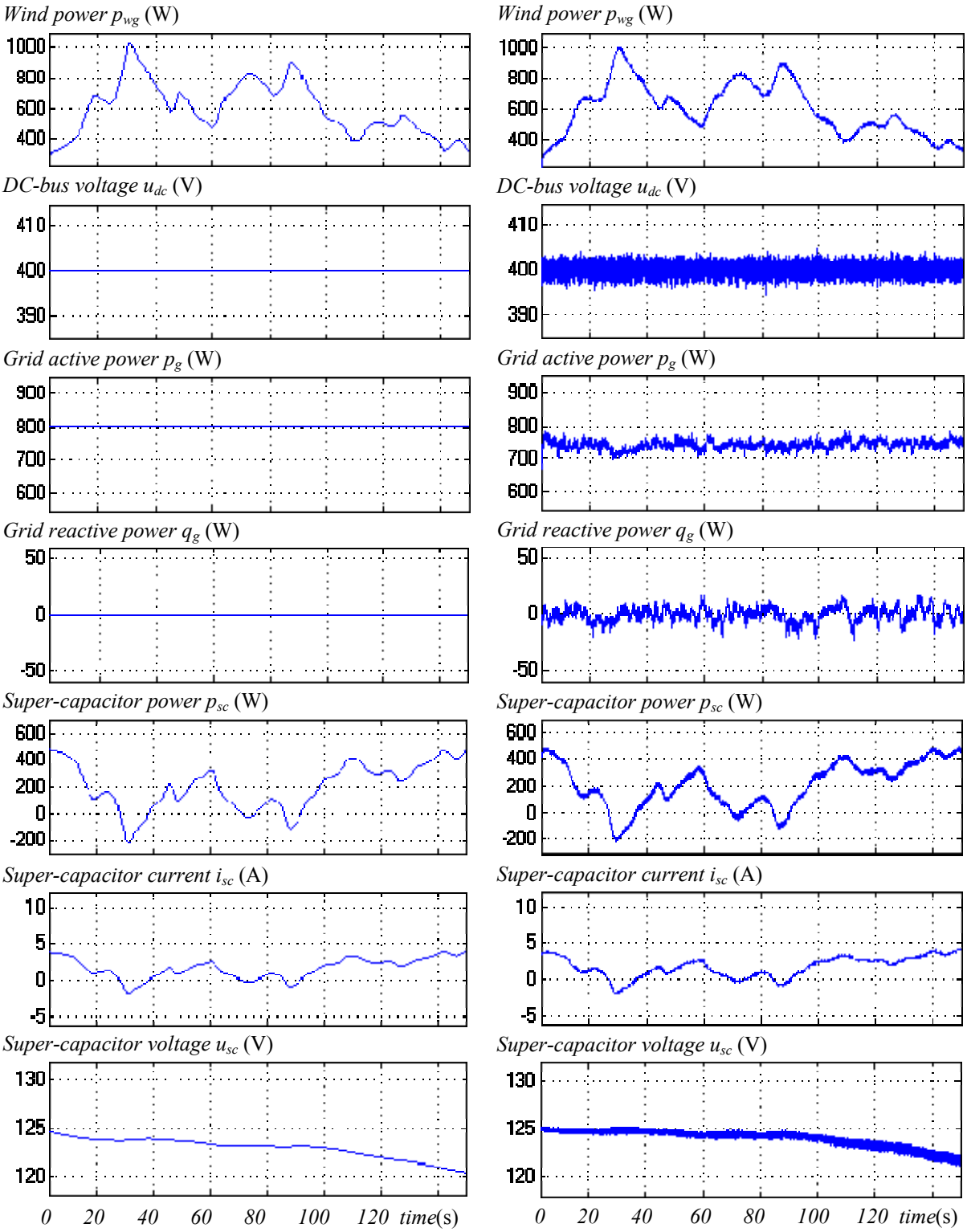

(a) simulation results (b) experimental results

Figure II-50: Evolution test of the wind/super-capacitor hybrid generator with the grid following strategy

The DC-bus voltage is well regulated by the line current loop in the "grid following" strategy against the fluctuant wind power. The delivered grid power is smoothed because the super-capacitors based energy storage system absorbs or supplies the difference between the power requirement (p_{gc_ref}) and the generated wind power (p_{wg}) with its fast power dynamic.

II.4.3 Test of the power dispatching strategy

a) Test with power steps from the microgrid system operator

The dynamic performance of the "power dispatching" strategy is firstly tested with respect to the grid power requirements (Fig.II-51).

The wind power is set to zero in the test in order to highlight the performances of the super-capacitor power conversion system and the grid connection system. The same steps of the active and reactive grid power requirements are given as previously.

The DC-bus voltage is better regulated around 400V with less overshoots by the super-capacitors during the transients. Both the active and reactive power requirements are exactly achieved (1000W and 500VAR) because they are directly sent to the grid connection system as power references. So the power dispatching strategy can have a better performance on the power regulation than the grid following strategy.

The super-capacitors supply or absorb necessary powers to regulate the DC-bus voltage. Because of the power losses in the filters and power converters, the super-capacitor power is slightly more than the grid active power requirement ($p_{sc}>p_{gc\_ref}$) in the experimental results. The same kind of super-capacitor voltage drops can be observed in the experimental results during the transient.

b) Test with wind power fluctuations

The performance of the hybrid power system in "power dispatching" strategy is then tested with the same wind power profile and grid power requirements (Fig.II-52). The delivered grid power is smoothed and the DC-bus voltage is well regulated, because the super-capacitors based energy storage system absorbs or supplies the difference between the power requirement (p_{gc_ref}) and the generated wind power (p_{wg}) with its fast power dynamic.

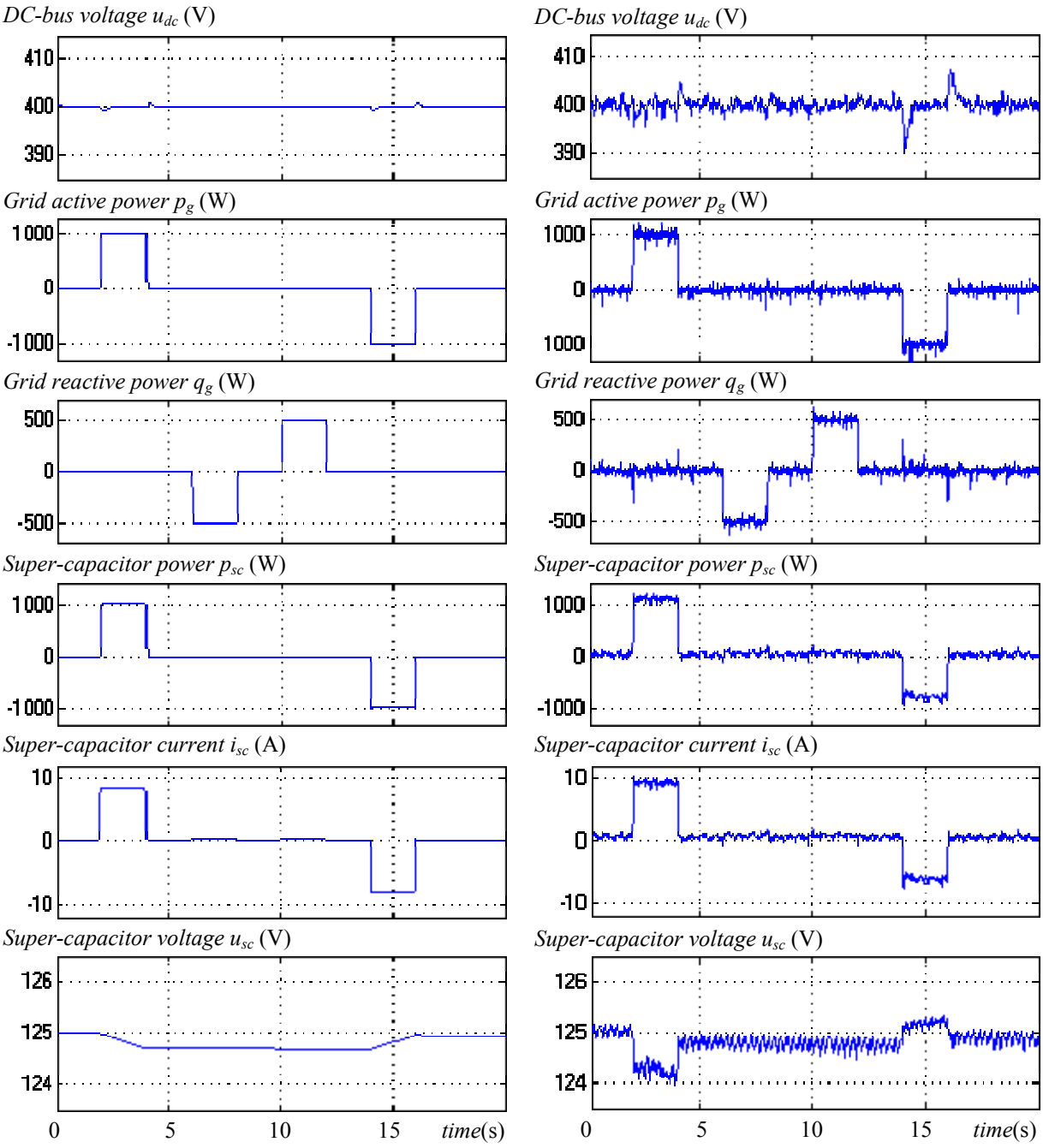

(a) simulation results (b) experimental results

Figure II-51: Dynamic test of the wind/super-capacitor hybrid generator in power dispatching strategy

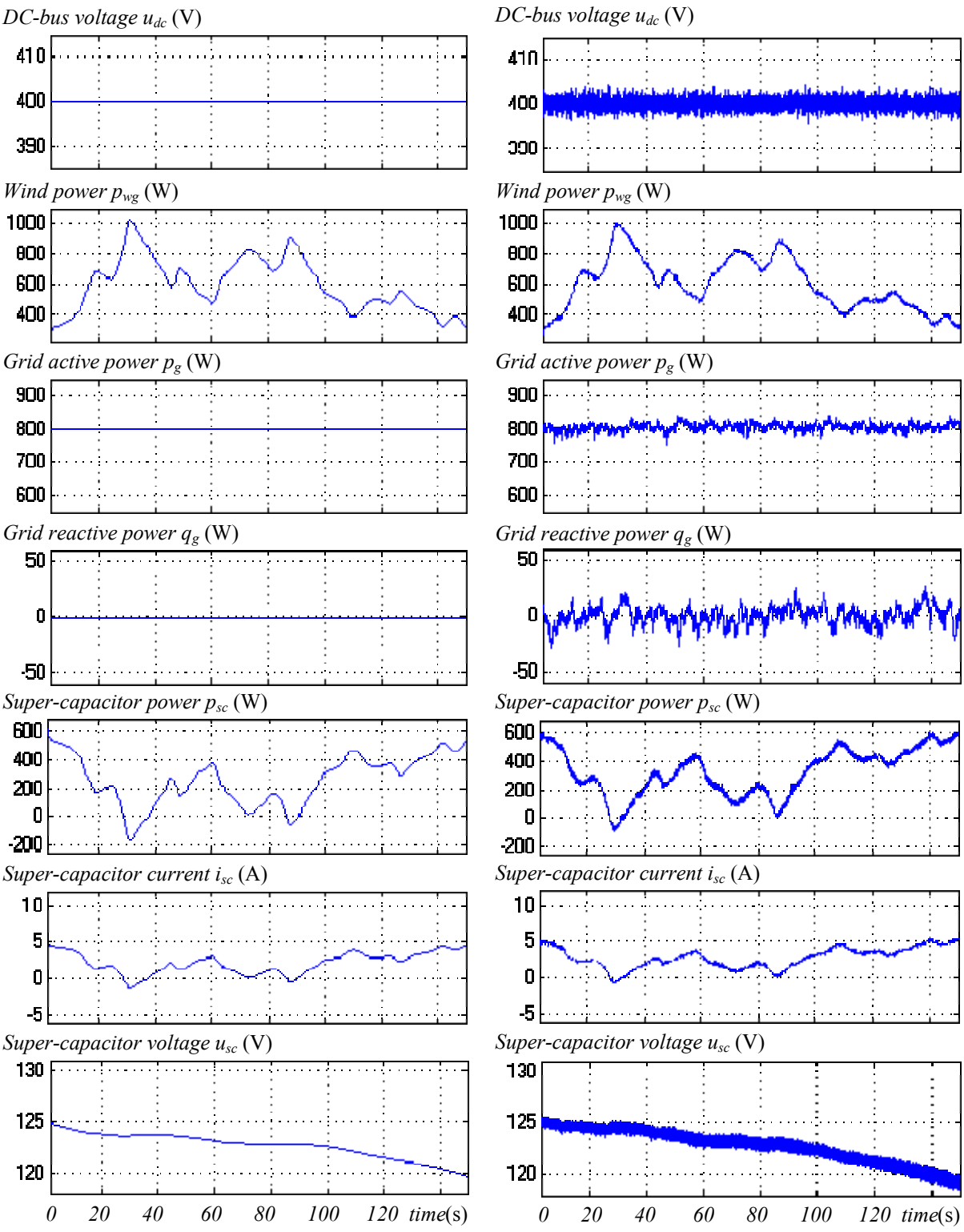

(a) simulation results (b) experimental results

Figure II-52: Evolution test of the wind/super-capacitor hybrid generator in power dispatching strategy

II.4.4 Discussion

For the super-capacitors assisted wind energy conversion system, two power balancing strategies are tested above: the grid following strategy and the power dispatching strategy. Thanks to the help of the super-capacitors based energy storage system, both power balancing strategies can be used. The DC-bus voltage is well regulated and the grid power requirements from the microgrid are well achieved. This is a great advantage since now the microgrid operator has the possibility to use this wind energy based generator as controllable power plant to supply some ancillary services for the microgrid.

From the simulation and experimental results, we find that the "power dispatching" strategy has better performances than the "grid following" strategy. With the grid following strategy, the grid power is used to regulate the DC-bus voltage and is adjusted and fluctuant all the time. Moreover, the power losses in the filters and in the power converters can not be exactly estimated and compensated in practice. When the power reference is attributed to the super-capacitors to supply the microgrid power requirements with the fluctuant wind power, the delivered grid power can not be exactly controlled as same as the microgrid system operator requires. With the power dispatching strategy, the microgrid power requirement is directly set for the grid connection system and can be more exactly satisfied.

According to the study, the super-capacitors are able to provide fast power dynamic, so they are suitable to filter the fast fluctuations of the wind power. However, due to the low energy density, its storage capacity is quite small if its power level is properly sized. Its storage level varies rapidly when the average wind power in a short period is different from the microgrid's power requirement. In the performance tests, since the average wind power (about 550W) during 150s is smaller than the microgrid's power requirement (800W), the extracted power from the super-capacitor is more than the stored power into them. As result, the storage level decreases from 125V to 120V, as well as the storage level from 75% to 69%. If the hybrid power system works in this way, the super-capacitors can not sustain for more than several minutes. However, in a microgrid operation, the power requirements are updated about every 15 or 30minutes. If the super-capacitor is sized according to the energy capacity, it is very expensive to add many super-capacitor modules. Moreover, the power capacity is much oversized and the super-capacitors will work far below its rated power for most of the time. Therefore, it is a huge waste of money and of power to use super-capacitors for storing a large amount of energy.

So another kind of energy storage system, which can store much more energy, should be added in the hybrid power system. Such a storage system should be cheap and have a high energy density in order to ensure the energy availability of the whole system for a long term.

In our study, we propose the use of the hydrogen based energy storage system because of many advantages, which have already been presented in Chap.I. It consists of fuel cells for energy backup from hydrogen and electrolyzers for energy storage into hydrogen. If we want to store more energy, we should increase the volume of the hydrogen tank and the effective cost power unit can be consequently reduced. Even more, we do not have to increase the power capacity of the fuel cell system and the electrolyzer system. The study of these two systems will be presented in the Chap.III and Chap.IV.

II.5 Conclusion

In this chapter, a wind energy conversion system is firstly presented, including the system modeling, control scheme and power balancing. Since, only the grid following power balancing strategy can be used, the DC-bus voltage is regulated by the line current control loop and the fluctuant wind power is totally delivered to the grid. This fact indicates that the grid power quality can not be ensured and some energy storage units should be associated in order to add some new control functions into the power system.

Then the super-capacitors assisted wind energy conversion system is studied. Different sources (wind generator, super-capacitors and the grid) are connected to a common DC bus through different power converters. The power balancing is very important for the control of the multi-source hybrid power system for the stability and efficiency reasons. We have proposed and tested two power balancing strategies: the “grid following” strategy and the “power dispatching” strategy. With this hybrid power system, the microgrid system operator can now modify its generated power as necessary.

Super-capacitors have fast power dynamic and can filter the fast fluctuations of the wind power and the peak power demand from the microgrid. However, an energy storage system with a high energy capacity is still needed to ensure the energy availability for a long-term operation. In our study, it refers to the hydrogen based long-term energy storage system including a fuel cell system and an electrolyzer system for power conversion. These two power systems will be presented in detail in the following chapters.

Chapter III

Fuel Cell for Energy Backup form Hydrogen

Chapter III Fuel Cell for Energy Backup from Hydrogen

Continuous depletion of oil supply and the gradual increase of oil prices have emphasized the need for a suitable energy alternative for our century's economy. The progress of fuel cell technologies makes the hydrogen a possible alternative energy carrier for the future. Fuel cell power generation becomes a more and more interesting and promising solution for both automotive industry and stationary power plants. In our study, the fuel cell system is proposed as an energy backup solution.

A systemic study of the fuel cell system is presented in this chapter. An overview is firstly presented, including the existing technologies, the operating principles, the fuel cell system, the technical challenges and the modeling methods. More specifically, a commercialized fuel cell system (Ballard Nexa^{TM} module) is used and is presented in detail. The modeling and control of the fuel cell system is detailed by using the Energetic Macroscopic Representation (EMR) as a graphical tool in order to give a better mathematical presentation. The modeling parameters are identified and validated through experimental studies. A flexible experimental test bench by using Hardware-In-the-Loop simulations has been used to test and validate our presented control system. It is presented in the end of this chapter. This fuel cell experimental test bench is finally used to set up an active generator, which is presented later in Chap.V.

III.1 Overview of fuel cells

III.1.1 Technologies

a) Classifications

The discovery of the fuel cell is generally attributed to Mr. William GROVE in 1845 [Gro 45]. With the ongoing development of the already successful steam engine and the later discovery of the internal combustion engine and its adaptation for the transport sector, fuel cells did not see any industrial development until the 20th century. Since then, different types of fuel cells have been developed. They are typically classified by either their operation temperature or the type of electrolyte as reported in Table III-1.

Proton Exchange Membrane Fuel Cell (PEMFC) or Polymer Electrolyte Fuel Cell is based on a solid polymer electrolyte. Fast start-up times, low temperature operation and high power densities make them an easy to use technology especially for portable or transport applications. CO poisons the catalyst and the hydrogen fuel has to be very pure. Because the polymer membrane has to be kept well humidified for good proton conduction, water management is one of the critical aspects of successfully running a PEMFC.

Direct Methanol Fuel Cell (DMFC) is similar in construction to PEMFCs. Since liquid methanol can be used as a fuel, no external fuel processing is required and high energy storage densities can be achieved. Unfortunately, the polymer membrane is not impermeable to liquid methanol and the resulting fuel crossover reduces overall system efficiency.

Alkaline Fuel Cell (AFC) is based on a liquid, concentrated *KOH* electrolyte. AFCs can operate with non-precious metal catalysts (typically nickel) and therefore have a cost advantage over other types of FCs. The use of a liquid electrolyte requires an additional electrolyte re-circulation system. Unfortunately, CO_2 is a poison for the liquid electrolyte and

needs to be scrubbed from process air. Typically, the use of AFCs has been limited to niche applications such as military and space applications.

Phosphoric Acid Fuel Cell (PAFC) is based on a liquid acid electrolyte. Due to their higher operating temperature, they are less sensitive to *CO* impurities in the fuel and water management is less of an issue. Additionally, they exhibit excellent long term stability. Their relatively long start-up times and low power densities limit their application to stationary power or co-generation plants.

Molten Carbonate Fuel Cell (MCFC) is based on a liquid molten carbonate electrolyte and generally exhibit very high conversion efficiencies. A high operating temperature allows direct use of non noble catalysts along with direct internal processing of fuels such as natural gas. Relatively long start-up times and low power densities again limit their application to stationary power or co-generation plants.

Solid Oxide Fuel Cell (SOFC) is based on a solid oxide electrolyte conducting oxygen O^{2-} ions. As with the MCFC, the high operating temperature translates into non-noble catalysts, direct internal hydrocarbon fuel processing and high quality waste heat that can be used in combined-cycle power plants. Additionally, high power densities along with high efficiencies can be attained. Slow start-up times dictate their primary use as stationary power or co-generation plants.

Table III-1: Overview of the operating characteristics of the different fuel cells [Hoo 03]

Fuel Cell Type	Electrolyte	Charge Carrier	Temperature	Fuel
PEMFC	solid	H^+	50-90°C	H_2
DMFC	solid	H^+	50-90°C	CH_3OH
AFPC	liquid	OH^-	60-250°C	H_2
PAFC	liquid	H^+	160-250°C	H_2
MCFC	liquid	CO_3^{2-}	about 650°C	H_2, CO, CH_4
SOFC	solid	O^{2-}	750-1000°C	H_2, CO, CH_4

b) Advantages

Fuel cell power generation becomes a more and more interesting and promising solution for both automotive industry and stationary power plants. Fuel cell systems become attractive thanks to many advantages over the conventional systems, such as:

- low pollution (or in some cases zero emission solutions);
- relatively high efficiency (55 – 65% stack);
- relatively high power density (>1MW/m^3 stack);
- direct energy conversion (no combustion);
- silent operation (stack);
- fuel flexibility;
- ability of modular installations for load matching;
- high reliability;
- size flexibility;
- rapid load following capability (PEMFC compared to the internal combustion engines).

III.1.2 Operating principles

Depending on the type of fuel cell and the used fuel, the reaction mechanisms may be different from each other. We choose PEM fuel cells to consider the operation description, moreover the main concept remains the same as for the other types of fuel cells. Within the PEM fuel cells, hydrogen and oxygen are converted into water while generating electricity. A schematic diagram of the processes occurring in a PEM fuel cells [Gra 07] is shown in Fig.III-1.

Both reactant gases are supplied under pressure into the flow channels of the plate. At the anode side the ***hydrogen oxidation reaction*** forms protons and electrons:

$$H_2 \xrightarrow{catalyst} 2H^+ + 2e^- \qquad \text{(III-1)}$$

Released protons and electrons are transferred through the membrane to the cathode catalyst layer and the external electrical load, respectively. At the cathode side the oxygen is consumed by the ***oxygen reduction reaction*** along with the protons and electrons and liquid water is produced as the product with heat:

$$\frac{1}{2}O_2 + 2e^- + 2H^+ \xrightarrow{catalyst} H_2O + Heat \qquad \text{(III-2)}$$

As a result, the overall chemical reaction of the fuel cell is represented as follows:

$$H_2 + \frac{1}{2}O_2 \longrightarrow H_2O + Heat + Electrical\ Energy \qquad \text{(III-3)}$$

In order to technically exploit such a reaction, the two chambers are separated through an electrically insulating (i.e. no electron conduction) and gas-impermeable ***membrane electrolyte assembly***, which is capable of conducting protons. The area in contact with the membrane is called ***catalyst layer***, which is covered with a platinum catalyst on both anode and cathode sides.

Adjacent to the catalyst layers on both sides of the membrane is a porous, electrically conducting ***gas diffusion layer***. It allows reaction gases (i.e. hydrogen and oxygen) to flow to the reaction sites on the catalyst layer and product water to flow back out.

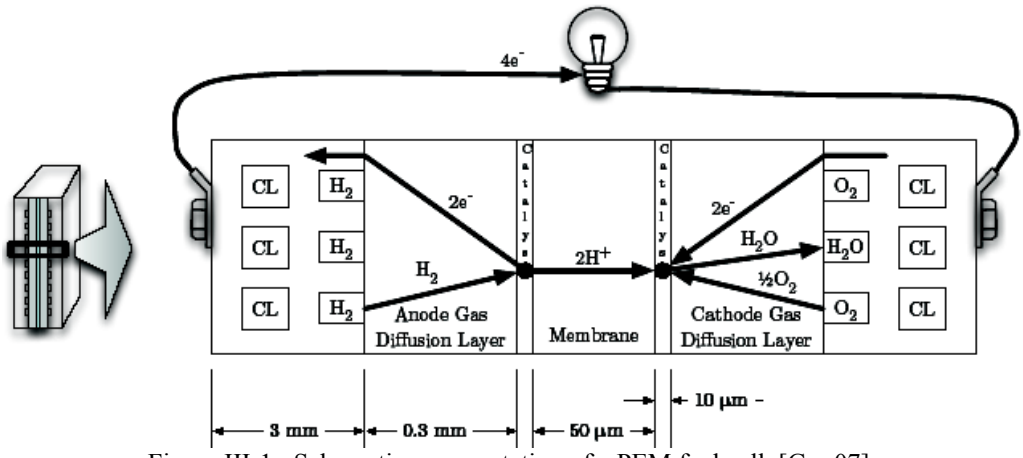

Figure III-1: Schematic representation of a PEM fuel cell. [Gra 07].

III.1.3 Fuel cell system

a) Fuel cell stack

The fuel cell stack is the key component of a fuel cell system and performs the main function of energy conversion within the system (Fig.III-2) [Ast 08]. Due to the fact that the voltage of a single fuel cell is quite small (between $1V$ and $0.5V$ depending on the current density) the desired voltage can only be produced by a series connection of cells. Such a collection of cells in series is called a "stack". This configuration corresponds to an electrical series connection of the single elements. The reaction gases and cooling liquid are supplied to the cells through a parallel network of supply channels.

One of the commonly used methods for cell interconnection in practice is to use a "bipolar plate". This makes connections all over a cathode of one cell and an anode of the next cell (hence "bipolar"). At the same time the bipolar plate helps to feed oxygen to the cathode and fuel gas to the anode. This distribution of the reactant gases over the electrodes is done using a "flow field" formed into the surface of the plate, usually a fairly complex serpentine pattern.

The heat, which is generated during the electrochemical reaction, is transferred to the bipolar plates through conduction. Then it is either transmitted to the ambient air through specially designed cooling fins or it is evacuated from the system through a cooling liquid (CL) circulating within the bipolar plates.

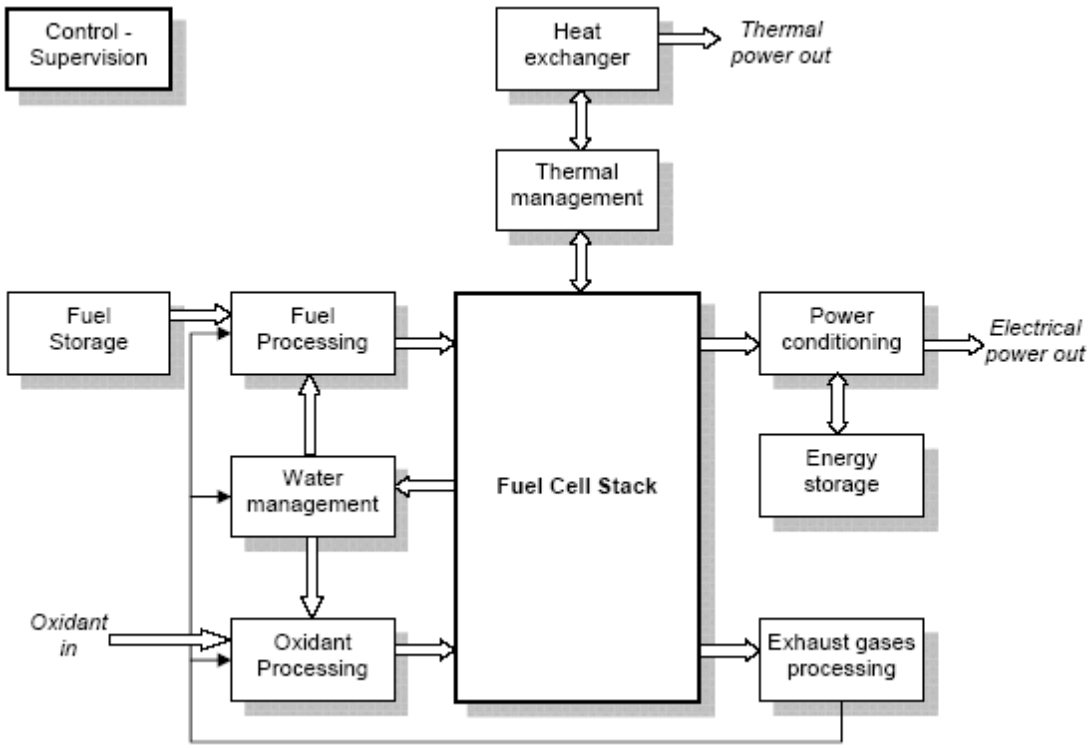

Figure III-2: Fuel cell system scheme [Ast 08].

b) Fuel cell auxiliaries

For a proper operation, a fuel cell system needs many auxiliaries, which are also called "Balance of Plant (BoP)" components. If the fuel cell stack is intrinsically able to respond quickly to the load changes, the auxiliary subsystems (hydrogen supply, air compressor, gas humidification, coolant circuit) respond much more slowly. This apparent contradiction

decreases the reliability and performance of the entire fuel cell system [Spa 03]. Fig.III-2 presents a general scheme of a fuel cell system.

The fuel must first be produced and/or stored. Then, it is finally processed (mostly in terms of pressure, hydration, and flow regulation) before arriving in the fuel cell stack. The oxidant must also be processed in the same way. For both fuel and oxidant gases, the water, which is produced by the fuel cell stack can be removed from the exhaust gases and can be reused in the hydration of incoming gases. Since the electrochemical reaction is exothermal and the fuel cell stack must be operated in a dedicated temperature range, a thermal management is essential. Moreover, the gas supply and the stack thermal management are strongly coupled with the gas hydration level control. The electrical power conditioning (in association with, or not in association with, an energy storage device) and the overall control of the whole system are also very important for an advanced fuel cell system.

There are many fuel cell stack manufacturers, few complete system suppliers exist. Investment costs are still high at present and depend on cell materials (Pt catalyst, graphite, membrane) and on the manufacturing mode. For the purpose of both energy savings and pollutant emissions, the whole fuel cell system should be well designed and global optimized. As mentioned above, many technological challenges have to be solved before that efficient, competitive, reliable fuel cell power generators can be seen in the market.

III.1.4 Technical challenges

Among the different technological challenges, some of them concern mainly electrochemical, mechanical or thermal engineering researchers. Obviously, the first research area concerns ***electrochemical and material engineering researches*** on the FC stack itself. The power density should be increased, whereas the amount of noble catalyst should be reduced. Moreover, temperature and water management related issues are of the highest importance. The temperature should increase for low-temperature FC stacks (to reduce water management problems) and decrease for higher-temperature FC stacks (to reduce the thermal stress on the materials and the startup time). The second large research area deals with ***hydrogen production, distribution, or storage*** [Jou 03]. It is clear that hydrogen is not a primary power source but an energy carrier. Today, hydrogen is usually produced by reforming oil or natural gas (in this case, a fossil fuel has to be available and carbon is emitted) or by electrolysis (in this case, electricity has to be provided). The reforming solution is based on a time-limited resource and also suffers from hydrogen purity problems.

For electrical engineering researchers, the challenges concern mainly the fuel cell's electrical behavior and the auxiliaries. Auxiliaries are required to feed the stack with reactants, to ensure the thermal equilibrium (temperature regulation or limitation), to perform the output power conditioning (storage devices and power converters) and to supervise the system. Four main research issues need to be considered:

- ***Power efficiency***: The electrical efficiency of the electrochemical conversion is quite high, between 50% and 60%, but it has to supply its own auxiliaries. To keep the global efficiency as high as possible, the auxiliary consumption has to be minimized (particularly, the motor compressor or the blower) and their efficiency has to be optimized (power conversion system).

- ***Power dynamic***: The auxiliaries dominate the dynamic of the fuel cell system. In comparison with the electrochemical time response of the fuel cell stack (below milliseconds), they take much longer time to be regulated, such as the flow regulators and valves (seconds and milliseconds), the air compressor (a few seconds) and the humidification system (a few minutes).
- ***Power buffer***: In general, the system is assisted by batteries. Super-capacitors and flywheels can also be used. At least, the power buffer has to supply the supervision system during startup and emergency shutdown. Moreover it can also be sized to balance the stack power by supplying the peak power demand and improving the time response to transient load changes.
- ***Power control***: It consists of the control of each auxiliary system (including closed-loop controls) and a global supervision of the fuel cell system. The global supervision must guarantee the safe operation of the stack. Moreover, it has to control the power flows among the different energy sources in a fuel cell based hybrid power system [Dav 09].

III.1.5 Modeling methods

The modeling is an important aspect in fuel cell system development since it facilitates a better understanding of the features and parameters affecting the performance of fuel cells and fuel cell systems. There are different approaches for fuel cell modeling, which can be classified by using different criteria (Table III-2) [Ast 08].

The first criterion is related to the **system boundary**, which defines the area of interest of the model:

- fundamental cell level (electrodes, membrane);
- middle stack level (fuel cell stack);
- high system level (stack with auxiliary system).

The fuel cell models can also be subdivided into ***empirical and theoretical*** ones. The theoretical (or mechanistic) models normally use the basic, phenomenological equations. For example, the Nernst-Planck equation describes the species transport, the Stefan-Maxwell equation is used for the gas-phase transport, the Butler-Volmer equation for the fuel cell voltage. Spatial dimensions are the key criteria for mechanistic models. For instance, to describe the fuel cell phenomenon of mass transport limitation at least a one-dimensional model is required. For a proper treatment of the thermal and water management, except electrochemical relationships, the model should contain also thermodynamic and fluid dynamic equations. They are normally applied in two or three dimensions and can provide an appropriate representation of almost all processes in a fuel cell and a fuel cell system. Depending on its focus and complexity level, the model may provide details like fuel flow pattern, current density distribution, voltage and pressure drops in the stack. Such a model is normally an appropriate tool for detailed system studies, since it allows a high flexibility in applications with a wide range of operating conditions. Usual drawbacks of such models are the time demand for their development and validation, due to the difficulties in the achievement of the detailed fuel cell stack features.

The other approach to model the FC is empirical. It is based on fitting experimental data by a set of mathematical functions. Usually, these models are related to the particular fuel cell experimental data specific to each application and operating condition. They typically do not

provide as many details as theoretical ones but may serve as a fast start into fuel cell modeling and a simplified basis for engineering applications.

The fuel cell models can also be classified into ***steady-state models and transient-state models*** (or a special intermediary case, the ***quasi-steady-state models***). This criterion is especially useful for system engineers. Steady-state models describe one operating point in each step. They are used mainly for parametric studies like sizing components in the system (stack and/or auxiliary systems), calculating amounts of materials (e.g. catalyst) and specification of the auxiliaries' parameters. The transient models are useful for the design of both the system's electrical and thermal interfaces, as well as the dynamic properties of the auxiliary equipments. The objective of the fuel cell system modeling and simulation could be focused on both stationary and transportation fuel cell applications.

Table III-2: Summary of major FC modeling features [Har 04]

System boundary	Model approach	Spatial dimension	Complexity/ details	Time domain
Electrode (gas channels, catalyst layer), fuel cell, stack, system	Theoretical (mechanistic), empirical, semi-empirical	Zero to three dimensions	Electrochemical, thermodynamic, fluid dynamic, control	Steady-state, quasi-steady-state, transient-state

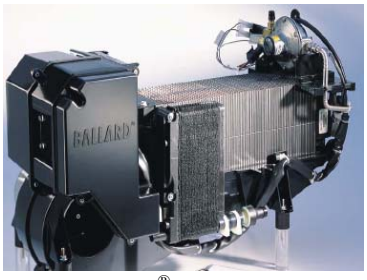

(a) Ballard® fuel cell stack

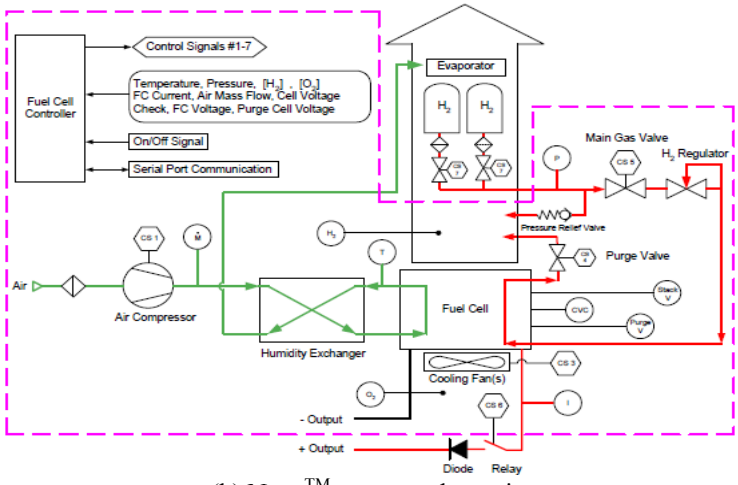

(b) Nexa™ system schematic

(c) Installation of the fuel cell system

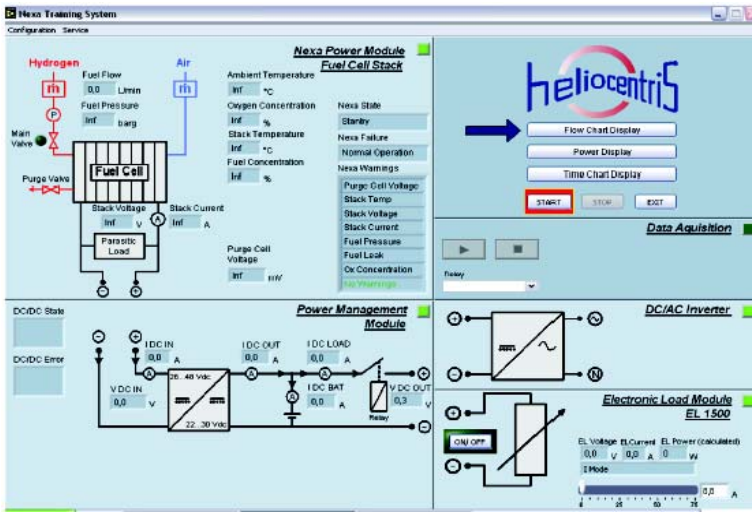

(d) Control panel from the computer screen

Figure III-3: Studied fuel cell system (Ballard Nexa™)

III.2 Studied fuel cell system

III.2.1 Introduction

A Ballard Nexa™ power module is studied in our study. It is a compact, low-maintenance and fully automated fuel cell system, which is designed for the back-up power markets. It provides up to 1200W DC power with supplied hydrogen and air. Water and heat are the only by-products of the reaction. So the Nexa™ module is extremely quiet and produces zero harmful emission. Moreover, it operates at low pressure, with minimized parasitic losses and enhanced system reliability. Furthermore, it does not require external fuel humidification and it is air-cooled. The overall system design is then simplified.

The Ballard® fuel cell stack contains 47 cells of 100 cm^2 in series (Fig.III-3a), as well as all necessary auxiliary systems for the fuel cell operation. Hydrogen, oxidant air and cooling air must be supplied to the unit (Fig.III-3b). Exhaust air, product water and coolant exhaust is emitted. The power conversion system is required to regulate the output electrical power. All these auxiliary systems are integrated in a rolling cabinet (Fig.III-3c). A communication interface must be provided to provide start/stop signals and to receive serial port communications. A computer is equipped to visualize and control the operations (Fig.III-3d).

In this section, this commercial fuel cell plant will be modeled and then be used to evaluate the feasibility of the proposed hybrid power system.

III.2.2 System operation

a) Fuel cell stack

The fundamental component of the Ballard® fuel cell consists of two electrodes, which are separated by a polymer membrane electrolyte. Each electrode is coated on one side with a thin platinum catalyst layer. The electrodes with catalyst and membrane together, form the membrane electrolyte assembly (Fig.III-4a).

Gases (hydrogen and air) are supplied to the electrodes through channels formed in flow field plates. Hydrogen flows through the channels to the anode where the platinum catalyst promotes its separation into protons and electrons. The free electrons are conducted in the form of usable electric current through an external circuit, while the protons migrate through the membrane electrolyte to the cathode. At the cathode, oxygen from the air with electrons from the external circuit and protons, are combined to form pure water and heat.

Individual fuel cells are gathered into a fuel cell stack to provide the required electrical power. A single fuel cell produces about 1V at open circuit and about 0.6V at full load. On one hand, cells are stacked together in series to provide the required voltage. On the other hand, the current of a fuel cell is proportional to its active area. Consequently, the fuel cell stack geometry can be tailored to provide the desired output voltage, current and power characteristics.

b) Fuel cell auxiliaries

The security issues are very important but are not detailed here. We focus on the operating principles of the auxiliaries (Fig.III-4b).

Power Conditioning: The fuel cell stack provides an unregulated DC power. A power conversion system is required to adapt the output electrical power. Due to the slow transient response of the auxiliary systems, power buffers are sometimes integrated through power electronic system to supply the peak power demand and to improve the time response to transient load changes.

Fuel processing: The Nexa^{TM} power module operates with pure, dry hydrogen from any suitable source (hydrogen tank or hydride bottle). The fuel processing system monitors and regulates the hydrogen supply. The pressure regulator maintains the pressure during the operation by continuously replenishing hydrogen, which is consumed in the fuel cell reaction.

Oxidant processing: A small compressor provides excess oxidant air to the fuel cell stack in order to sustain the fuel cell reaction. The compressor speed is adjusted to suit the current demand of the fuel cell stack. Oxidant air is humidified before reaching the fuel cells to maintain the membrane saturation for the fuel cell lifetime. A humidity exchanger transfers both fuel cell product water and heat from the wet cathode outlet to the dry incoming air. Excess product water is collected and discharged from the system.

Cooling system: A cooling fan is located on the bottom of the power module, blows air through vertical cooling channels in the fuel cell stack. The fuel cell operating temperature can be maintained at 65°C by varying the speed of the cooling fan. The hot air from the cooling system may also be used in an energy cogeneration system for building heating in some cases.

System control and supervision: The overall control and supervision should be implemented for the security reasons and for improving performances, by receiving various input signals from the onboard sensors, like stack temperature, hydrogen pressure, stack current and voltage, air mass flow, etc.

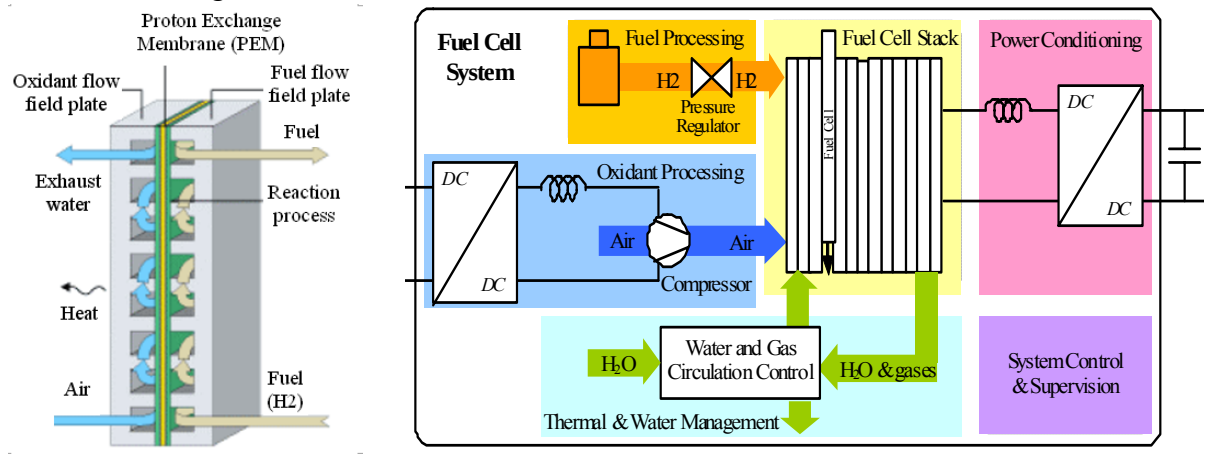

(a) Operation of a fuel cell [Pri 02] (b) Operation principles of the studied fuel cell system

Figure III-4: Bloc diagram of a fuel cell system including the stack and its auxiliaries

Therefore, a fuel cell system is a very complex multi-physic system. Some graphical tools are used in order to present the system modeling and the control. The modeling and control of the studied fuel cell system will be presented by using the Energetic Macroscopic Representations (See Appendix C).

III.3 Modeling of the fuel cell stack

III.3.1 Open-circuit voltage

A fuel cell directly converts chemical energy into electrical energy. The chemical energy released from the fuel cell can be calculated from the change in Gibbs free energy (ΔG), which is the difference between the Gibbs free energy of the product and the Gibbs free energy of the reactants. The Gibbs free energy is used to represent the available energy to do external work. For the hydrogen/oxygen fuel cell, the basic chemical reaction is shown in (II-3), and the change in the Gibbs free energy (ΔG) in a hydrogen fuel cell reaction is expressed as:

$$\Delta G_{fc} = G_{H2O} - G_{H2} - G_{O2} \tag{III-4}$$

with ΔG_{fc}: the change in Gibbs free energy of the hydrogen fuel cell reaction [J];
G_{H2O}: the Gibbs free energy of H_2O [J];
G_{H2}: the Gibbs free energy of H_2 [J];
G_{H2O}: the Gibbs free energy of O_2 [J].

The change in Gibbs free energy varies with both temperature and pressure [Lar 00],

$$\Delta G_{fc} = \Delta G_0 - (T_{fc} - T_0)\Delta S_0 - RT_{fc} \ln\left(\frac{p_{H2\_fc} p_{O2\_fc}^{0.5}}{p_{H2O\_fc}}\right). \tag{III-5}$$

with ΔG_0: the change in Gibbs free energy at standard pressure (1 bar) [J];
ΔS_0: the entropy change in standard temperature;
T_0: the standard temperature [K];
T_{fc}: the temperature of the fuel cell [K];
p_{H2_fc}: the partial pressure of the hydrogen [bar];
p_{O2_fc}: the partial pressure of the oxygen [bar];
p_{H2O_fc}: the partial pressure of the water vapor [bar];
R: the universal gas constant 8.31451 [J/(kg·K)].

The change in Gibbs free energy of the reaction in Eq.III-5 at standard pressure varies with different reaction temperatures (Table III-3). Its value is negative and means that the energy is released from the reaction.

Table III-3: Change in Gibbs free energy of hydrogen fuel cell at various temperatures at standard pressure

From of Water Product	Temperature °C	ΔG_0 (kJ/mole)
Liquid	25	-237.2
Liquid	80	-228.2
Gas	80	-226.1
Gas	100	-225.2
Gas	200	-220.4
Gas	400	-210.3
Gas	600	-199.6
Gas	800	-188.6
Gas	1000	-177.4

We consider that all of the Gibbs free energy is converted to electrical energy, which is the electrical work used to move an electrical charge around a circuit. For each mole of

hydrogen, two moles of electrons pass around the external circuit and the resulted electrical work (charge × voltage) is

$$Electrical\ work\ done = -nFE \tag{III-6}$$

with n: number of moles of electrons (=2 moles);
F: Faraday constant (=96485 Coulombs), electrical charge of 1 mole of electrons;
E: the voltage of the fuel cell [V].

This resulted electrical work would be equal to the change in Gibbs free energy if the system is reversible. In practice, the fuel cell process is not reversible, some of the chemical energy is converted to heat and the fuel cell voltage V_{cell} is less than the theoretical value. By using thermodynamic values of the standard-state entropy change, the open circuit voltage (E_{fc}) of the fuel cell can be expressed as [Amp 95]

$$E_{fc} = 1.229 - 0.85 \times 10^{-3}(T_{fc} - 298.15) + 4.3085 \times 10^{-5} T_{fc} \ln(p_{H2\_fc} p_{O2\_fc}^{0.5}) \tag{III-7}$$

It can be rewritten into two parts.

$$R_{fc\_1}: \quad E_{fc} = E_{0\_fc} - \Delta E_{fc}, \tag{III-8}$$

where

$$E_0 = \frac{\Delta G_0}{-2F} = 1.229 \tag{III-9}$$

and

$$R_{fc\_2}: \Delta E_{fc} = 0.85 \times 10^{-3}(T_{fc} - 298.15) - 4.3085 \times 10^{-5} T_{fc} \ln(p_{H2\_fc} p_{O2\_fc}^{0.5}) \tag{III-10}$$

The term E_{fc} is the theoretical thermodynamic voltage due to the change in Gibbs free energy varies at standard-state condition (25°C and 1 bar). ΔE_{fc} is the voltage drop, which depends on the temperature and pressures.

III.3.2 Operating voltage

When the fuel cell operates, the actual cell voltage V_{cell} is less than the open-circuit voltage E_{fc},

$$R_{fc\_3}: V_{cell\_fc} = E_{fc} - \Delta V_{fc}. \tag{III-11}$$

The voltage drop ΔV_{fc} is the result of several irreversible losses, such as activation losses, ohmic losses and concentration losses, which depend on the current density (j_{fc}) [Lar 00]

$$R_{fc\_4}: \Delta V_{fc} = A_{fc} \ln\left(\frac{j_{fc}}{j_{0\_fc}}\right) + r_{fc} j_{fc} + B_{fc} \ln\left(1 - \frac{j_{fc}}{j_{\lim\_fc}}\right) \tag{III-12}$$

where A_{fc} and j_{0_fc} are the parameters for the activation losses, r_{fc} is the parameters for the ohmic losses, B_{fc} and j_{lim_fc} are the parameters for the concentration losses. The current density j_{fc} is described as:

$$R_{fc\_5}: j_{fc} = \frac{i_{fc}}{S_{fc}} \tag{III-13}$$

with j_{fc}: the fuel cell current density;
i_{fc}: the fuel cell current;
S_{fc}: the active surface area.

III.3.3 Stack modeling

For the fuel cell stack of n_{fc} cells in series, the gas flow (q_{H2_fc} and q_{O2_fc}) of the consumed H_2 and O_2 are described with the Faraday law:

$$R_{fc\_6}:\ q_{H2\_fc} = \frac{n_{fc}}{2F} i_{fc} \tag{III-14}$$

$$R_{fc\_7}:\ q_{O2\_fc} = \frac{n_{fc}}{4F} i_{fc} \tag{III-15}$$

And the output voltage of the stack V_{fc} can be deduced as follows:

$$R_{fc\_8}:\ u_{fc} = n_{fc} V_{cell} \tag{III-16}$$

Since the fuel cell operation is not reversible in practice, the energy losses are converted to heat. In order to present the losses by thermal flow, we define a variable "entropy flow" (ΔS). Then we can describe the power losses in the fuel cell open-circuit voltage as

$$R_{fc\_9}:\ \Delta S_{E\_fc} = n_{fc} \frac{\Delta E_{fc} i_{fc}}{T_{fc}} \tag{III-17}$$

and the power losses in the fuel cell operation as

$$R_{fc\_10}:\ \Delta S_{V\_fc} = n_{fc} \frac{\Delta V_{fc} i_{fc}}{T_{fc}} \tag{III-18}$$

The total power losses by thermal flow can be described as

$$R_{fc\_11}:\ \Delta S_{tot\_fc} = \Delta S_{E\_fc} + \Delta S_{V\_fc} \tag{III-19}$$

III.3.4 Graphical representation

We can see that a fuel cell stack is a very complex multi-physic component, and many variables are used in its modeling. In order to organize all relations among the different input and output variables, the modeling equations are depicted by in a COG (Appendix D) and by an equivalent macroscopic presentation (REM) (Fig.III-5). We can see four quantities, which should be controlled by the auxiliary systems:

- the current (i_{fc}) should be controlled by the power conditioning system;
- the hydrogen pressure (p_{H2_fc}) should be controlled by the hydrogen handling system;
- the oxygen pressure (p_{O2_fc}) should be controlled by the oxygen handling system;
- the temperature (T_{fc}) should be controlled by the thermal management system.

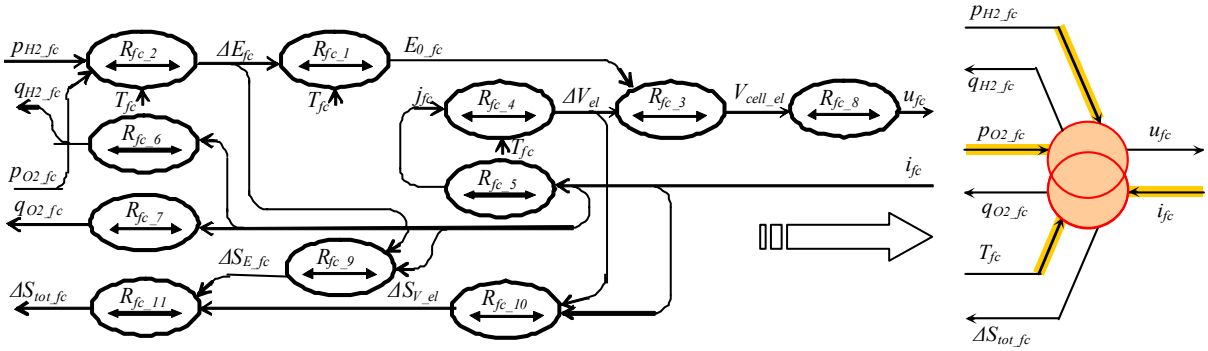

Figure III-5: COG and EMR of a fuel cell stack modeling

III.4 Modeling and control of the auxiliary systems

III.4.1 Modeling and control of the power conditioning system

The fuel cell stack supplies unregulated DC power,

$$p_{fc} = u_{fc} i_{fc} . \tag{III-20}$$

It should be adapted before being applied to the load. Since the fuel cell is considered as a voltage source (u_{fc}), the power can be controlled by regulating the fuel cell current (i_{fc}). A ***choke filter*** is needed to set this current (i_{fc}),

$$\frac{di_{fc}}{dt} = \frac{u_{fc} - u_{m\_fc\_ref}}{L_{fc}} \tag{III-21}$$

where u_{m_fc} is the average value of the chopper's modulated voltage. The ***DC chopper*** is described by average values as below,

$$\begin{cases} u_{m\_fc} = m_{fc} u_{dc} \\ i_{m\_fc} = m_{fc} i_{fc} \end{cases} \tag{III-22}$$

where m_{fc} is the chopper's duty ratio and i_{m_fc} is the average value of the chopper's modulated current. The voltage of the DC bus (u_{dc}) can be considered as a constant voltage source, which is maintained by the other sources in the studied hybrid power system.

An EMR is used to organize the modelling equations (Fig.III-6) of the power conditioning system. We can see a causal path from the duty ratio (m_{fc}) of the chopper to the fuel cell current (i_{fc}). In order to control the fuel cell current, the control scheme is obtained by inverting this path (Fig.III-6). The reference value (m_{fc_ref}) of the chopper's duty ratio is obtained by inverting the equation (II-22),

$$m_{fc\_ref} = \frac{u_{m\_fc\_ref}}{\hat{u}_{dc}} \tag{III-23}$$

where $u_{m\_fc\_ref}$ is the reference of the chopper's average modulated voltage. It is set by the current corrector (PI) to keep the fuel cell current equal to the desired value i_{fc_ref},

$$u_{m\_fc\_ref} = PI\left(i_{fc\_ref} - \hat{i}_{fc}\right) + \hat{u}_{fc} \tag{III-24}$$

The used equations in the EMR are summarized in (Table III-4)

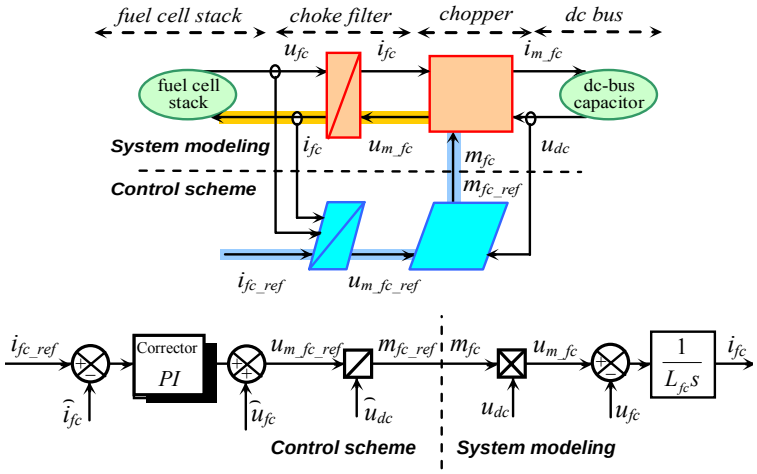

Figure III-6: EMR and block diagram of the power conditioning modeling and control

Table III-4: Summary of modeling equations and control algorithms for the oxidant processing

	Modeling equations	Control algorithms
choke filter	$\frac{di_{fc}}{dt} = \frac{u_{fc} - u_{m\_fc\_ref}}{L_{fc}}$	$u_{m\_fc\_ref} = PI\left(i_{fc\_ref} - \hat{i}_{fc}\right) + \hat{u}_{fc}$
chopper	$\begin{cases} u_{m\_fc} = m_{fc} u_{dc} \\ i_{m\_fc} = m_{fc} i_{fc} \end{cases}$	$m_{fc\_ref} = \frac{u_{m\_fc\_ref}}{\hat{u}_{dc}}$

III.4.1 Modeling of the fuel processing system

The pressurized H_2 is stored in a bottle. It should be released and humidified before arriving at the anode. In practice, the pressure regulation is performed instantaneously, so we can assume a hydrogen supply with a wished constant pressure (p_{H2_fc}). Hence the fuel processing unit is modeled as an energy source in the EMR (Fig.III-7).

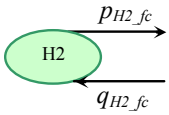

Figure III-7: EMR of fuel processing modeling as an energy source

III.4.2 Modeling and control of the oxidant processing system

The pressurized O_2 with a releaser can also be used to supply the fuel cell and the same modeling can be used for the oxidant processing as for the fuel processing (Fig.III-8).

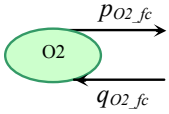

Figure III-8: EMR of oxidant processing modeling as an energy source

In our study, an air compressor is used to supply the O_2 into the fuel cell. A simplified model is used for the oxidant processing system [Chr 07]:

- The electrode and the manifold are represented by a ***lumped volume***.
- The air is sent into the electrode by a compressor, which is modeled with a simplified ***compressor law*** and the ***turbine inertia***.
- The compressor is driven by a ***DC machine***, which is connected to a ***DC chopper*** and a ***filter inductor***.

Theoretically, the air pressure should be controlled and the reference of the air flow ($q_{air\_fc\_ref}$) is the output of the pressure controller. In practice, the reference of the air flow ($q_{air\_fc\_ref}$) is directly set proportional to the fuel cell current (i_{fc}) in order to supply enough or more oxygen than consumed. In order to control the oxygen supply, the rest of the control scheme is obtained by inverting the modelling equations or by inserting some variable controllers.

An EMR is used to organize the modelling equations and the control algorithms (Fig.III-9). The used equations are summarized in (Table III-5).

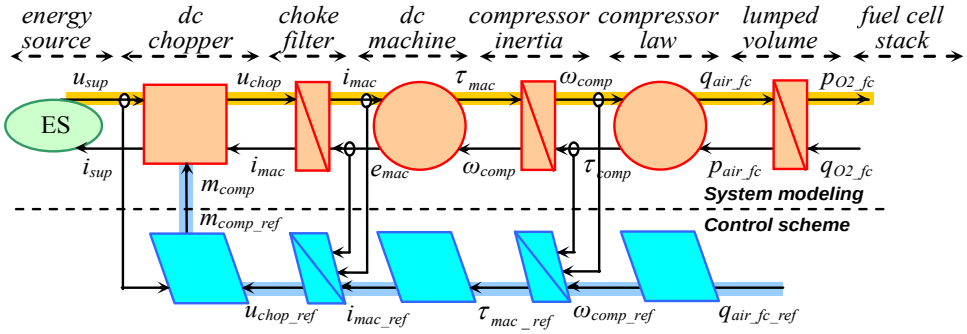

Figure III-9: EMR of oxidant processing modeling and control

Table III-5: Summary of modeling equations and control algorithms for the oxidant processing

	Modeling equations	Control algorithms
dc chopper	$\begin{cases} u_{chop} = m_{comp} u_{sup} \\ i_{sup} = m_{comp} i_{mac} \end{cases}$	$m_{comp\_ref} = \frac{1}{\hat{u}_{sup}} u_{chop\_ref}$
choke filter inductor	$\frac{di_{mac}}{dt} = \frac{1}{L_{mac}}(u_{chop} - e_{mac})$	$u_{chop\_ref} = PI(i_{mac\_ref} - \hat{i}_{mac}) + \hat{e}_{mac}$
dc machine	$\begin{cases} \tau_{mac} = k_\tau i_{mac} \\ e_{mac} = k_\omega \omega_{comp} \end{cases}$	$i_{mac\_ref} = \frac{1}{k_\tau} \tau_{mac\_ref}$
compressor inertia	$\frac{d\omega_{comp}}{dt} = \frac{1}{J_{comop}}(\tau_{mac} - \tau_{comp})$	$\tau_{mac\_ref} = PI(\omega_{comp\_ref} - \hat{\omega}_{comp}) + \hat{\tau}_{comp}$
compressor laws	$\begin{cases} q_{air} = k_q \omega_{comp} \\ \tau_{comp} = k_p p_{air} \end{cases}$	$\omega_{comp\_ref} = \frac{1}{k_{O2}} \hat{q}_{air}$
lumped volume	$\frac{dp_{O2\_fc}}{dt} = \frac{RT_{fc}}{V_{lump}}(k_{O2} q_{air\_fc} - q_{O2\_fc})$	$q_{air\_ref} = \frac{1}{k_{O2}} q_{O2\_fc\_ref} = \frac{n_{fc}}{4Fk_{O2}} i_{fc\_ref}$

III.4.3 Modeling and control of the thermal management system

The fuel cell operating temperature (T_{fc}) can be maintained in a certain range with a controlled air flow by varying the speed of the cooling fan. The temperature of the fuel cell stack (T_{fc}) depends on the balance between the created entropy flow (ΔS_{tot_fc} by the fuel cell stack) and the released entropy flow (Q/T_{air}) by the air [His 08]. The modeling of the thermal management consists of the ambient air (the low temperature source), a thermal flow regulator and an equivalent thermal capacity (Fig.III-8).

The ambient air has a constant temperature, which is lower than the temperature of the fuel cell stack.

The thermal flow regulator is performed by the cooling fan here. By adjusting the air flow, the thermal flow, which is released to the outside of the fuel cell stack, can be regulated:

$$Q'_{cl} = \sigma_{cl}(T_{fc} - T_{amb}) = k_{cl} q_{cl}(T_{fc} - T_{amb}) \qquad \text{(III-25)}$$

with Q'_{cl}: the thermal flow released by the cooling air from the fuel cell stack;
T_{fc}: the temperature of the fuel cell stack;
T_{amb}: the temperature of the ambient air;
σ_{cl}: the equivalent thermal conductivity of the cooling air;

q_{cl}: the cooling air flow;
k_{cl}: a constant coefficient.

The thermal capacity of the fuel cell stack is used to make appear the time-dependent thermal behavior.

$$\frac{dT_{fc}}{dt} = \frac{\Delta S_{tot\_fc} - Q'_{cl} / T_{amb}}{C_{t\_fc}} \tag{III-26}$$

where C_{t_fc} is the specific thermal capacitance of the fuel cell stack.

In order to regulate the temperature T_{fc}, the control scheme is obtained by inverting the path of the modeling equations, which connects the cooling air flow (q_{cl}) to the temperature (T_{fc}). An EMR is used to organize the modelling equations and the control algorithms (Fig.III-10). The used equations are summarized in (Table III-6).

Table III-6: Summary of modeling equations and control algorithms for the oxidant processing

	Modeling equations	Control algorithms
Thermal flow regulator	$Q'_{cl} = k_{cl} q_{cl} (T_{fc} - T_{amb})$	$q_{cl} = \frac{1}{k_{cl}(\hat{T}_{fc} - \hat{T}_{amb})} Q'_{cl\_ref}$
Thermal capacity	$\frac{dT_{fc}}{dt} = \frac{\Delta S_{tot\_fc} - Q'_{cl}}{C_{t\_fc}}$	$Q'_{cl\_ref} = PI(T_{fc\_ref} - \hat{T}_{fc})$

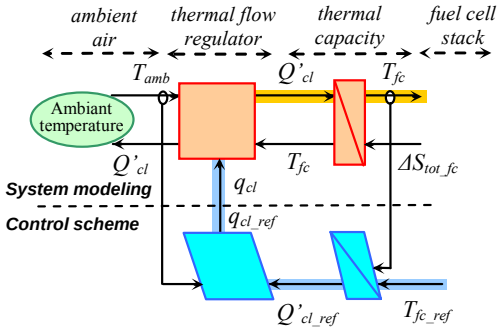

Figure III-10: EMR of the thermal management modeling and control

III.4.5 Overall control and supervision system

With all EMRs of the fuel cell stack and the auxiliary systems, we obtain the EMR of the system modeling and the control scheme of the whole fuel cell system (Fig.III-11). The overall control and supervision is represented in EMR by a strategy block (purple pictogram in Figure III-11). The supervision unit of the fuel cell system should ensure the security and the efficiency of the whole fuel cell system, by taking into account the working capacity of each subsystem and all measured variable values. Some control decisions should be made with anticipated forecasting. Some control signals should be conditioned and adapted according to the control capacity of each subsystem (eg. Fuel cell power p_{fc}). In case of subsystem's failure, alarming system should be triggered and the system should stand by or automatically stop in sequence if necessary.

The overall control of the fuel cell system is the control interface between inside and outside. It receives external requirements from outside the fuel cell system and "translates" them into internal instruction through some controllable variables' references (eg. fuel cell

current i_{fc_ref} and pressures p_{H2} and p_{O2}) or through some operation intervals (eg. fuel cell temperature T_{fc_ref}).

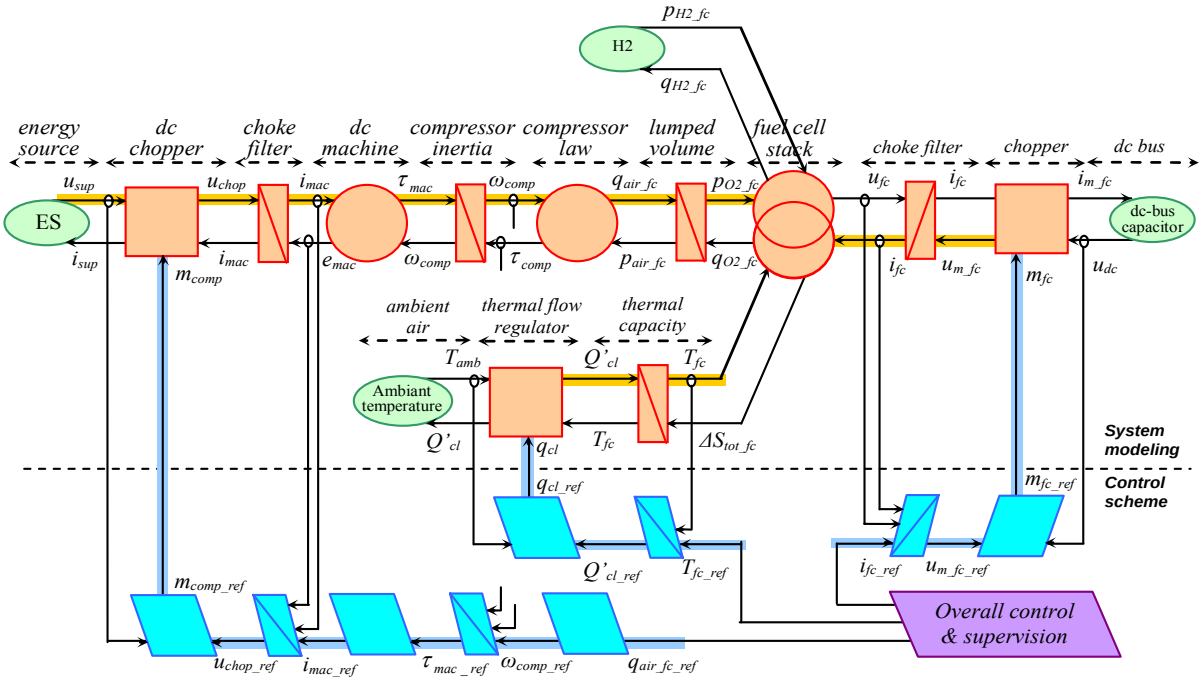

Figure III-11: EMR of the fuel cell system modeling and control

a) Pressures

According to the pressure level of the reactants, the fuel cell can be divided into two categories: pressurized fuel cell and atmospheric fuel cell. For pressurized fuel cells, the reaction performance varies with the pressure conditions. Moreover, the differential pressure between the two electrodes should be controlled below a certain level (eg. 0.1bar) to avoid breaking the membrane. Therefore, the pressures should be precisely controlled both in the anode and in the cathode. The pressure references (p_{H2_ref} and p_{O2_ref}) should be set, and the sophisticated pressure control loops should be considered to control the air flow in order to precisely control the reactant pressures and the differential pressure for security and efficiency reasons.

In our study, we use the atmospheric fuel cells. Since the (opened) system is well sized and the reactants' pressures are both near the atmospheric pressure, the differential pressure is in the required interval. In practice, the air flow reference (q_{air_ref}) is given according to the estimation of the oxygen consumption with the fuel cell current, but 1.5 times or twice more than consumed in the reaction.

$$q_{air\_fc\_ref} = \frac{1}{k_{O2}} q_{O2\_fc} = \frac{n_{fc}}{4Fk_{O2}} i_{fc\_ref} \qquad \text{(III-27)}$$

where k_{O2} is an empirical parameter and is based on the concentration of the oxygen in the air and the required surplus oxygen supply.

b) Temperature

The operation temperature interval is required according to the type of the fuel cell. The fuel cell temperature should be controlled in this interval for efficiency and security reasons. The temperature control system can be more or less sophisticated. With an accurately controlled cooling system (by circulating water), the overall control unit needs only to set the

temperature reference (T_{fc_ref}), which is used by the control loop to set the water flow reference. With a less precisely control cooling system (by cooling fan), the overall control system should directly control the cooling system's power. For example, when the fuel cell supplies a high power, a high power reference for the cooling fan should be given, in order to prevent the temperature increasing upon the upper limit for security reasons. When the fuel cell supplies a low power, a less power reference is given for the cooling fan for efficiency reasons.

c) Power

The fuel cell stack supplies an unregulated DC power,

$$p_{fc} = u_{fc} i_{fc} . \tag{III-28}$$

with a very non-linear characteristic. Since the fuel cell is considered as a voltage source (u_{fc}), the power can be controlled by regulating the fuel cell current (i_{fc}). So the power reference (p_{fc_ref}) of the fuel cell stack can be converted into the current reference (i_{fc_ref}). Two methods can be used.

- ***by a division operator***: The current reference (i_{fc_ref}) can be obtained by dividing the power reference (p_{fc_ref}) by the measured fuel cell voltage (u_{fc}),

$$i_{fc\_ref} = \frac{p_{fc\_ref}}{\widehat{u}_{fc}} . \tag{III-29}$$

- ***by a look-up table***: The static model of the fuel cell stack can be implemented in a look-up table. For each power reference (p_{fc_ref}), a current reference (i_{fc_ref}) can be directly found in the table in order to avoid the division by zero,

$$i_{fc\_ref} = LUT\left(p_{fc\_ref}\right). \tag{III-30}$$

d) Dynamic

Due to the low-dynamics of the auxiliary systems, the power dynamic should be limited. So the supervision system should verify the power reference's dynamic and should limit its variation rate in an acceptable level. Two solutions can be considered:

- A slope limiter for the power reference (p_{fc_ref}) or for the current reference (i_{fc_ref}) to limit the rate of variation, before sending the reference to the control loop;
- A low-pass filter can be applied for the power reference (p_{fc_ref}) or the current reference (i_{fc_ref}) to slow down the variation, before sending the reference to the control loop.

Since the power slope of the fuel cell is limited, a power buffer is usually necessary as an auxiliary energy source. In general, batteries are often used, but flywheels and super-capacitors are also encountered. This auxiliary energy source should at least supply the supervision system during startup and emergency shutdown. Moreover, it can also be used to balance the fuel cell stack power according to the power requirement from the load, by supplying the peak power demand and improving the time response to transient load changes. In this case, the power mission can be accomplished with the help of the power buffer and the supervision unit can put in priority the security and lifetime of the fuel cell stack.

III.5 Modeling simplification and identification

III.5.1 Simplification of the modeling

The goal of the work is to integrate the fuel cell system in the hybrid power system with some power management algorithms. So we focus on the electrical characteristics of the fuel cell system and some auxiliary parts can be simplified.

The fuel cell stack is intrinsically able to quickly react to the load changes, since the electrical and electrochemical time constants are very small. The auxiliaries (hydrogen supply, air compressor, gas humidification, cooling circuit and membrane hydration) react much slower, with some time constants that are several hundreds or thousands times higher. So the global dynamic of the fuel cell system is generally considered slow and the power slope (which is required by the load) should be limited enough, so that we can consider a quasi steady-state operation during which the partial pressures (p_{H2} and p_{O2}), the temperature (T_{fc}) and the membrane hydration can be considered constant. As result, the modeling of the fuel cell system can be simplified and the corresponding REM is shown in Fig.III-12.

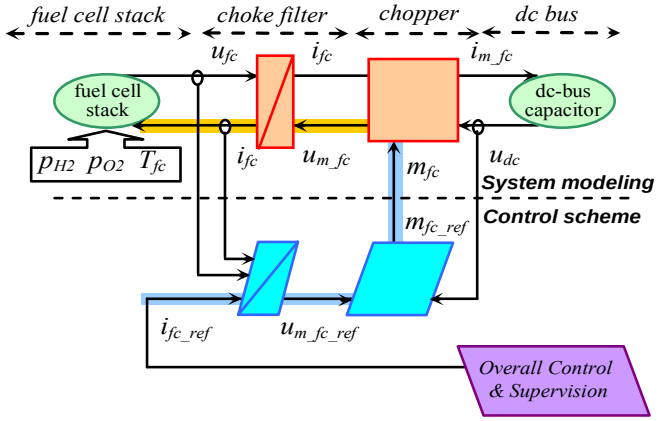

Figure III-12: EMR of a simplified fuel cell system's modeling and control

III.5.2 Experimental characterization of the fuel cell behavior

In order to evaluate the influence of the temperature on the stack voltage, several tests are performed on a Ballard Nexa™ 1200W power module (47 cells of 100 cm^2 in series) at the University of Lille. This fuel cell system has been presented in Paragraph III.2. The voltage-current curves have been recorded for different temperatures: 35°C, 45°C, 55°C and 65°C. We find that the stack voltage increases with the temperature (Fig.III-13).

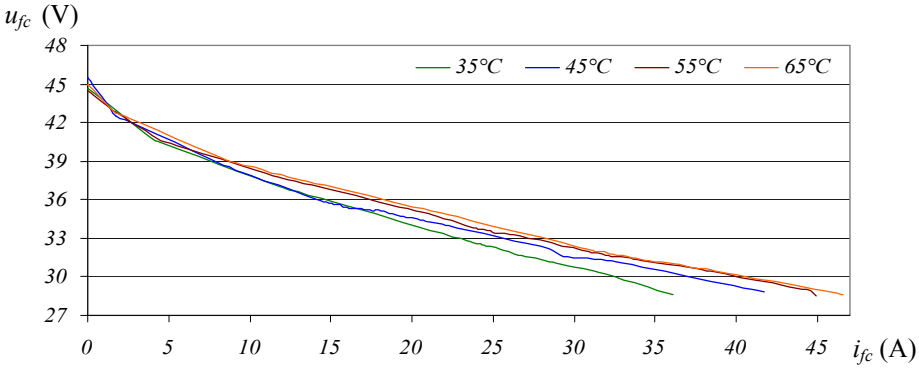

Figure III-13: The fuel cell stack current-voltage characteristics curves for different temperatures (35°C, 45°C, 55°C and 65°C)

III.5.3 Identification of the modeling parameters

In order to validate the fuel cell stack modeling, some modeling parameters should be identified in Eq. II-12:

- A_{fc}: the Tafel slope for the activation losses;
- j_{0_fc}: the minimal current density for the activation losses;
- r_{fc}: the equivalent specific resistance for the ohmic losses;
- B_{fc} : the empiric coefficient for the concentration losses;
- j_{lim_fc} : the maximal current density for the concentration.

For the studied fuel cell stack with 47 cells of 100cm^2 in series, the modeling parameters are identified at 65°C (Table III-5). And these parameters are validated by comparison with the experimental curves (Fig.III-18).

Table III-5: Modeling parameters of the fuel cell modeling in 65°C

p_{H2}	p_{O2}	T_{fc}	A	j_o	B	j_{lim}	r
1bar	0.2bar	65°C	0.027	2μA/cm^2	0.027	2A/cm^2	0.5Ω·cm^2

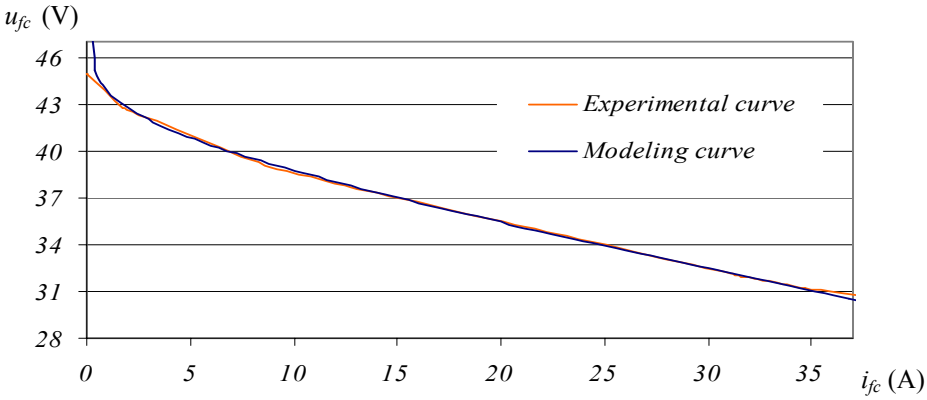

Figure III-14: Comparison between the modeling curve and experimental curve of the fuel cell stack in 65°C

III.5.4 Dynamic limitations in transient states

According to recent works on a 1.2kW PEMFC (Ballard) [Sch 05] and a 0.5kW PEMFC (ZSW) [Tho 06], one of the main weak points of the FC is the fact that its time constants are dominated by the temperature and the fuel delivery system. As result, fast load demand will cause a high voltage drop in a short time, which is known as fuel starvation phenomena [Cor 04][Vah 04] and is harmful for the fuel cell stack [Tho 05][Puk 04]. Thus, to use the fuel cell in dynamic applications, the control system should limit its current or power slope, for example, 4A/s^{-1} for a 0.5kW-12.5V PEMFC [Tho 07]; 2.5kW/ s^{-1} for a 40kW-70V PEMFC [Rod 05]; and 500W/ s^{-1} for a 2.5kW-22V PEMFC [Cor 05].

The studied fuel cells have also an active area of 100cm^2 as the ZWS fuel cell, which is used in [Tho 07]. The same current slope of 4A/s is used for our fuel cell system and it corresponds to a power slope of about 125W/s. The time evolutions of the electrical variables are simulated separately with the current slope limiter and the power slope limiter. In Fig.III-

15a, a current ramp is given from 0.1A to 16A, then from 16A to 32A, and finally from 32A to 0.1A. In Fig.III-15b, a power ramp is given from 5W to 500W, then from 500W to 1000A, and finally from 1000W to 5W.

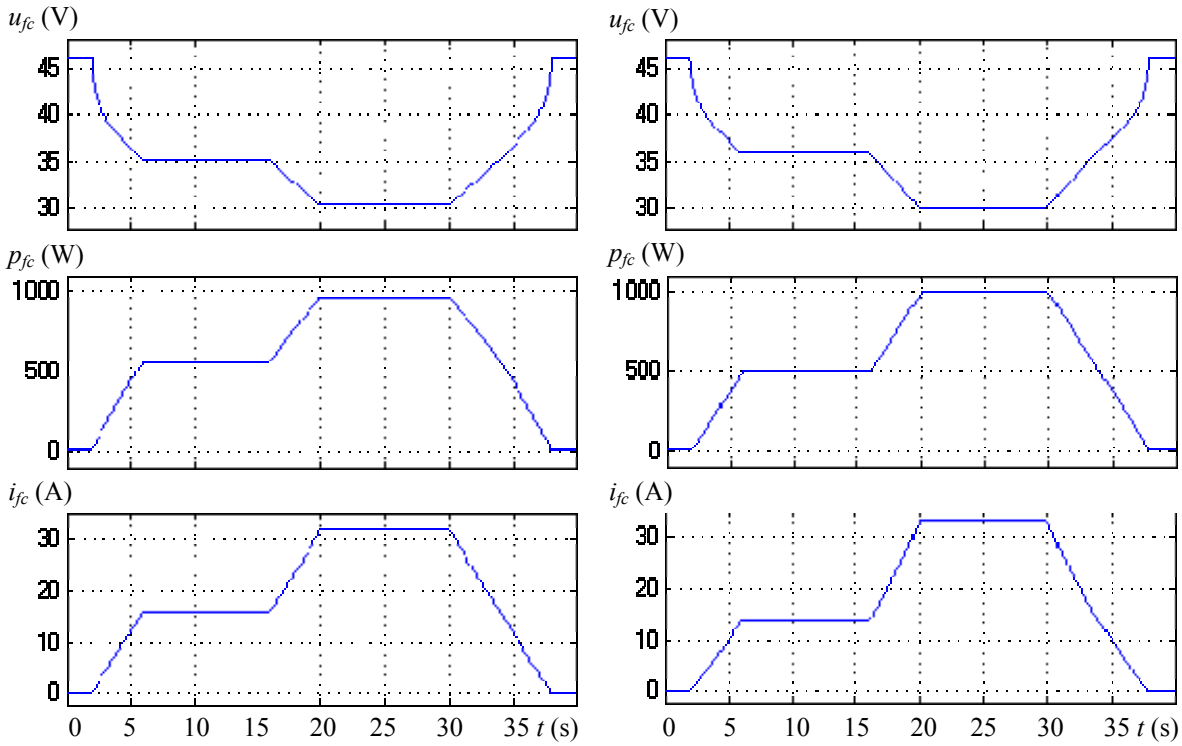

(a) Limitation with a current slope (b) Limitation with a power slope

Figure III-15: Evolution of the electrical variables with a limited slope

III.6 Real-time fuel cell emulator

In our study, we need to test the power balancing and energy management strategies of the hybrid power system on an experimental test bench. In order to make the experimental test bench more flexible, we have decided to build a real-time emulator of the fuel cell system instead of implementing on a real fuel cell system. The real-time emulator has also many other advantages, as explained in the Paragraph I.4.2. In this section, we present the fuel cell emulator by Hardware-In-the-Loop (HIL) simulation.

III.6.1 Structure of the fuel cell Emulator

The fuel cell emulator works like a current dependent voltage source (Fig.III-16a). It can be divided into two stages: the power electronic stage and the control stage (Fig.III-16b).

The power electronic stage consists of a dc-voltage supply and a buck converter including a chopper, a choke and a capacitor (Fig.II-16b). It is properly designed and sized to set the same voltage (u_{fc_emu}) as in the real fuel cell voltage (u_{fc}) according to the measured current (i_{fc}) and the used fuel cell system's models.

The control stage consists of the chopper's driving card, the measurement instruments, the Digital Signal Processing (DSP) card and the interfacing card. A feed-back closed loop is used to control the emulator's output voltage (u_{fc_emu}). The voltage reference u_{fc_ref} is calculated from the fuel cell modeling. The fuel cell modeling is implemented in the DSP card.

For a simplified modeling, the partial pressures (p_{H2} and p_{O2}), the stack temperature (T_{fc}) can be set constant as given parameters. For a more complex modeling, all needed auxiliary modeling and control functions can be algorithmically implemented in the DSP card, then the time evolutions of other quantities (T_{fc}, p_{H2} and p_{O2}) can also be observed through the emulator.

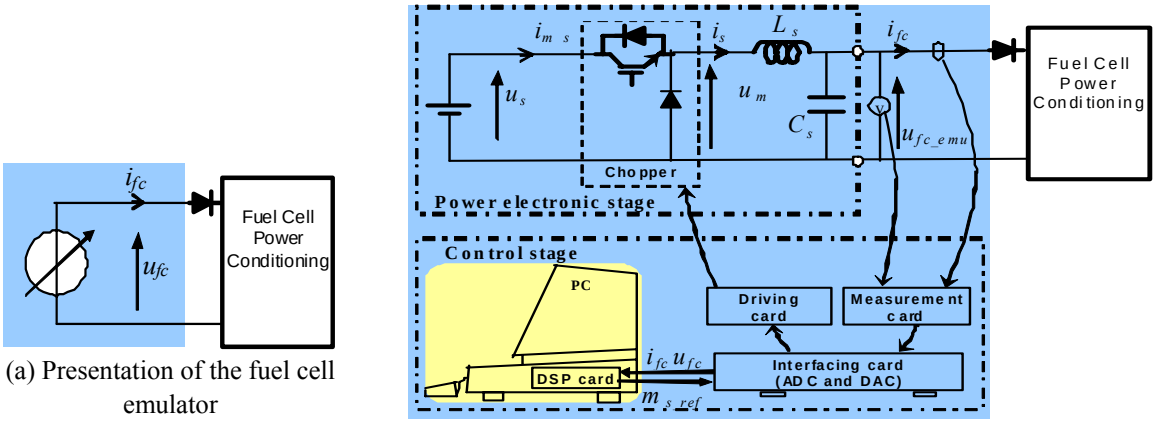

(a) Presentation of the fuel cell emulator as equivalent voltage source

(b) Structure of the fuel cell emulator

Figure III-16: Structure of the fuel cell emulator

III.6.2 Modeling and control of the fuel cell emulator

The EMR of the power electronic stage modeling and the control scheme of the fuel cell emulator are shown in Fig.III-17 and the used modeling equations and control algorithms are summarized in Table III-7.

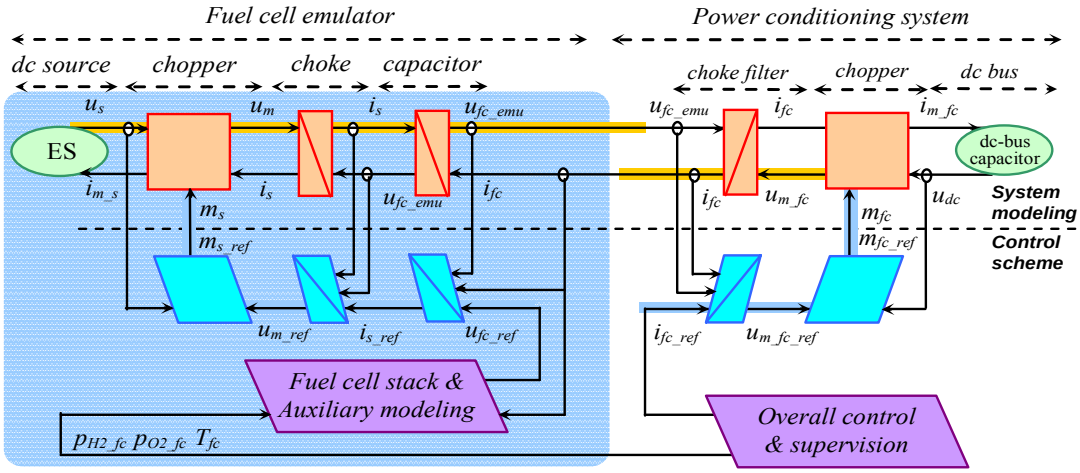

Figure III-17: EMR of modeling and control scheme for the fuel cell emulator and power conditioning unit

Table III-7: Summary of modeling equations and control algorithms for the fuel cell emulator

	Modeling equations	Control algorithms
Chopper	$\begin{cases} u_m = m_s u_s \\ i_{m\_s} = m_s i_s \end{cases}$	$m_{s\_ref} = \dfrac{u_{m\_ref}}{\hat{u}_s}$
Choke	$\dfrac{di_s}{dt} = \dfrac{u_m - u_{fc\_emu}}{L_s}$	$u_{m\_ref} = PI(i_{s\_ref} - \hat{i}_s) + \hat{u}_{fc}$
Capacitor	$\dfrac{du_{fc}}{dt} = \dfrac{i_s - i_{fc}}{C_s}$	$i_{s\_ref} = PI(u_{fc\_ref} - \hat{u}_{fc}) + \hat{i}_{fc}$

a) Emulator modeling

For the power stage, the power supply is modeled by a constant voltage source (u_s). An average model is used for the ***chopper***,

$$\begin{cases} u_m = m_s u_s \\ i_{m\_s} = m_s i_s \end{cases} \tag{III-31}$$

where u_m and i_{m_s} are the average values of the chopper's modulated voltage and modulated current. The ***choke inductor*** current i_s can be described as below,

$$\frac{di_s}{dt} = \frac{u_m - u_{fc\_emu}}{L_s}. \tag{III-32}$$

The voltage across the ***capacitor*** (u_{fc_emu}) is used as the emulated fuel cell voltage,

$$\frac{du_{fc\_emu}}{dt} = \frac{i_s - i_{fc}}{C_s}. \tag{III-33}$$

b) Emulator control

The task of the emulator control is to make the output voltage (u_{fc_emu}) equal to the real fuel cell voltage (u_{fc}) according to the sensed current and the implemented current/voltage characteristic (Fig.II-14).

The control scheme is divided in two parts (Fig.III-17). The first stage is the power electronic stage control. It consists to regulate the output voltage (u_{fc}) in order to make it equal to the reference value (u_{fc_ref}) by a voltage control controller,

$$i_{s\_ref} = PI(u_{fc\_ref} - \hat{u}_{fc}) + \hat{i}_{fc}. \tag{III-34}$$

The obtained reference value (i_{s_ref}) is used as the current reference in the current controller,

$$u_{m\_ref} = PI(i_{s\_ref} - \hat{i}_s) + \hat{u}_{fc}. \tag{III-35}$$

Then the reference of the averaged modulated voltage (u_{m_ref}) is used to generate the duty ratio reference (m_{s_ref}) of the chopper with the measured dc voltage (u_s),

$$m_{s\_ref} = \frac{u_{m\_ref}}{\hat{u}_s} \tag{III-36}$$

The second stage is the modeling of the studied fuel cell stack and auxiliary systems. It consists to calculate the emulated fuel cell's output voltage according to the pressures, the temperature (T_{fc}) and the current (i_{fc}), which is set by the fuel cell power conditioning unit. This current (i_{fc}) is measured and is sent to the "Fuel cell stack and auxiliary modeling" (Table III-5 with the equations from EqIII-7 to Eq.III-16) in the DSP card as the fuel cell current and the voltage of the emulated fuel cell (u_{fc_ref}) can be calculated.

III.6.3 Implementation of the fuel cell emulator

The experimental implementation of the fuel cell emulator is shown in Fig.III-18. The power electronic stage consists of a dc-voltage supply and a buck converter including a chopper, a choke and a capacitor. The control stage consists of an analogical control card for the current control loop and a digital control board (DSpace 1002) for the voltage control loop and the algorithmic modeling of the fuel cell system. The parameters, which are used in the fuel cell emulator implementation, are given in Table III-8.

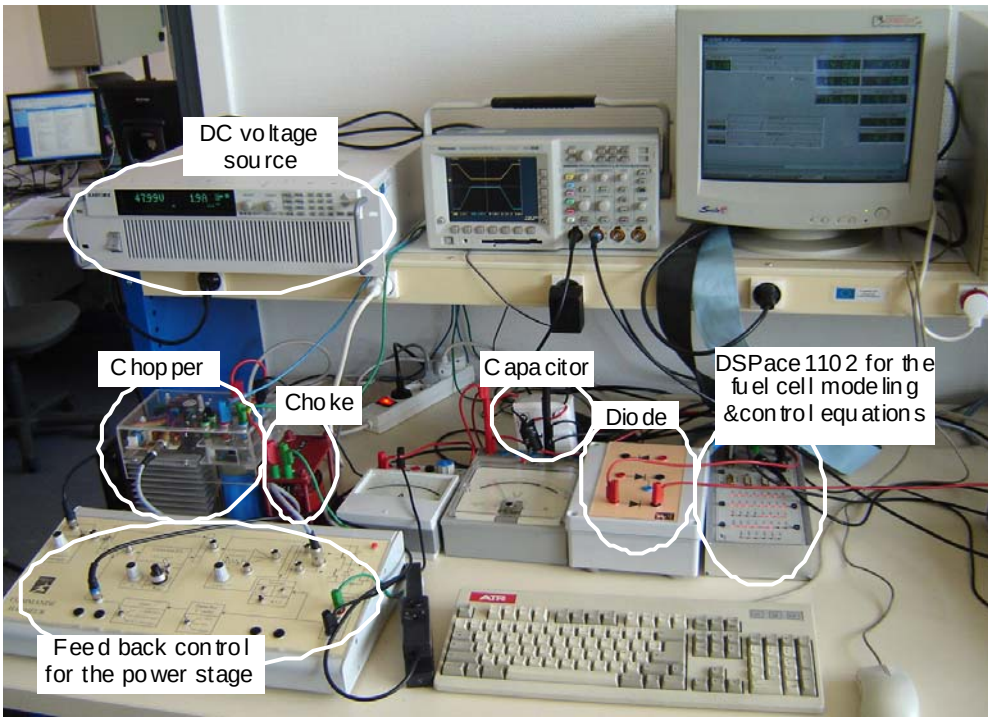

(a) Photo

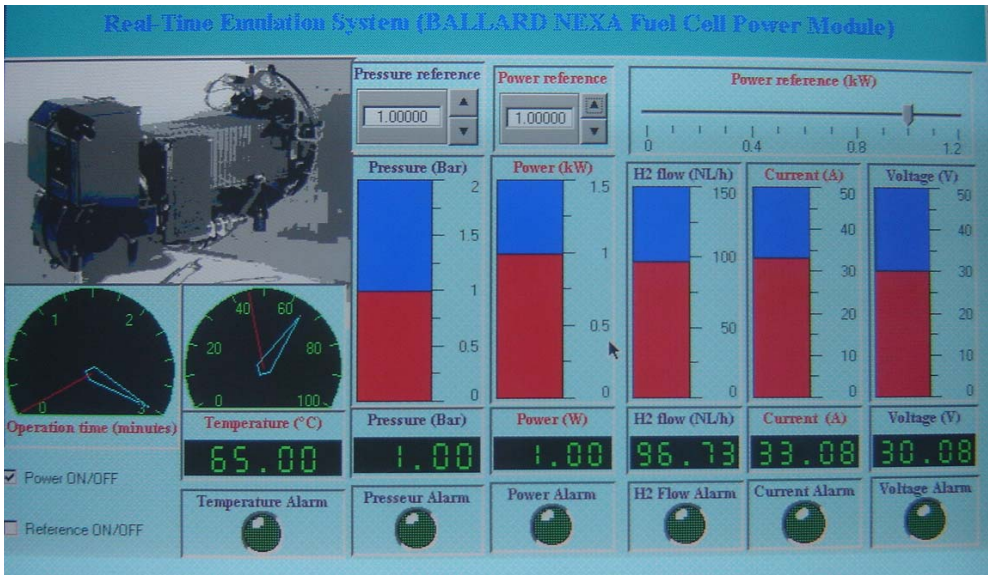

(b) Control panel

Figure III-18: Experimental implementation of the fuel cell emulator

Table III-8: Parameters of the Fuel Cell Emulator

u_s	60	V	L_s	10	mH
L_{fc}	10	mH	C_s	22	µF

III.6.4 Experiment results

By taking into account the fuel cell's power dynamic limit, we give the same power ramp in the fuel cell emulator's experimental test, as in the simulation (Fig.III-15). The same

electrical behaviors are found in the experimental results (Fig.III-19) as in the simulation (Fig.III-15b).

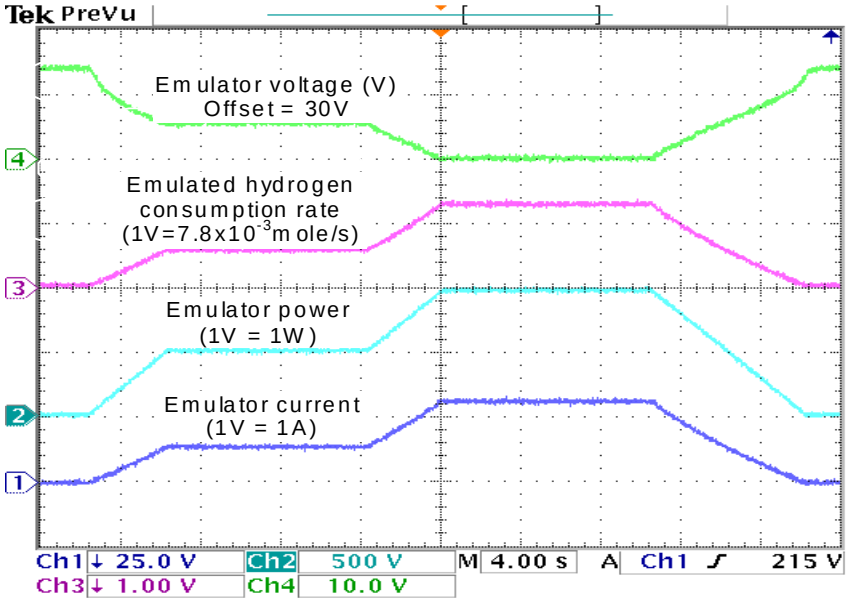

Figure III-19: Time evolution of the emulated variables

Therefore, the fuel cell emulator can be used to test our studied hybrid power system, in order to experimentally test the added control functions and the different power balancing and energy management strategies, which will be presented in Chap.V.

III.7 Conclusion

In this chapter, a system analysis of the studied fuel cell power module is presented. An overview is given on the existing technologies, the operating principles, the fuel cell system, the technical challenges and the modeling methods. In our study, a 1200W Ballard Nexa™ power module is used. The system modeling and control scheme of the studied fuel cell system is presented with the Energetic Macroscopic Representation (EMR) in order to give a better presentation. The modeling parameters are experimentally identified and validated. This model is used to build a fuel cell emulator by Hardware-In-the-Loop simulation. This emulator is a flexible experimental test bench, which will be used to set up the hybrid power system in order to test the control function, power balancing and energy management strategies for the active generator, which will be presented in Chap.V.

Chapter IV

Electrolyzer for Energy Storage into Hydrogen

Chapter IV Electrolyzer for Energy Storage into Hydrogen

The water electrolyzer is an ideal solution for the hydrogen production on site without CO_2 emission. It can avoid the costs of bottled hydrogen delivery and stock management. In the next chapter, we will test this solution to store the surplus energy from intermittent renewable energies.

In this chapter, a system analysis of the electrolyzer is presented. An overview is firstly presented, including the existing technologies, the operating principles, the system performances and commercialized products. More specifically, the CETH GENHY 100® electrolyzer system is used in our study and is presented in detail. A modeling and control scheme of this electrolyzer system is presented graphically by using the Energetic Macroscopic Representation (EMR) in order to give a synthetic view of the whole system. The modeling parameters are validated with experimental tests. The control system is designed in order to use the electrolyzer as a controlled load to damp high power surplus from the wind generator. Finally, a flexible experimental test bench by using Hardware-In-the-Loop simulation is presented in the end of this chapter and validated through performance comparisons. This electrolyzer experimental test bench will be used to implement the active generator in Chap.V.

IV.1 Overview of electrolyzers

IV.1.1 Technologies

There are three existing electrolyzer technologies: (1) the alkaline technology, which is the most developed and mature; (2) the Proton Exchange Membrane (PEM) or Solid Polymer Electrolyte (SPE) technology, which is equivalent to PEM Fuel Cell; (3) the Steam Vapor technology, which is analogue to the Solid Oxide Fuel Cell. Fig.IV-1 compares the electrical characteristics of the three electrolyzer technologies [Wen 91]. The steam vapor electrolyzer has the lowest operating voltage but the maximum current density is still low. Moreover, there are many problems in terms of materials and fabrication and only prototypes exist. The alkaline and PEM electrolyzer are presented as follows.

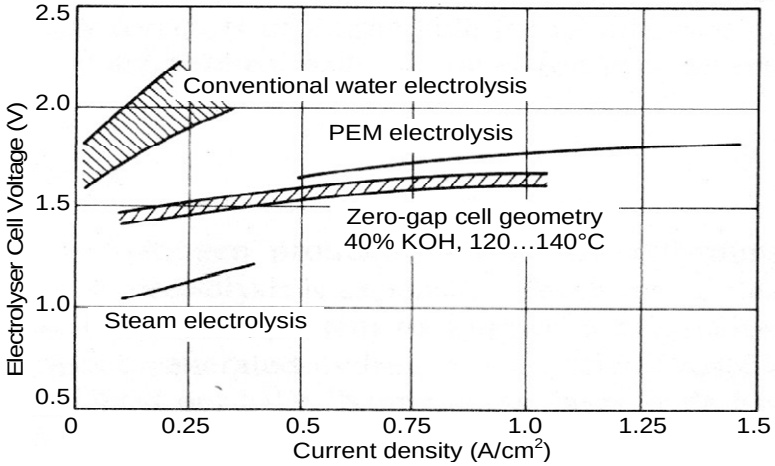

Figure IV-1: Electrical characteristic of different types of electrolyzers [Wen 91].

The alkaline electrolyzers are configured as unipolar (tank) or bipolar (filter press) designs. In the unipolar design (Fig.IV-2a), electrodes are alternatively suspended in a tank that is filled with a solution of electrolyte (potassium hydroxide in pure water). In this design, the cells are connected in parallel and operate at 1.9V-2.5V. The alkaline electrolyzers are very simple to manufacture and repair. However, they usually operate at lower current densities and lower temperatures. [Kon 75].

The bipolar design (Fig.IV-2b) has alternating layers of electrodes and separation diaphragms that are clamped together. The cells are connected in series to obtain higher stack voltages. Since the cells are relatively thin, the overall stack can be considerably smaller than the unipolar design. The bipolar design has the reduced stack size, the higher current densities and the ability to produce higher pressure gas. However, it is more complicated to repair it [Kin 78].

In a PEM electrolyzer, the electrolyte is contained in a thin, solid and ion-conducting membrane [Kon 75] rather than the aqueous solution in the alkaline electrolyzers. This allows the H^+ ion (i.e., proton) to transfer from the anode side of the membrane to the cathode side and separates the hydrogen and oxygen gases. Oxygen is produced at the anode side and hydrogen is produced on the cathode side. The most commonly used membrane material is Nafion® from Dupont. PEM electrolyzers use the bipolar design and can be made to operate at a high differential pressure across the membrane.

Electrolyzer technologies are in fast development and important improvements are being made in the following field: (1) the change of geometry, in order to reduce the ohmic losses and to increase the volumetric power density; (2) the increase of the operating temperature, in order to improve the electrolyte conductivity and to reduce the electrode voltage drop; (3) the development of new catalysts, in order to activate the electrochemical reaction easier and to reduce the voltage drops; (4) the increase of operating pressure, in order to operate in higher temperatures and to increasing electrolyte conductivity.

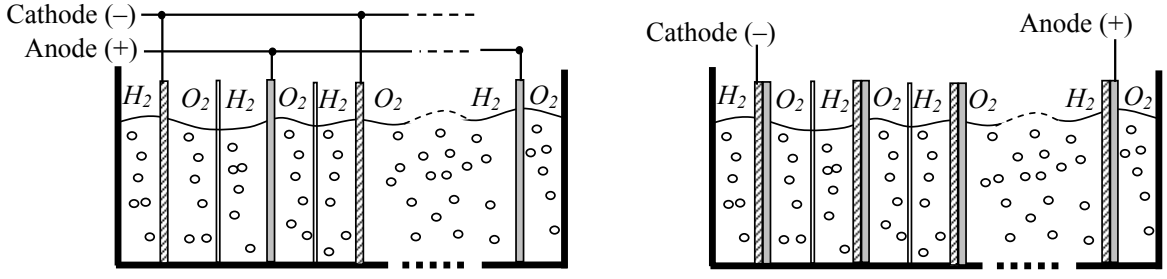

(a) Unipolar Design (b) Bipolar Design

Figure IV-2: Alkaline electrolyzer designs

IV.1.2 Operating principles

An electrolyzer splits water into hydrogen and oxygen when it is electrically supplied. An electrolyzer cell is made up of: (1) two electrodes, which activates the electrochemical reactions; (2) an electrolyte permitting the ionic transfers; (3) a membrane between the two electrodes. The operating principles of alkaline electrolyzers and PEM electrolyzers are illustrated in Fig.IV-3. Their technical differences are summarized in Table IV-1.

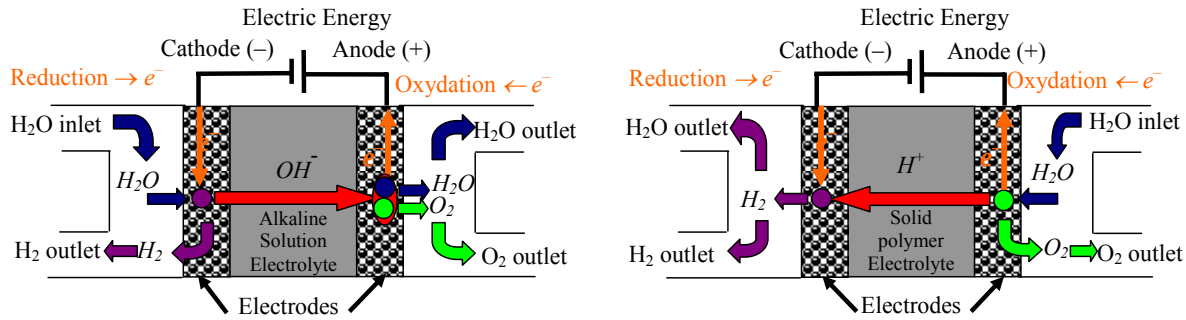

(a) Alkaline electrolyzer (b) PEM electrolyzer

Figure IV-3: Operating principles of electrolyzers

Table IV-1: Technical comparison between alkaline electrolyzers and PEM electrolysers

	Alkaline Electrolyzer	**PEM Electrolyzer**
Electrolyte	Alkaline solution	Solide polymer electrolyte
Charge carrier	OH^-	H^+
Cathode reaction	$4H_2O + 4e^- \rightarrow 2H_2 + 4OH^-$	$4H^+ + 4e^- \rightarrow 2H_2$
Anode reaction	$4OH^- \rightarrow O_2 + 2H_2O + 4e^-$	$2H_2O \rightarrow O_2 + 4H^+ + 4e^-$
Global reaction	$4H_2O \rightarrow 2H_2 + O_2 + energy$	$4H_2O \rightarrow 2H_2 + O_2 + energy$

IV.1.3 System performance

a) Electrolyzer stack

The electrolyzer stack is the key component of an electrolyzer system and performs the main function of energy conversion within the system, as well as the fuel cell stack in the fuel cell system. Since the voltage of a single cell is quite small, a number of cells should be connected in series to obtain a higher voltage, which can be used by other electrical systems.

The electrical characteristics of an electrolyzer stack depend on the used electrolyzer technology (see above); on the number of cells (which determines the operating voltage of the stack); and on the active area (which defines the maximum current of the stack).

Fig.IV-4 shows the electrical characteristics of an alkaline cell. The open circuit voltage is about 1.23V. When the current increases, losses become important and the operating voltage increases. The alkaline cell voltage is usually limited to 2V.

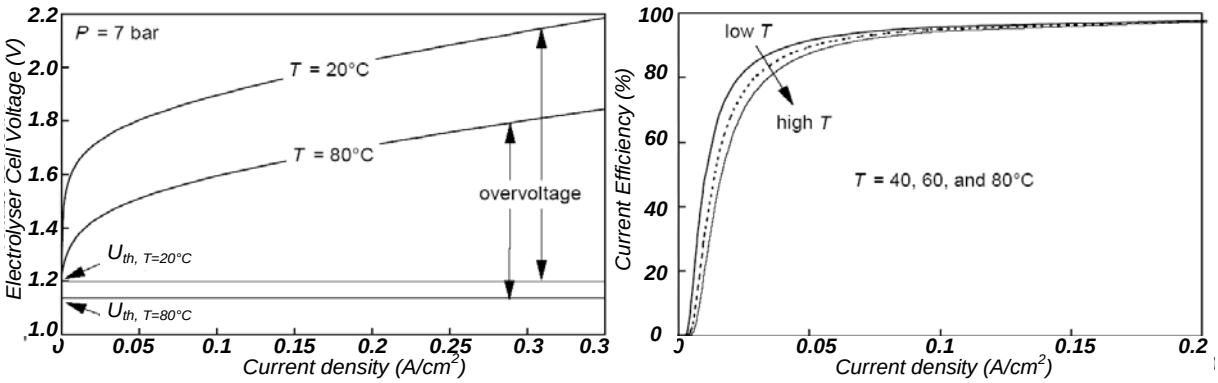

Figure IV-4: Influence of the temperature and the current on voltage efficiency and current efficiency (alkaline electrolyzer) [Ull 98]

The voltage efficiency, which is also called the energy efficiency, is the ratio of the consumed electrical energy on the global used energy of the reaction. This global energy is the enthalpy, equal to 286kJ/mol at standard condition, equivalent to the thermodynamic voltage equal to 1.48V. The energy efficiency is simply calculated by dividing the thermodynamic voltage by the cell voltage,

$$\eta_{v\_el} = \frac{U_{th}}{U_{cell\_el}} \qquad \text{(IV-1)}$$

with η_{v_el}: energy efficiency or voltage efficiency of an electrolyzer cell (%);
U_{cell_el}: operating voltage of an electrolyzer cell (V);
U_{th}: thermodynamic potential (V).

The voltage efficiency decreases when the current increases. It is higher than 74% in case of 2V limitation.

The gas production of an electrolyzer is directly proportional to the current if the current efficiency or Faraday efficiency is constant.

$$q_{H2\_el} = \eta_{i\_el} \frac{n_{el}}{2F} I_{el} \qquad \text{(IV-2)}$$

with η_{i_el}: Faraday efficiency or current efficiency of an electrolyzer cell (%);
q_{H2_el}: hydrogen flow, produced by the electrolyzer (mol/s);
n_{el}: number of the electrolyzer cells in series;
F: Faraday constant (electrical charge of 1 mole of electrons), 96485 Coulombs;
I_{el}: current of the electrolyzer (A).

The current efficiency results from the reduction of the gas production due to the migration and recombination of hydrogen and oxygen across the membrane without energy recuperation. This efficiency is usually close to 1.

The power efficiency, or global efficiency, of the electrolyzer stack is evaluated by multiplying the voltage efficiency and the current efficiency,

$$\eta_{p\_el} = \eta_{v\_el} \times \eta_{i\_el}\,, \qquad \text{(IV-3)}$$

where η_{p_el} is the power efficiency of an electrolyzer stack (%).

The gas purity is another essential performance criterion. A part of the gases crosses the membrane. They do not recombine and reduces the purity of produced gases. It becomes dangerous when there is about 4% of hydrogen in oxygen (lower explosive limit) or 4% oxygen in hydrogen. A gas purity measurement unit is needed and this measurement decreases generally the Faraday efficiency.

b) Important parameters

Two parameters, the operating temperature and the pressure, influence the electrolyzer performance, especially the voltage efficiency, the current efficiency and the gas purity.

Increasing the temperature reduces the stack operating voltage because the amount of energy needed to initiate the reaction (activation) is reduced. In other words, the reactions at the electrodes are increased, which lowers the voltage drop (losses) at the electrodes. In addition, the open-circuit voltage of the electrolyzer cells is reduced. So the voltage efficiency (overall energy efficiency) thus increases with the operating temperature (Fig.IV-4). But this can increase the mechanical stress of the other component in the electrolyzer system and the current efficiency and the gas purity decrease with the temperature [Ull 98].

There are also advantages for the electrolyzers to operate at high pressures. These include reductions in specific power consumption, a reduced need for gas compressors and smaller electrolyzer cells.

c) Electrolyzer system

The auxiliary systems ensure the management of the gases, the water, the heat, the pressures and the electrical supply for the electrolyzer stack. They are composed of different sensors, regulators, valves and power electronic converters. All these elements consume a part of the energy, which is supplied to the electrolyzer system. Therefore, the global efficiency of the component (different to the cell efficiency) is defined by the following equation.

$$\eta_{sys\_el} = \frac{p_{gas\_el}}{p_{sys\_el}} = \frac{\eta_{p\_el}\, p_{sta\_el}}{p_{sta\_el} + p_{aux\_el}} \qquad \text{(IV-4)}$$

with η_{sys_el}: global efficiency of an electrolyzer system (%);
η_{p_el}: global efficiency of an electrolyzer stack (%);
p_{gas_el}: power produced in gas form (W);
p_{sys_el}: power consumed by the whole electrolyzer system (W);
p_{sta_el}: power consumed by the electrolyzer stack (W);
p_{aux_el}: power consumed by the auxiliaries of the electrolyzer system(W).

Therefore, even if the power efficiency of an electrolyzer stack is quite high (70-80%) thanks to the directly electrochemical conversion, the global efficiency of an electrolyzer can be reduced (40-50%) due to the intrinsic consumptions by the auxiliary systems.

IV.1.4 Commercialized products

The first applications of electrolyzers were the hydrogen production on site with high power units (30kW to 700kW). The present market is more diversified (hospital, laboratory) but there are also some low power units (5kW). Table IV-1 shows some electrolyzer manufacturers and the main characteristics of their commercialized electrolyzer.

Table IV-2: Main manufacturers of electrolyzer, developed technologies [Dis 01]

Manufacturers	Electrolyte type	Power range	Operating Pressure	Global efficiency	Price
Casale Chemicals SA (Metkon-Alyzer)	Alkaline	2-350kW	5-30bar		5-6€/W
Norks Hydro	Alkaline	35-200kW	15bar	65%	7-8€/W
Vandenborre Hydrogen Systems (Stuart Energy)	Alkaline	3-200kW	10-30bar	74%	3-4€/W
ErreDue	Alkaline		6bar	60%	1-2€/W
Teledyne	Alkaline	0-550kW	7-15bar	58%	3-4€/W
Linde	Alkaline	150W-70kW	2-4bar	62%	
GHW	Alkaline	500kW-2MW	5-30bar		
PIEL (ITL Technology)	Alkaline	2-55kW	3-18bar	48-75%	
Proton Energy (Diamond Lite)	PEM	2-35kW	13bar	60%	7-8€/W
GENHY (CETH)	PEM	0-30kW	2-10bar	70-80%	
Giner, Inc. and Giner Electrochemical Systems	PEM	15-50kW	30-200bar		

The investment cost varies according to the producers. It depends on the cost of the cell, the auxiliaries and the manufacturing mode. The electrolyzer lifetime is long, about 15-20 years for alkaline electrolyzers (manufacturer guarantees) and 150000 hours according to manufacturers of PEM electrolyzers.

IV.2 Studied electrolyzer system

IV.2.1 Introduction

The studied electrolyzer system is GENHY 100® from the European Company of Hydrogen Technologies (CETH). CETH develops, builds and sells hydrogen production and purification systems. Their electrolyzers can be powered from primary renewable energy sources (photovoltaïc arrays, windmills, micro hydraulic plants, etc.) and can also operate in combination with the grid.

The studied electrolyzer stack consists of 7 cells of 75cm^2 in series (Fig.IV-5a). The PEM technologies are used for reduced maintenance, high capacity, no corrosive electrolyte and safe operation. It can work at 800W in maximal power and at 500W in nominal power. The stack covers a range of hydrogen production flow from 5Nl/h (normal liter per hour) to 100Nl/h. The system is designed to produce hydrogen and oxygen from 2bar to 10bar. The pressure comes from electrochemical forces, without any mechanical compression, for energy efficiency improvement.

(a) Electrolyzer stack

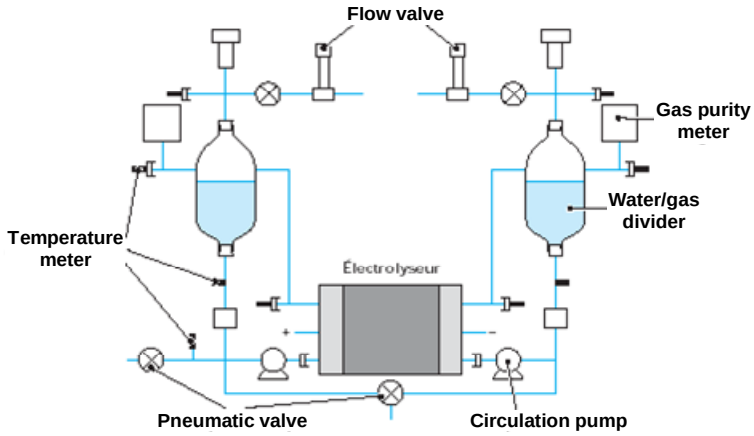

(b) Block diagram of the electrolyzer system

(c) Electrolyzer system

(d) Automatic control unit

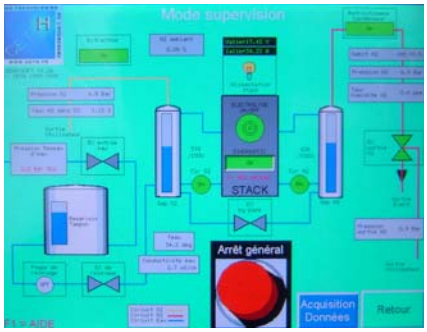

(e) Supervision Screen

Figure IV-5: Studied electrolyzer system (CETH GENHY 100®) [Cet 08]

Auxiliary systems (Fig.IV-5b) are integrated to provide deionized water to each cell and to collect separately generated hydrogen and oxygen. The system also integrates separation and purification means (which remove water traces in the hydrogen stream), pressure regulation means and monitoring and control systems.

The electrolyzer stack and the auxiliary systems are integrated in a compact cabinet (Fig.IV-5c).

IV.2.2 System operation

Remote-control industrial computer is implemented with user friendly tactile screen (Fig.IV-5d). The operation can be directly visualized and ordered through the tactile screen (Figure IV5e). Three automated modes of operation can be performed: storage in metal hydride tanks, H_2 supply for fuel cells and storage in pressurized vessel. The system control can be simplified as shown in Fig.IV-6.

- ***Power conversion***: The electrical power is controlled by a power conversion system, which consists of a stable voltage source, a DC chopper, a filter L_{el} and a filter C_{el}.
- ***Hydrogen handling***: The hydrogen is sent to a metal hydride with a constant pressure, so the hydrogen pressure in the electrolyzer is regulated with an electrovalve (open or closed).
- ***Oxygen handling***: The oxygen is outlet into the atmosphere and the oxygen pressure in the electrolyzer is also regulated with an electrovalve. It should be closed to the hydrogen pressure in order to reduce the membrane's mechanical stress.
- ***Water management***: The water is supplied by a circulating pump with a constant flow, which is sufficient for the reaction requirement and the system cooling need.
-

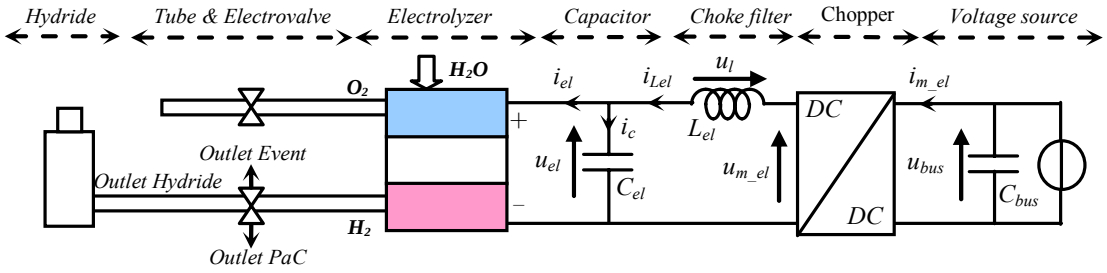

Figure IV-6: Block diagram of the simplified electrolyzer system.

IV.2.3 Experimental tests

An experimental test is firstly done in order to verify the system control and to characterize the timing evolution of the following phisical variables: the temperature T_{el}, the current i_{el}, the voltage u_{el} and the hydrogen pressure p_{H2} (Fig.IV-7).

Some observations can be highlighted. The stack voltage (u_{el}) is a control input and the current (i_{el}) varies with the stack voltage according to the electrolyzer's electrical behavior.

- The voltage supply is limited in variation slope: 0.25V/s for the startup from 0V to 10.5V ($t_1 - t_2$), and 0.05V/s for changing the operating point ($t_5 - t_6$; $t_{15} - t_{16}$; $t_{17} - t_{18}$; $t_{19} - t_{20}$; $t_{21} - t_{22}$);
- The regulation of the hydrogen pressure is performed by an electrovalve. To increase the pressure, the valve is closed and the pressure increases according to the hydrogen

production rate ($t_3 - t_4$; $t_7 - t_8$; $t_9 - t_{10}$; $t_{11} - t_{12}$). To decrease the pressure, the valve is opened and the pressure decreases quickly. If the pressure decreases too much, the valve is closed and the pressure comes back ($t_{13} - t_{14}$). So the electrovalve works more like a switch, whose duty cycle can be used to control the hydrogen outlet flow.

- The temperature has much influence on the stack voltage. The voltage decreases while the temperature increases ($t_2 - t_5$; $t_6 - t_{15}$).
- A pressure below 7bar has a little influence on the stack voltage ($t_6 - t_{15}$).

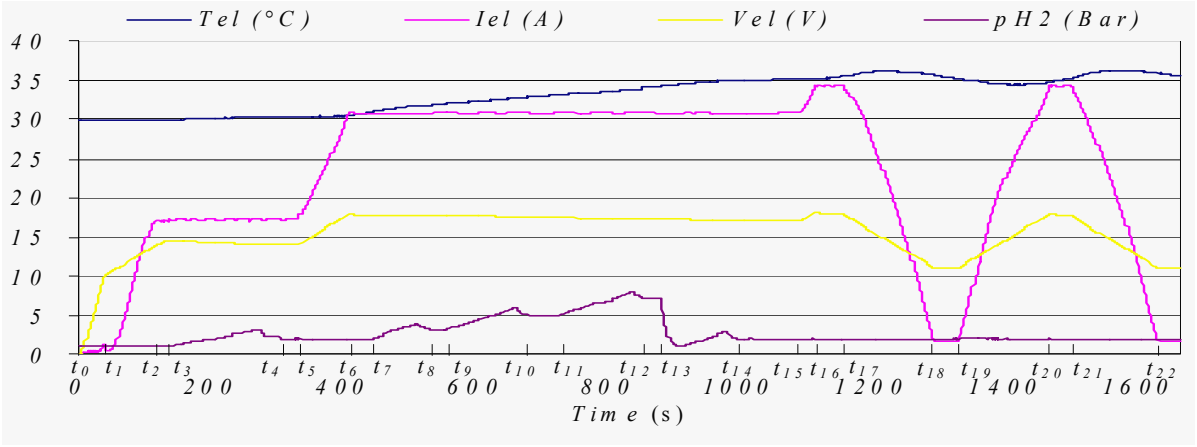

Figure IV-7: Evolution of the main variables in the electrolyzer stack temperature T_{el}, current I_{el}, voltage V_{el} and hydrogen pressure p_{H2}.

IV.3 Modeling of the electrolyzer stack

IV.3.1 Open-circuit voltage

An electrolyzer converts electrical energy into chemical energy. It is the inverse process of the electrochemical reaction in a fuel cell as explained in Paragraph III.2.2. The exchanged chemical energy can be calculated from the change in Gibbs free energy (ΔG_{el}), which is the difference between the Gibbs free energy of the product and the Gibbs free energy of the reactants.

$$\Delta G_{el} = G_{H2} + G_{O2} - G_{H2O} \qquad \text{(IV-5)}$$

with ΔG_{el}: Change of Gibbs free energy in the electrolyzer [J];
ΔG_{H2O}: Gibbs free energy of H_2O [J];
ΔG_{H2}: Gibbs free energy of H_2 [J];
ΔG_{H2O}: Gibbs free energy of O_2 [J].

The change in Gibbs free energy varies with both temperature and pressure [Lar 00],

$$\Delta G_{el} = \Delta G_0 - (T_{el} - T_0)\Delta S_0 - RT_{el} \ln\left(\frac{p_{H2O\_el}}{p_{H2\_el}\, p_{O2\_el}^{0.5}}\right). \qquad \text{(IV-6)}$$

with ΔG_0: change in Gibbs free energy at standard pressure (1 bar), [J];
ΔS_0: the entropy change in standard temperature;
T_0: the standard temperature [K];
T_{el}: temperature of the electrolyzer [K];
p_{H2_el}: partial pressure of the hydrogen in the electrolyzer [bar];

p_{O2_el}: partial pressure of the oxygen [bar];
p_{H2O_el}: partial pressure of the water vapor [bar]
R: universal gas constant 8.31451 J/(kg·K).

In the electrolyzer reaction, the signes of the ΔG_0 and ΔS_0 change and the movement direction of the electrons changes too. As result, the same equation can be obtained for the open-circuit voltage of the electrolyzer cell,

$$R_{el\_1}: \quad E_{el} = E_0 + \Delta E_{el} \tag{IV-7}$$

where

$$E_0 = \frac{\Delta G_0}{2F} = 1.229 \tag{IV-8}$$

and

$$R_{el\_2}: \Delta E_{el} = -0.85 \times 10^{-3}(T_{el} - 298.15) + 4.3085 \times 10^{-5} T_{el} \ln(p_{H2\_el} p_{O2\_el}^{0.5}) \tag{IV-9}$$

IV.3.2 Operation voltage

During the electrolyzer operation, the actual cell voltage V_{cell_el} is higher than the open-circuit voltage,

$$R_{el\_3}: \quad \Delta V_{el} = V_{cell\_el} - E_{el} \tag{IV-10}$$

The voltage drop ΔV_{el} results from several irreversible losses, such as activation losses, ohmic losses and concentration losses, which depend on the current density (j_{el}) [Lar 00]

$$R_{el\_4}: \quad \Delta V_{el} = A_{el} \ln\left(\frac{j_{el}}{j_{0\_el}}\right) + r_{el} j_{el} + B_{el} \ln\left(1 - \frac{j_{el}}{j_{\lim\_el}}\right) \tag{IV-11}$$

where A_{el} and j_{0_el} are the parameters for the activation losses, r_{el} is the parameter for the ohmic losses, B_{el} and j_{lim_el} are the parameters for the concentration losses. And the current density can be obtained by the reciprocal function of Eq.IV-11 through interpolation with a look-up table,

$$R^{-1}{}_{el\_4}: \quad j = R^{-1}{}_{el\_4}(\Delta V_{el}) \tag{IV-12}$$

Then the current of the stack i_{el} is obtained:

$$R_{el\_5}: \quad i_{el} = S_{el} j_{el} \tag{IV-13}$$

with j_{el}: fuel cell current density;
i_{el}: fuel cell current;
S_{el}: active surface area.

IV.3.3 Stack modeling

For the electrolyzer stack of n_{el} cells in series, the production rates of the H_2 and O_2 (q_{H2} and q_{O2}) are described with the Faraday law:

$$R_{el\_6}: \quad q_{H2\_el} = \frac{n_{el}}{2F} i_{el} \tag{IV-14}$$

$$R_{el\_7}: \quad q_{O2\_el} = \frac{n_{el}}{4F} i_{el} \tag{IV-15}$$

The cell voltage can be deduced from the stack voltage u_{el}:

$$R_{el\_8}: \quad V_{cell\_el} = \frac{1}{n_{el}} u_{el} \tag{IV-16}$$

Since the electrolyzer operation is not reversible in practice, the energy losses are converted to heat. In order to present the losses by thermal flow, we define a variable "entropy flow" (ΔS). Then we can describe the power losses in the fuel cell open-circuit voltage as

$$R_{el\_9}: \quad \Delta S_{E\_el} = n_{el} \frac{\Delta E_{el} i_{el}}{T_{el}} \tag{IV-17}$$

and the power losses in the electrolyzer operation as

$$R_{el\_10}: \quad \Delta S_{V\_el} = n_{el} \frac{\Delta V_{el} i_{el}}{T_{el}} \tag{IV-18}$$

The total power losses in thermal flow can be described as

$$R_{el\_11}: \quad \Delta S_{tot\_el} = \Delta S_{E\_el} + \Delta S_{V\_el} \tag{IV-19}$$

IV.3.4 Graphical representation

We can see that an electrolyzer stack is a very complex multi-physic system and many variables are used for its mathematical modeling. In order to highlight the causal relations among the different variables, the modeling equations are organized in a COG and EMR (Fig.IV-8). We can see four quantities, which should be controlled by the auxiliary systems:

- the current (i_{el}) should be controlled by the power conditioning system;
- the hydrogen pressure (p_{H2_el}) should be controlled by the hydrogen handling system;
- the oxygen pressure (p_{O2_el}) should be controlled by the oxygen handling system;
- the temperature (T_{el}) should be controlled by the thermal management system.

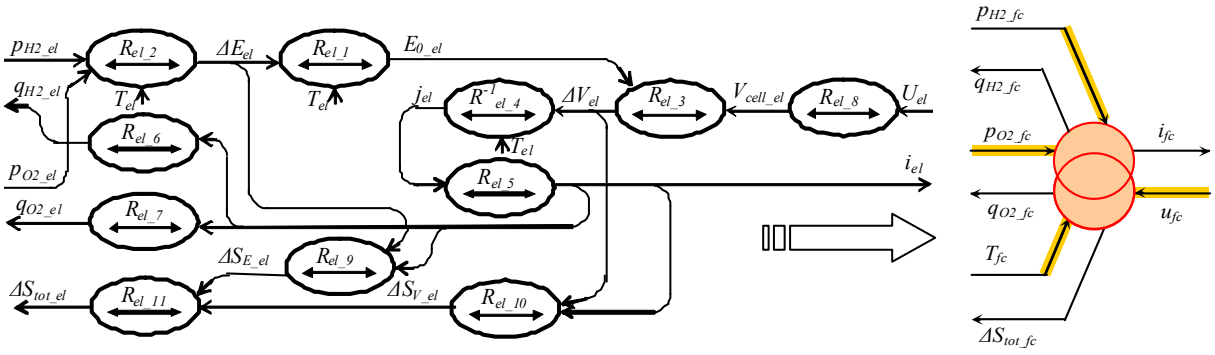

Figure IV-8: COG and EMR of an electrolyzer stack modeling

IV.4 Modeling and control of the auxiliary systems

IV.4.1 Power conversion system

The electrical characteristic of the electrolyzer stack is very non-linear and logarithmic functions have been used for the modeling. As shown in Fig.IV-8, the electrolyzer stack is considered as a current source (i_{el}) here.

Capacitor: A capacitor is needed to set the voltage (u_{el}) across the electrolyzer (Fig.IV-6).

$$\frac{du_{el}}{dt} = \frac{i_{Lel} - i_{el}}{C_{el}}. \tag{IV-20}$$

Choke filter: The current (i_{Lel}) comes from a choke filter, which is modeled as:

$$\frac{di_{Lel}}{dt} = \frac{u_{m\_el} - u_{el}}{L_{el}}. \tag{IV-21}$$

where u_{m_el} is the average value of the chopper's modulated voltage.

Chopper: The average modeling of the chopper is described as below,

$$\begin{cases} u_{m\_el} = m_{el} u_{dc} \\ i_{m\_el} = m_{el} i_{Lel} \end{cases}. \tag{IV-22}$$

where i_{m_el} is the average value of the chopper's modulated current.

DC-bus: The voltage of the DC bus (u_{dc}) is considered here as a constant voltage source, which is maintained by the other sources in the hybrid power system. And m_{el} is the chopper's duty ratio.

The objective of the control scheme is to set the electrolyzer voltage (u_{el}) in order to control the supplied electrical power or the produced hydrogen flow.

The EMR of the power conditioning unit is shown in Fig.IV-9 and the used equations are summarized in Table IV-3. An action path appears from the control input of the DC chopper (m_{el}) to the electrolyzer voltage (u_{el}). The control system of the power conversion system is obtained by inverting this path. It relies on three control functions: a voltage controller, a current controller and a chopper controller.

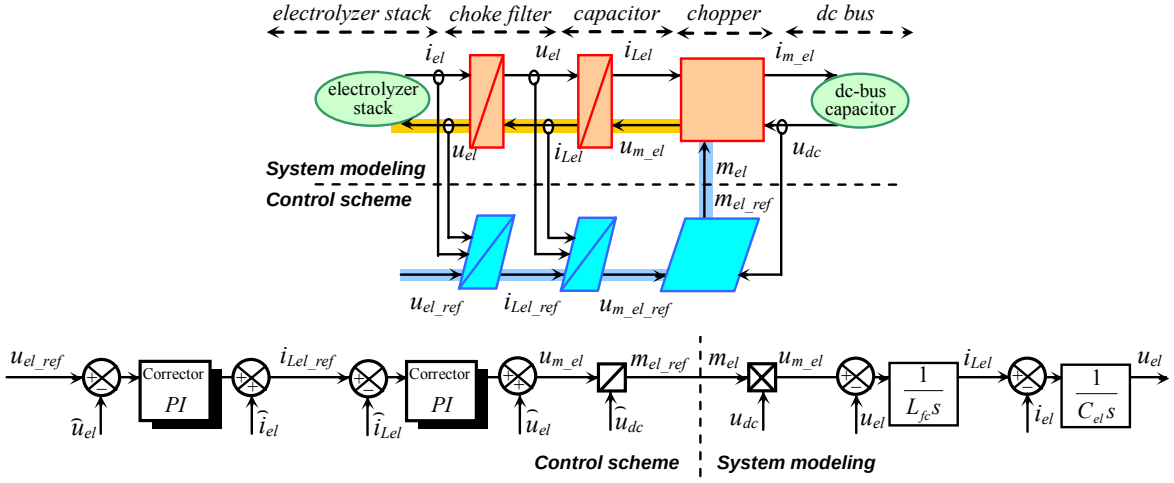

Figure IV-9: EMR and block diagram of the power conversion system modeling and control

Table IV-3: Summary of modeling equations and control algorithms for the oxidant processing

	Modeling equations	Control algorithms
Capacitor	$\frac{du_{el}}{dt} = \frac{i_{Lel} - i_{el}}{C_{el}}$	$i_{Lel\_ref} = PI\left(u_{el\_ref} - \hat{u}_{el}\right) + \hat{i}_{el}$
Choke filter	$\frac{di_{Lel}}{dt} = \frac{u_{m\_el} - u_{el}}{L_{el}}$	$u_{m\_el\_ref} = PI\left(i_{Lel\_ref} - \hat{i}_{el}\right) + \hat{u}_{el}$
Chopper	$\begin{cases} u_{m\_el} = m_{el} u_{dc} \\ i_{m\_el} = m_{el} i_{Lel} \end{cases}$	$m_{el\_ref} = \frac{u_{m\_el\_ref}}{\hat{u}_{dc}}$

Voltage Controller: The electrolyzer voltage is controlled with a PI corrector and a compensation of the electrolyzer current (i_{el}):

$$i_{Lel\_ref} = PI\left(u_{el\_ref} - \hat{u}_{el}\right) + \hat{i}_{el} \tag{IV-23}$$

Current Controller: Another PI corrector is needed to keep the choke current (i_{Lel}) equal to the desired value (i_{Lel_ref}) with a compensation of the electrolyzer voltage (u_{el}):

$$u_{m\_el\_ref} = PI\left(i_{Lel\_ref} - \hat{i}_{el}\right) + \hat{u}_{el} \tag{IV-24}$$

Chopper Controller: With the reference of the averaged chopper's modulated voltage, the reference value m_{el_ref} of the chopper's duty ratio is obtained by inverting Eq.IV-23.

$$m_{el\_ref} = \frac{u_{m\_el\_ref}}{\hat{u}_{dc}} \tag{IV-25}$$

IV.4.2 Hydrogen handling system

The produced hydrogen should be handled and sent to the pressurized hydrogen storage unit (hydride bottles or hydrogen tanks). The organization of modeling equations of the hydrogen handling system is presented in an EMR (Fig.IV-10)

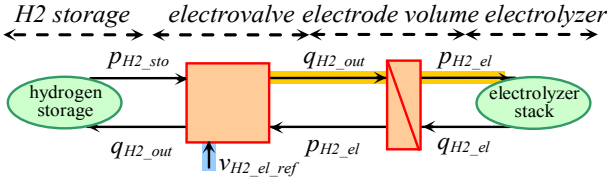

Figure IV-10: EMR of the hydrogen handling system modeling.

The hydrogen storage unit can be modeled as an equivalent pressure source, whose pressure (P_{H2_sto}) depends on the quantity of the stored hydrogen. For most of the time, the pressure (P_{H2_sto}) varies very slowly (for hydrogen tanks) or can be considered as a constant value (for hydrides). Moreover, the hydrogen pressure in the hydride (used in our study) is lower than the pressure (P_{H2_el}), which comes from electrochemical forces of the reaction. A mechanical compression (gas compressor) can be avoided.

An electrovalve is used to control the outlet hydrogen flow.

$$q_{H2\_el\_out} = v_{H2\_el}\frac{p_{H2\_el} - p_{H2\_sto}}{R_{H2\_el}} \tag{IV-26}$$

with q_{H2_out}:the hydrogen outlet flow from the electrolyzer (mol/s);
v_{H2_el}: the state of the hydrogen-side electrovalve, open or closed (1 or 0);
p_{H2_el}: the hydrogen pressure in the electrolyzer (bar);
p_{H2_sto}: the hydrogen pressure in the storage unit (bar);
R_{H2_el}: the equivalent hydraulic resistor of the hydrogen-side tube.

The volume of the electrode can be described through the ideal gas law:

$$\frac{dp_{H2\_el}}{dt} = \frac{q_{H2\_el} - q_{H2\_out}}{C_{el}} = \frac{q_{H2\_el} - q_{H2\_out}}{V_{H2\_el}/RT_{el}} \tag{IV-27}$$

with p_{H2_el}: the hydrogen pressure in the electrode (bar);
q_{H2_el}: the hydrogen production rate (mol/s);

q_{H2_out}: the hydrogen outlet flow (mol/s);
C_{H2_el}: the equivalent volume capacity of the hydrogen-side electrode;
V_{H2_el}: the volume of the hydrogen-side electrode;
T_{el}: the temperature of the electrolyzer.

A hysteresis controller is used to control the hydrogen pressure in the electrode. The measured pressure (p_{H2_el}) value is compared with the reference pressure value ($p_{H2\_el\_ref}$).

$$\begin{cases} v_{H2\_el\_ref} = 1, & if\ p_{H2\_el\_ref} - \hat{p}_{H2\_el} > \Delta p_{H2\_el}; \\ v_{H2\_el\_ref} = v_{H2\_el}, & if\ -\Delta p_{H2\_el} \geq p_{H2\_el\_ref} - \hat{p}_{H2\_el} \geq \Delta p_{H2\_el}; \\ v_{H2\_el\_ref} = 0, & if\ p_{H2\_el\_ref} - \hat{p}_{H2\_el} < -\Delta p_{H2\_el}. \end{cases} \quad \text{(IV-28)}$$

where Δp_{H2_el} is the hysteresis interval of the hydrogen pressure controller.

IV.4.3 Oxygen handling system

The produced oxygen can be stored in a storage unit for future use. In our study, it is outlet in the atmosphere. The similar modeling and control scheme can be applied to the oxygen handing system (Fig.IV-11).

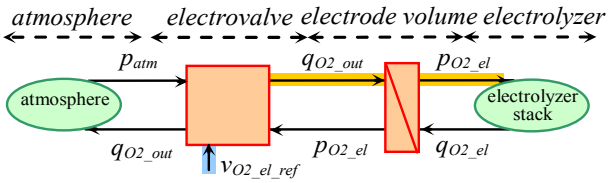

Figure IV-11: EMR of the oxygen handling system modeling.

The atmosphere can be modeled as an equivalent constant pressure source, which is much lower than the oxygen pressure in the electrode.

An electrovalve is used to control the outlet oxygen flow.

$$q_{O2\_el\_out} = v_{O2\_el} \frac{p_{O2\_el} - p_{atm}}{R_{O2\_el}} \quad \text{(IV-29)}$$

with q_{O2_out}:the oxygen outlet flow from the electrolyzer (mol/s);
v_{O2_el}: the state of the oxygen-side electrovalve, open or closed (1 or 0);
p_{O2_el}: the oxygen pressure in the electrolyzer (bar);
p_{atm}: the oxygen pressure in the storage unit (bar);
R_{O2_el}: the equivalent hydraulic resistor of the oxygen-side tube.

The volume of the electrode can be described by the ideal gas law,

$$\frac{dp_{O2\_el}}{dt} = \frac{q_{O2\_el} - q_{O2\_out}}{C_{O2\_el}} = \frac{q_{O2\_el} - q_{O2\_out}}{V_{O2\_el} / RT_{el}} \quad \text{(IV-30)}$$

with p_{H2_el}: the hydrogen pressure in the electrode (bar);
q_{H2_el}: the hydrogen production rate (mol/s);
q_{H2_out}: the hydrogen outlet flow (mol/s);
C_{O2_el}: the equivalent volume capacity of the oxygen-side electrode;
V_{O2_el}: the volume of the oxygen-side electrode;
T_{el}: the temperature of the electrolyzer.

A hysteresis controller is used to control the oxygen pressure in the electrode. The measured pressure (p_{O2_el}) value is compared with the reference pressure value ($p_{O2\_el\_ref}$).

$$\begin{cases} v_{O2\_el\_ref} = 1, & if\ p_{O2\_el\_ref} - \hat{p}_{O2\_el} > \Delta p_{O2\_el}; \\ v_{O2\_el\_ref} = v_{H2\_el}, & if - \Delta p_{O2\_el} \geq p_{O2\_el\_ref} - \hat{p}_{O2\_el} \geq \Delta p_{O2\_el}; \\ v_{O2\_el\_ref} = 0, & if\ p_{O2\_el\_ref} - \hat{p}_{O2\_el} < -\Delta p_{O2\_el}. \end{cases} \quad \text{(IV-31)}$$

where Δp_{O2_el} is the hysteresis interval of the oxygen pressure controller.

IV.4.4 Water and thermal management system

The circulation of water is performed by water pumps. It is used to supply the necessary water, which is needed for the electrochemical reaction and the membrane humidification. It is also used to release the heat, which is created by the reaction, in order to maintain the stack temperature (T_{el}) of the electrolyzer.

The temperature of the stack (T_{el}) depends on the balance of the created entropy flow (ΔS_{tot} by the fuel cell stack) and the released entropy flow (Q/T_{H2O} by the circulating water) [His 08]. It should be maintained in a certain range. However, in the studied electrolyzer system, the water flow is fixed according to the worst condition. In other words, even if the stack works with its maximal power, the water flow is always able to maintain the temperature under maximal level. The EMR of the water and thermal management system modeling is shown in Fig.IV-12.

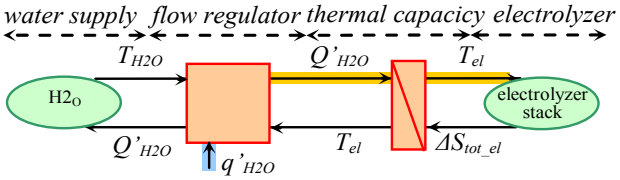

Figure IV-12: EMR of the water and thermal management system modeling.

The water supply can be considered as a constant temperature source.

The water flow regulator is not actually used in our studied system and we assume that a fixed water flow is imposed no matter how much heat the stack creates by reaction. It can be served as a regulation input in the future with some system modification. The thermal flow according to the performed water flow can be expressed as follows:

$$Q'_{H2O} = k_{cl} q_{cl} \left(T_{el} - T_{H2O} \right) \quad \text{(IV-32)}$$

with T_{el}: the temperature of the electrolyzer stack;
T_{H2O}: the temperature of the water source;
k_{cl}: the constant coefficient;
q_{cl}: the cooling water flow.

The thermal capacity of the electrolyzer stack is used to make appear the time-dependent thermal behavior.

$$\frac{dT_{el}}{dt} = \frac{\Delta S_{tot\_el} - Q'_{H2O}}{C_{t\_H2O}} \quad \text{(IV-33)}$$

where ΔS_{H2O} is the thermal flow evacuated by the circulating water and C_{t_H2O} is the specific thermal capacitance of the electrolyzer stack.

IV.4.5 Macroscopic representation of the electrolyzer system

If we combine the EMRs of the stack and the auxiliary systems together, we obtain the EMR of the whole electrolyzer system (Fig.IV-13). Different control inputs are highlighted in the EMR. More or less complicated control means can be implemented for the electrolyzer's operation through these control inputs.

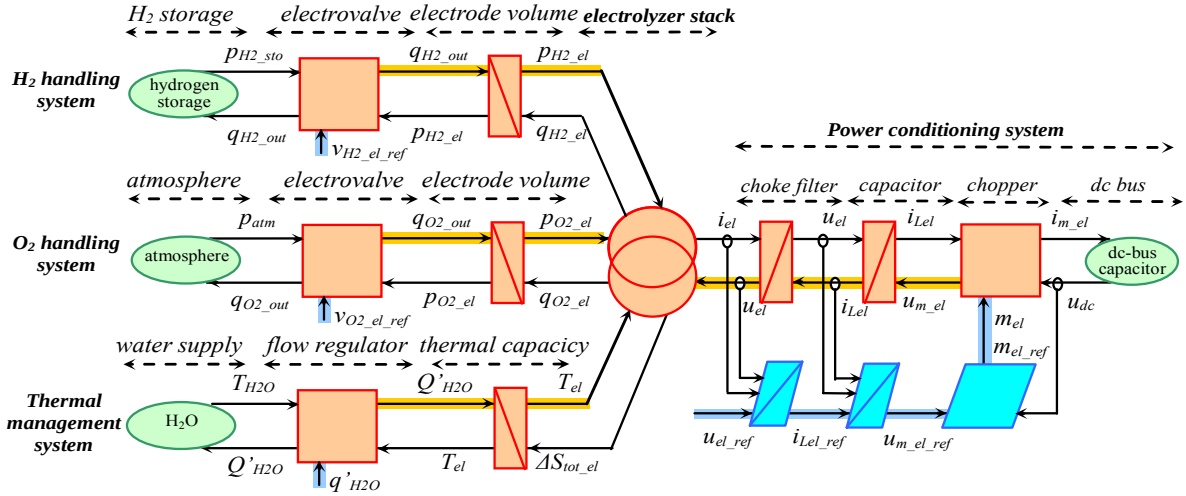

Figure IV-13: EMR of the electrolyzer system modeling.

IV.5 Modeling simplification and identification

IV.5.1 Simplification of the modeling

The goal of the work is to integrate an electrolyzer system in the hybrid power system with some power management algorithms. So we focus on the electrical characteristics of the electrolyzer system. Some auxiliaries can be simplified.

The electrolyzer stack is intrinsically able to quickly react to the load changes, since the electrical and electrochemical time constants are very small [Leb 07]. The auxiliaries (hydrogen and oxygen handling system, water and thermal management) react much slower. So the global dynamic of the electrolyzer system is generally slow. The power slope, which is required by the load, should be limited. Therefore, we can consider a quasi steady-state operation, during which the pressures (p_{H2} and p_{O2}) and the temperature (T_{el}) can be considered constant (well maintained). As result, the modeling and control scheme of the electrolyzer system can be simplified by assuming the physical quantities as constant parameters (Fig.IV-14).

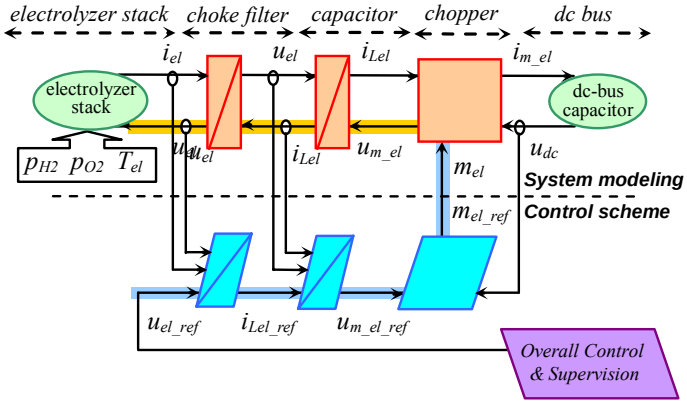

Figure IV-14: Simplified EMR of the electrolyzer system modeling and control.

IV.5.2 Experimental characterization of the electrolyzer behavior

In order to evaluate the influence of the temperature and the pressures on the stack voltage, several tests are performed on a CETH GENHY 100® electrolyzer system (7 cells of 75cm^2 in series) at the Ecole des Mines de Douai. It has been presented in Paragraph IV.2.

a) Influence of the temperature

Several tests are performed in order to evaluate the influence of the temperature on the stack voltage. The pressures (p_{H2_el} and p_{O2_el}) have been set to 7bar, and the voltage-current curves have been recorded for different temperatures: 31°C, 35°C, 40°C and 45°C (Fig.IV-15). We find that the stack voltage decreases with the temperature.

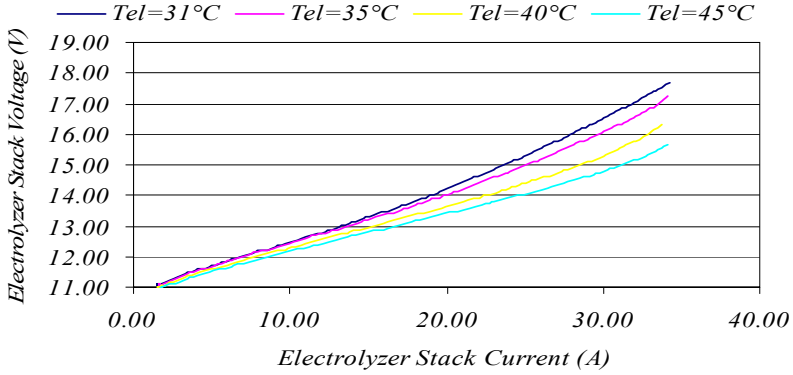

Figure IV-15: Experimental current-voltage characteristics at 7bar with different temperatures (31°C, 35°C, 40°C and 45°C)

b) Influence of the pressure

Several tests are performed with the same temperature (T_{el}=45°C) in order to evaluate the influence of the pressure on the stack voltage. The voltage-current curves have been recorded for different pressures: from 2bar to 7bar (Fig.IV-16). We find that the stack voltage does not vary much with the pressure for the studied system, because 7bar is still too low to modify the stack's voltage-current curve.

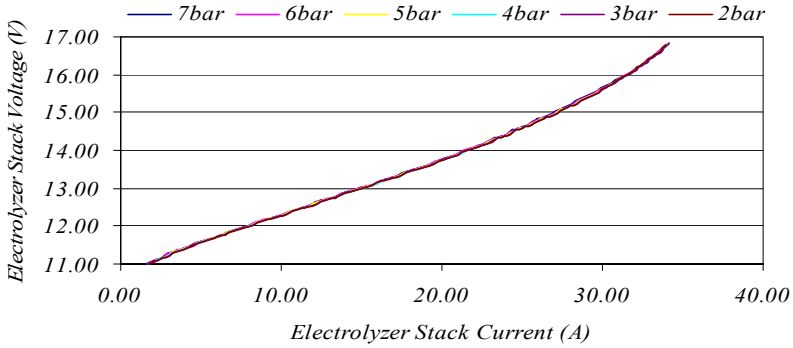

Figure IV-16: Experimental current-voltage characteristics at 45°C with different pressures (from 2bar to 7bar)

IV.5.3 Identification of the modeling parameters

In order to validate the electrolyzer stack modeling, some modeling parameters should be identified in Eq.IV-11:

- A_{el}: the Tafel slope for the activation losses;
- j_{0_el}:the minimal current density for the activation losses;
- r_{el}: the equivalent specific resistance for the ohmic losses;
- B_{el} : the empiric coefficient for the concentration losses;
- j_{lim_el} : the maximal current density for the concentration.

For the studied electrolyzer stack with 7 cells of 75cm^2 in series, the modeling parameters are identified at 45°C and 7bar (Table IV-4). These parameters are used in our simplified modeling and are validated by comparison of the obtained characteristic from simulation results and experimental measurements (Fig.IV-17).

Table IV-4: Modeling parameters of the electrolyzer stack at 45°C and 7bar

p_{H2}	p_{O2}	T_{el}	A	j_o	B	j_{lim}	r
7bar	1.4bar	45°C	0.0441	30μA/cm^2	0.228	0.58A/cm^2	0.5Ω·cm^2

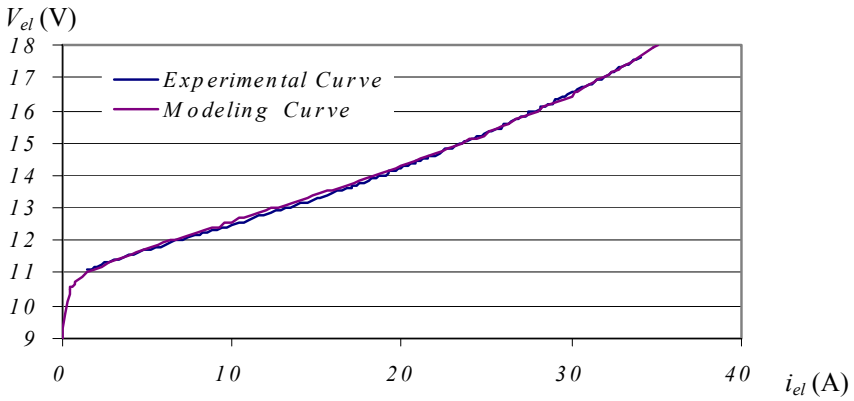

Figure IV-17: Comparison between the modeling curve and experimental curve at 7bar and 45°C

IV.5.4 Dynamic limitations in transient states

The dynamic of the electrolyzer system is dominated by the auxiliary systems (eg. gas handling systems and thermal management system). In practice, the power dynamic of the electrolyzer system should be limited for efficiency and security reasons. For example, when the electrical operating point is stepped, the gas handling systems take some time to regulate the pressures in a good level in order to reduce the mechanic stress of the membrane; the thermal management system takes more time to ensure a homogenous heat evacuation in order to avoid some dangerous hot point on the membrane.

The evolutions of the electrical variables are simulated firstly with a limited voltage slope and then with a limited power slope. In Fig.IV-18a, a voltage ramp of 1.25V/s is given from 10.5V to 13V, then from 13V to 15.5V, and finally from 15V.5V to 10.5V. In Fig.IV-18b, a power ramp of 62.5W/s is given from 5W to 250W, then from 250W to 500W, and finally from 500W to 5W.

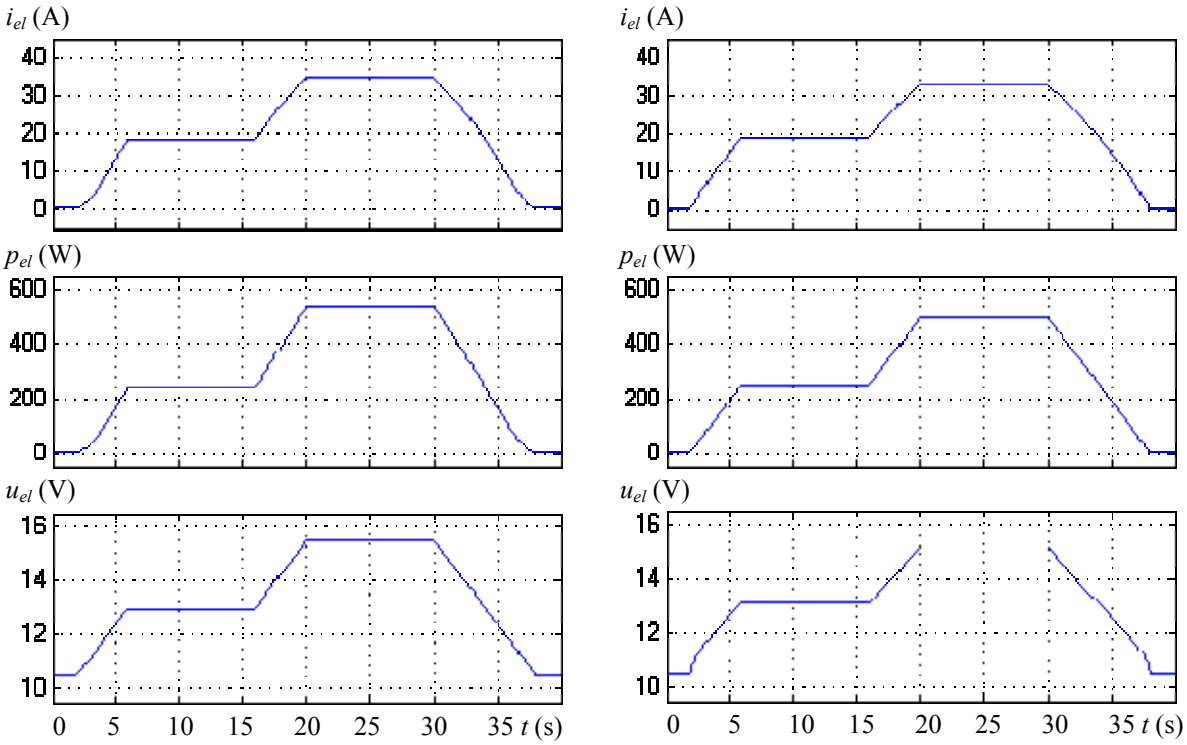

(a) Limitation with a voltage slope (b) Limitation with a power slope

Figure IV-18: Evolution of the simulated electrical variables with limited slope

IV.6 Real-time electrolyzer emulator

In our study, we need to test the power balancing and energy management strategies of the hybrid power system on an experimental test bench. In order to make the experimental test bench more flexible, we have decided to build a real-time emulator of the electrolyzer system instead of using the studied commercial electrolyzer system. Its power slope is limited too slow in comparison with its power range (Fig.IV-7) and we do not have access to modify it for implementing interested control functions in our application [Cet 07]. Moreover, the real-time emulator has also many other advantages in comparison with the real components, as explained in the Paragraph I.5.2. In this section, we present the fuel cell emulator by Hardware-In-the-Loop (HIL) simulation [Zho 09].

IV.6.1 Structure of the electrolyzer emulator

The emulator works as a current source like the real electrolyzer (Fig.IV-19a). It can be divided into two stages: the power electronic stage and the control stage (Fig.IV-19b).

The power electronic stage consists of a dc-voltage supply and a buck converter including a chopper, a choke and a capacitor. It is properly designed and sized to set the same voltage (u_{el}) as in a real electrolyzer system according to the measured current (i_{el}) and the used electrolyzer system's models.

The control stage consists of the chopper's driving card, the measurement instruments, the digital control board (DSpace 1102) and the interfacing card. A feed-back closed loop is used to make the emulator's output current (i_{el_emu}) equal to the current reference (i_{el_ref}),

which is calculated from the electrolyzer modeling with the sensed voltage (u_{el}). The electrolyzer modeling is implemented in the DSpace 1102. For a simplified modeling, the partial pressures (p_{H2} and p_{O2}), the stack temperature (T_{el}) can be set constant as given parameters. For a more complex modeling, all needed auxiliary modeling and control functions can be algorithmically implemented in the DSP card. The time evolutions of other quantities (T_{el}, p_{H2} and p_{O2}) can also be observed through the emulator.

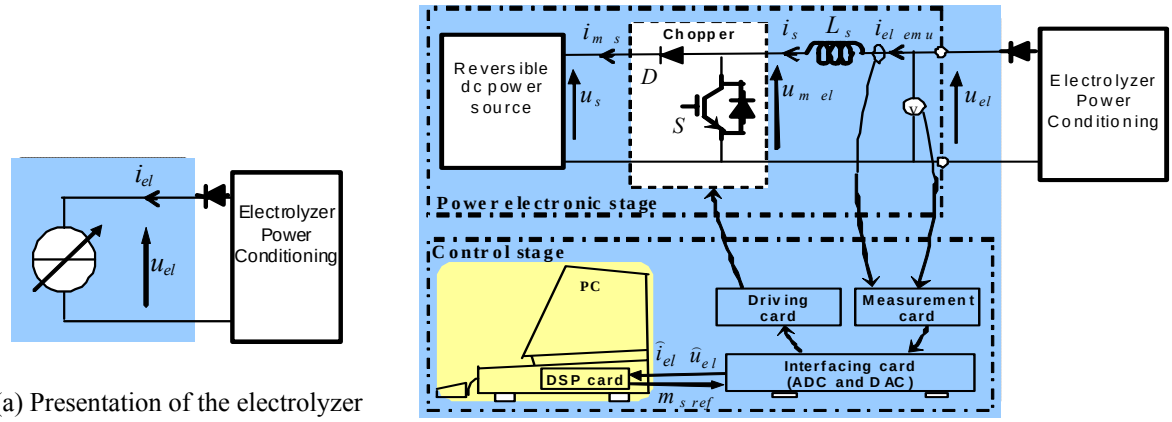

(a) Presentation of the electrolyzer emulator as equivalent current source

(b) Structure of the electrolyzer emulator

Figure IV-19: Structure of the Electrolyzer emulator

IV.6.2 Modeling and control of the electrolyzer emulator

The EMR of the power electronic stage modeling and the control scheme of the electrolyzer emulator are shown in Fig.IV-20 and all the used modeling equations and control algorithms are summarized in Table IV-5.

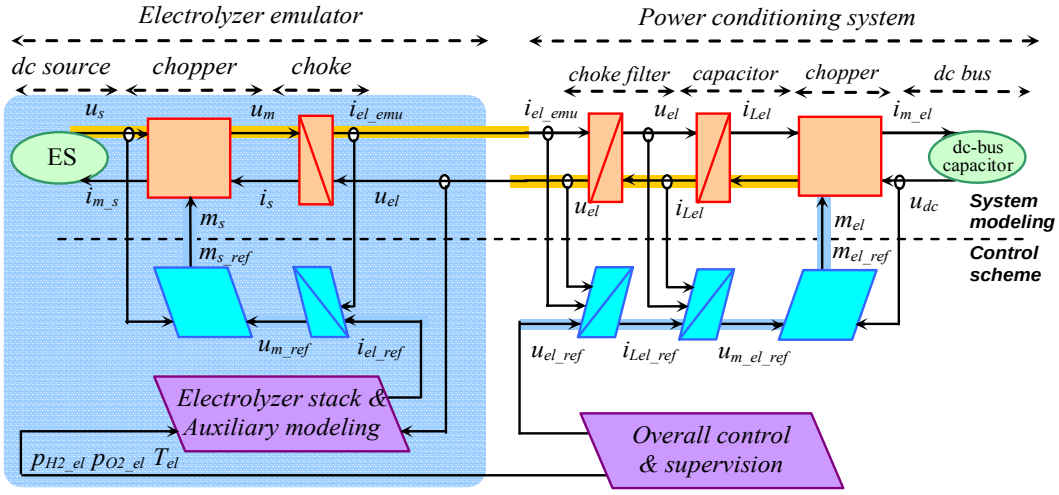

Figure IV-20: EMR of modeling and control scheme for the electrolyzer emulator.

Table IV-5: Summary of modeling equations and control algorithms for the fuel cell emulator

	Modeling equations	Control algorithms
Chopper	$\begin{cases} u_m = m_s u_s \\ i_{m\_s} = m_s i_s \end{cases}$	$m_{s\_ref} = \dfrac{u_{m\_ref}}{\hat{u}_s}$
Choke	$\dfrac{di_{el\_emu}}{dt} = \dfrac{u_{el} - u_m}{L_s}$	$u_{m\_ref} = \hat{u}_{el} - PI(i_{el\_ref} - \hat{i}_{el\_emu})$

a) Emulator modeling

For the power stage, the power supply is modeled by a constant voltage source (u_s). An average model is used for the ***chopper***:

$$\begin{cases} u_m = m_s u_s \\ i_{m\_s} = m_s i_s \end{cases}, \tag{II-34}$$

where u_m and i_{m_s} are the average values of the chopper's modulated voltage and modulated current. The ***choke*** current (i_{el_emu}) can be described as below,

$$\frac{di_{el\_emu}}{dt} = \frac{u_{el} - u_m}{L_s} \tag{II-35}$$

b) Emulator control

As shown in Fig.IV-20, the current from the emulator can be adjusted by the control input of the DC chopper (m_{s_ref}). The strategy consists to set a reference value of the current from the previously presented current-voltage characteristic. The control scheme is divided in two parts (Fig.IV-20).

The first one is the power electronic stage control. It consists to regulate the output current (i_{el_emu}) to make it equal to the reference value (i_{el_ref}) by a PI corrector and a compensation of the electrolyzer voltage,

$$u_{m\_ref} = \hat{u}_{el} - PI(i_{el\_ref} - \hat{i}_{el\_emu}) \tag{II-36}$$

Then the reference of the averaged modulated voltage (u_{m_ref}) is used to generate the duty ratio reference (m_{s_ref}) of the chopper with the measured dc voltage (u_s),

$$m_{s\_ref} = \frac{u_{m\_ref}}{\hat{u}_s} \tag{II-37}$$

The second stage is the modeling of the electrolyzer stack and auxiliary systems. It consists to calculate the emulated electrolyzer's output current according to the pressures, the temperature and the voltage (u_{el}), which is set by the electrolyzer power conditioning unit. This voltage (u_{el}) is measured and is sent to the "Electrolyzer stack and auxiliary modeling" in the DSP card as the electrolyzer voltage. Then the current of the emulated electrolyzer (i_{el_ref}) is then calculated with this voltage and serves as the reference for the current control loop.

IV.6.3 Implementation of the electrolyzer emulator

The implementation of the electrolyzer emulator is shown in Fig.IV-21. The power electronic stage consists of a regenerative DC voltage source, a DC chopper, a choke and a diode. The control stage consists of an analogical control card for the current control loop and a digital control board (DSpace 1002) for the mathematical modeling of the electrolyzer system. The parameters, which are used in the electrolyzer emulator implementation, are given in Table IV-6.

Different auxiliary system models and their control algorithms can also be implemented in the DSP card, according to different purposes and methods. For example, we can implement the auxiliary system's model described above to establish the relation between the electrolyzer and the hydrogen storage. The variation of the different physical quantities can

also be simulated in the DSP card and verified via the computer desk in real time, such as the hydrogen outlet flow rate and the hydrogen pressure in the storage.

Table IV-6: Parameters of the electrolyzer emulator

u_s	60	V	L_s	10	mH
L_{el}	10	mH	C_{el}	22	µF

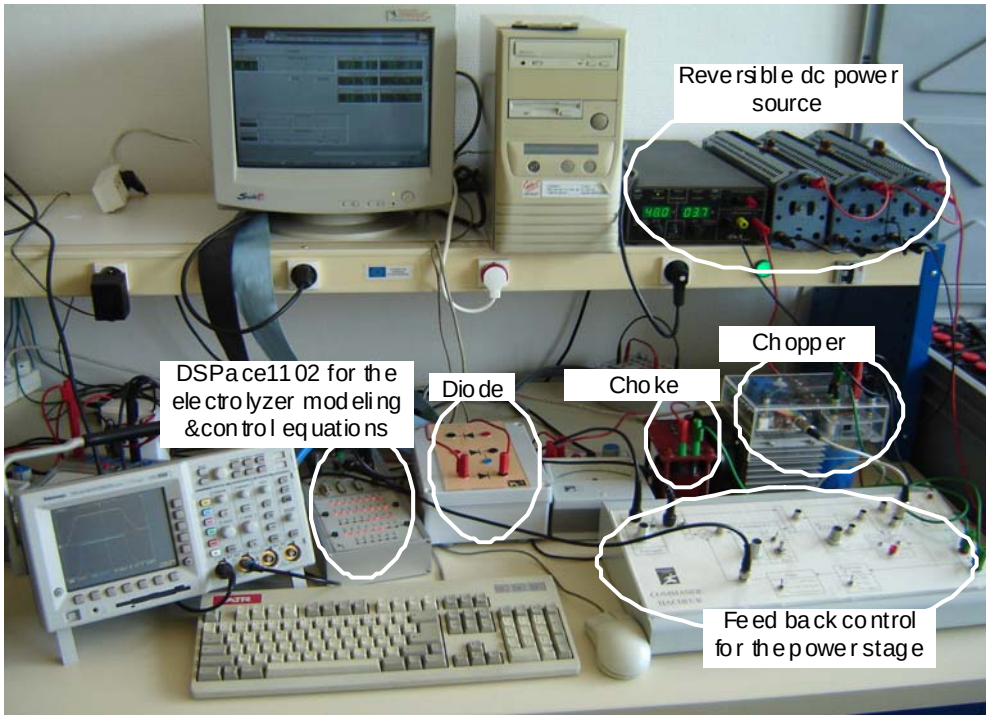

(a) Photo

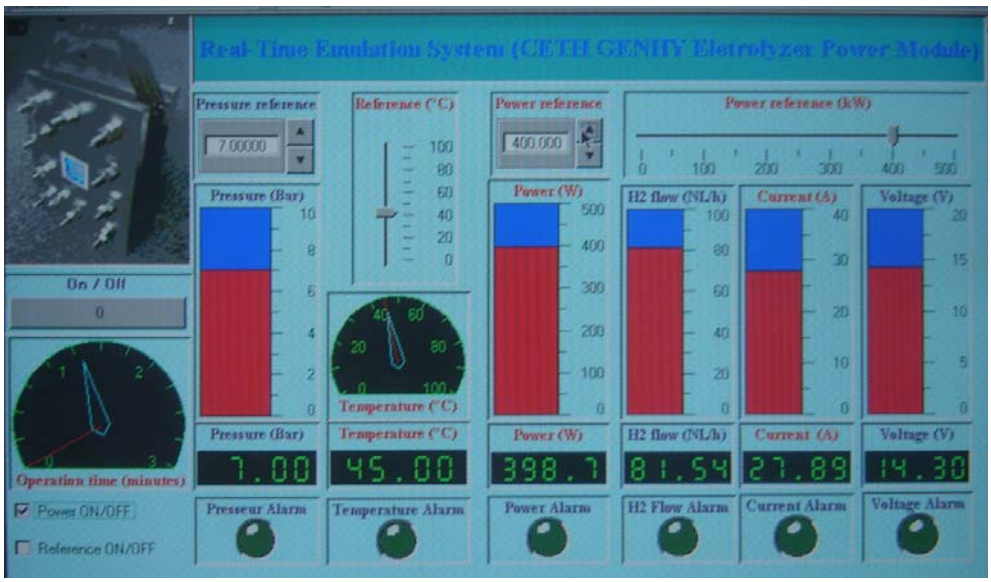

(b) Control panel

Figure IV-21: Implementation of the electrolyzer emulator

IV.6.4 Experimental results

By taking into account the electrolyzer's power dynamic limit, we give the same power ramp for the fuel cell emulator's experimental test, as in the simulation. Experimental results show that the same electrical behaviors are found (Fig.IV-22) as in the simulation (Fig.IV-18b). Therefore, the electrolyzer emulator should be able to help the test bench assessment of our studied hybrid power system, in order to experimentally test the added control function and the different power balancing and energy management strategies, which will be presented in Chap.V.

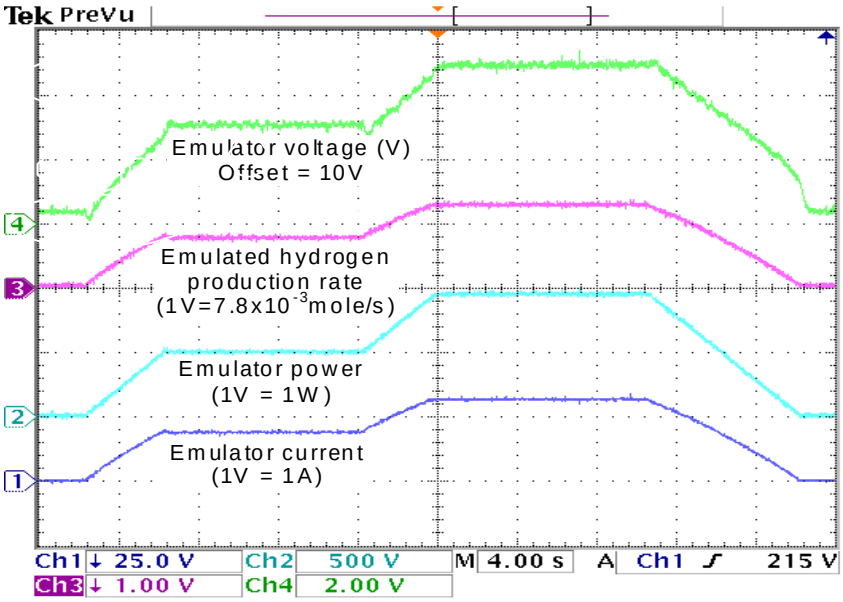

Figure IV-22: Time evolution of the emulated variables

IV.7 Conclusion

In this chapter, a system analysis of an electrolyzer system is presented. An overview is given on the existing technologies, the operating principles, the electrolyzer system, the commercialized products. In our study, the 500W CETH GENHY100® is studied. The system modeling and control scheme is presented with the Energetic Macroscopic Representation (EMR) in order to give a better presentation. The modeling parameters are experimentally identified and validated. This model is used to build an electrolyzer emulator by Hardware-In-the-Loop simulation. This emulator is a flexible experimental test bench, which is used to assess the hybrid power system in order to test the control function, power balancing and energy management strategies for the active generator, which will be presented in Chap.V.

Chapter V

Active Wind Generator

Chapter V Active Wind Generator

In the previous chapters, the modeling and control schemes of the wind/super-capacitors hybrid power system, the fuel cell system and the electrolyzer system have been separately studied. In Chap.I, we have shown that super-capacitors are able to filter fast wind power fluctuations. In order to have a local energy reserve, the fuel cell system and the electrolyzer system are integrated together to build a wind/hydrogen/super-capacitors hybrid power system, which is presented in this chapter.

Different control strategies have been presented for the energy management of the hybrid power system in several applications. These strategies are based on the evolution of the state of the system [Aya 07], on the fuzzy control or the neural control [Haj 07] [Mor 06], on the DC-bus regulation [Mar 06] [Tho 09], on the passitivity and the plate systems [Pay 07] [Bec 06]. In this chapter, the study consists of the system modeling and the design of control system, including the power balancing and energy management strategies. The objective is to set up an active wind generator, which can work like a classical power plant to supply the same powers as asked by a microgrid system operator. Several cases are studied to compare the performances with simulations and practical implementation.

V.1 Modeling of the active wind generator

V.1.1 Presentation

The hydrogen based long-term energy storage system, including fuel cells and electrolyzers, is integrated into the wind/super-capacitor based hybrid power system. Because of many advantages (presented in Paragraph I.3), the DC-coupled structure is used. Different sources are connected to the common DC bus through different power converters (Fig.V-1) [Zho 08]. Thus, four types of sources are used in the hybrid power system:

- the renewable energy conversion system: wind generator (WG);
- the fast-dynamic energy storage system: super-capacitor (SC);
- the long-term energy storage system: fuel cell system (FC) and electrolyzer system (EL);
- the grid as a three-phase voltage source.

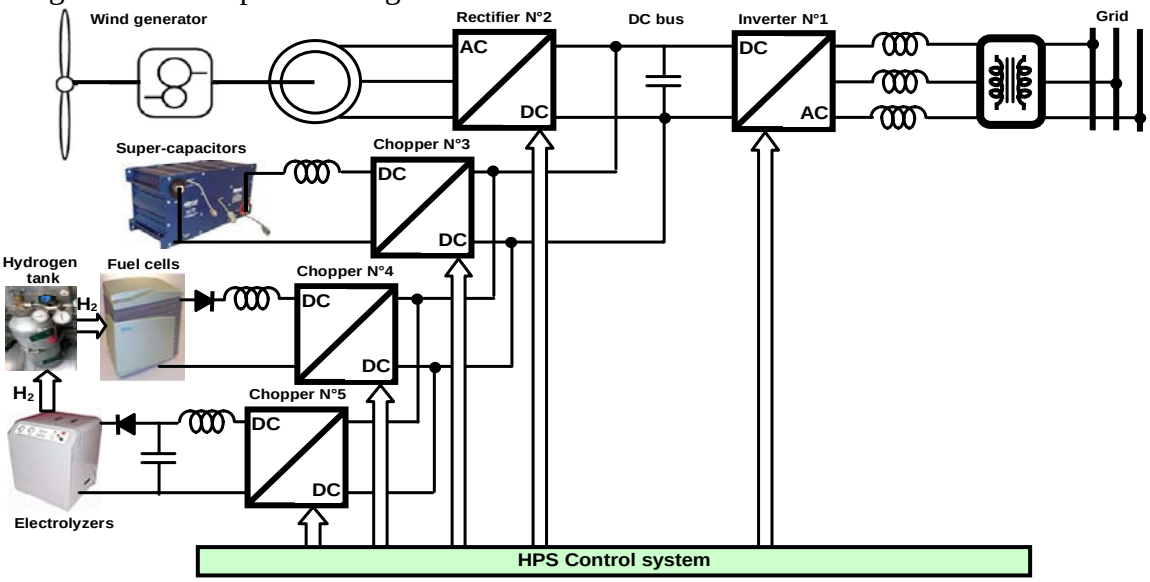

Figure V-1: Structure of the active wind generator.

In order to make the hybrid power system work like a classical active generator to participate in grid management, the coordination of these different sources is very important. So the modeling and control of each source's power conversion system should be studied in detail, as well as the overall power balancing and energy management strategies.

V.1.2 Equivalent average modeling

Equivalent average models of the power converters are used in our study because they are sufficient for the design of the power balancing and energy management strategies. Moreover, they can significantly reduce the simulation time during analysis work. By adding the equivalent average modeling of the power conversion system of the fuel cells and the electrolyzers in the wind/super-capacitors hybrid power system (Fig.II-34), we obtain the equivalent average modeling of the active wind generator (Fig.V-2). It shows that five sources are connected to the DC-bus through five power converters. These five power converters are used to introduce control inputs for each power conversion system, in order

- to extract the maximal power from the wind generator;
- to maintain a constant DC-bus voltage;
- to provide the power exchange with the microgrid;
- to ensure the availability of each energy storage system.

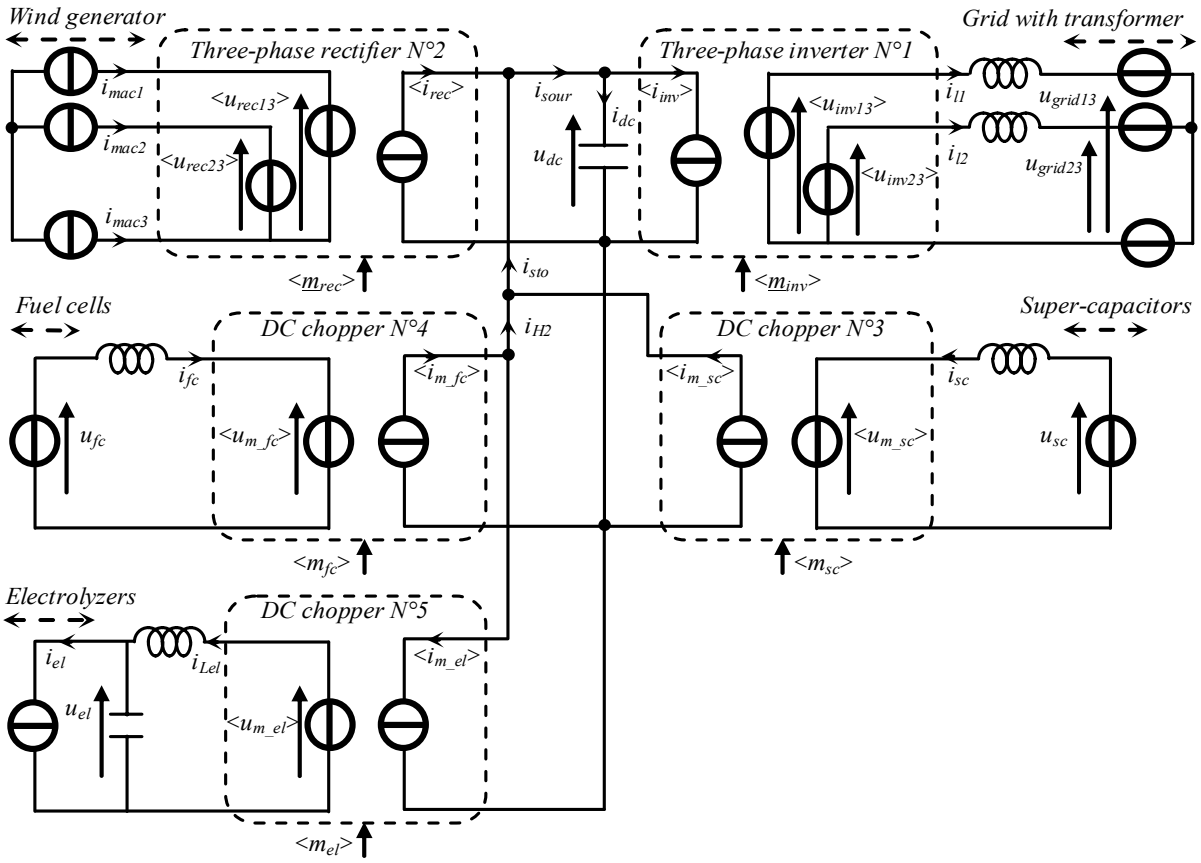

Figure V-2: Equivalent electrical diagram of the active wind generator

V.1.3 DC-bus modeling

In this hybrid power system, five energy sources are connected to the common DC bus via different power converters. So the DC-coupling modeling should be adapted with the newly added power conversion systems of the fuel cells and the electrolyzers (Fig.V-3):

$$i_{inv} = i_{sour} - i_{dc} \quad \text{(V-1)}$$

$$i_{sour} = i_{rec} + i_{sto} \quad \text{(V-2)}$$

$$i_{sto} = i_{m\_sc} + i_{H2} \quad \text{(V-3)}$$

$$i_{H2} = i_{m\_fc} + i_{m\_el} \quad \text{(V-4)}$$

with i_{inv}: the modulated current of the grid inverter N°1;
i_{rec}: the modulated current of the wind generator rectifier N°2;
i_{m_sc}: the modulated current of the super-capacitor chopper N°3;
i_{m_fc}: the modulated current of the fuel cell chopper N°4;
i_{m_el}: the modulated current of the electrolyzer chopper N°5.
i_{sto}: the sum of the modulated currents from energy storage systems;
i_{H2}: the sum of the modulated currents from fuel cells and electrolyzers;
i_{sour}: the sum of the modulated currents from the wind generator and the energy storage systems. The DC-bus voltage is expressed as:

$$C_{dc}\frac{du_{dc}}{dt} = i_{dc} \quad \text{(V-5)}$$

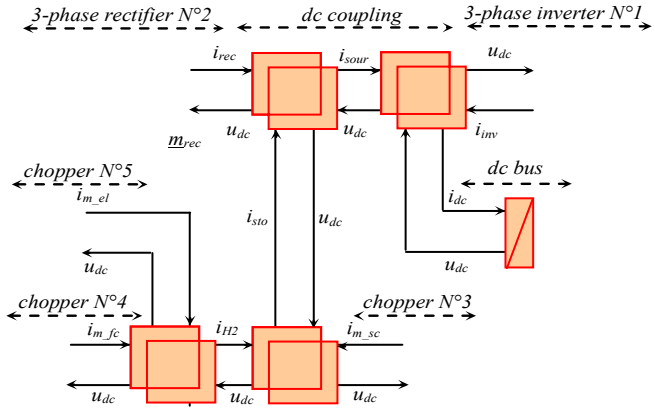

Figure V-3: EMR of the DC bus in the active wind generator

V.1.4 Energetic macroscopic representation

The EMRs of each source's power conversion system modelling have already been presented in the previous chapters (Fig.II-8, Fig.II-31, Fig.III-6 and Fig.IV-9). By combining these EMRs, we obtain the EMR of the entire active wind generator (Fig.V-4).

Five action paths appear from the control inputs of the five power converters to the different physical quantities (i_l, T_{gear}, i_{sc}, i_{fc}, u_{el}):

- from the three-phase inverter N°1 ($\underline{m}_{inv}$) to the line currents ($\underline{i}_l$);
- from the three-phase rectifier N°2 ($\underline{m}_{rec}$) to the gearbox torque (T_{gear});
- from the chopper N°3 (m_{sc}) to the super-capacitors current (i_{sc});
- from the chopper N°4 (m_{fc}) to the fuel cell current (i_{fc});
- from the chopper N°5 (m_{el}) to the electrolyzer voltage (u_{el}).

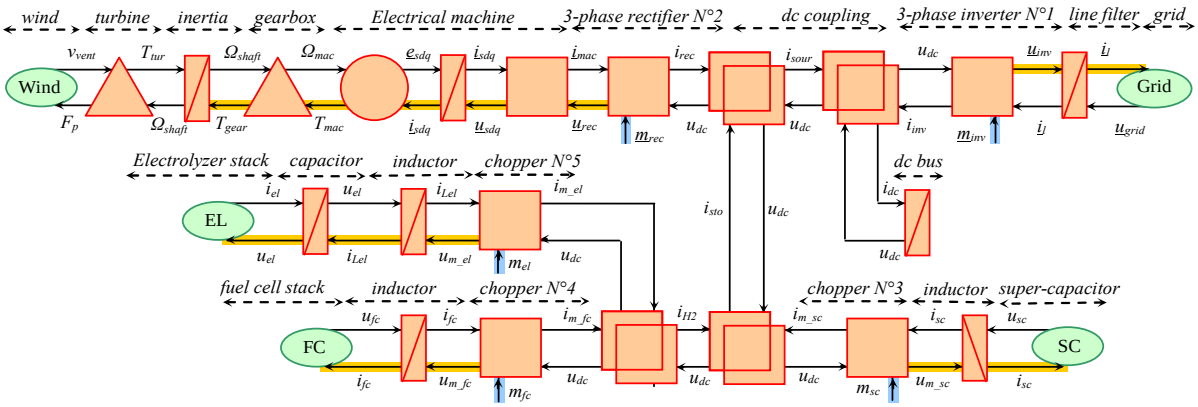

Figure V-4: EMR of the power conversion system in the active wind generator

V.2 Control of the active wind generator

V.2.1 Hierarchical control structure

As for the wind energy conversion system and for the wind/super-capacitors hybrid power system (Fig.II-9 and Fig.II-37), we have used a hierarchical structure of the control system (Appendix C).

In the studied active wind generator, five sources are considered: the wind generator (WG), the super-capacitors (SC), the fuel cells (FC), the electrolyzers (EL) and the grid connection (GC). Five power converters are used to regulate the power exchanges among them. So in the control system, five SCUs and five ACUs are used for the control of the five sources, a common PCU and a common MCU are used for the power balancing and the energy management of the entire hybrid power system (Fig.V-5).

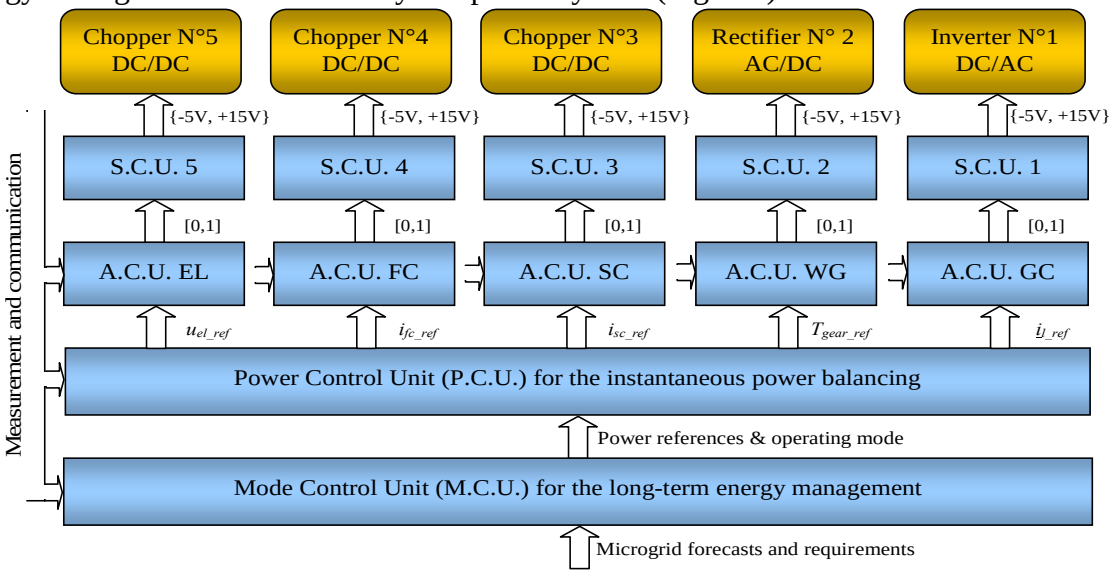

Figure V-5: Hierarchical control structure for the active wind generator.

In the SCU of each converter, the IGBT drivers and PWM techniques are used to control the switching legs. These units are not the main concerns of the study, so they will not be detailed here. However, the control algorithms in the ACU should be presented in order to highlight the physical quantities, which can be used for the power flow control among the different energy sources.

V.2.2 Automatic control unit

The control tasks of each dynamical quantity are the same as previously explained. The torque (T_{gear}) must be controlled in order to implement a maximum power point tracking strategy for the wind generator. The voltage across the electrolyzer, as well as the currents from the fuel cells and the super-capacitors, must be controlled for regulating the power exchange with the storage systems.

The global control scheme of the entire active wind generator is obtained by combining all these control schemes, which have been presented in the previous chapters. They are organized with the help of the Energetic Macroscopic Representation (Fig.V-6). Six references (i_{dc_ref}, i_{l_ref}, T_{gear_ref}, i_{sc_ref}, i_{fc_ref}, u_{el_ref}) must be set to interface the automatic control units with the power control unit. As result, the Automatic Control Units (ACU) of the control system consist of the control schemes of each power conversion system (Fig.V-7).

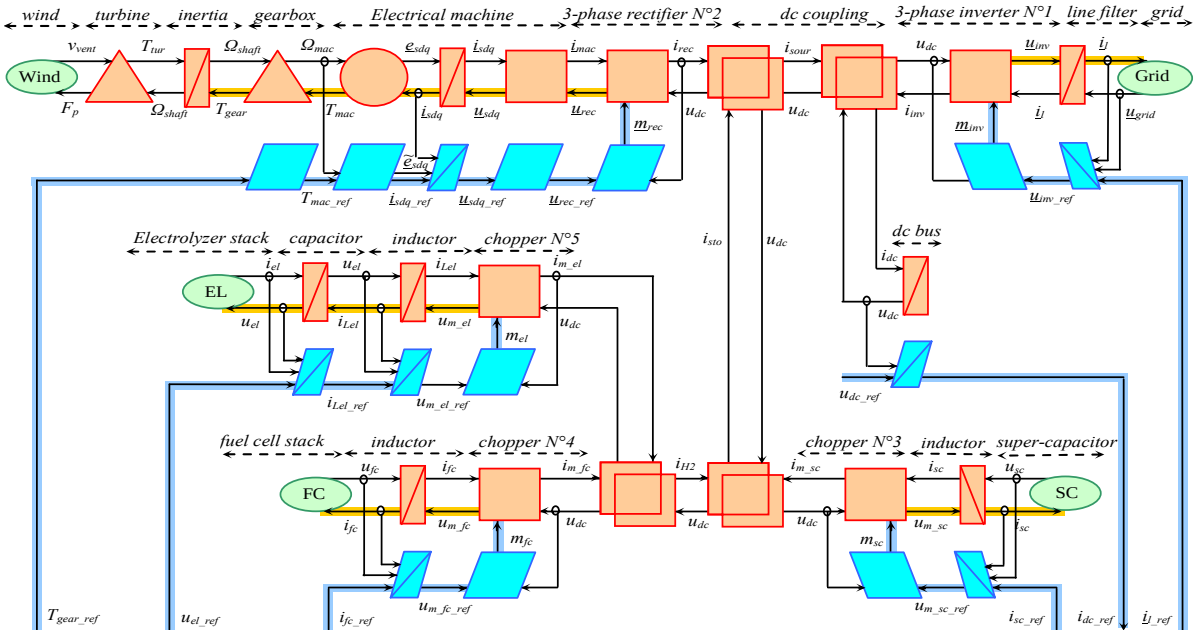

Figure V-6: EMR of the active wind generator with the control scheme.

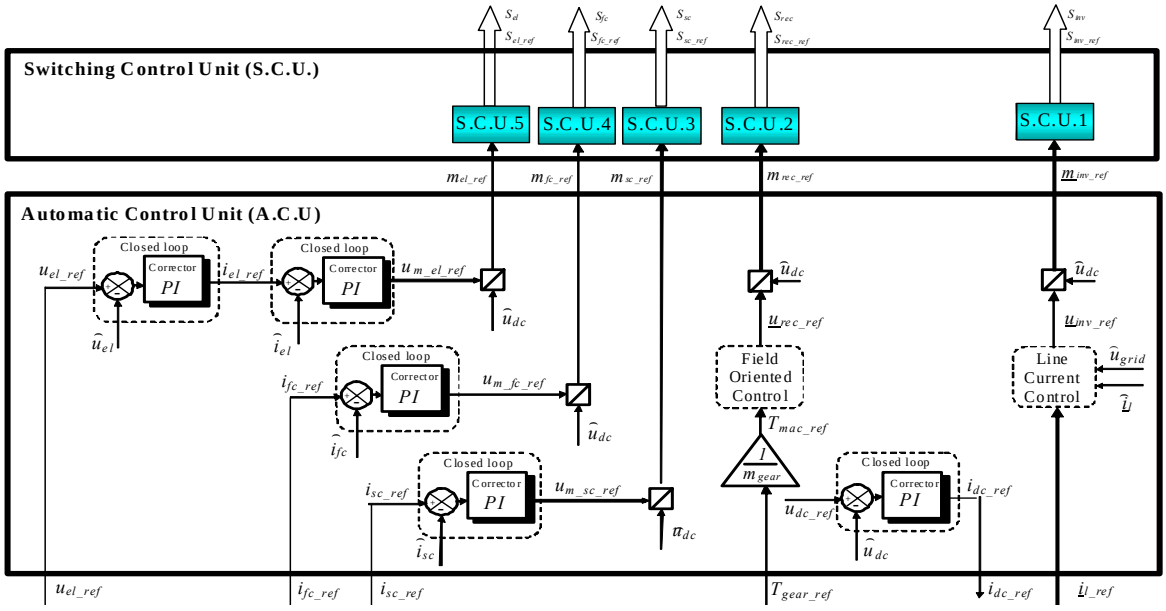

Figure V-7: Block diagram of the automatic control units for the active wind generator.

V.2.3 Power control unit

a) Layout of the power control unit

The Power Control Unit is divided into two levels: the Power Control Level (PCL) and the Power Sharing Level (PSL).

The Power Control Level is the interface between the powers and the other quantities. The Power Sharing Level coordinates the power flow exchanges among the different energy sources with different power balancing strategies. They are presented here in detail with the help of the Multi-Level Representation (Fig.V-8), which has been developed by Peng LI in 2008 [Li 08].

b) Power control level

The power flow exchanges with various sources can be controlled only via the related five references (u_{el_ref}, i_{fc_ref}, i_{sc_ref}, T_{gear_ref}, $\underline{i}_{l\_ref}$ in Fig.V-7). Therefore, the expressions of the powers should be deduced and these equations are used in order to obtain the control algorithms (Table V-1). In order to focus on the power exchanges with the different sources around the DC bus, the instantaneously exchanged power with the choke, the losses in the filters and the losses in the power converters are neglected. Only the sources' powers and the exchanged power with the DC-bus capacitor are taken into account here.

Table V-1: Power calculation and power control algorithms for the active wind generator.

Energy source	Power flow calculation	Controllable variable calculation
DC-bus capacitor	***Int0***: $p_{dc} = u_{dc} i_{dc}$	***Int0e***: $p_{dc\_ref} = \hat{u}_{dc} i_{dc\_ref}$
Grid connection	***Int1***: $\begin{cases} p_g = u_{13} i_1 + u_{23} i_2 \\ q_g = \sqrt{3}(u_{13} i_1 - u_{23} i_2) \end{cases}$	***Int1c***: $\begin{cases} i_{l1\_ref} = \dfrac{(2\hat{u}_{13} - \hat{u}_{23}) p_{g\_ref} + \sqrt{3}\hat{u}_{23} q_{g\_ref}}{2\hat{u}_{13}^2 - 2\hat{u}_{13}\hat{u}_{23} + 2\hat{u}_{23}^2} \\ i_{l2\_ref} = \dfrac{(2\hat{u}_{23} - \hat{u}_{13}) p_{g\_ref} - \sqrt{3}\hat{u}_{13} q_{g\_ref}}{2\hat{u}_{13}^2 - 2\hat{u}_{13}\hat{u}_{23} + 2\hat{u}_{23}^2} \end{cases}$
Wind generator	***Int2***: $p_{wg} = \Omega_{tur} T_{gear}$	***Int2c***: $T_{gear\_ref} = \dfrac{1}{\hat{\Omega}_{tur}} p_{wg\_ref}$
Super-capacitors	***Int3***: $p_{sc} = u_{sc} i_{sc}$	***Int3c***: $i_{sc\_ref} = \dfrac{1}{\hat{u}_{sc}} p_{sc\_ref}$
Fuel cells	***Int4***: $p_{fc} = i_{fc} u_{fc}$	***Int4c***: $i_{fc\_ref} = \dfrac{1}{\hat{u}_{fc}} p_{fc\_ref}$
Electrolyzers	***Int5***: $p_{el} = i_{el} u_{el}$	***Int5c***: $u_{el\_ref} = \dfrac{1}{\hat{i}_{fc}} p_{fc\_ref}$

For the energy storage systems, the powers are calculated by multiplying the measured currents and the measured voltages (***Int3, Int4*** and ***Int5*** in Table V-1). The references of the controllable variables are given by dividing the power reference with the measured current or the measured voltages (***Int3c, Int4c*** and ***Int5c*** in Table V-1).

For the wind energy conversion system, a maximal power point tracking (MPPT) strategy is used to extract the maximum power of the available wind energy according to a non-linear characteristic in function of the speed. It receives the measured rotational speed (Ω_{tur}) and sets a desired power reference (p_{wg_ref}) (***Int2*** and ***Int2c*** in Table V-1).

The output of the DC-bus voltage control loop is the current reference (i_{dc_ref}) of the DC-bus capacitor, and its product with the measured DC-bus voltage gives the power reference (p_{dc_ref}) for the DC-bus voltage regulation (***Int0e***). The powers, which are exchanged with the grid, can be calculated through the "two-wattmeter" method (***Int1*** and ***Int1c*** in Table V-1).

The reference of the controllable variables should be limited while the powers are divided by a too small value. A look-up table can sometimes be used to avoid divisions by zero. For example, the non-linear static model of the electrolyzer stack can be implemented in a look-up table to translate each power reference into a voltage reference.

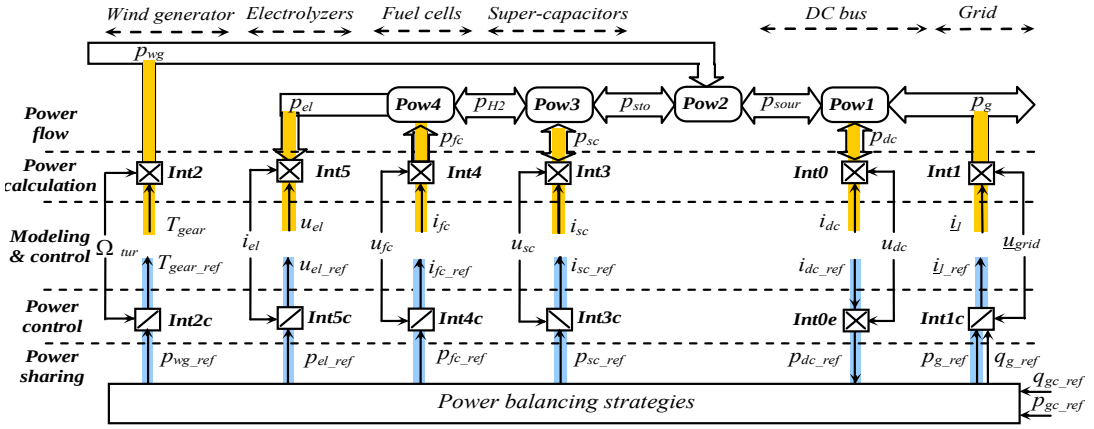

Figure V-8: Multi-Level Representation of the power modeling and control for the active wind generator

c) Power sharing level

The Power Sharing Level is used to implement the power balancing strategies in order to coordinate the various sources in the hybrid power system (Fig.V-9). It will be explained in the following paragraphs.

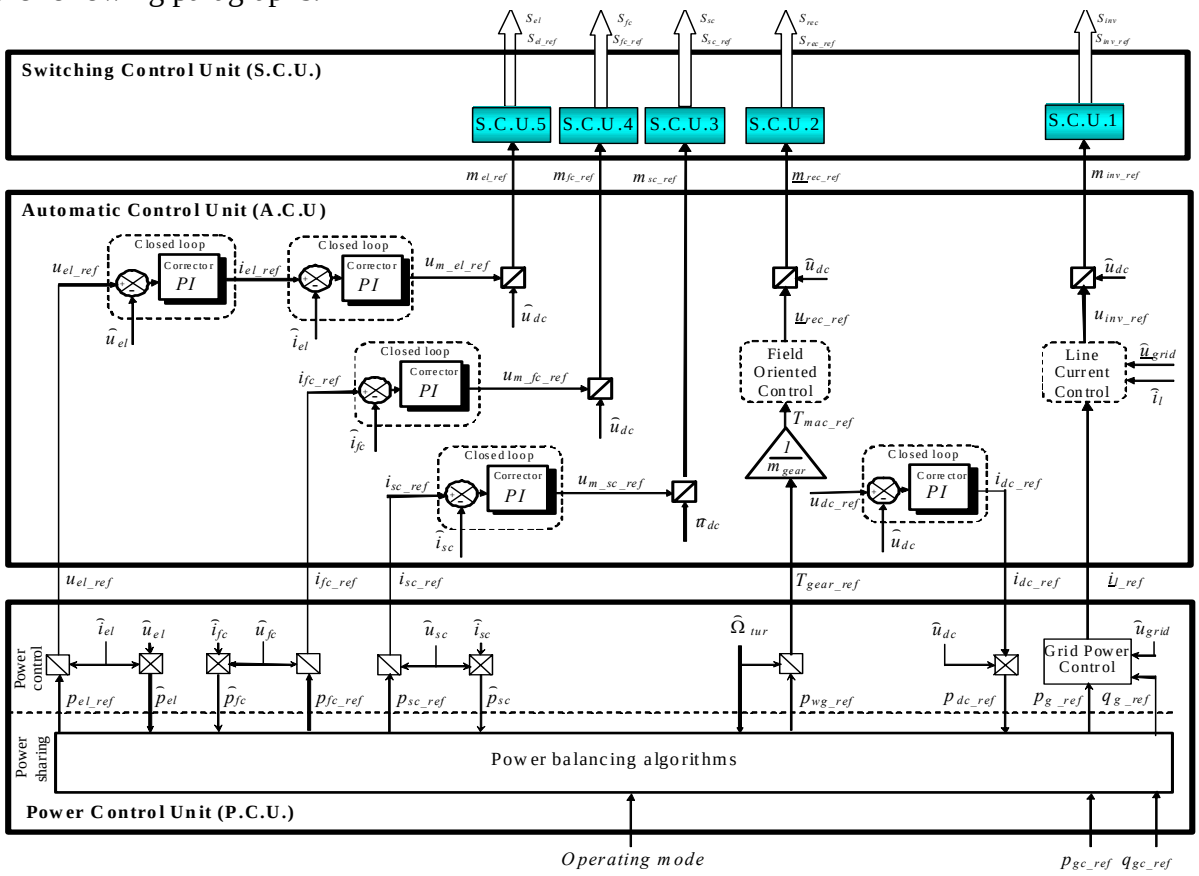

Figure V-9: Block diagram of the hierarchical control system of the active wind generator.

V.3 Power balancing strategies for the active wind generator

V.3.1 Role of the power balancing

The power balancing plays a very important role in the control system of the hybrid power system. It leads directly to the stability of the hybrid power system. In the studied wind energy conversion system, all power exchanges are performed via the DC-bus (Fig.V-10) and have an impact on the DC-bus voltage (u_{dc}):

$$\frac{dE_{dc}}{dt} = C_{dc} u_{dc} \frac{du_{dc}}{dt} = p_{dc} = p_{sour} - p_g = p_{wg} + p_{sc} + p_{fc} - p_{el} - p_g . \quad \text{(V-6)}$$

with E_{dc}: the energy stored in the DC-bus capacitor;
p_{dc}: the resulted power into the DC-bus capacitor;
p_{wg}: the power, which is injected into the DC bus from the wind generator;
p_{fc}: the power, which is injected into the DC bus from the fuel cell;
p_{sc}: the power, which is injected into the DC bus from the super-capacitor;
p_{el}: the power, which is extracted from the DC bus into the electrolyzer;
p_g: the power, which is extracted from the DC bus into the grid;
p_{sour}: the total power from the sources.

So the instantaneous power balancing is very important for the stability of the whole system and should be well performed to regulate the DC-bus voltage.

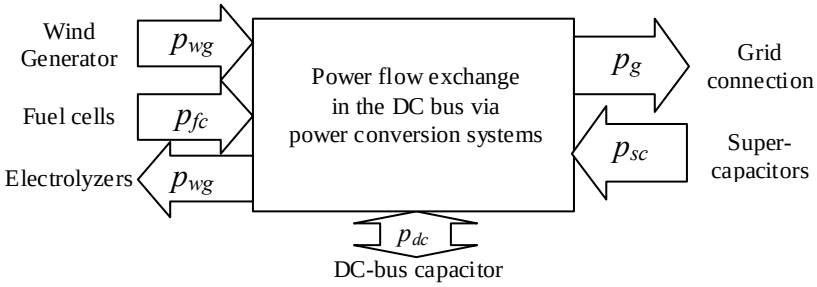

Figure V-10: Power flow exchanges around the DC bus in the active wind generator

V.3.2 Power flow modeling

According to the power exchange, the power flows inside this hybrid power system is organized with four equations according to Eq.V-1, Eq.V-2, Eq.V-3 and Eq.V-4 (Fig.V-11):

$$\textbf{\textit{Pow1:}}\ p_g = p_{sour} - p_{dc} , \quad \text{(V-7)}$$

$$\textbf{\textit{Pow2:}}\ p_{sour} = p_{sto} + p_{wg} , \quad \text{(V-8)}$$

$$\textbf{\textit{Pow3:}}\ p_{sto} = p_{H2} + p_{sc} , \quad \text{(V-9)}$$

$$\textbf{\textit{Pow4:}}\ p_{H2} = p_{fc} - p_{el} , \quad \text{(V-10)}$$

with p_{sour}: the total power, which arrives at the DC bus from the sources;
p_{sto}: the total power, which arrives at the DC bus from the storage systems;
p_{H2}: the total power, which arrives at the DC bus from the long-term storage system.

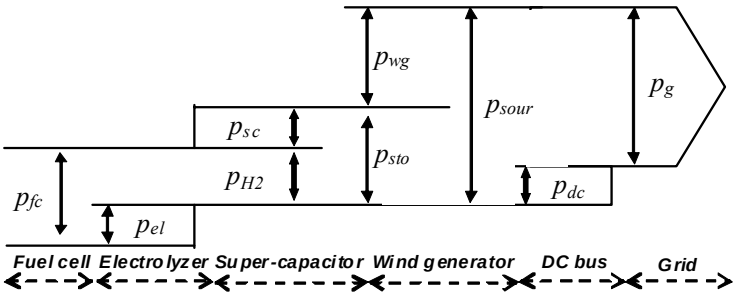

Figure V-11: Power balance inside the active wind generator

The grid power (p_g) must be equal to the power reference (p_{gc_ref}) sent by the microgrid system operator. The DC power (p_{dc}) must be equal to the required value (p_{dc_ref}) to regulate the DC-bus voltage (u_{dc}0 to a constant value. Hence the sources' total power (p_{sour}) can be adjusted by regulating the total power from storage units (p_{sto}). So the power flows are supervised with the power references, which must be calculated by the Power Sharing Level of the Power Control Unit (Fig.V-8).

In this wind/hydrogen/super-capacitor hybrid power system, five power electronic converters are used to regulate the power transfer with each source. The three-phase rectifier is used to control the wind generator with a MPPT strategy. The three-phase inverter in the grid connection system and the DC choppers in the other power conversion systems can be used for the DC-bus voltage regulation and the grid power control. According to the chosen power flow, two power balancing strategies can be implemented [Zho 09]:

- ***the grid following strategy*** uses the line current loop to regulate the DC-bus voltage;
- ***the power dispatching strategy*** uses the line current loop to control the grid active power, and the DC-bus voltage is regulated with the wind generator and storage units.

V.3.3 Grid following strategy

With the grid following strategy, the DC-bus voltage is regulated by adjusting the exchanged power with the grid, while the wind generator works in MPPT strategies. In Fig.V-12, it is depicted by a closed loop ($p_{dc\_ref} \rightarrow p_{g\_ref} \rightarrow p_g \rightarrow p_{dc}$). So the required power for the DC-bus voltage regulation (p_{dc_ref}) is used to calculate the grid power reference (p_{g_ref}),

$$\textbf{Pow1e:}\quad p_{g\_ref} = \widehat{p}_{sour} - p_{dc\_ref}\,. \tag{V-11}$$

The sources' total power (p_{sour}) is a disturbance and should also be taken into account.

$$\textbf{Pow2e:}\quad \widetilde{p}_{sour} = \widetilde{p}_{wg} + \widetilde{p}_{sto}\,. \tag{V-12}$$

$$\textbf{Pow3e:}\quad \widetilde{p}_{sto} = \widehat{p}_{sc} + \widehat{p}_{H2}\,. \tag{V-13}$$

$$\textbf{Pow4e:}\quad \widetilde{p}_{H2} = \widehat{p}_{fc} - \widehat{p}_{el}\,. \tag{V-14}$$

The energy storage systems help the wind energy conversion system to satisfy the power references, which are asked by the microgrid operator. In steady state, the DC-bus voltage is regulated and the averaged power exchange with the DC-bus capacitor can be considered as zero in the equation (***Pow1***). Hence in steady state, the grid power (p_g) is equal to the total power from the sources (p_{sour}). If the microgrid system operator sets a power requirement (p_{gc_ref}), it must be equal to the sources' power reference (p_{sour_ref}) as shown in Fig.V-12:

$$\textbf{Pow1c:}\ p_{sour\_ref} = p_{g\_ref} = p_{gc\_ref}. \tag{V-15}$$

In order to help the wind energy conversion system to respect the active power requirement, the energy storage systems should be coordinated to supply or absorb the difference between this power requirement (p_{gc_ref}) and the fluctuant wind power (p_{wg}) as shown in Fig.V-12:

$$\textbf{Pow2c:}\ p_{sto\_ref} = p_{sour\_ref} - \tilde{p}_{wg}. \tag{V-16}$$

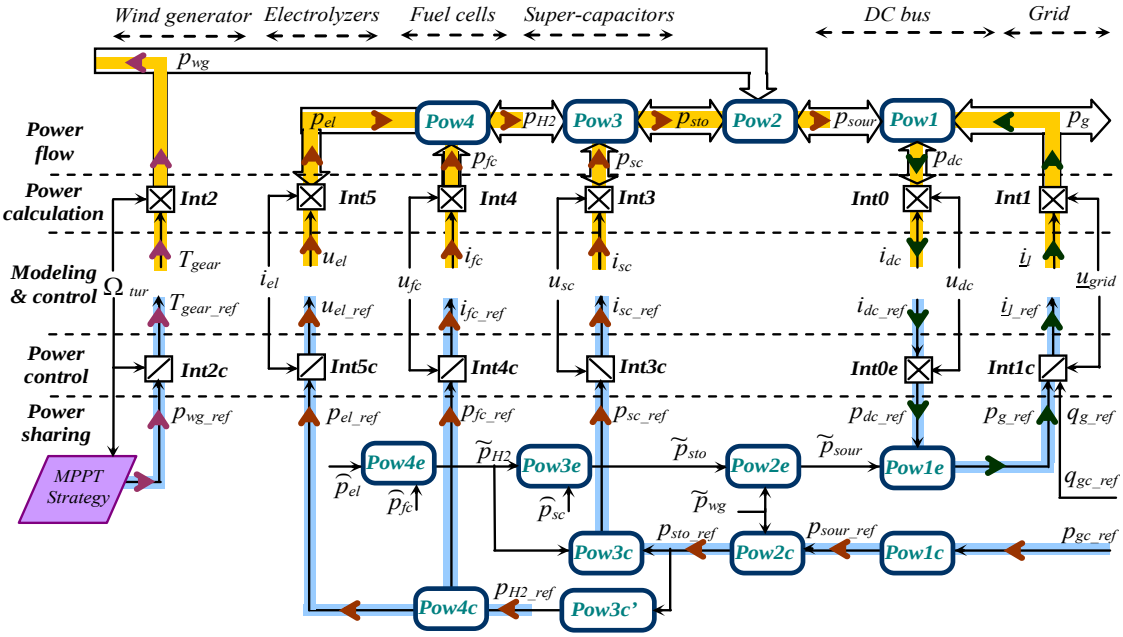

Figure V-12: Multi-Level Representation of the grid following strategy for the power sharing

Among the energy storage systems, the fuel cells and the electrolyzers are the main energy exchangers because a large quantity of hydrogen can be stored for enough energy availability. For efficiency reasons the fuel cell and the electrolyzer should not work at the same time. The activation of the fuel cell or the activation of the electrolyzer depends on the sign of the reference (p_{H2_ref}). Thus a selector assigns the power reference (p_{H2_ref}) to the fuel cell (p_{fc_ref}) or to the electrolyzer (p_{el_ref}) according to the sign of p_{H2_ref} (Fig.V-12),

$$\textbf{Pow4c:}\ \begin{cases} if: P_{H2\_ref} > 0, & P_{fc\_ref} = P_{H2\_ref}, & P_{el\_ref} = 0; \\ if: P_{H2\_ref} = 0, & P_{fc\_ref} = 0, & P_{el\_ref} = 0; \\ if: P_{H2\_ref} < 0, & P_{fc\_ref} = 0, & P_{el\_ref} = \left| p_{H2\_ref} \right|. \end{cases} \tag{V-17}$$

However, the power reference (p_{sto_ref}) is a fast varying value due to the fluctuant wind power (p_{wg}) and the varying grid power (p_g). In order to avoid the fast chattering problem when it is close to zero, it should be slowed down. Moreover, the fuel cells and the electrolyzers have relatively slow power dynamics, fast varying power reference are not welcome for their operating lifetime. So a Low-Pass Filter (*LPF*) with a slope limiter should be added (Fig.V-12):

$$\textbf{Pow3c':}\ p_{H2\_ref} = \frac{1}{1+\tau s}\left(p_{sto\_ref}\right). \tag{V-18}$$

where τ is the time constant of the Low-Pass Filter. Its value should be set large enough according specific application by taking into account the power dynamics of the fuel cells and the electrolyzers as well as the size of the super-capacitors.

The super-capacitors are not made for a long-term energy backup unit because they have limited energy storage capacities due to their low energy density. However, they have vey fast power dynamics and can supply fast varying powers and power peaks. They can be used as auxiliary power system of the fuel cells and the electrolyzer to fill the power gaps during their transients (Fig.V-12),

$$\textbf{Pow3c:}\ p_{sc\_ref} = p_{sto\_ref} - \widehat{p}_{H2} = p_{sto\_ref} - \widehat{p}_{fc} + \widehat{p}_{el}\,. \qquad \text{(V-19)}$$

The block diagram of the grid following strategy for the active wind generator is shown in Fig.V-13.

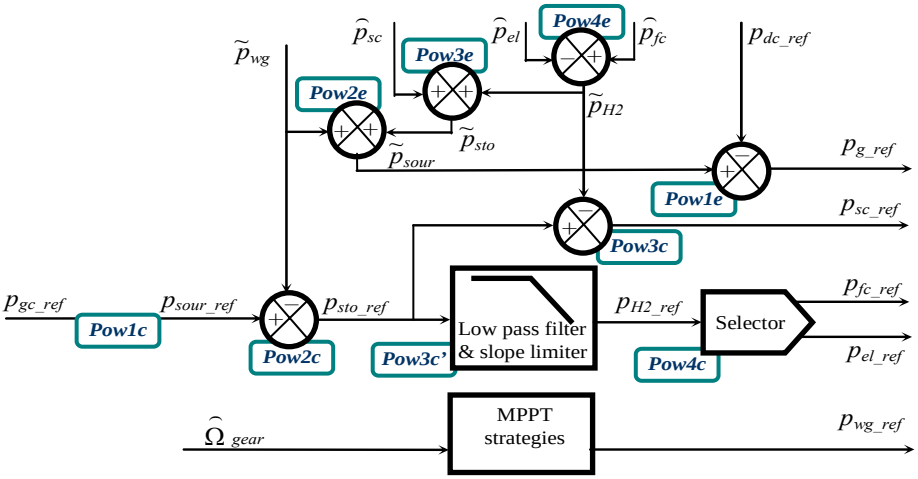

Figure V-13: Block diagram of the grid following strategy for the power sharing.

V.3.4 Power dispatching strategy

The total power (p_{sour}) from the energy storage and the wind generator can also be used to provide the necessary DC power (p_{dc}) for the DC-bus voltage regulation (Fig.V-14). In this case, the necessary total power reference (p_{sour_ref}) must be calculated by taken into account the required power for the DC-bus voltage regulation (p_{dc_ref}) and the measured grid power (p_g) as disturbance input by using the inverse equation of ***Pow1*** (Fig.V-14),

$$\textbf{Pow1c:}\ p_{sour\_ref} = p_{dc\_ref} + \widehat{p}_{g}\,. \qquad \text{(V-20)}$$

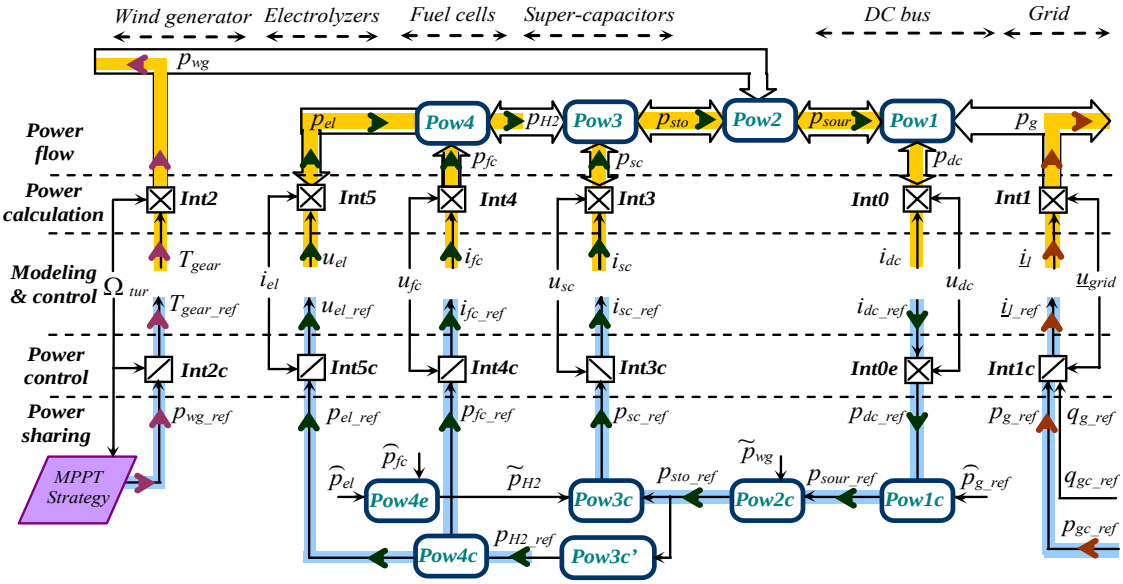

Figure V-14: Multi-Level Representation of the power dispatching strategy for the power sharing

Then the total power reference of the storage systems is deduced by taking into account the fluctuant wind power with the inverse equation of ***Pow2*** (Fig.V-14),

$$\textbf{Pow2c:}\ p_{sto\_ref} = p_{sour\_ref} - \tilde{p}_{wg}\,. \tag{V-21}$$

This power reference is shared among the fuel cells, the electrolyzers and the super-capacitors in the same way as explained above,

$$\textbf{Pow3c':}\ p_{H2\_ref} = \frac{1}{1+\varpi}\left(p_{sto\_ref}\right), \tag{V-22}$$

$$\textbf{Pow4c:}\ \begin{cases} if: P_{H2\_ref} > 0, & P_{fc\_ref} = P_{H2\_ref}, & P_{el\_ref} = 0; \\ if: P_{H2\_ref} = 0, & P_{fc\_ref} = 0, & P_{el\_ref} = 0; \\ if: P_{H2\_ref} < 0, & P_{fc\_ref} = 0, & P_{el\_ref} = \left|p_{H2\_ref}\right|. \end{cases} \tag{V-23}$$

$$\textbf{Pow3c:}\ p_{sc\_ref} = p_{sto\_ref} - \tilde{p}_{H2} = p_{sto\_ref} - \hat{p}_{fc} + \hat{p}_{el}\,. \tag{V-24}$$

And now, the grid power reference (p_{g_ref}) is free to be used for the grid power control. The microgrid system operator can directly set power requirements (p_{gc_ref} and q_{gc_ref}) for the grid connection system,

$$p_{g\_ref} = p_{gc\_ref}\,. \tag{II-25}$$

Therefore, the hybrid power system can directly supply the required powers for providing the ancillary services to the microgrid, like the regulations of the grid voltage and frequency.

The block diagram of the grid following strategy for the active wind generator is shown in Fig.V-15.

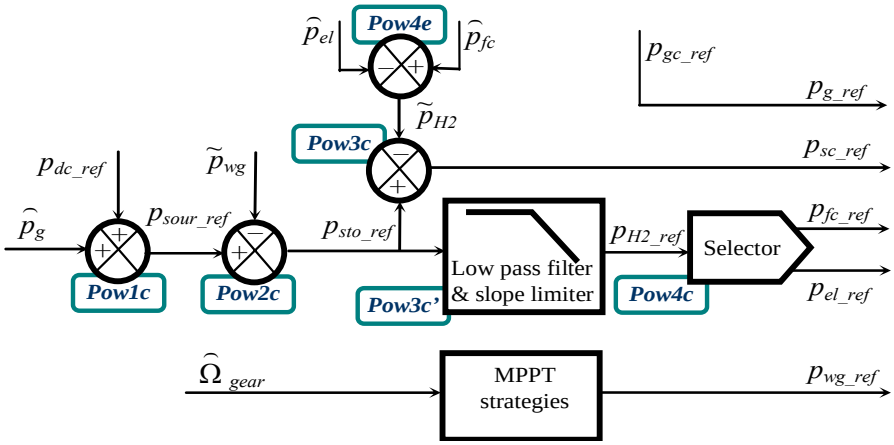

Figure V-15: Block diagram of the power dispatching strategy for the power sharing.

V.4 Experimental tests

V.4.1 Experimental implementation

An experimental test bench of the active wind generator has been built to test the different power balancing strategies. Several real-time emulators are used in our system (Fig.V-16). Previously, we have presented the experimental implementation of the wind energy conversion system (Paragraph II.2.2). It enables to have similar power dynamics and characteristics as a real wind generator. The wind power emulator is used to provide the needed wind power profile, which has been presented in Chap.II. The fuel cell emulator and the electrolyzer emulator are used to provide the same electrical behavior as the real fuel cell

stack and the electrolyzer stack, which have been presented in Chap.III and in Chap.IV. They are integrated into the wind/super-capacitor hybrid power system, which is presented in Chap.II, in order to build the experimental test bench of the active wind generator. The test bench of the active wind generator is controlled by a Digital Signal Processor DSpace 1103. The emulators of the fuel cells and the electrolyzers are respectively controlled by DSpace 1102 (Fig.V-16).

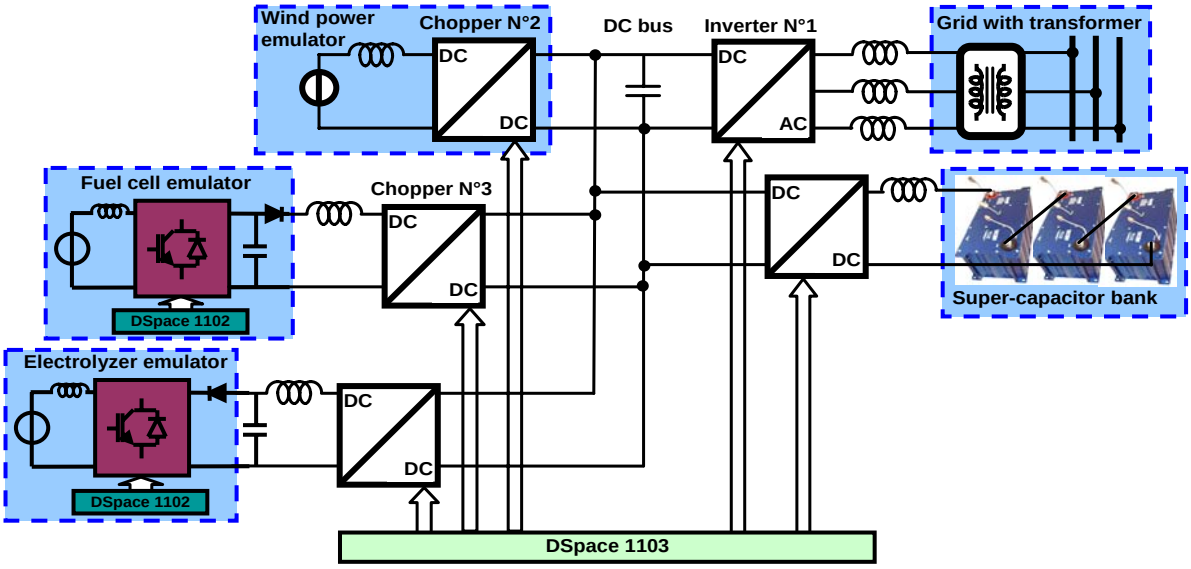

(a) System implementation

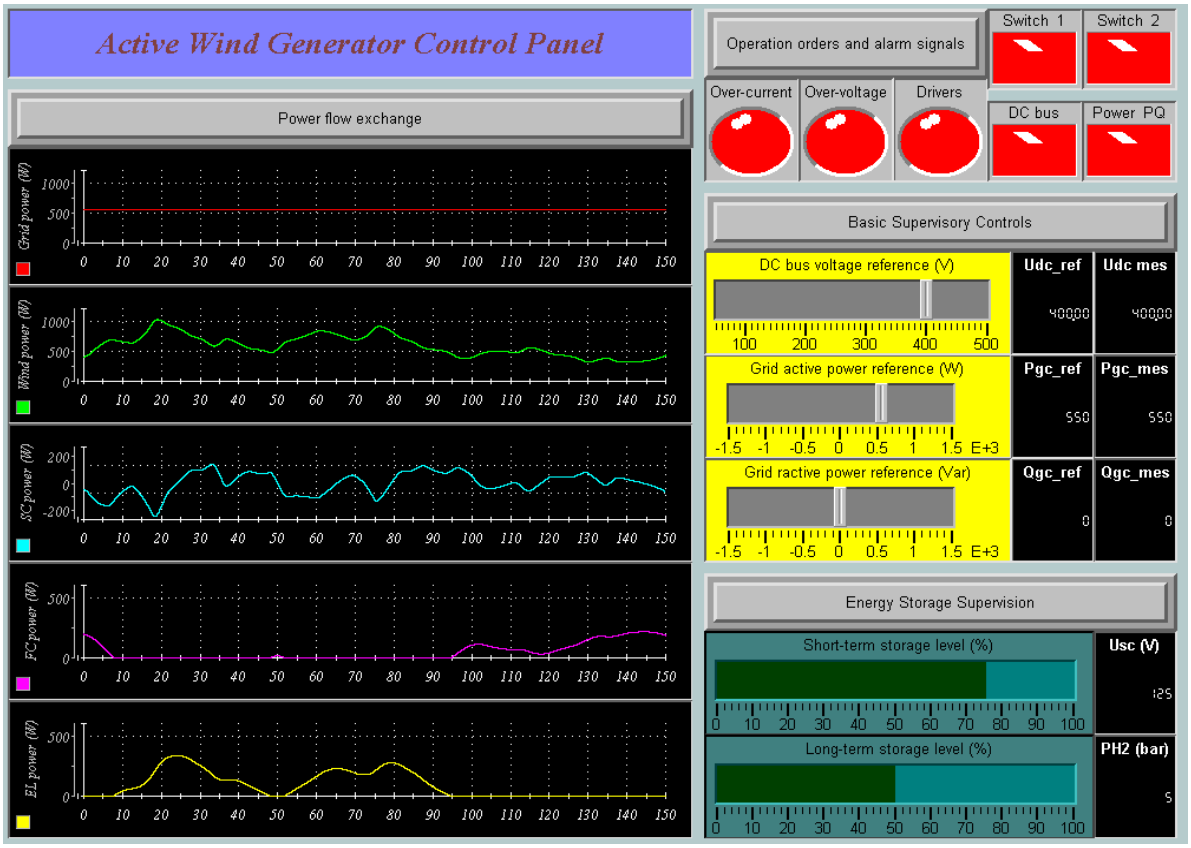

(b) Control panel

Figure V-16: Implementation of the experimental test bench for the active wind generator.

The sizing of the fuel cell stack and the electrolyzer stack is adapted by using the modeling parameters of Table V-2 in the Hardware-In-the-Loop simulation in order to be interfaced in the experimental test bench. Three "BOOSTCAP" super-capacitors modules (160F and 48V) are connected in series (Table V-3). Therefore, the equivalent capacitor of the super-capacitor bank is about 53F and the maximal voltage is about 144V. Two power balancing strategies are respectively tested and compared. With this experimental test bench, it is possible to apply our proposed hierarchical control system for the active generator and to test it with the developed power balancing strategies.

Table V-2: Implementation parameters for the fuel cell and the electrolyzer emulators

	Number of cells	**Active surface**	**Nominal power**	**Time constant**
Fuel cells	156	25 cm^2	1 kW	5 s
Electrolyzers	70	15 cm^2	1 kW	5 s

Table V-3: Implementation parameters for the super-capacitors bank

	Module voltage	**Module capacitance**	**Module number**	**Stored energy**
Super-capacitors	48 V	160 F	3	0.15 kWh

V.4.2 Test of the grid following strategy

In order to test the grid following strategy, the same fluctuant wind power profile is used during 150 seconds as in Chap.II. The active power requirement from the microgrid is assumed to be p_{gc_ref}=600W. The experimental results are compared with the simulation results (Fig.V-17).

The DC-bus voltage is well regulated around 400V. Thanks to the energy storage systems, the active power, which is exchanged with the grid, is well regulated.

For the energy storage systems, when the generated wind power is more than 600W the electrolyzer is activated to absorb the power difference. When the generated wind power is less than 600W, the fuel cell is activated to compensate the power difference. Since the power dynamic of the fuel cells and the electrolzyer are limited by a low-pass filter with a 5s time constant. They are not able to filter the fast fluctuations of the wind power. Therefore, the super-capacitors supply or absorb the rest of the required power in order to respect the microgrid's power requirement ($p_{sour}=p_{gc\_ref}$=600W). The grid active power is slightly less than the microgrid's requirement ($p_g<p_{gc\_ref}$=600W) because different power losses in the filers and in the power converters are not taken into account in the system study.

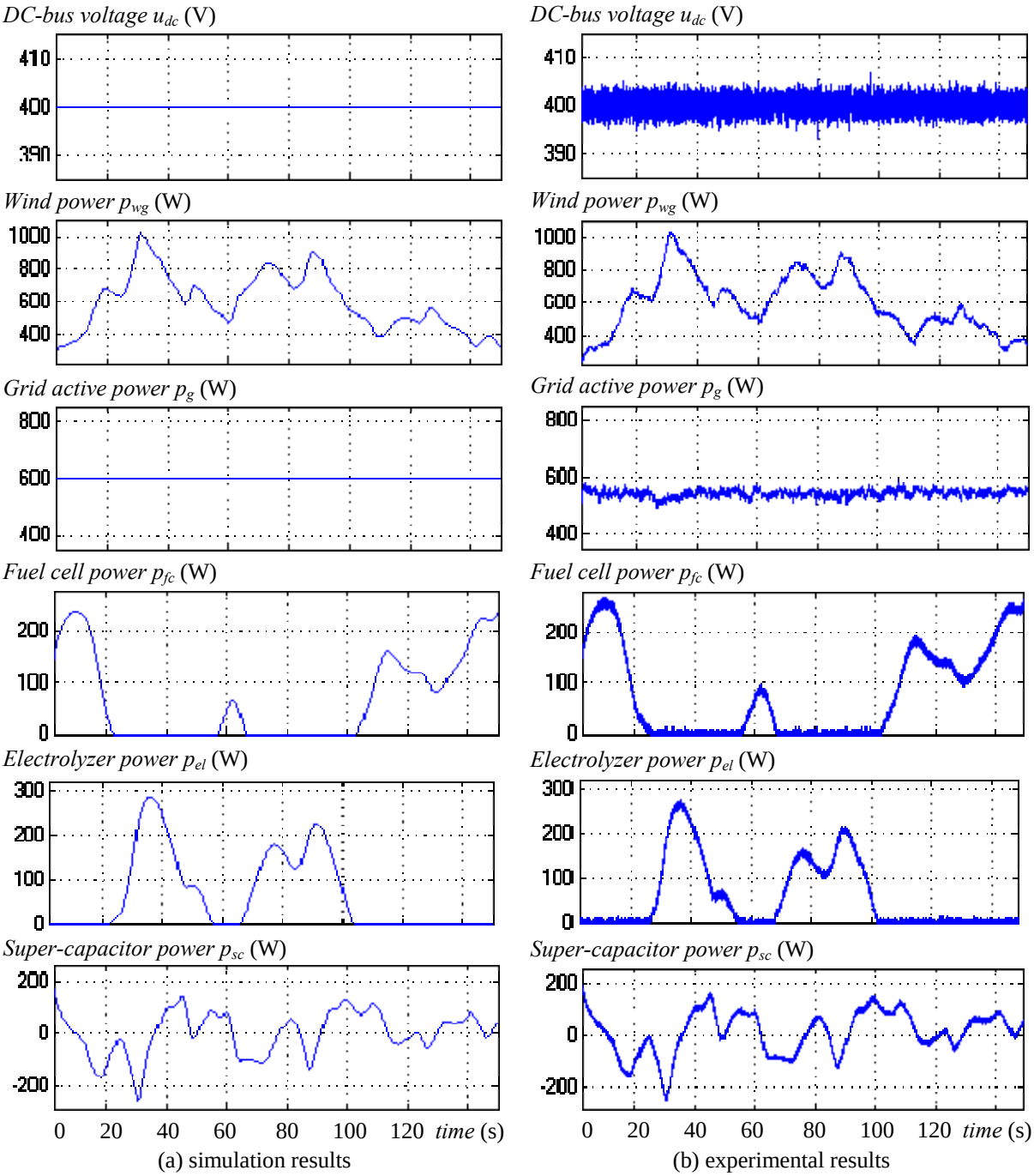

(a) simulation results (b) experimental results

Figure V-17: Time evolution of the powers inside the active wind generator with the grid following strategy

The voltages and the currents of the super-capacitors, the fuel cells and the electrolyzers are shown in Fig.V-18. Thanks to the help of the fuel cells and the electrolyzers, the voltage of the super-capacitor has not varied much. It means that the super-capacitors can still work during a long time with the help of the long-term energy storage systems.

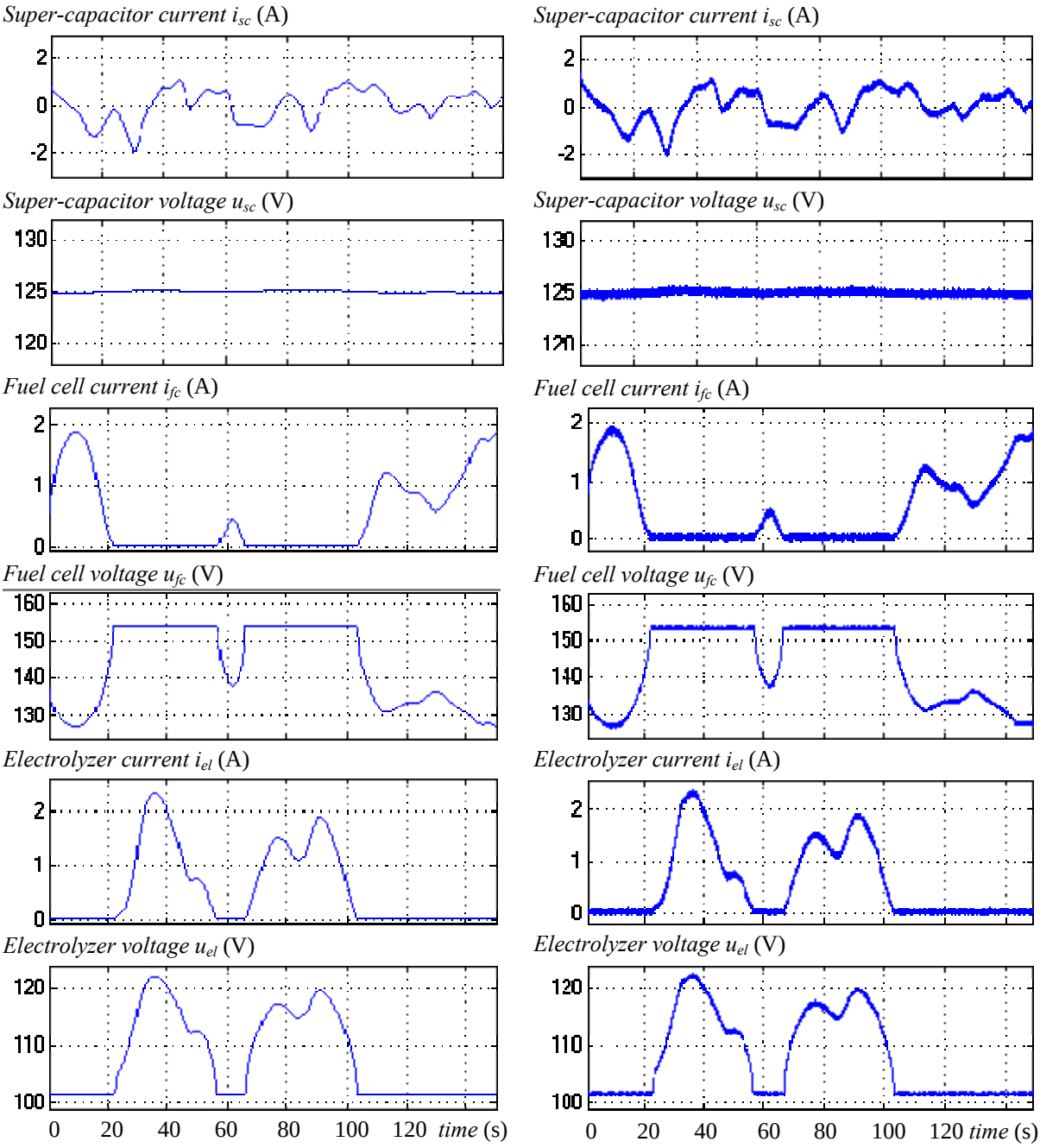

(a) simulation results (b) experimental results

Figure V-18: Time evolution of the storage systems' currents and voltages with grid following strategy

V.4.3 Test of the power dispatching strategy

The power dispatching strategy has also be tested with the same wind power profile and the same power requirement p_{gc_ref}=600W. Experimental results are compared with the simulation results (Fig.V-19). The active power, which is delivered to the grid, is well regulated. It is exactly equal to the microgrid's requirement (p_g=p_{gc_ref}=600W) because the line current control loop regulates directly the grid powers.

The DC-bus voltage is well regulated by the energy storage units against the fluctuant wind power. They are controlled to supply or to absorb necessary powers in order to maintain

constant the DC-bus voltage. Since the power losses in the filters and in the power converters are not taken into account in the study, the sum of the powers, which are supplied by the storage systems, is slightly more than the microgrid's requirement ($p_{sto}>p_{gc\_ref}$).

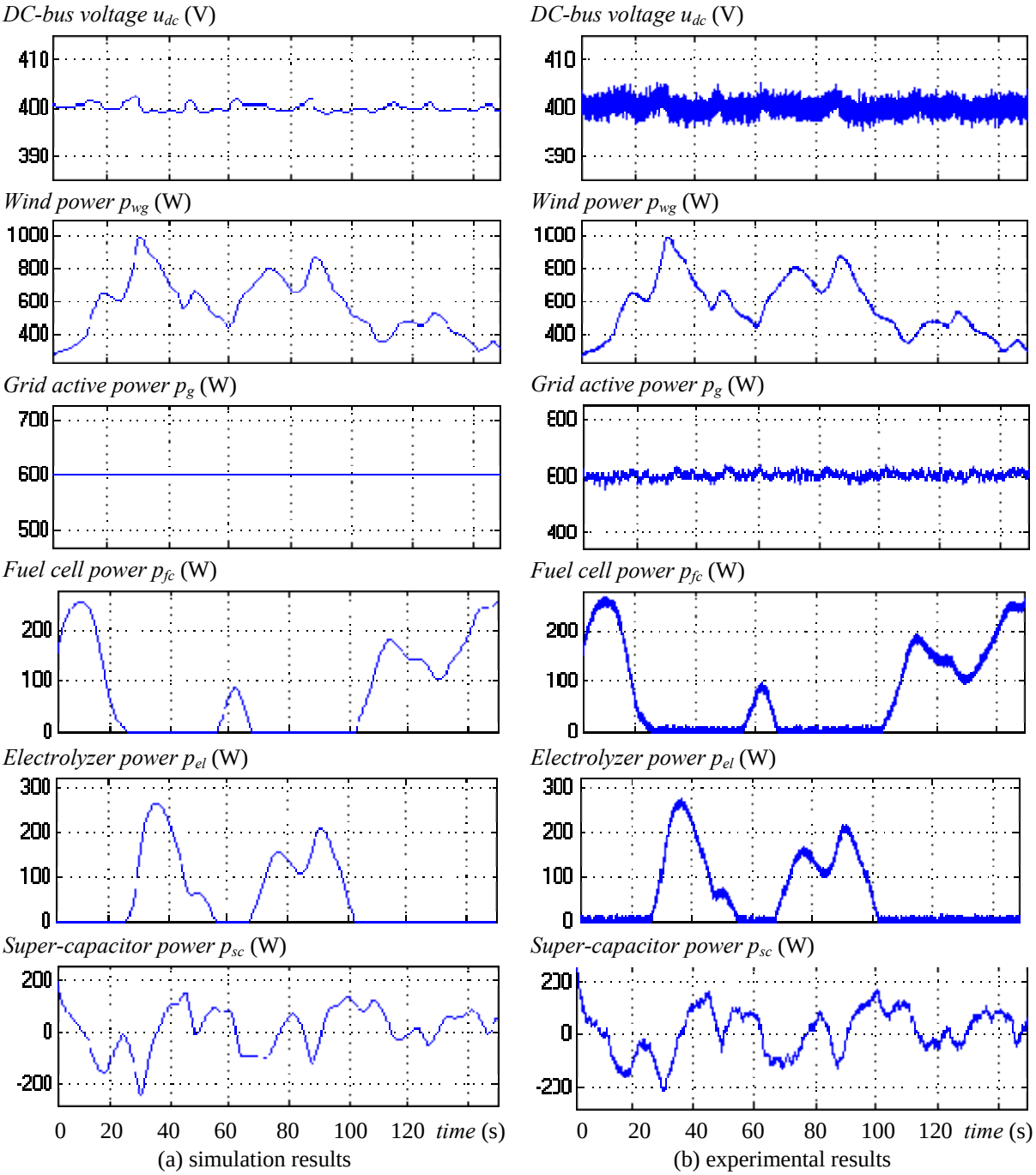

(a) simulation results (b) experimental results

Figure V-19: Time evolution of the powers inside the active wind generator with power dispatching strategy

The voltages and the currents of the super-capacitors, the fuel cells and the electrolyzers are shown in Fig.V-20. Similar results can be found here as in Fig.V-18.

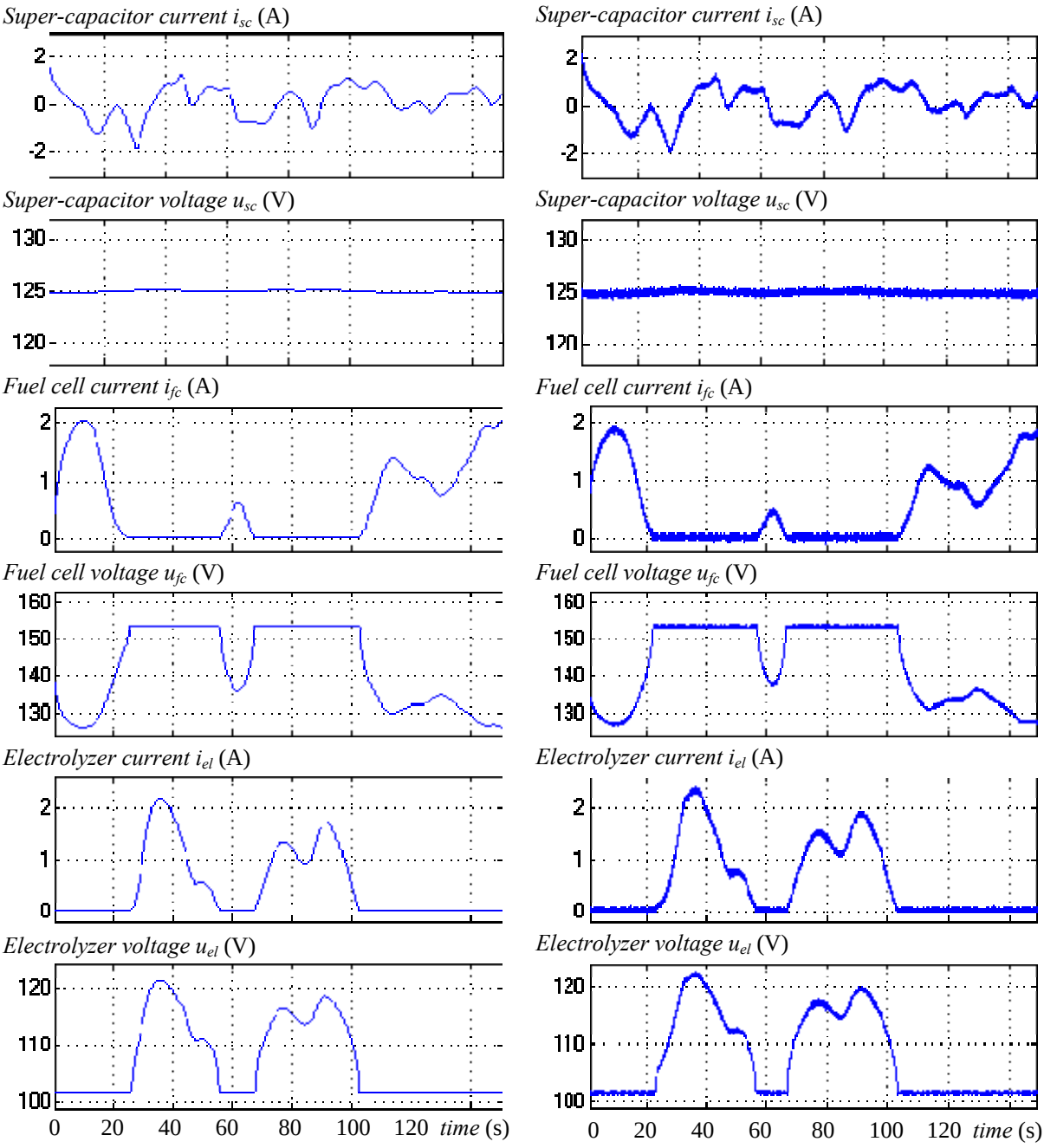

(a) simulation results (b) experimental results

Figure V-20: Time evolution of the storage systems' currents and voltages with power dispatching strategy

V.4.4 Comparison and discussion

Two power balancing strategies are tested above: the grid following strategy and the power dispatching strategy. Thanks to the help of energy storage systems, the DC-bus voltage and the grid powers can be well regulated while the wind generator is working in MPPT strategy to extract the maximum available wind energy.

Because of their high power dynamic, the super-capacitors are used for the transient regulation tasks. They can help to regulate the grid active power with the "grid following"

strategy and they can also help to regulate the DC-bus voltage with the “power dispatching” strategy. As result, the active wind generator can work in both power balancing strategies.

Because of its high energy capacity, the hydrogen based energy storage system ensures the energy availability of the active wind generator. Thanks to the help of the fuel cells and the electrolyzers, the storage level of the super-capacitor has not varied much. It means that the super-capacitors can continue working during a long period against the continuously fluctuant wind power. So the active wind generator can work like a classical power generator to provide ancillary services to the power system of the microgrid and to ensure the system’s power quality.

By comparing the two power balancing strategies with their experimental test results (Fig.V-17 and Fig.V-19), we see that the grid active power is better regulated in “grid following” strategy than in “power dispatching” strategy. In grid following strategy, the grid power varies continuously because the line current control loop regulates the DC-bus voltage and the grid power is adjusted all the time. In power dispatching strategy, the DC-bus voltage is regulated by the super-capacitors and the grid power can be directly used to supply the same power as required by the microgrid system operator. So if the active generator is required to provide necessary powers to participate in the microgrid management, the power dispatching strategy is preferred for more precisely controlling the grid powers.

With the same wind power profile, the similar power evolutions are found for the energy storage units. These two power balancing strategies have the similar impacts on the energy storage levels, because they are both developed based on the same power balance equations.

V.5 Energy management of the active wind generator

V.5.1 Studied microgrid

In our study, the active wind generator is connected to a microgrid and helps it to manage the network (Fig.V-21).

If the microgrid is fed only by the active wind generator, the energy storage systems should be sized large enough and operated robustly according to the load capacity of the microgrid. For example, the fuel cell system’s capacity should correspond to the nominal load of the microgrid and the electrolyzer system’s capacity corresponds to the wind generator’s nominal power. The super-capacitor should be able to supply the peak load during the transient. In this case, the fuel cells become the main power supply and the wind generator becomes a supplementary primary power source. Moreover, the very large hydrogen storage system should be equipped and hydrogen import from outside of the region should be possible. This is not a cost-effective solution nowadays and the purpose of profiting from the renewable energy is partially lost. The super-capacitors must be sized to filter wind power fluctuations and load demand variations.

If the microgrid is also fed by other power plants, the active wind generator can provide a continuously smooth power while the wind turbine works in MPPT strategy in order to maximize the use of the wind energy. In this case, the fuel cell system and the electrolyzer system should be sized according to the wind generator’s capacity, since, in the worst case,

the active wind generator is disconnected and all wind power is then stored in H_2. The super-capacitor system is then sized to filter wind power fluctuations.

In our study, the studied microgrid is fed by an active wind generator, a micro gas turbine and other power plants (Fig.V-21) [Fra 08]. When the renewable energy generator can not supply enough power, the micro gas turbine and the other power plants can be activated to feed the microgrid. It must be noted that since the storage units are associated in the active wind generator, a security margin exists for the energy supply. It is a very important point because now the microgrid system operator has a sufficient time delay to change the power planning of other power plants before the active generator shuts down. Moreover, the microgrid can be connected to the distribution network and necessary power exchanges can be performed between the microgrid and the distribution network.

The objective of the energy management is that the active wind generator can supply a prescribed power during a time interval (eg. 30 minutes), which is required by the microgrid system operator. This power reference is calculated one period before according to the forecasting of the wind condition.

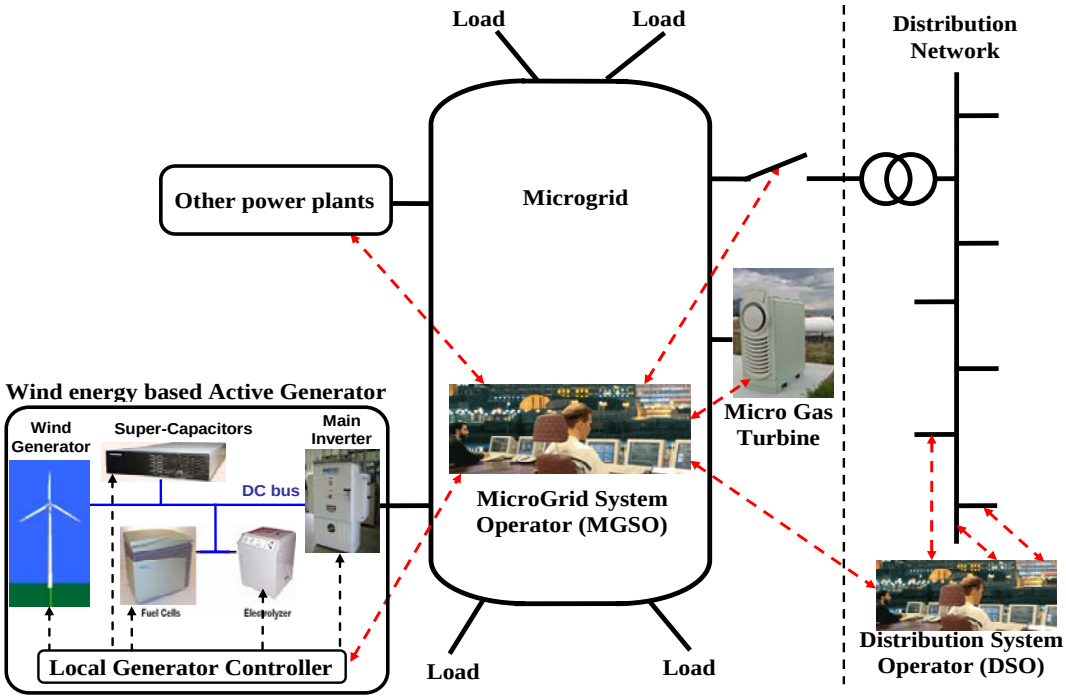

Figure V-21: Studied microgrid

V.5.2 Energy management

a) Role of the microgrid system operator

The energy is the integral of the power time evolution $p(t)$ during a time interval ΔT. If the time interval is fixed, the energy demand (E) can be expressed by an average power requirement ($<p>$) during a period (ΔT),

$$E = \int_{t_0}^{t_0+\Delta T} p(t)dt = \Delta T \cdot < p > . \qquad \text{(V-26)}$$

The microgrid system operator forecasts the wind profile $v_{wind}(t)$ and calculates the total expected energy (E_{wind}) with the estimated wind power ($\tilde{p}_{wind}(t)$) that the wind turbine can

capture and can generate during each time interval in a day. The power requirement p_{gc_ref} is obtained by dividing this estimated wind energy by the time interval,

$$p_{gc\_ref}(n\Delta T) \approx \frac{1}{\Delta T}\tilde{E}_{wind}\Big|_{n\Delta T}^{(n+1)\Delta T} = \frac{1}{\Delta T}\int_{n\Delta T}^{(n+1)\Delta T}\tilde{p}_{wind}(t)dt = \frac{1}{\Delta T}\int_{n\Delta T}^{(n+1)\Delta T} f\left(\tilde{v}_{wind}(t)\right)dt. \qquad \text{(V-27)}$$

b) Role of the active generator

A classical power plant can supply a smooth constant power according to the microgrid's requirement during the period. However, the wind generator can only supply a continuously fluctuant power because the actual wind speed is very fluctuant and will never be the same as the forecasted wind profile. These fast fluctuating power differences can be filtered by the super-capacitors based energy storage system, if the super-capacitor voltage is not too high or too low. Moreover, the forecasted wind energy and the real available wind energy can not be exactly the same. These energy differences can be stored or compensated by the hydrogen based energy storage system (by using fuel cells and electrolyzers), if the hydrogen tank is not full or empty (as the pressure is too high or too low).

This operating scheme is only possible if all storage levels are in a good range for the next period. Then the normal power requirements will be attributed and the active power generator works in a normal operating mode with all storage systems in normal states (as well as we discussed above).

Therefore, the storage level of each energy storage system should be monitored by an energy management unit. If the storage levels are not in a good range for the next period (30 minutes) according to the necessary energy estimations, they should be adjusted during the next period. And the power planning, which is required by the microgrid system operator, should also be modified for the next period. Then the active power generator works in other operating modes during which at least one storage level is not in a good range.

The energy management must ensure the energy availability of the active wind generator by monitoring and adjusting the storage level of each energy storage system. The communication with the microgrid system operator is thus necessary because it must coordinate the different power plants with upgraded their power planning for the next period.

V.5.3 Mode control unit

a) Presentation

The energy management strategies can be implemented in the Mode Control Unit (MCU) of the hierarchical control system (Appendix C) by determining the operating mode (M) of the hybrid power system. Each operating mode corresponds to a group of power balancing algorithms in the Power Sharing Level (PSL) of the Power Control Unit (PCU). The chosen power balancing algorithms perform the desired energy management purpose corresponding to the chosen operating mode.

The operating modes are determined in the Mode Control Unit according to the fast dynamic energy storage level ($Level_{sc}$) and the long-term energy storage level ($Level_{H2}$) (Fig.V-22). The super-capacitor voltage (u_{sc}) is used to characterize the fast-dynamic energy storage level. The hydrogen pressure (P_{H2}) in the tank is used to characterize the long-term energy storage level.

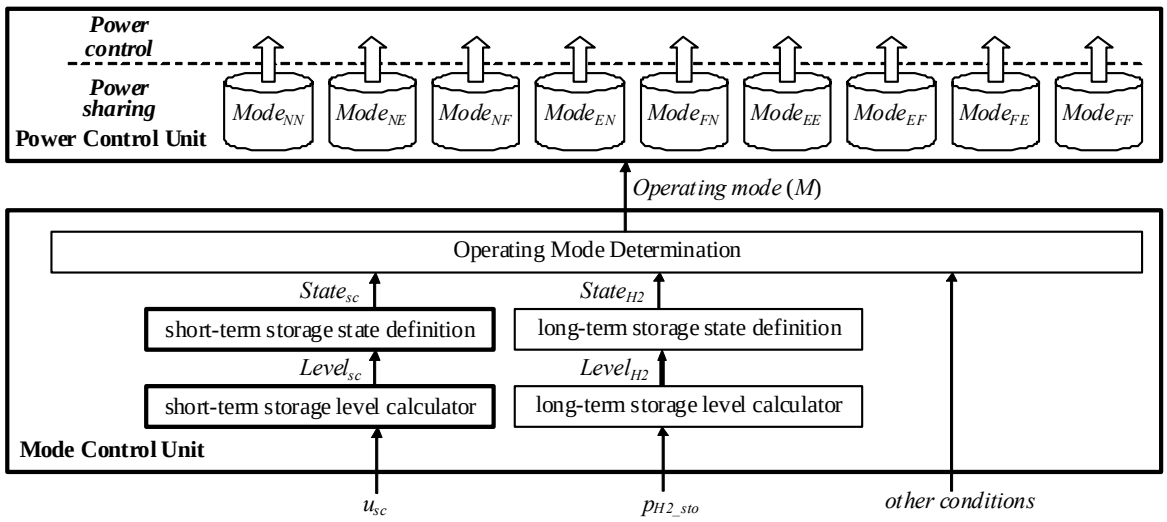

Figure V-22: Block diagram of the Mode Control Unit for the active wind generator

b) Short-term storage level

The short-term storage level can be expressed by the super-capacitor voltage and is indicated in percentage in the "short-term storage level calculator" of the Mode Control Unit (Fig.V-22):

$$Level_{sc} = \frac{E_{sc}}{E_{sc\_\max}} = \frac{C_{sc}u_{sc}^2/2}{C_{sc}u_{sc\_\max}^2/2} = \frac{u_{sc}^2}{u_{sc\_\max}^2}. \qquad \text{(V-28)}$$

with E_{sc}: the energy, which is stored in the super-capacitors;

E_{sc_max}: the maximal energy, which can be stored in the super-capacitors;

u_{sc}: the voltage across the super-capacitors;

u_{sc_max}: the maximal voltage across the super-capacitors banks;

C_{sc}: the equivalent capacitance of the super-capacitor banks.

For efficiency and security reasons, the operating fast dynamic storage level is limited from 25% to 95%. It corresponds to an operating voltage from 50% to 97.5% of the maximal voltage. In our study, three BOOSTCAP 48V super-capacitor modules are used in series and the maximal voltage is thus 144V. So the operating voltage range of the super-capacitors is from 72V to 140.4V (Table V-4).

Table V-4: Fast-dynamic energy storage level vs. the super-capacitor voltage

Fast-dynamic storage level ($Level_{sc}$):	0%	25%	30%	50%	90%	95%	100%
Super-capacitor voltage (u_{sc}):	0V	72V	78.9V	101.8V	136.6V	140.4V	144V

In order to avoid the chattering phenomena, two hysteresis operators are used to define the short-term storage state ($State_{sc}$) by the "short-term storage state definition" of the Mode Control Unit (Fig.V-22) with $Empty_{sc}$, $Normal_{sc}$ and $Full_{sc}$ (Fig.V-23).

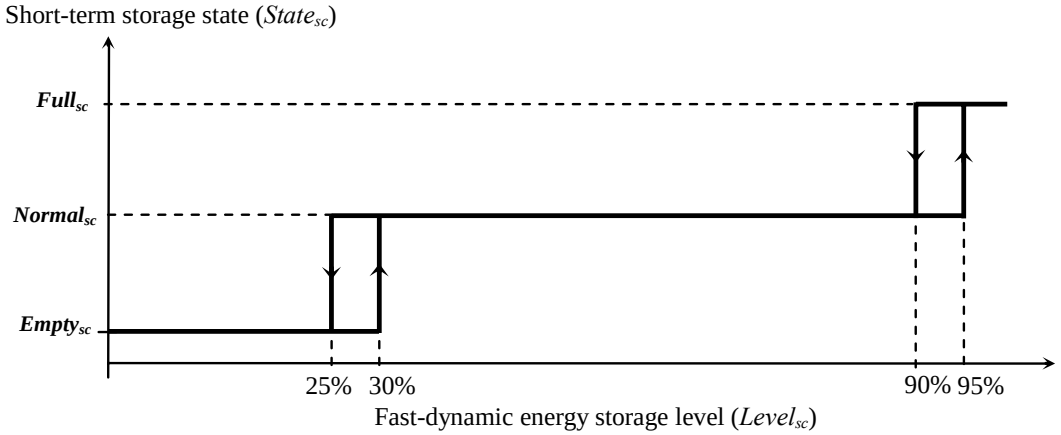

Figure V-23: Hysteresis control of the short-term recovering modes.

c) Long-term energy storage level

The long-term energy storage level can be expressed by the hydrogen pressure in the tank and is indicated in percentage in the "long-term storage level calculator" of the Mode Control Unit (Fig.V-22):

$$Level_{H2} = \frac{E_{H2}}{E_{H2\_\max}} = \frac{M_{H2}k_{HHV}}{M_{H2\_\max}k_{HHV}} = \frac{P_{H2}V_{H2}k_{HHV}/RT}{P_{H2\_\max}V_{H2}k_{HHV}/RT} = \frac{P_{H2}}{P_{H2\_\max}}. \qquad \text{(V-29)}$$

with E_{H2}: the energy, which is stored in the tank in hydrogen form;

E_{H2_max}: the maximal energy, which can be stored in the tank in hydrogen form;

M_{H2}: the number of moles of the hydrogen, which is stored in the tank;

M_{H2_max}: the maximal number of moles of the hydrogen in the tank;

P_{H2}: the hydrogen pressure in the tank;

P_{H2_max}: the maximal hydrogen pressure in the tank;

V_{H2}: the volume of the hydrogen tank;

k_{HVV}: the higher heating value, corresponding to the stored energy in 1 mole of hydrogen (302kJ/mol), or to the stored energy in $1m^3$ of hydrogen ($3.51kWh/Nm^3$) in stardard condition (T=25°C and P_{H2}=1bar).

The energy capacity of a hydrogen tanks can be easily sized with the volume of the tanks and the maximal pressure that the tanks can support. In our study, a 100L/20bar hydrogen tank is considered. The energy storage capacity is about 7kWh. If the fuel cell system should supply a 1000W rated power, it can stand up to about 7 hours due to its global power efficiency. For efficiency and security reasons, the operating pressure is limited from 2bar to 18bar. The long-term storage level is then limited from 10% to 90% (Table V-4).

Table V-5: Long-term energy storage level vs. the hydrogen pressure in the tank

Long-term storage level ($Level_{sc}$):	0%	10%	15%	50%	90%	95%	100%
Hydrogen pressure in the tank (P_{H2}):	0bar	2bar	3bar	10.8bar	18bar	19bar	20bar

In order to avoid the chattering phenomena, two hysteresis operators are used to define the short-term storage state ($State_{H2}$) by the "long-term storage state definition" of the Mode Control Unit (Fig.V-22) with $Empty_{H2}$, $Normal_{H2}$ and $Full_{H2}$ (Fig.V-24).

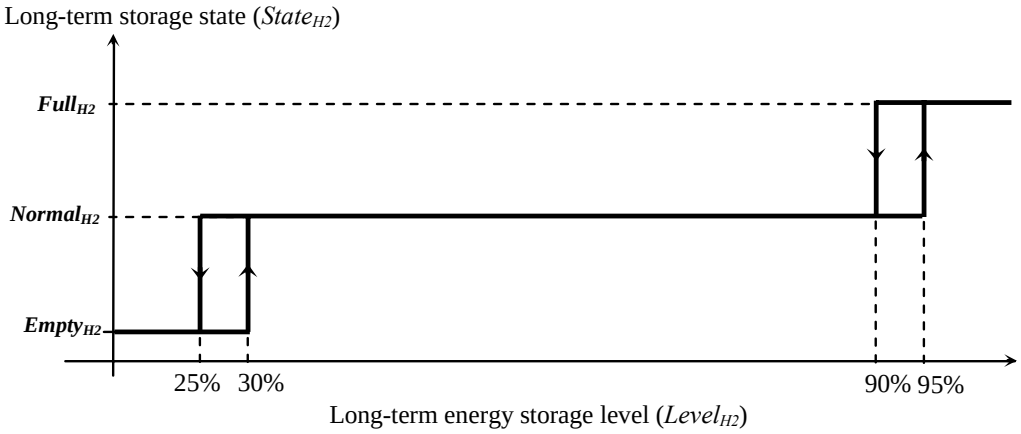

Figure V-24: Hysteresis control of the long-term recovering modes for the active wind generator.

d) Determination of the operating mode

According to the states of the energy storage systems ($State_{sc}$ and $State_{H2}$), four kinds of operating modes (including nine specific modes) can be defined in the "operating mode determination" of the Mode Control Unit for the active wind generator (Fig.V-22):

- Normal operating mode ($Mode_{NN}$)
- Short-term recovering modes ($Mode_{NE}$, $Mode_{NF}$)
- Long-term recovering modes ($Mode_{EN}$, $Mode_{FN}$)
- Entire recovering modes ($Mode_{EE}$, $Mode_{EF}$, $Mode_{FE}$, $Mode_{FF}$)

All these possible operating modes with respect to the energy storage systems are summarized and are determined by a look-up table (Table V-6).

Table V-6: Possible operating modes (M) for the active wind generator

$State_{sc}$ / $State_{H2}$	$Empty_{SC}$	$Normal_{SC}$	$Full_{SC}$
$Empty_{H2}$	$Mode_{EE}$	$Mode_{EN}$	$Mode_{EF}$
$Normal_{H2}$	$Mode_{NE}$	$Mode_{NN}$	$Mode_{NF}$
$Full_{H2}$	$Mode_{FE}$	$Mode_{FN}$	$Mode_{FE}$

For a specified operating mode, a group of power balancing algorithm is then applied in the Power Sharing Level of the Power Control Unit (Fig.V-22). As discussed above, the power dispatching strategy has better performances on the grid power control than the grid following strategy. So we consider only the power dispatching strategy for each operating mode in the following paragraphs.

V.5.4 Normal operating mode

When all energy storage systems are available (with their storage levels in a good range), $M=Mode_{NN}$, the active wind generator works in the normal operating mode. The power balancing algorithms, which are shown in Fig.V-15, can be directly used without any modification by the mode switching (Fig.V-25).

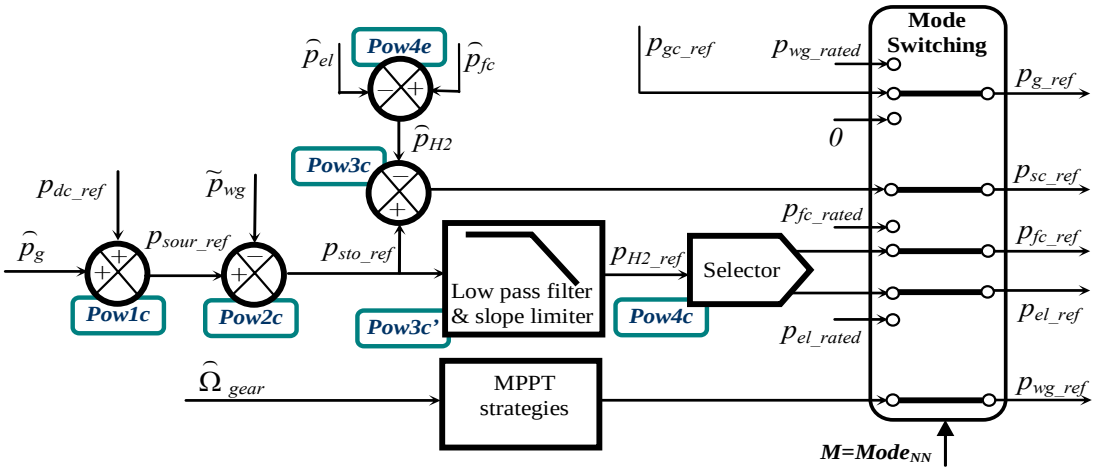

Figure V-25: Block diagram of the power dispatching strategy in normal mode

V.5.5 Short-term recovering modes

In short-term recovering modes, only the storage level ($Level_{sc}$) is out of the normal range and should be adjusted. The fuel cell or the electrolyzer should work under their nominal power until the storage level of the super-capacitor is recovered. At the same time, the power requirements from the microgrid system operator can still be respected.

a) Full super-capacitor mode

When the super-capacitor voltage increases above 140.4V, the short-term energy storage level is too high ($Level_{sc}$>95) for the super-capacitors to operate in the same way as in the normal mode. The long-term energy storage level is still in a good range and the active wind generator begins to work in the "full super-capacitor mode". Special energy management strategy should be performed to recover the short-dynamic energy storage level ($Level_{sc}$) as soon as possible, while the active grid power is always well regulated to achieve the microgrid's power requirement.

In this case, the look-up table of the Operating Mode Determination (Table V-6) gives $M=Mode_{NF}$. The "mode switching" modifies only the electrolyzer power reference (p_{el_ref}) (Fig.V-26). It should be equal to its rated power,

$$p_{el\_ref} = p_{el\_rated} . \qquad \text{(V-30)}$$

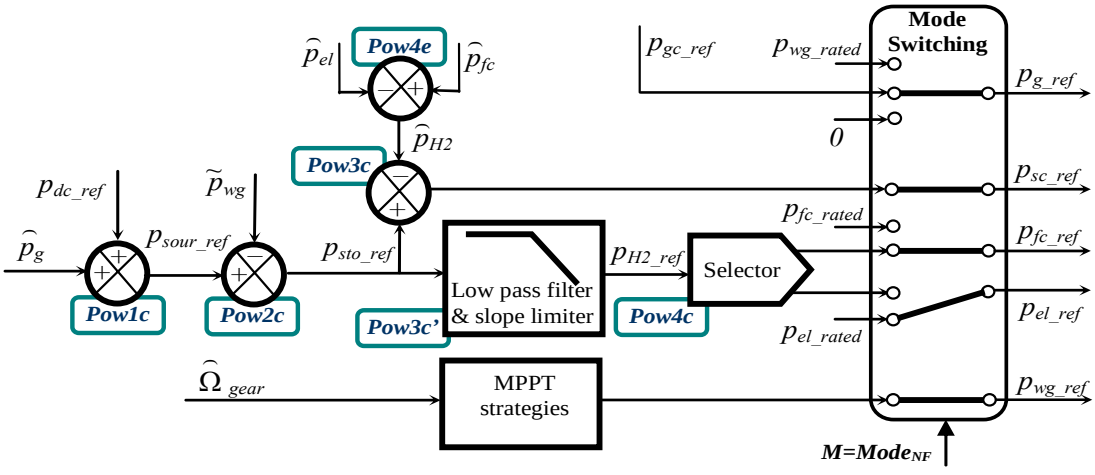

Figure V-26: Block diagram of the power dispatching strategy in "full-SC" mode

As result, the electrolyzers consume more power than required and the super-capacitors start to be discharged for returning back to its normal state. Of course, the transient should be limited with a power slope. With the same power control algorithms for the other source, the super-capacitor will be automatically discharged.

b) Empty super-capacitor mode

When the super-capacitor voltage decreases below 72V, the short-term energy storage level is too low ($Level_{sc}$<25) for the super-capacitor to continue operating in the same way as in the normal mode. The long-term energy storage level is still in a good range and the active wind generator begins to work in the "empty super-capacitor mode". Special energy management strategy should be performed to recover the fast-dynamic energy storage level as soon as possible, while the active grid power is always well regulated to achieve the microgrid's power requirement.

In this case, the look-up table of the Operating Mode Determination (Table V-6) gives $M=Mode_{NE}$. The "mode switching" modifies only the fuel cell power reference (p_{fc_ref}) by the mode switching (Fig.V-27). It should be equal to its rated power,

$$p_{fc\_ref} = p_{fc\_rated} . \quad \text{(V-31)}$$

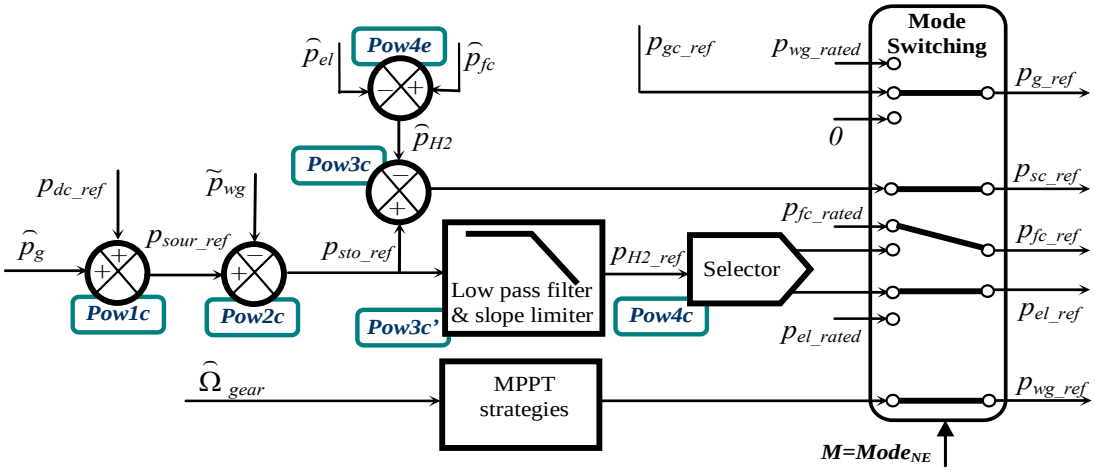

Figure V-27: Block diagram of the power dispatching strategy in "empty-SC" mode

As result, the fuel cells generate more power than required and the super-capacitors start to be recharged for returning back to its normal state. Of course, the transient should be limited with a power slope. With the same power control algorithms for the other sources, the super-capacitor will be automatically recharged.

V.5.6 Long-term recovering modes

In long-term recovering modes, the storage level ($Level_{H2}$) is out of the normal range and should be adjusted. Because the active wind generator has a problem of the energy availability now, the grid power reference can no long be the same as the microgrid power requirements. Thus, the microgrid system operator should be informed of this situation, it should attribute more power requirements or less power requirements for other power plants to overcome this special period.

a) Full hydrogen mode

When the hydrogen pressure in the tank increases above 18bar, the long-term energy storage level is too high ($Level_{H2}$>90%) for the hydrogen tank to store more hydrogen. So the electrolyzer system can not operate in the same way as in the normal mode. The short-term storage level is still in a good range and the active wind generator begins to work in the "full hydrogen mode". Special energy management strategy should be performed to recover the long-term energy storage level.

In this case, we have $M=Mode_{FN}$, the grid power reference (p_{gc_ref}) of the active wind generator should be modified in order to ask the electrolyzers to consume more hydrogen from the H_2 storage. It can be a higher value, which corresponds to (for example 50%) more energy than the forecasted wind energy during the next periods, until a good hydrogen pressure is recovered.

Or it can also be set with the rated power value (p_{gc_rated}) of the active wind generator (Fig.V-28).

$$p_{gc\_ref}(n\Delta T) = p_{gc\_rated}. \tag{V-32}$$

Then the fuel cell will be activated alone to supply the complement power between the actual wind power (p_{wg}) and the active wind generator's rated power (p_{gc_rated}), because this value of p_{wg} will never be higher than p_{gc_rated}. As result, the hydrogen tank will be discharged since the hydrogen is used by the fuel cell to supply the power to the grid.

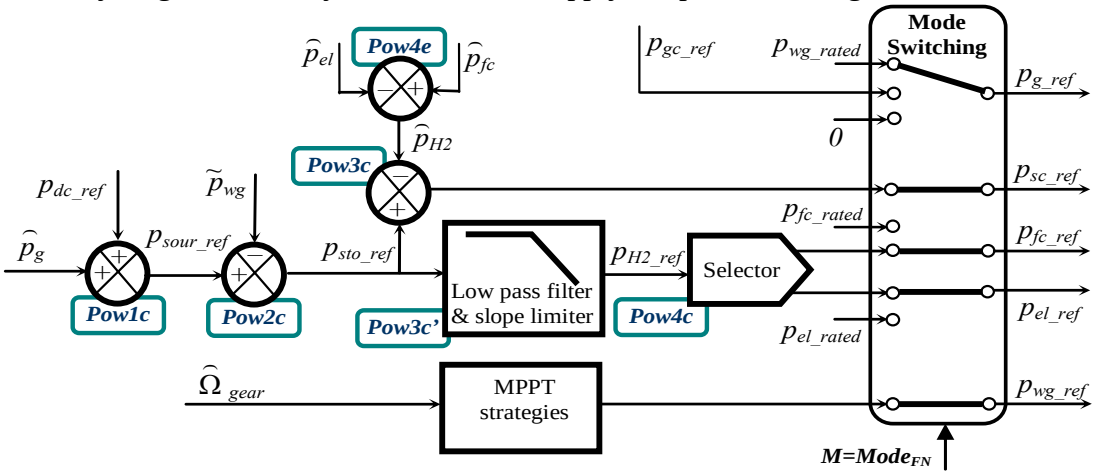

Figure V-28: Block diagram of the power dispatching strategy in "full-H2" mode

b) Empty hydrogen mode

When the hydrogen pressure in the tank decreases below 18bar, the long-term energy storage level is too low ($Level_{H2}$<10%) for the hydrogen tank to release more hydrogen. So the fuel cell system can not operate in the normal mode. The short-term storage level is still in a good range and the active wind generator begins to work in the "empty hydrogen mode". Special energy management strategy should be performed to recover the long-term energy storage level.

In this case, we have $M=Mode_{EN}$, the grid power reference (p_{gc_ref}) of the active wind generator should be modified in order to ask the fuel cells to produce more hydrogen for the H_2 storage. It can be a lower value, which corresponds to (for example 50%) less energy than the forecasted wind energy during the next periods, until the hydrogen pressure is recovered.

Or it can also be set to zero (Fig.V-29),

$$p_{gc\_ref}(n\Delta T) = 0. \tag{V-33}$$

Then the electrolyzer system will be activated alone to absorb the power difference between the actual wind power (p_{wg}) and the zero power reference, because this value of p_{wg} will never be smaller than 0. As result, the hydrogen tank will be recharged with the hydrogen which is produced with the generated wind power.

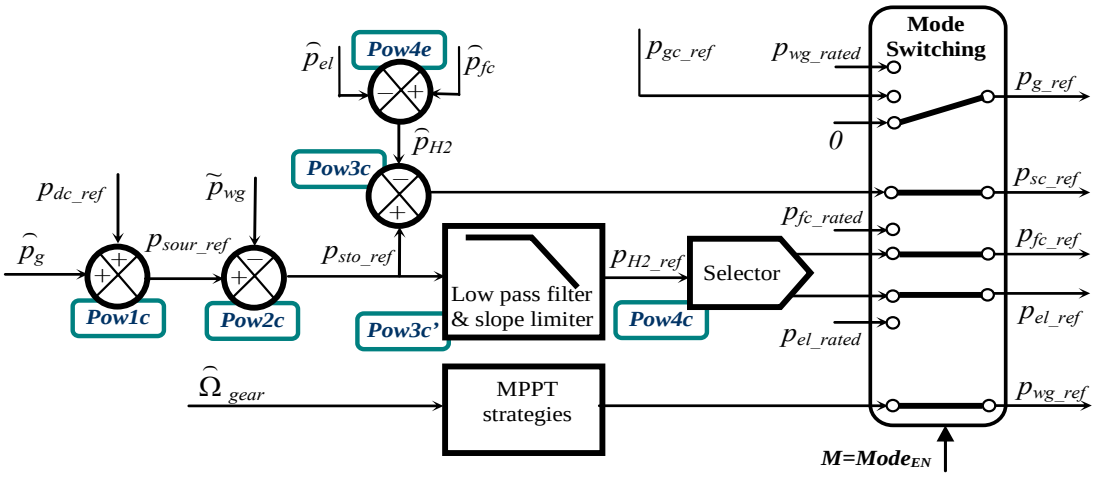

Figure V-29: Block diagram of the power dispatching strategy in "empty-H2" mode.

V.5.7 Entire recovering modes

We have introduced five specific operating modes (with $M=Mode_{NN,}$, $M=Mode_{NF,}$, $M=Mode_{NE,}$, $M=Mode_{FN,}$, $M=Mode_{EN,}$) in the previous paragraphs. In all of these five operating modes, even if one of the two energy storage systems can not work normally, the wind generators can always work in a MPPT strategy to extract the maximum of the available wind energy if the wind speed is medium.

When both storage levels are out of their normal ranges, we have $M=Mode_{FF,}$, $M=Mode_{FE,}$, $M=Mode_{EF,}$, $M=Mode_{EE}$ in Table V-6, and the active wind generator works in the "entire recovering modes". None of the energy storage systems can properly operate and the active wind generator enters into an extremely abnormal situation.

We will not present them in detail, because the active wind generator is not "active" during this operating mode. In this case, we have two possible solutions.

- Either the wind generator works in a MPPT strategy and the grid following strategy is used to regulate the DC bus voltage and to deliver a fluctuant wind power to the grid. In this case, we loose the ancillary service for the microgrid management from the active wind generator, but we have still the power production.
- Or a constant power can be exchanged with the microgrid to recover the long-term storage level ($Level_{H2}$), and the wind generator should be stopped or should supply a constant power if a necessary wind speed is available. When $Level_{H2}$ is recovered, the active wind generator can operate in the "short-term recovering mode" to recover the short-term storage level ($Level_{sc}$). In this case, the wind power production is limited, but the active wind generator can provide ancillary service to the grid as soon as possible.

V.6 Performance tests of the energy management strategies

V.6.1 Presentation

The energy management strategy test should be performed for a long time range, so numerical simulations are used to test the performance. The main objective is to monitor the variation of the storage levels in order to evaluate these energy management strategies, so only the power models are used in this part. The same parameters are used in these tests as in the previous sections

V.6.2 Normal operating mode

In the normal operating mode, the two storage levels are both in a good range (u_{sc}=125V and P_{H2}=10bar). The same wind power profile is given and is repeated during 150 minutes (9000 seconds). The grid power is updated every period of 25 minutes (1500 seconds). The test results are shown in Fig.V-30.

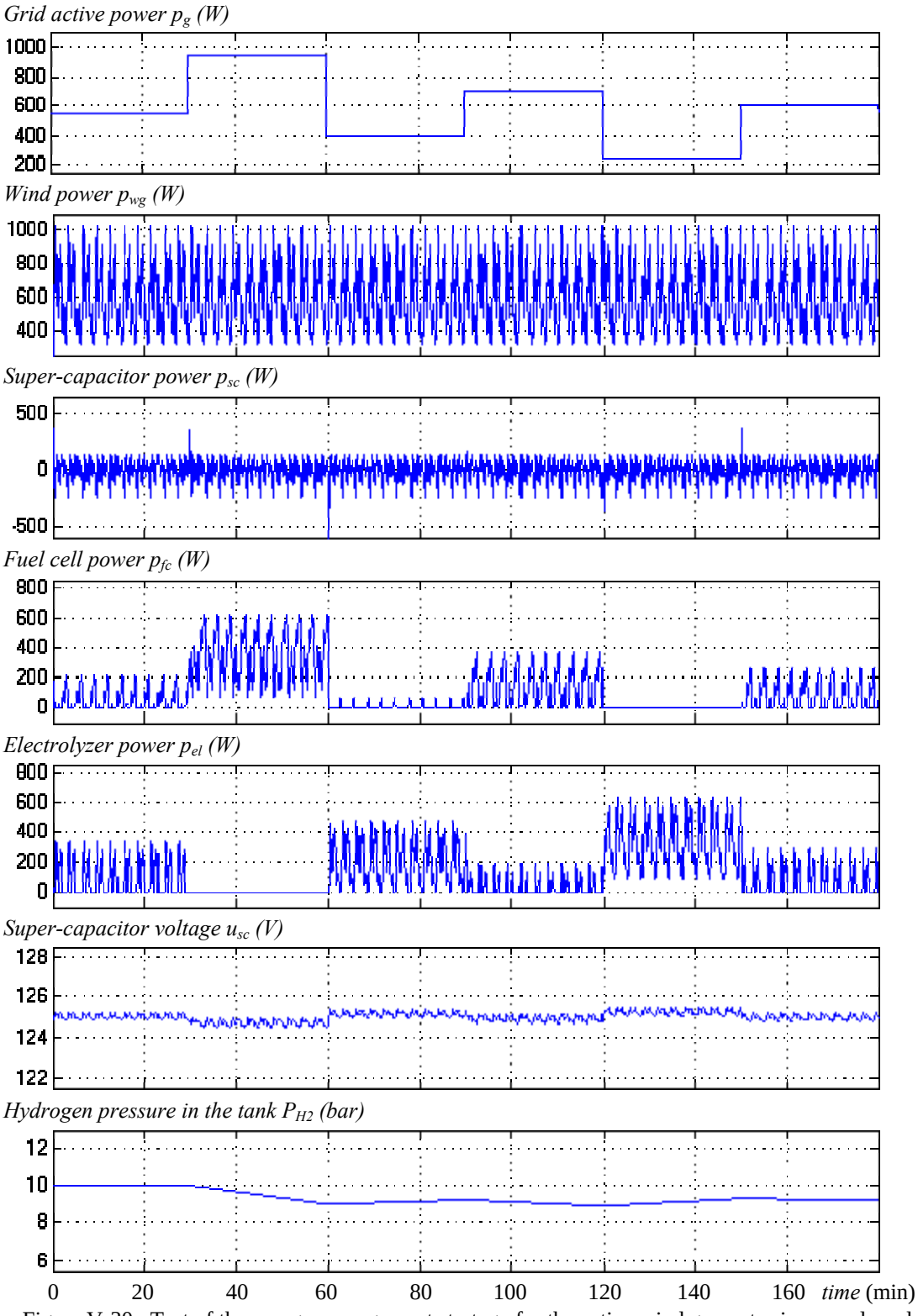

Figure V-30: Test of the energy management strategy for the active wind generator in normal mode

With the proposed power balancing strategies, the super-capacitor voltage has not much varied, thanks to the available long-term energy storage system. With a good wind generation forecasting, the grid power reference (p_{gc_ref}=550W) is close to the average wind power (from 0 to 30min), and the hydrogen pressure in the tank does not vary much. When the forecasted

wind generation is not very accurate, the long-term storage system should store or release more energy in order to ensure the energy availability of the active wind generator and the long-term storage level varies (from 30minutes to 180minutes).

V.6.3 Short-term recovering modes

When the short-term storage level ($Level_{sc}$) goes out of the good range (from 25% to 95%), the active wind generation works in short-term recovering mode. Two tests are performed to evaluate the energy management strategies in short-term recovering mode, respectively for the "full super-capacitor mode" (Fig.V-31) and the "empty super-capacitor mode" (Fig.V-32).

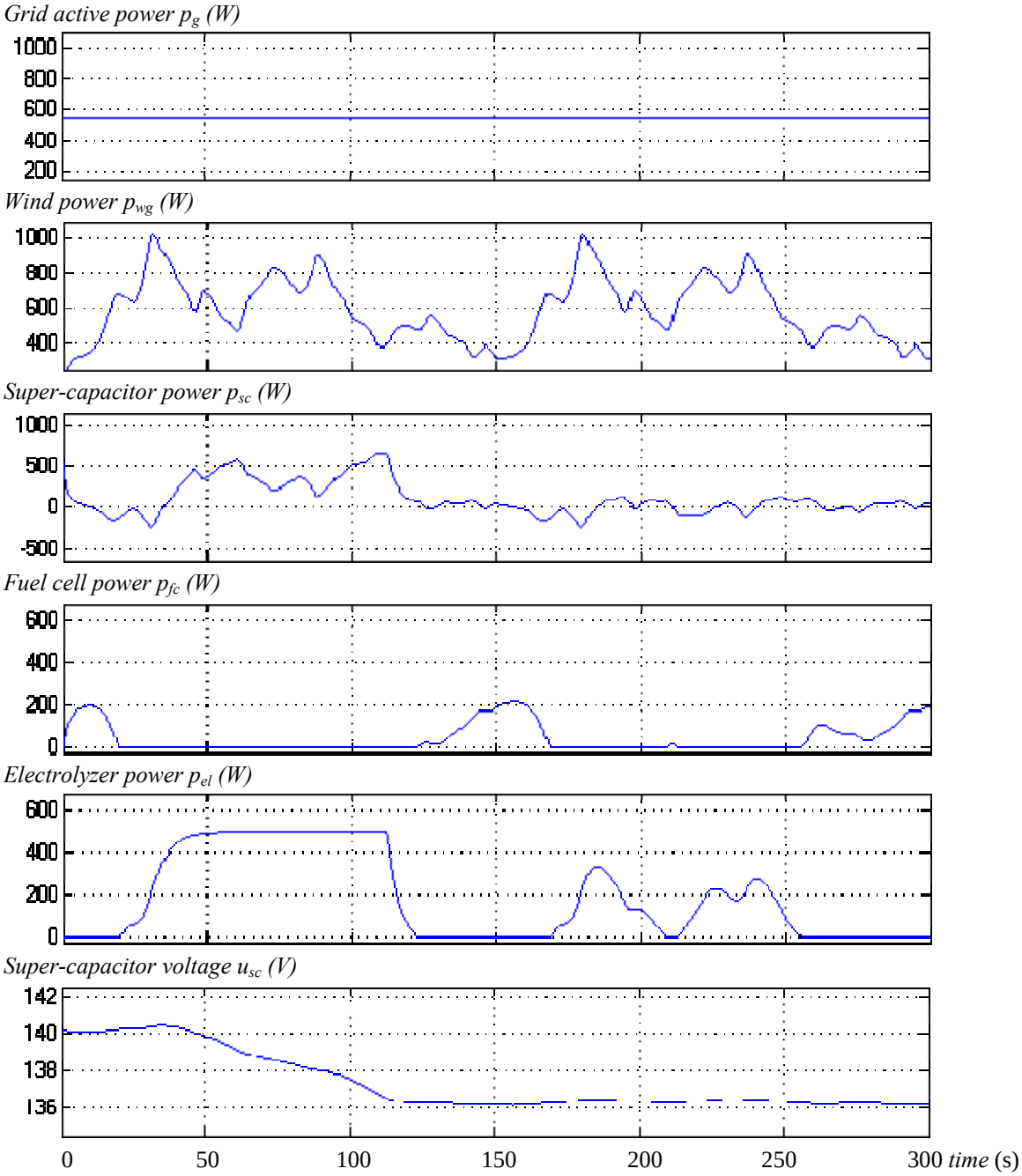

Figure V-31: Test of the energy management strategy for the active wind generator in "full-SC" mode

When the super-capacitor voltage goes above 140.4V ($Level_{sc}$=95%), the "full super-capacitor mode" should be started immediately. A constant power reference (500W) is sent to the electrolyzer and the fuel cell is deactivated until the super-capacitor voltage is back below 136.6V ($Level_{sc}$=90%) (Fig.V-31).

When the super-capacitor voltage goes below 72V ($Level_{sc}$=25%), the "empty super-capacitor mode" should be started immediately. A constant power reference (500W) is sent to the fuel cell and the electrolyzer is deactivated until the super-capacitor voltage is back above 78.9V ($Level_{sc}$=30%) (Fig.V-32).

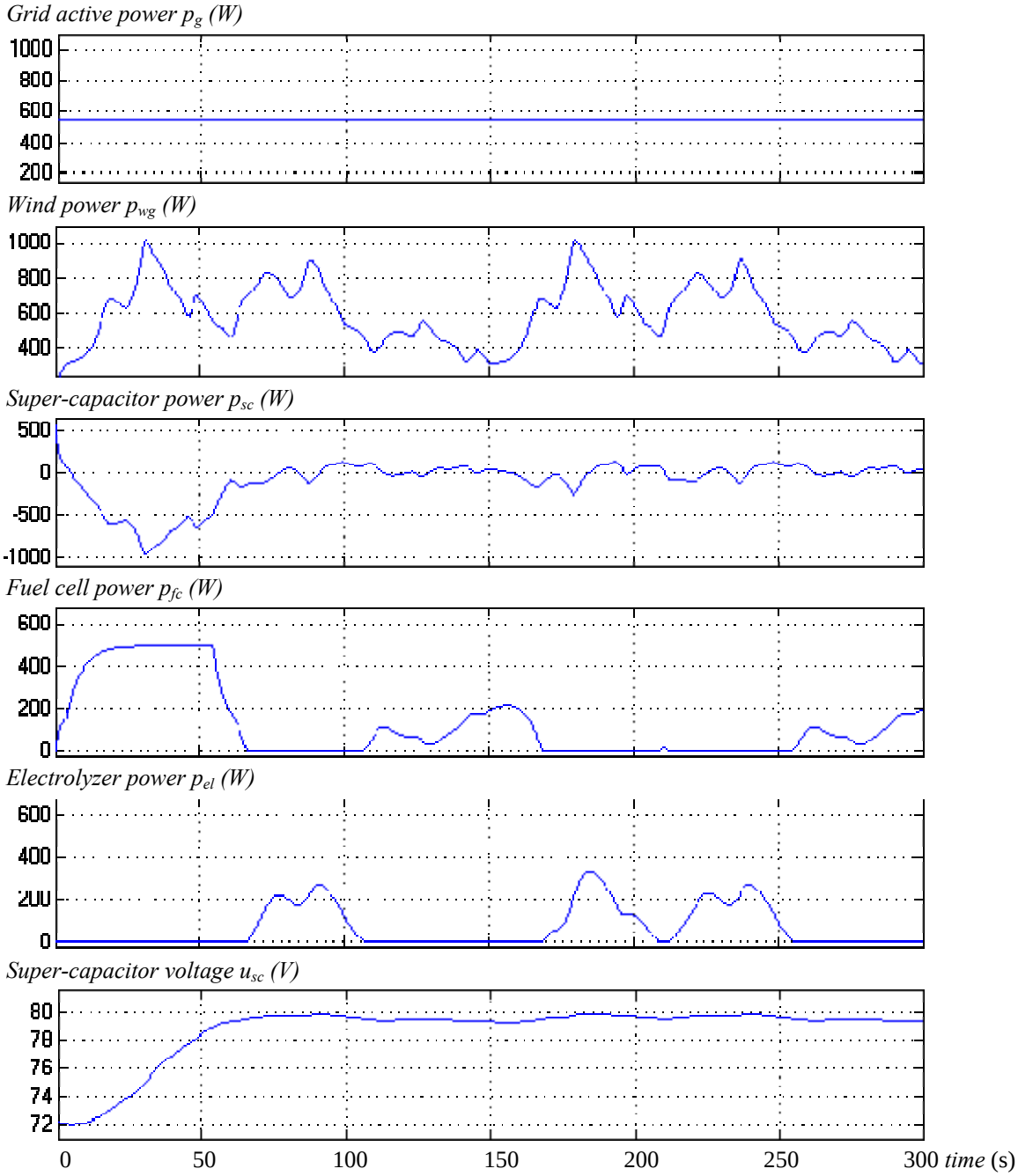

Figure V-32: Test of the energy management strategy for the active wind generator in "empty-SC" mode

V.6.4 Long-term recovering modes

When the long-term storage level ($Level_{H2}$) goes out of the good range (from 10% to 90%), the active wind generation works in long-term recovering mode. Two tests are performed to evaluate the energy management strategies in long-term recovering mode, respectively for "full hydrogen mode" (Fig.V-33) and "empty hydrogen mode" (Fig.V-34).

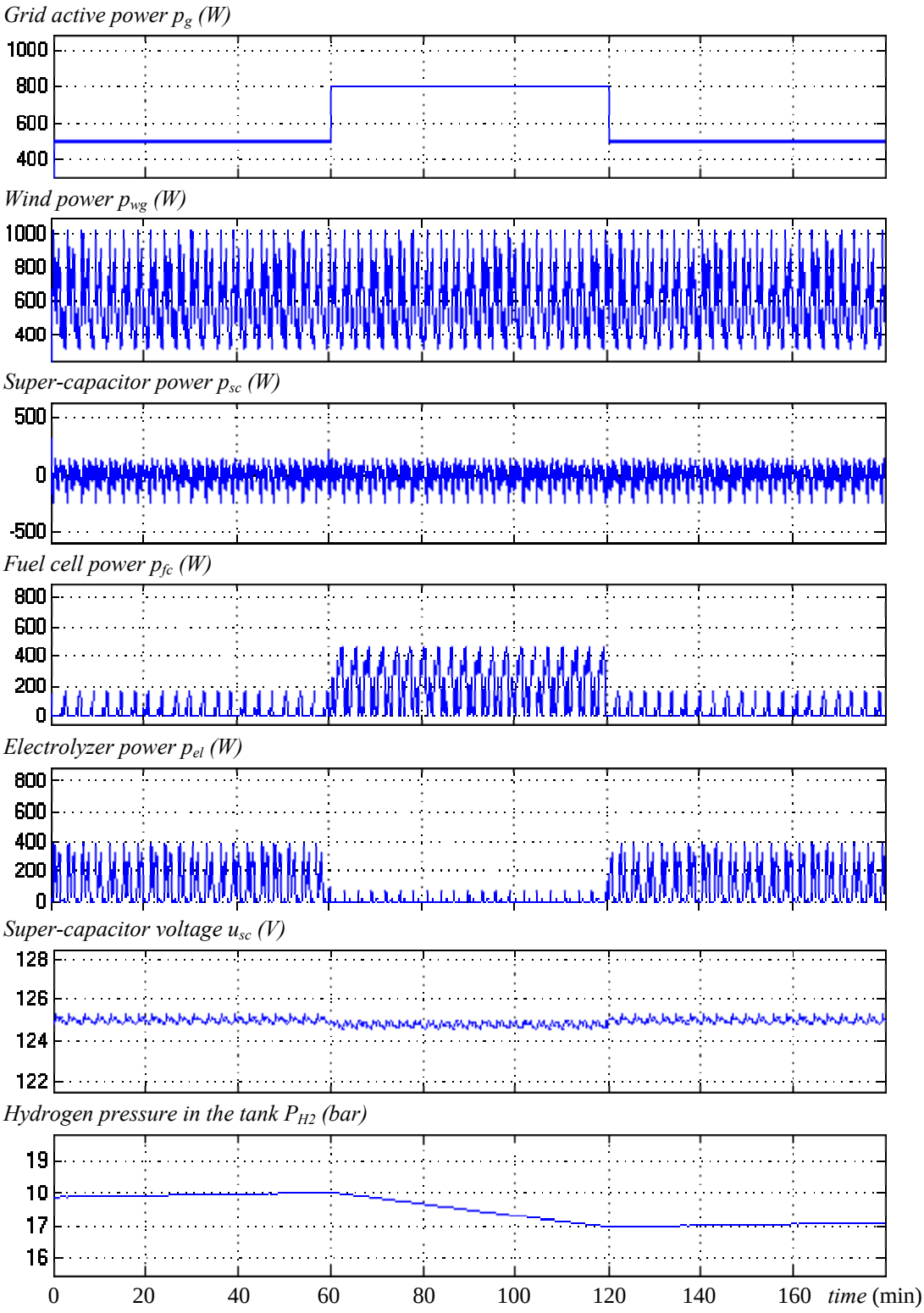

Figure V-33: Test of the energy management strategy for the active wind generator in "full-H2" mode

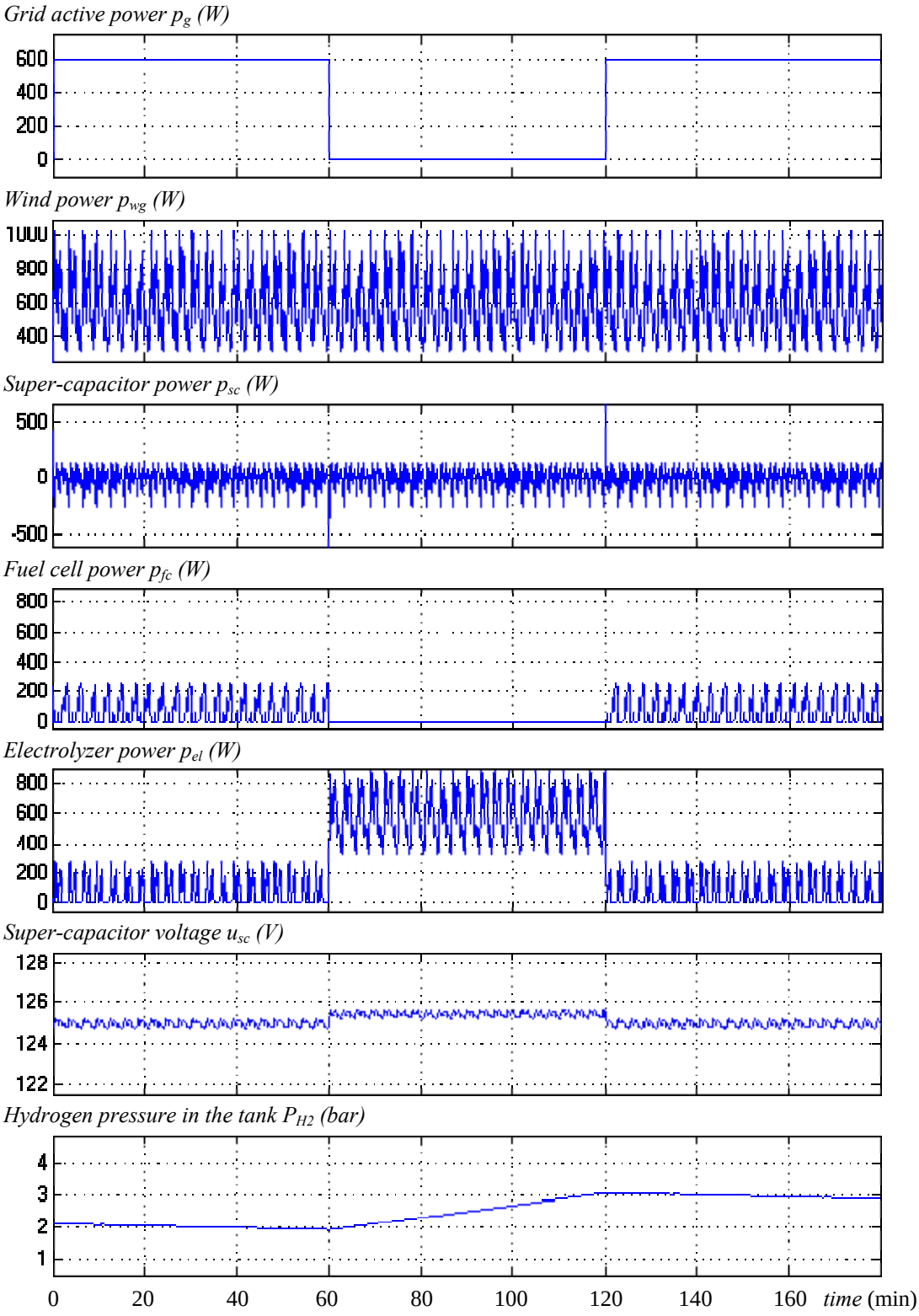

Figure V-34: Test of the energy management strategy for the active wind generator in "empty-H2" mode

When the hydrogen pressure in the tank goes above 18bar ($Level_{sc}$=90%), the "full hydrogen mode" should be started for the next period of 30 minutes. The microgrid system operator should attribute a higher active power requirement (800W for example) than the value, which is obtained by wind condition forecasting (600W). With the properly used power

balancing strategy, the fuel cells supply more power than the electrolyzers consume and the hydrogen pressure in the tank increases. The normal operating mode will be restarted only if the hydrogen pressure in the tank is back below 17bar ($Level_{sc}$=85%) in the previous period. (Fig.V-33).

When the hydrogen pressure in the tank goes below 2bar ($Level_{sc}$=10%), the "empty hydrogen mode" should be started for the next period of 30 minutes. The microgrid system operator should attribute a lower active power requirement (0W for example) than the value, which is obtained by wind condition forecasting (600W). With the properly used power balancing strategy, the electrolyzers consume more power than the fuel cells supply and the hydrogen pressure in the tank decreases. The normal operating mode will be restarted only if the hydrogen pressure in the tank is back above 3bar ($Level_{sc}$=15%) in the previous period. (Fig.V-34).

V.6.5 Discussion

a) Power balancing and energy management

Power balancing deals with the instantaneous power flow control among the different sources. As result, it leads to directly two basic control functions: DC-bus voltage regulation and grid power regulation. With the presence of the fast-dynamic energy storage system and the long-term energy storage system, both the "grid following" strategy and the "power dispatching" strategy can be used for the power balancing of the proposed active wind generator. Because of the better performance on the grid power regulation, the "power dispatching" strategy is preferred.

Energy management deals with the monitoring and control of the energy storage levels by taking decisions on the system's operating mode. As result, it leads to the energy sustainability of the power system. The thresholds of the storage levels are not invariable, but should be adapted with the available equipments and the user's requirements.

b) Sizing of the storage systems

The sizing of the storage systems depends on the system requirement.

If the total conventional generator power is extremely larger than the integrated wind generator, the fluctuant wind power has even no impact on the system's power quality. So the wind generator can work like a passive generator and no energy storage systems are needed.

If the microgrid is partially fed by the wind generator, smooth wind powers are required in order to ensure the system's power quality and even to provide sometimes some services to the power system. In this case, energy storage systems are needed to build an active wind generator. They should only be sized according to the wind generator's rated power, in order to supply or to absorb the rated wind power in the worst case.

If the microgrid is mainly fed by the wind generator, the energy storage system of the active wind generator should be sized according to the microgrid's capacity. Because of the fluctuant and random characteristics of the wind condition, the active wind generator should supply the system even if there is no wind.

The sizing of the storage systems is relatively easy. In order to adapt the power level (voltage and current), corresponding cell numbers and active surface areas can be easily calculated for the fuel cell stack and the electrolyzer and the number of the modules in series

and the number of the modules in parallel can also be easily calculated for the super-capacitor bank.

The specified sizing of the storage systems will not change the power balancing and energy management strategies. Only the storage levels' thresholds need to be adjusted. So the discussed methodologies can be applied to the DC-coupled hybrid power system of different power scales.

V.6.6 Efficiency analysis

In a classical wind energy conversion system, the generated wind energy, which is sent to the DC bus, is totally delivered to the grid. This energy efficiency of this energy conversion system can be considered as 100%, if all kinds of power losses are ignored.

In the studied active wind generator, two kinds of energy storage system are integrated through the DC bus. A part of the generated wind power is exchanged with them before being delivered to the grid. So the round-trip efficiency of the storage systems should be taken into account to evaluate the system efficiency (Fig.V-35).

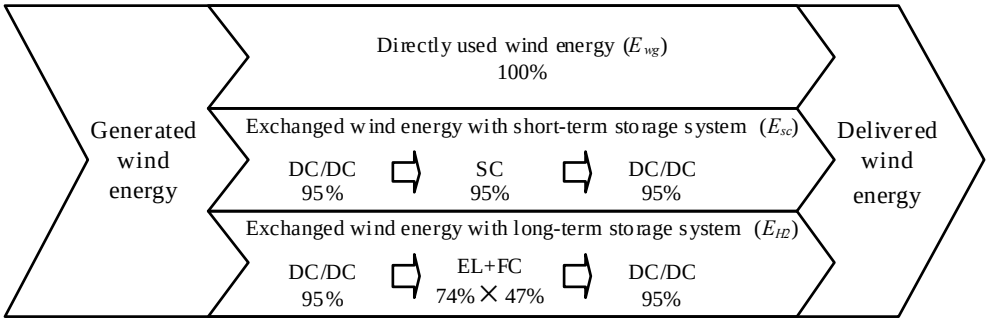

Figure V-35: Energy exchange inside the active wind generator

The assumed efficiencies of each component are listed in Table V-7. Therefore, the round-trip efficiency of the fast-dynamic storage system is about 85.74% (0.95×0.95×0.95). The round-trip efficiency of long-term energy storage by hydrogen is 31.38% (0.95×0.74×0.47×0.95). If the intrinsic losses (for example, the powers, which are consumed by the auxiliary systems, like compressors) are taken into account, the round-trip efficiency is 29.84% [Li 08a]. The system efficiency can be obtained by using the following equation,

$$\eta_{tot} = \frac{E_{del}}{E_{gen}} = \frac{E_{wg} + \eta_{H2}E_{H2} + \eta_{sc}E_{sc}}{E_{wg} + E_{H2} + E_{sc}} = \alpha_{wg} + 85.74\%\alpha_{H2} + 29.84\%\alpha_{sc} \qquad \text{(V-34)}$$

with E_{gen}: the generated wind energy, which is sent to the DC bus;
E_{del}: the delivered wind energy from the DC bus to the grid
E_{wg}: the energy, which is directly delivered to the grid from the wind generator;
E_{H2}: the energy, which is exchanged with the long-term energy storage system;
E_{sc}: the energy, which is exchanged with the fast-dynamic energy storage system;
η_{H2}: the round-trip efficiency of long-term energy storage system (29.84%);
η_{sc}: the round-trip efficiency of fast-dynamic energy storage system (85.74%);
η_{tot}: the system efficiency of the active wind generator;
α_{wg}: the energy distribution ratio of E_{wg} in E_{gen};
α_{H2}: the energy distribution ratio of E_{H2} in E_{gen};
α_{sc}: the energy distribution ratio of E_{sc} in E_{gen}.

Table V-7: The round-trip efficiency of the storage systems

Super-capacitors bank	Fuel cell system	Electrolyzer system	DC-DC converters	Fast-dynamic storage	Long-term storage
95%	47%	74%	95%	85.74%	29.84%

The system efficiency is 88.5% (with α_{wg}=79.1%, α_{sc}=5.6% and α_{H2}=15.3%) in normal operating mode with p_{wg_ref}=550W during 150 minutes. It becomes 85.0% (with α_{wg}=74.1%, α_{sc}=5.6% and α_{H2}=20.3%) for the scenario, which is presented in Fig.V-30. We can see that the energy distribution ratios (α_{wg}, α_{H2} and α_{sc}) depend on many factors. For examples:

- If the wind power is less fluctuant, less energy is exchanged with the energy storage systems, so the directly transferred wind energy (α_{wg}) is increased and the system efficiency η_{tot} is also increased.
- If the wind forecast is more precise, α_{wg} can be increased, α_{H2} can be reduced and the system efficiency η_{tot} can be improved.

Possible values of the system efficiency are calculated in Table.V-8 according to different energy distribution ratios.

Table V-8: Possible system efficiencies according to different energy distribution ratios

α_{wg} \ α_{H2}	0.0	0.1	0.2	0.3	0.4	0.5	0.6	0.7	0.8	0.9	1.0
0.0	85%	80%	75%	69%	63%	58%	53%	46%	41%	36%	29%
0.1	87%	81%	76%	71%	65%	59%	54%	48%	42%	37%	–
0.2	88%	83%	78%	72%	66%	61%	55%	49%	44%	–	–
0.3	91%	84%	79%	74%	67%	62%	57%	51%	–	–	–
0.4	92%	86%	80%	75%	69%	63%	58%	–	–	–	–
0.5	93%	87%	82%	76%	71%	65%	–	–	–	–	–
0.6	95%	88%	83%	78%	72%	–	–	–	–	–	–
0.7	96%	91%	84%	79%	–	–	–	–	–	–	–
0.8	97%	92%	86%	–	–	–	–	–	–	–	–
0.9	99%	93%	–	–	–	–	–	–	–	–	–
1.0	100%	–	–	–	–	–	–	–	–	–	–

Some extremely cases are explained as follows:

- when no storage devices are used and the wind power is totally delivered to the grid, the system efficiency is considered as 100% (orange);
- when only super-capacitors are used, the possible values of system efficiency are presented in the second column (blue);
- when only hydrogen devices are used, the possible system efficiencies are presented in the diagonal (green);
- with both energy storage systems, the system efficiency should probably stay in the triangle area (purple);
- the other values of the system efficiency will rarely appear if the system works in normal operating mode (white).

V.6.7 Cost evaluation

The economic and technical performance should be evaluated for the multi-source hybrid power system, like cost and efficiency of each component and of the whole system. Table.V-9 presents the actual costs (2008) and the expected costs (2015-2020) of the components [Zou 07] [Bec 08].

Some similar economic and technical metrics have also been proposed and have been applied to compare different hybrid power systems based on solar energy (PV/Batteries, PV/H2 and PV/Batteries/H2) [Li 08c]. Due to the short lifetime and high price, the batteries are not suitable for long-term energy storage. The lowest cost with a better efficiency can be obtained by using batteries for short-term energy storage and hydrogen devices for long-term storage (Table.V-10).

Table V-9: Techno-economic statistics of different components [Zou 07] [Bec 08]

	Efficiency	**Lifetime**	**Present cost**	**Expected cost (2015)**	**Cost Reduction**
Photovoltaic Panels	14%	25 year	10200 $/kW	8000 $/kW	22%
Wind Turbines	30%	25 year	1200 $/kW	1200 $/kW	Stable
Power Converters	95%	10 year	1000 $/kW	1000 $/kW	Stable
Fuel cells	47%	5 year	2000 $/kW	500 $/kW	75%
Electrolyzers	74%	10 year	1500 $/kW	500 $/kW	67%
Super-capacitors	95%	20 year	300 $/kW		
Batteries	90%	5 year	120 $/kWh		
Hydrogen tanks	100%	20 year	30 $/kWh		

Table V-10: Comparison of system efficiency and electricity cost for a PV based hybrid power systems [Li 08c]

	PV/Batteries	**PV/H2**	**PV/Batteries/H2**
System Efficiency	81.76%	43.71%	71.30%
Electricity Cost	0.95$	1.16$	0.88$

For our system, the system efficiency varies from 54% to 87% if properly operated (Table.V-8). Although the super-capacitors are more expensive than batteries, wind energy is much cheaper than solar energy, the electricity cost of the active wind generator will be comparable with PV/Batteries/H2 hybrid power system (0.88$). Moreover, more we need an energy storage capacity, cheaper cost we have for per unit of energy, and more benefits we make from this active wind generator. Because, we do not need to over size the fuel cell system and the electrolyzer, but only need to increase hydrogen reserve. On the contrary, it is very expensive to increase the number of batteries for this purpose. After all, with fast developing control technique and reducing component price, the electricity cost of the active wind generator can be probably much reduced.

V.7 Conclusion

The hydrogen based long-term energy storage system (based on fuel cells and electrolyzers which are presented in Chap.III and in Chap.IV) has been finally added in the super-capacitors assisted wind energy conversion system (which is presented in Chap.II), in order to ensure the energy availability of the system. In this chapter, the system study is presented, including the system modeling and the control design. The different power balancing and energy management strategies are proposed to transform the wind/H2/super-capacitors hybrid power system into an active wind generator. This active wind generator works like classical power plants, which can supply smooth and controllable powers to satisfy the microgrid power requirements, in spite of the continuous fluctuation of the wind power.

Both power balancing strategies can be used for the active wind generator. They are tested in simulation and in experimental implementation. The results shows that the “power dispatching” strategy has better performances in DC-bus regulation and in the grid power control than the “grid following” strategy.

Different operating modes of the active wind generator are defined according to the related energy storage levels. Different energy management strategies are proposed for storage level's recovering. Their performances are respectively tested by simulations for long-time operations and proved to be able to bring the storage levels back in the normal operating ranges.

Finally, some techno-economic evaluations are discussed. The system efficiency depends much on the power balancing and energy management strategies. They can be well increase by improving the control strategies. The cost of the system is still very high, however, this situation will be improved with the fast developing technologies and continuously reduced price of the components.

Conclusion

Conclusion

In the previous chapters, the modeling and control schemes have been separately studied for the wind/super-capacitor based hybrid power system, the fuel cell system and the electrolyzer system. The objective is to design an active wind generator, which can work like a classical power plant to provide ancillary services to the electrical system of the microgrid. They are finally integrated together to form a wind/hydrogen/super-capacitors hybrid power system. The study consists of the design of the power balancing and energy management strategies. Several tests have been done to compare the performances with simulations and experiences. In this chapter, a summary of the dissertation is presented, some conclusions are driven and some recommendations for future work are also brought.

Summary of the Thesis Work

Recall of the context and the methodologies

In this PhD dissertation, the introduction of wind generators in a microgrid is considered. In order to overcome the wind power's intermittent and fluctuant characteristics, energy storage systems should be added in. Different energy storage technologies are compared. Finally the hydrogen-related technologies including fuel cells and electrolyzers are chosen to ensure the energy availability of the system and the super-capacitors are chosen to ensure fast power dynamics.

The objective of this research work is to design the control system and the energy management system of all units in order to form an active wind generator. The used tools and methodologies are presented in the first chapter of the dissertation. The equivalent continuous modeling method and some graphical tools are introduced, as the Causal Ordering Graph (COG), the Energetic Macroscopic Representation (EMR) and the Multi-Level Representation (MLR). The design method of the control system is also recalled. Real-time emulators can provide the same electrical behaviour of the emulated components, so they are enough in our study to test the experimentally implemented control functions and the power balancing strategies.

Wind energy conversion system

A classical wind energy conversion system is firstly studied. It consists of a wind energy generation system and a grid connection system, which are connected through two back to back power inverters. The system modelling and the control design are studied by using graphical tools (REM and MLR). When the wind generator works in MPPT strategy, the grid connection system regulates the DC-bus voltage and the fluctuant wind power is delivered to the grid. A wind power emulator is experimentally implemented to provide the same fluctuant power profile as a wind generator.

Because the wind energy production is very difficult to predict, the power balancing between the production and the consumption becomes very difficult. So this fluctuant wind power has very bad impacts on the power quality of the electrical system of the microgrid. As

solutions, the energy storage system are used to set up a hybrid power system with additional control functions, in order to make the power generation more controllable and flexible.

Wind/super-capacitors hybrid power system

A super-capacitor based fast-dynamic energy storage system is added to the DC bus in order to filter the fast fluctuations of the wind power. The modelling and control of this wind/super-capacitors hybrid power system are studied with the help of graphical tools (REM and MLR). Two power balancing strategies are presented. With the "grid following" strategy, the grid connection system regulates the DC-bus voltage and the super-capacitor helps the wind generator to satisfy the power requirement from the microgrid. With the "power dispatching" strategy, the grid connection system controls the delivered power to the grid and the super-capacitors regulate the DC-bus voltage against the fluctuant wind power. Both power balancing strategies are experimentally tested.

Fuel cell for energy backup from hydrogen

An overview has been given on the existing fuel cell technologies, the operating principles, the fuel cell system, the technical challenges and the modeling methods. In our study, a 1200W Ballard Nexa™ power module is studied, including the system modeling and control design. The modeling parameters are experimentally identified. This model is used to build a fuel cell emulator to provide the same electrical behavior as the studied fuel cell stack. It has been used to assess the hybrid power system in order to test the control functions, the power balancing and energy management strategies for the active generator.

Electrolyzer for energy storage into hydrogen

An overview has been given on the existing electrolyzer technologies, the operating principles, the electrolyzer system and the commercialized products. In our study, the 500W CETH GENHY100® power module is studied. The system modeling and control scheme is presented with EMR in order to give a better presentation. The modeling parameters are experimentally identified. This model is used to build an electrolyzer emulator to provide the same electrical behavior as the studied electrolyzer stack. It has been used to assess the hybrid power system in order to test the control functions, the power balancing and energy management strategies for the active generator.

Active wind generator

Finally, the DC-coupled wind/hydrogen/super-capacitors hybrid power system has been considered. The modelling and control of the entire system are studied with the help of graphical tools (REM and MLR). The different power balancing and energy management strategies are proposed to transform the hybrid power system into an active wind generator. This active wind generator works like a classical power plant, which can supply smooth and controllable powers to satisfy the microgrid power requirements, in spite of the continuous fluctuations of the wind power.

Two power balancing strategies can be used for the active wind generator. They are tested in simulation and in experimental implementation. Different operating modes of the active wind generator are defined according to the related energy storage levels. Different energy management strategies are also proposed for storage level's recovering. Their performances

are respectively tested by simulations for long-time operations and are proved to be able to bring the storage levels back in the normal operating ranges.

Discussions and Conclusions

Hybrid power system for active generator

In order to make an active generator from renewable energies, a hybrid power system is required because of the intermittent availability and fluctuant characteristics of the renewable energy sources. Three types of power sources are required :

- renewable energy generation systems (for supplying primary energy);
- fast-dynamic energy storage systems (for improving power quality);
- long-term energy storage systems (for ensuring energy availability).

Different devices can be chosen for each type of power sources according to local condition and power requirements. But the three types of power sources must be coordinated to perform an active generator for providing ancillary services to the electrical system of the microgrid.

Control system for active generator

A hierarchical control is implemented for the active wind generator. It can be divided into four levels:

- the Switching Control Unit (SCU);
- the Automatic Control Unit (ACU);
- the Power Control Unit (PCU);
- the Mode Control Unit (MCU)

The SCU and ACU are both low-level control functions and can be separately designed with standard methods and techniques. The PCU and MCU are both high-level control functions and should be designed for the entire system according to some specific requirements. So the PCU and the MCU are the main concern of an active generator's control system. We have proposed and tested two power balancing strategies in the PCU to make a smooth and flexible power generation from the active wind generator. We have also proposed several energy management strategies in the MCU in order to ensure and recover the energy availability of the active wind generator.

Power balancing strategies

In order to transform the hybrid power system into an active generator, it is very important to coordinate the different power sources, especially their power flows. The DC-bus voltage is the direct consequence of the power flow exchange among the different sources, and it should be well regulated for the system's stable operation. The delivered power to the grid is another consequence of the power flow exchange among the different sources; it should be precisely controlled to provide ancillary services to the power system of the microgrid. This is an advanced control function.

In wind energy conversion system without any energy storage system, when the wind generator works with a MPPT strategy, only the grid connection system can be used to regulate the DC-bus voltage. The fluctuant wind power is totally delivered to the microgrid.

The wind energy conversion system works like a passive generator, whose power supply does not depends on microgrid's requirement but on the climate condition.

In the hybrid power system, with the help of the energy storage systems, the DC-bus voltage and the grid power can be both controlled with a well implemented power balancing strategy. Two power balancing strategies are discussed in our study. With the "grid following" strategy, the grid current control loop regulates the DC-bus voltage, the energy storage systems are coordinated to help the wind generator to satisfy the power requirements from the microgrid. With the "power dispatching" strategy, the grid connection system controls the delivered power to the grid and the energy storage systems regulate the DC-bus voltage against the fluctuant wind power. Both power balancing strategies are experimentally tested and compared. We find that the "power dispatching" strategy has better performances on the grid power control than the "grid following" strategy.

Energy management strategies

Two kind of energy storage systems are used in the hybrid power system. The fast-dynamic storage system is sized according to the required power level (for following the fast varying peak power). The long-term storage system is sized according to the required energy capacity (for ensuring the energy availability during hours, days or months). Their storage level has been monitored in order to ensure the "good health" of the active generator. When the grid power requirement and the available wind power are different, the storage levels will vary. When a storage level goes out of the good range, an energy management strategy must be performed by defining an operating mode and by choosing the right power balancing algorithms for the active generator.

The implemented energy management strategies results in the following performances. When the fast-dynamic storage level goes out of the normal zone, the active generator itself can bring it back with the help of the long-term storage system and without modifying the grid power task. When the long-term energy storage level goes out of the normal zone, it can only be brought back by modifying the grid power requirement. In all these cases, the wind generator can always work with a MPPT strategy to make the maximum benefits from the wind energy without any bad impact on the electrical grid.

Recommendation for Future Work

High power-scale implementation

The active wind generator has been designed with a small power scale. The control functions and the power balancing strategies have been experimentally tested and validated. In order to obtain an industrial and commercial prototype, an experimental implementation with a larger power scale is suggested to investigate the problems, which may occur with high voltages and a high current

Experimental assessment

In our experimental tests, we focus on the power balancing strategies and the coordination of the different types of energy storage systems. So some real-time emulators are used to

provide required conditions of the experimental test. However, a real wind generator, a fuel cell system and an electrolyzer system will be necessary to design a commercial plant.

Techno-economic and environmental evaluation

In this work, we focus on the control functions of the active wind generator. Only a simple discussion on the efficiency and the cost of the system is given. The efficiency of the active wind generator depends on the power balancing and energy management strategies. The cost of the system depends on the improving control techniques and the reducing price of components. But no precise evaluations are given in this work. They should be evaluated precisely with a sophisticated algorithm and some statistics, by taking into account the technical evolution three types of sources and the environmental benefits. That will be very useful for the future practical use.

AC-coupled hybrid power system

In our study, a DC-coupled structure is chosen for the hybrid power system assessment because of different advantages. In this case, all energy sources should be close from each other. However, sometime the needed energy sources are dispersed far from each other because of geographical reasons. Then the AC-coupled structure can be used for the hybrid power system. Therefore, it will also be very useful to test the performance of an AC-coupled hybrid power system.

Appendix

Appendix

Appendix A: The ongoing research & development on Distributed Generation

Table A-1: The ongoing research & development on Distributed Generation

In Europe	
IRED's projects (Integration of Renewable Energy Sources and Distributed Generation into Electricity Grid) see http://www.ired-cluster.org	
Terminated project	Over 100 partners, 34M euro (see the web site for more detail)
Project FENIX	Flexible Electricity Networks to Integrate the eXpected Energy Evolution (22 partners 7.8M Euro)
Project SOLID-DER	Coordination Action to Consolidate RTD Activities for Large-Scale Integration of DER into the European Electricity Market (15 partners 1.5M Euro)
Project MORE MICROGRIDS	Large Scale Integration of Micro-Generation to Low Voltage Grids (22 partners 7.8M Euro)
Project DER-LAB	Network of Excellence for Decentralized Energy Resources and Preparation of Standards (11 partners 4.1M Euro)
In the United States	
Supported by **DOE** (Department of Energy) and **CEC** (California Energy Commission) See http://www.energy.gov and http://www.energy.ca.gov	
CERTS projects	Consortium for Electric Reliability Technology Solutions - The CERTS Microgrid Concept (2002) - Autonomous Control of Microsources (2006) - CERTS Microgrid Testbed (2006)
GE Global Research Microgrid	Development and demonstration of a microgrid energy management (MEM) framework for a broad set of microgrid applications that provides a unified controls, protection, and energy management platform
Other U.S. Microgrid RD&D	- Distributed Utility Integration Test (DUIT) - development of IEEE P1547.4, Draft Guide for Design, Operation, and Integration of Distributed Resource Island Systems with Electric Power Systems
In Japan	
NEDO's projects (New Energy Technology Department) See http://www.nedo.go.jp/english	
2004-2007	Demonstrative project on new power network systems
2003-2007	Demonstrative projection of regional power grids with various new energies
2003-2007	Demonstrative project on grid-interconnection of clustered photovoltaic power generation systems
2004-2007	Wind power stabilization technology development project
In Canada	
CANMET projects (Energy Technology Center) See http://canmetenergy-canmetenergie.nrcan-rncan.gc.ca	
Remote Microgrids Applications	Applications of autonomous microgrids for remote locations by electrification of electrically non-integrated areas, often geographical islands.
Grid-Connected Microgrid Applications	Investigate full-scale development, field demonstration, and experimental performance evaluation of: - frequency and voltage control methods/algorithms and the available technologies, under various microgrid operation modes - transition between grid-connected and islanded modes, and vice versa - high DER penetration and its impact on the host grid and interaction phenomena between DERs.
Planned Microgrid Islanding	One central element within the microgrid concept used to maintain continuity of supply during planned outages; e.g., substation maintenance periods.
Development of MV Test Line	To upgrade one of HQ's MV distribution lines for testing various concepts, methods, algorithms, and technologies related to DER integration, smart distribution system concepts, and microgrids.

Appendix B: Equivalent Continuous Modeling of Power Converters

B.1 Fundamental recall

Equivalent continuous models of the power electronic converters are sufficient for our study, because we do with the power balancing and energy management strategies of a hybrid power system in order to transform it into an active generator [Rob 01][Rob 02]. In our study, three types of power converters are used: 1) the DC chopper, 2) the three-phase inverter and 3) the three-phase rectifier. They are all connected to a DC-bus capacitor. The studies with the equivalent continuous modeling of power converters are carried out under the following assumptions:

- switches are ideal;
- switchings are instantaneously;
- switches are considered as short circuits in ON state and as open circuits in OFF state.

A switching function (s_{ij}) is defined for each power switch. It represents the ideal commutation order and takes the values 1 when the switch is closed (ON) and 0 when it is opened (OFF).

$$s_{ij} \in \{0,1\} \; with \begin{cases} i \in \{1,2,3\} n° \; of \; the \; leg \\ j \in \{1,2\} n° \; of \; the \; switch \; in \; the \; commutation \; circuit \end{cases}$$

As ideal power switches are considered, the switches in a same commutation circuit are in complementary states:

$$s_{i1} + s_{i2} = 1 \qquad \forall i \in \{1,2,3\}$$

B.2 Equivalent continuous modeling

a) DC chopper modeling

In our power electronic structure a DC chopper is located between a current source and a voltage source. For the super-capacitor storage system, the current source is the choke L_{sc} and generates the current i_{sc}. The DC-bus capacitor is the voltage source and generates the voltage (u_{dc}) (Fig.B-1).

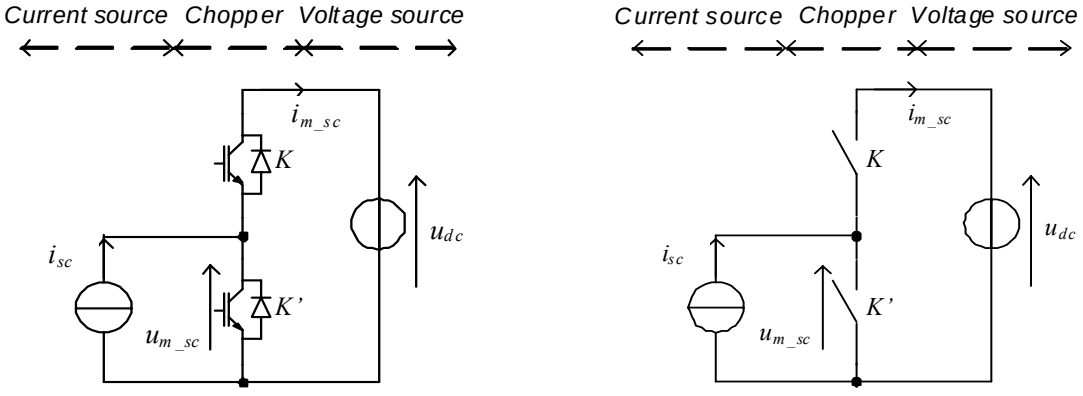

(a) Electrical diagram of the DC chopper (b) DC chopper with ideal switches

Figure B-1: Diagram of the DC chopper in the super-capacitor storage system

The modulation functions of the DC chopper can be expressed from the switching function ($s_{sc11}$of the first switch in the commutation circuit:

$$m_{sc} = s_{sc11}.$$

Then the modulated voltage u_{m_sc} and the modulated current i_{m_sc} of the DC chopper are obtained as follows:

$$\begin{cases} u_{m\_sc} = m_{sc} u_{dc} \\ i_{m\_sc} = m_{sc} i_{sc} \end{cases}.$$

In practice, a connection controller is used to create the two complementary switching functions (s_{sc11} and s_{sc12}) with necessary dead times from the modulation function m_{sc}. Then the switching functions are converted into ON/OFF signal for each semi-conductor switch through some drivers and optocouplers. The modulation function m_{sc} is obtained by comparing an average modulation function $<m_{sc}>$ with a triangular signal ξ (Fig.B-2).

In theory, when the modulation frequency of the carrier signal ξ is much higher than the frequency domain of the control signal (which is a continuous value for the DC chopper), the average modulation function can be obtained as follows:

$$< m_{sc} >= \frac{1}{\Delta t}\int_{to}^{to+\Delta t} m_{sc}(t)dt + m_{sc}(t_0).$$

By considering that the voltage u_{dc} and the current i_{sc} are constant during the time interval Δt, the average values of the modulated voltage$<u_{m_sc}>$ and the modulated current $<i_{m\_sc}>$ are expressed as follows:

$$\begin{cases} < u_{m\_sc} >=< m_{sc} > u_{dc} \\ < i_{m\_sc} >=< m_{sc} > i_{sc} \end{cases}.$$

As result, the equivalent average model of the DC chopper is obtained and the electrical diagram is shown in Fig.B-3. Finally, a variable $<m_{sc}>$ can be used to model the DC chopper.

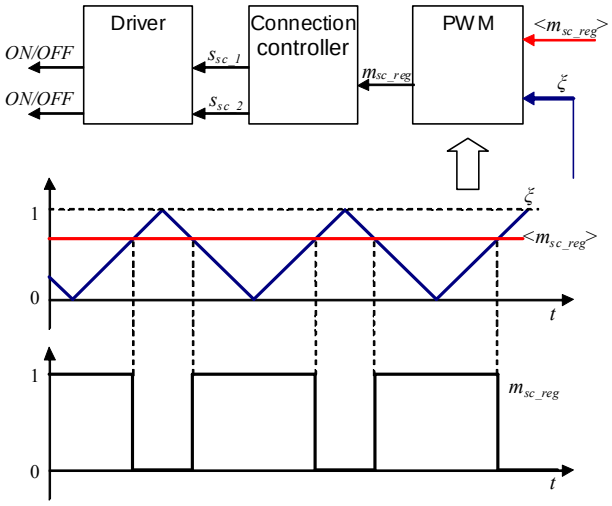

Figure B-2: Classical PWM method

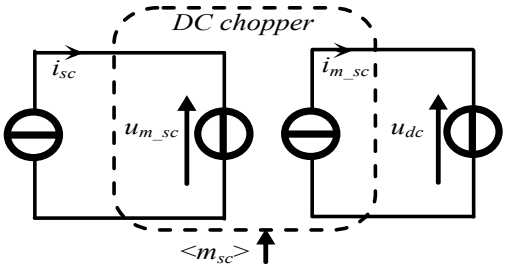

Figure B-3: Equivalent average electrical diagram of the DC chopper

b) Three-phase inverter modeling

In our study, a three-phase voltage source inverter VSI is used to connect the DC bus to the AC grid [Fra 99]. The task is to invert in real time the DC voltage into AC modulated voltages. The three-phase VSI is located between a three-phase current source and a voltage source. For the grid power conversion system, the current sources come from the choke filters and is set to generate the AC line current ($\underline{i}_{line}=[i_{line\_1}\ \ i_{line\_2}]^T$) and the voltage source comes from the DC bus and is set to generate the DC-bus voltage (u_{dc}) (Fig.B-4).

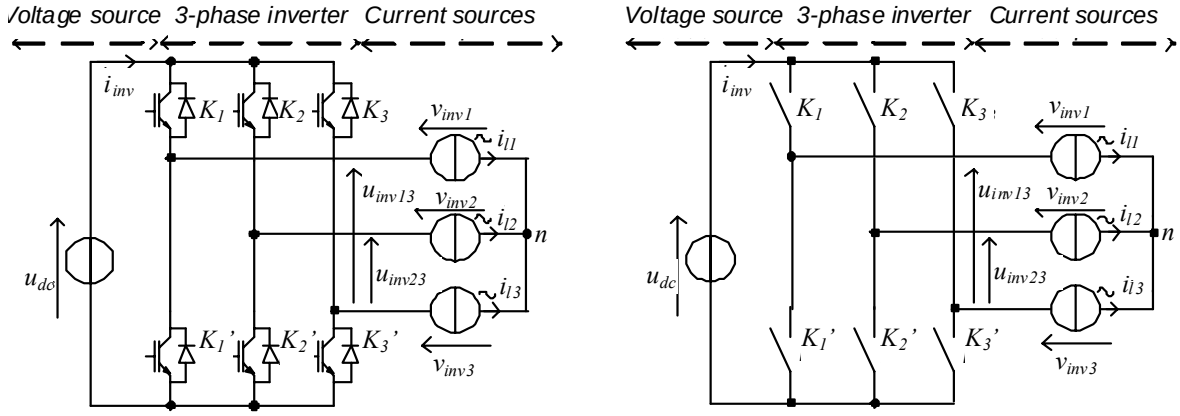

(a) Electrical diagram of the three-phase inverter (b) Three-phase inverter with ideal switches

Figure B-4: Diagram of the three-phase inverter in the grid power conversion system

The modulation functions ($\underline{m}_{inv}=[m_{inv13}\ \ m_{inv23}]$) of the three-phase inverter can be expressed from the switching functions ($\underline{s}_{inv}=[s_{inv11}\ s_{inv21}\ s_{inv31}]$) of first switches of the three commutation circuits :

$$\underline{m}_{inv}(t)=\begin{bmatrix} m_{inv13}(t) \\ m_{inv23}(t) \end{bmatrix}=\begin{bmatrix} 1 & 0 & -1 \\ 0 & 1 & -1 \end{bmatrix}\begin{bmatrix} s_{inv11}(t) \\ s_{inv21}(t) \\ s_{inv31}(t) \end{bmatrix}.$$

Then the modulated voltage ($\underline{u}_{inv}=[u_{inv13}\ u_{inv23}]^T$) and the modulated current i_{inv} of the three-phase inverter are obtained from the DC-bus voltage and the line currents ($\underline{i}_l=[i_{l1}\ i_{l2}]$), which are considered constant during the time window Δt :

$$\begin{cases} \underline{u}_{inv}(t)=\underline{m}_{inv}(t)\ u_{dc} \\ i_{inv}(t)=\underline{m}_{wg}^{T}(t)\ \underline{i}_l \end{cases}.$$

In practice, a connection controller is used to create the six switching functions {s_{inv11}, s_{inv12}, s_{inv21}, s_{inv22}, s_{inv31}, s_{inv32}} with necessary dead times from the modulation function m_{inv}. Then the switching functions are converted into ON/OFF state of each switch through some drivers and optocouplers. The modulation function m_{inv} can be obtained by comparing an average modulation function $<m_{inv}>$ with a triangular signal ξ (Fig.B-5).

In theory, when the modulation frequency of the carrier signal ξ is much higher than the frequency domain of the control signals (which are sinusoidal values for the inverter) the average modulation function can be obtained as follows:

$$<\underline{m}_{inv}>=\frac{1}{\Delta t}\int_{to}^{to+\Delta t}\underline{m}_{inv}(t)dt+\underline{m}_{inv}(t_0).$$

Then the average values $<\underline{u}_{inv}>$ and $<i_{inv}>$ of the modulated voltage and the modulated current are expressed as follows:

$$\begin{cases} <\underline{u}_{inv}> = <\underline{m}_{inv}> u_{dc} \\ <i_{inv}> = <\underline{m}_{inv}^{T}> \underline{i}_{l} \end{cases}.$$

The voltage u_{dc} and the currents $\underline{i}_l$ are assumed to be constant during the switching period. As result, the equivalent continuous model of the three-phase inverter is obtained and the electrical diagram is shown in Fig.B-6. Finally, a vector $<\underline{m}_{inv}>$ can be used to model the three-phase inverter.

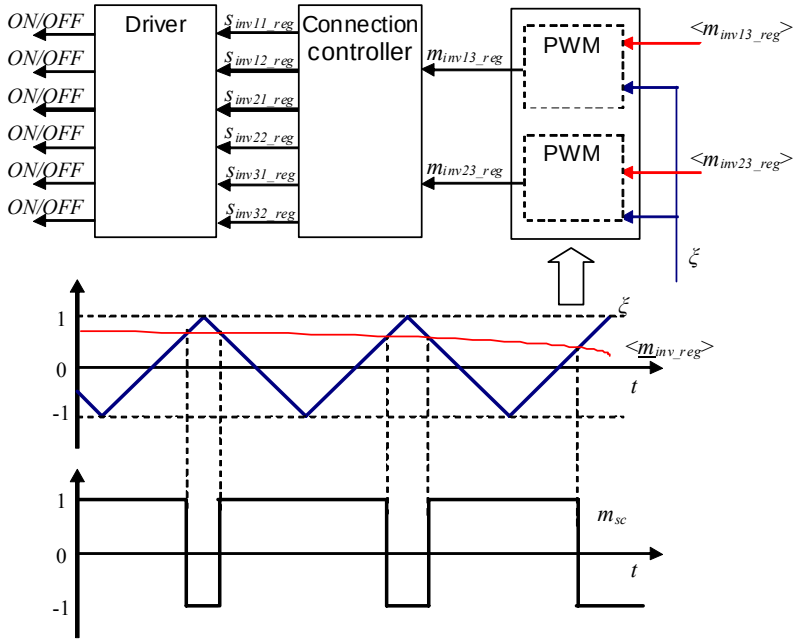

Figure B-5: Classical sinusoidal PWM method.

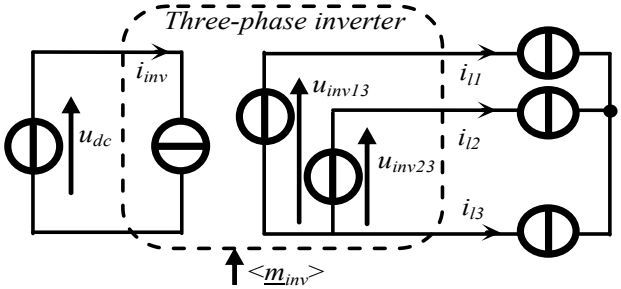

Figure B-6: Equivalent electrical diagram of the three-phase inverter

c) Three-phase rectifier modeling

A three phase rectifier is used to rectify three-phase sinusoidal currents from the machine of the wind generator. For the three-phase rectifier, similar relations are obtained for the average values of the modulated voltage ($<\underline{u}_{rec}>=[(<u_{rec13}>\ (<u_{rec23}>]^{T}$) and the modulated current ($<i_{rec}>$) from the DC-bus voltage u_{dc} and the currents ($\underline{i}_{mac}=[i_{mac1}\ i_{mac2}]^{T}$) of the electrical machine, with the averaged vector ($<\underline{m}_{rec}>=[<m_{rec13}>\ <m_{rec23}>]^{T}$) of the rectifier modulation functions:

$$\begin{cases} <\underline{u}_{rec}> = <\underline{m}_{rec}> u_{dc} \\ <i_{rec}> = <\underline{m}_{rec}^{T}> \underline{i}_{mac} \end{cases}.$$

As result, the equivalent continuous model of the three-phase inverter is obtained and the electrical diagram is shown in Fig.B-7. Finally, a vector $<\underline{m}_{rec}>$ can be used to model the three-phase inverter.

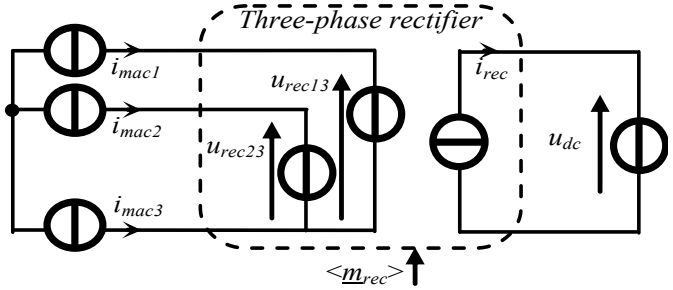

Figure B-7: Equivalent electrical average diagram of the three-phase rectifier

Appendix C: Control Structure of Power Systems through Power Converters

In a power system, power converters are usually used to introduce some control inputs for the power conversion. The structure of the control system can be divided into four different levels [Hau 99]:

- Switching Control Unit (SCU);
- Automatic Control Unit (ACU);
- Power Control Unit (PCU);
- Mode Control Unit (MCU).

A representation of a power system including renewable energy generators and energy storage systems is given as example (Fig.C-1). Different power converters are used to connect the different energy sources to the DC bus. The roles of each control unit in the control system are explained as below.

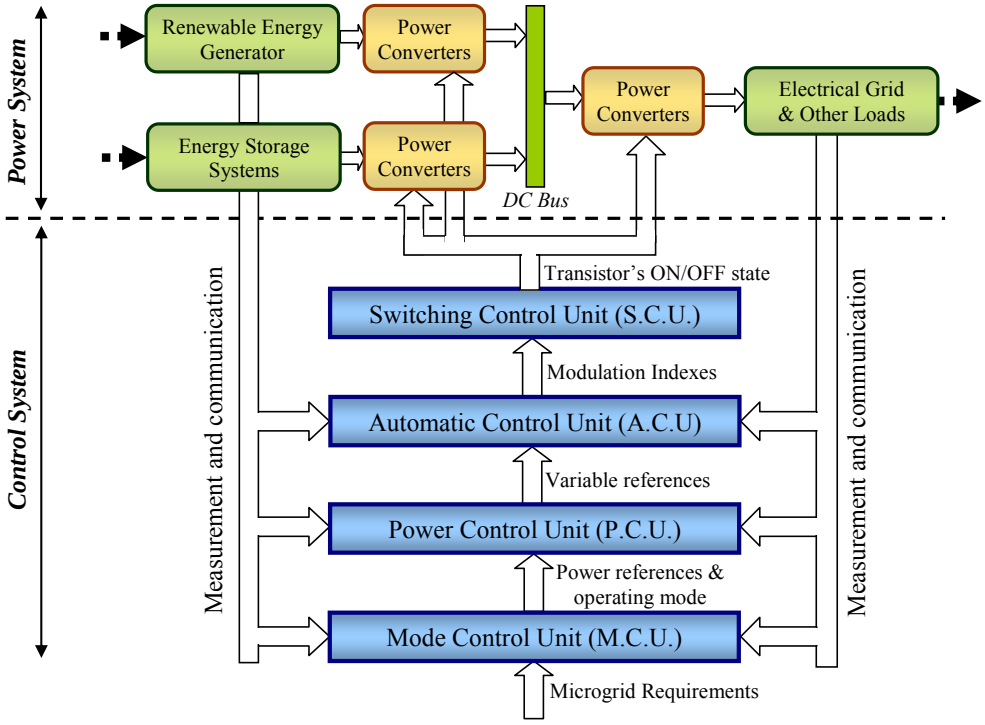

Figure C-1: Structure of a DC-coupled hybrid power system and its control system

The Switching Control Unit (SCU) is designed for each power converter as shown in Fig.2 and in Fig.5. In a SCU, the drivers with opto-couplers generate the transistor's ON/OFF signals from the ideal states of the switching function {0,1} and the modulation modules (eg. PWM) determine the switching function from the modulation function.

The Automatic Control Unit (ACU) is designed for each energy source and its power conversion system. In an ACU, the control algorithms calculate the modulation index of each power converter through the regulation of some physical quantities according to their reference values.

The Power Control Unit (PCU) is designed to perform the instantaneous power balancing of the entire hybrid power system. In a PCU, some power balancing algorithms are implemented to coordinate the power mission of the different energy sources with their power

conversion systems. It can be an algorithm base consisting of different power balancing algorithms targeting at a number of possible operation mode of the hybrid power system.

The Mode Control Unit (MCU) is designed for the energy management of the entire hybrid power system. In a MCU, the renewable energy generation capacity (like the climate condition and the generator's state) and the energy storage level (like the super capacitors' voltage and the stored hydrogen pressure) should be supervised to make the right decision of the operating mode in order to ensure good energy availability.

Appendix D: Causal Ordering Graph (COG)

Static relation

The COG is a graphical representation of mathematical equations, which can be used to model a system and to design its control structure [Hau 96][Hau 04]. Balloons with inside the equation number represent modeling relations. A static instantaneous relation has no time dependence. It will be depicted as a balloon with a bi-directional arrow as shown in Fig.D-1a. Physically, it can be said that the corresponding element has an external causality orientation. If the variable x is externally set, it is then the input and we get:

$$R_a:\ y(t) = R_a(x(t)).$$

To make the output y equal to a reference y_{ref}, an elementary control equation R_{ac}, obtained by inverting the modeling equation R_a to calculate the desired input variable x_{reg} from the reference y_{ref}.

$$R_{ac}:\ x_{reg}(t) = R_{ac}(y_{ref}(t)).$$

Dynamic relation

A time-dependent relation will be characterized by a unidirectional arrow in the balloon. Classically, dynamical systems are mathematically modeled by differential equations,

$$\frac{dy(t)}{dt} = ax(t) + b$$

This first order differential equation is typically a time-dependent relation, whose output is formed by integration. It is represented by (R_b) in Fig.9b,

$$R_b:\ y(t) = R_b(x(t), t).$$

Moreover the mathematical property of differential equations specifies that this equation type has an input-output orientation. Meanwhile for equation R_b, the variable $x(t)$ must be the input and $y(t)$ must be the output. Physically, it can be said that the element has an internal causality orientation. The pure inverse equation introduces large instabilities due to the differential term. Instead of inverting R_b, we can use a closed loop control with a corrector C_m to compensate the error signal between the measured output $\hat{y}$ and the reference y_{ref}.

$$R_{bc}:\ x_{reg}(t) = C_m(y_{ref}(t) - \hat{y}(t)).$$

(a) static relation (b) dynamic relation

Figure B-8: COG of static and dynamic relations with their control schemes.

Appendix E: Energetic Macroscopic Representation (EMR)

EMR is based on action-reaction principle, which organises the system as interconnected subsystems according to the integral causality. Inversion of the graphical description by using specific rules leads to a Maximal Control Structure of the system. It is very suitable for research/development of complex multi-physic system [Bou 07].

Interaction principle

The system is decomposed into basic subsystems in interactions (Table E-1): energy sources (green ovals), accumulation elements (orange rectangles), conversion element without energy accumulation (various orange pictograms) and coupling elements for energy distribution (orange overlapped pictograms). All the elements are interconnected according to the action and reaction principle using exchange variable (arrows). The product of action and reaction variables between two elements leads to the instantaneous power exchanged.

Table E-1: Elements of EMR and of control

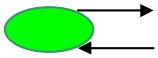	Source of energy	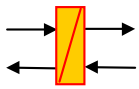	Element with energy accumulation	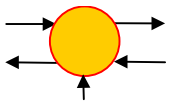	Electromechanical converter (without energy accumulation)
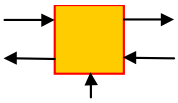	Electrical converter (without energy accumulation)	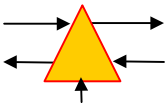	Mechanical converter (without energy accumulation)	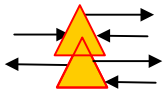	Mechanical coupling device (energy distribution)
	Control block without controller	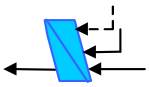	Control block with controller		Action and reaction variables

Causality principle

As in COG, only the integral causality is considered in EMR. This property leads to define accumulation element by a time-dependant relationship between its variables, in which its output is an integral function of its inputs. Other elements are described using relationships without time dependence. In order to respect the integral causality specific association rules are defined, but there are taught only in the expert level unit.

Inversion principle

The inversion based control theory has been initiated by COG. The control structure of a system is considered as an inversion model of the system because the control has to define the appropriated inputs to apply to the system from the desired output (Fig.E-1). In this method, relationships without time-dependence are directly inverted (with neither control nor measurement). Because the derivative causality is forbidden, a direct inversion of time-dependence relationships is not possible. An indirect inversion is thus made using a controller and measurements. These inversion rules have been extended to EMR (blue pictograms, see Table E-1): conversion elements are directly inverted and accumulation elements are inverted using controller. Moreover inversions of coupling element require distribution or weighted inputs. These inputs lead an organization of the energy distribution. This inversion methodology is another way to locate controllers and measurements or estimations.

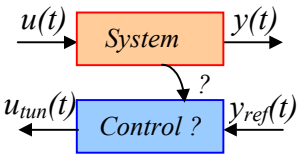

Figure E-1: Inversion-based control principle

Appendix F: Multi-Level Representation (MLR)

The Multi-Level Representation (MLR) has been recently proposed for a synthetic and dynamic description of the electromechanical conversion systems [Li 08]. The MLR has the same advantages as the EMR. Moreover, it integrates a power calculation level and a power flow level as well as their corresponding control levels, in order to solve the most important factor of the supervision for microgrid application. Here we take the Super-Capacitor Bank (SCB) power conversion system (Fig.F-1) as example to explain how to make and use a Multi-Level Representation (MLR).

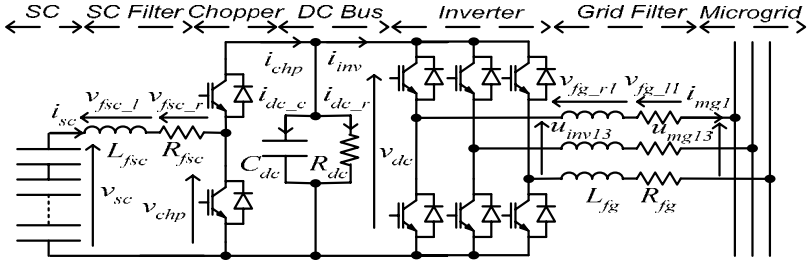

Figure F-1: Super-capacitor power conversion system

F.1 Multi-level modelling

Step 1: EMR level modeling

The SCB is composed of the Super Capacitor (SC), a SC filter, a chopper, a DC bus, an inverter and a three-phase grid filter (Fig.F-1). The first step of the SCB multi-level modeling is consists to gather dynamical equations of each element into '*ProX*' and '*ES*' macro blocs in order to obtain an *EMR* (Fig.F-3, *EMR* level).

1) Modeling of the SC (*macro bloc* '*Pro1*')

The super capacitor module is modeled as a voltage source. For the study of power system applications, the model of Zubieta and Bonert can be applied. Nevertheless, for the simplification of the study, the model with a resistor R_s and an ideal capacitor C_0 in series is used.

$$\frac{dv_C}{dt} = \frac{1}{C_0} i_{sc} \tag{F-1}$$

$$v_R = R_s i_{sc} \tag{F-2}$$

$$v_{sc} = v_C + v_R \tag{F-3}$$

2) Modeling of the filter ('*Pro2*')

The SC filter is modeled as an inductance (L_{fsc}) and a resistance (R_{fsc}) in series.

$$\frac{di_{sc}}{dt} = \frac{1}{L_{fsc}} v_{fsc\_l} \tag{F-4}$$

$$v_{fsc\_l} = v_{sc} - v_{chp} - v_{fsc\_r} \tag{F-5}$$

$$v_{fsc\_r} = R_{fsc} i_{sc} \tag{F-6}$$

3) Modeling of the chopper ('*Pro3*')

The chopper adapts the low voltage across the super capacitor to the desired voltage for the DC bus. An equivalent continuous model of the chopper is used by a mean value modulation function m_{chp}:

$$\begin{cases} v_{chp} = m_{chp} v_{dc} \\ i_{chp} = m_{chp} i_{sc} \end{cases}, \; m_{chp} \in [0,1] \tag{F-7}$$

4) Modeling of the grid-side DC bus ('*Pro4*')

The DC bus is considered as a capacitor (C_{dc}) and a resistance (R_{dc}) in parallel.

$$\frac{dv_{dc}}{dt} = C_{dc} i_{dc\_c} \tag{F-8}$$

$$i_{dc\_c} = i_{chp} - i_{inv} - i_{dc\_r} \tag{F-9}$$

$$i_{dc\_r} = \frac{1}{R_{dc}} v_{dc} \tag{F-10}$$

5) Modeling of the inverter ('*Pro5*')

An equivalent mean modeling of the power converters is sufficient for the study. It represents fundamental phase-to-phase voltage $\underline{u}_{inv}=[u_{inv13}, u_{inv23}]^T$ and line currents $\underline{i}_{mg}=[i_{mg1}, i_{mg2}]^T$ components as:

$$\underline{u}_{inv} = \underline{m}_{inv} \cdot v_{dc} \tag{F-11}$$

$$i_{inv} = \underline{m}_{inv}^T \cdot \underline{i}_{mg} \tag{F-12}$$

where $\underline{m}_{inv} = [m_{inv1}, m_{inv2}]^T$ is the modulation index vector. Line voltages $\underline{v}_{inv}=[v_{inv1n}, v_{inv2n}]^T$ are obtained by:

$$\underline{v}_{inv} = \frac{1}{3}\begin{bmatrix} 2 & -1 \\ -1 & 2 \end{bmatrix} \cdot \underline{u}_{inv} \tag{F-13}$$

6) Modeling of the three-phase filter ('*Pro6*')

The line current $\underline{i}_{mg}$ are deduced from the inverter voltages $\underline{u}_{inv}$ and the grid voltages $\underline{u}_{mg}=[u_{mg13}, u_{mg23}]^T$.

$$\frac{d}{dt}\underline{i}_{mg} = \frac{1}{L_{fg}} \underline{v}_{fg\_l} \tag{F-14}$$

$$\underline{v}_{fg\_l} = \frac{1}{3}\begin{bmatrix} 2 & -1 \\ -1 & 2 \end{bmatrix} (\underline{u}_{inv} - \underline{u}_{mg}) - \underline{v}_{fg\_r} \tag{F-15}$$

$$\underline{v}_{fg\_r} = R_{fg} \underline{i}_{mg} \tag{F-16}$$

where L_{fg} and R_{fg} are the inductance and resistance of the filter, the $\underline{v}_{fg\_l} = [v_{fg\_l1}, v_{fg\_l2}]^T$ and $\underline{v}_{fg\_r} = [v_{fg\_r1}, v_{fg\_r2}]^T$ are the voltages respectively across L_{fg} and R_{fg}.

7) Modeling of the microgrid ('*ES*')

The grid voltages $\underline{u}_{mg}$ is modeled by :

$$\underline{u}_{mg} = \begin{bmatrix} u_{mg13} \\ u_{mg23} \end{bmatrix} = \sqrt{2} A \begin{bmatrix} \sin(2\pi f t - \pi/6 + \theta_0) \\ \sin(2\pi f t - \pi/2 + \theta_0) \end{bmatrix} \tag{F-17}$$

where A is the rms value of the grid phase-to-phase voltage, f is the grid frequency and θ_0 is the initial angle of the grid voltage. The line currents $\underline{i}_{mg}$ are considered as disturbances for the microgrid.

Sept 2: Power calculation level

The second step for the multi-level modeling uses an interface, which is designed to calculate the different powers. They are classified in three terms: the intermediary powers between two elements, the exchanged powers with a storage element, and the losses (Table F-1). All equations of this level have been respectively gathered into the macro blocs named '*IntX*' in the '*Power Calculation*' level of the Fig.F-3.

Step 3: Power flow representation level

The third step for the multi-level modeling describes the power flow (Fig.F-2) from the super capacitor modules to the microgrid. The macro blocs, which are named '*PowX*' in the '*Power Flow*' level of the Fig.F-3, represent the modeling equations.

For the storage elements (as example the SC filter), the input power (P_{scf} from the SC) is separated into losses (P_{fsc_los}), the exchanged power with the storage unit (p_{fsc_sto}) and the output power (p_{fch}) is expressed as:

$$Pow1:\ p_{fch} = p_{scf} - p_{fsc\_los} - p_{fsc\_sto} \tag{F-18}$$

where p_{fsc_sto} is the total of the accumulation power ($p^{+}_{fsc\_sto}$) and the restitution power ($p^{-}_{fsc\_sto}$).

For the power electronic converters, the input power is equal to the output power since losses are neglected. The power flow from the SC to the microgrid is modeled by the following equations:

$$Pow2:\ p_{fch} = p_{chb} \tag{F-19}$$

$$Pow3:\ p_{bin} = p_{chb} - p_{dc\_los} - p_{dc\_sto} \tag{F-20}$$

$$Pow4:\ p_{bin} = p_{inf} \tag{F-21}$$

$$Pow5:\ p_{mgs} = p_{inf} - p_{fg\_los} - p_{fg\_sto} \tag{F-22}$$

These power equations are bidirectional. For the SCB, it is possible to perform the accumulation and the restitution of the power.

The complete multi-level modeling of the SCB is composed of three levels: *EMR*, *Power Calculation* and *Power Flow* (Fig.F-3).

F.2 Design of the control system

The global system has three control inputs in order to manage the system. The inverter has two independent modulation functions m_{inv1} and m_{inv2} using its switching orders. The chopper has only one modulation function m_{chp}. The control task is to reduce the power variations of the microgrid. The inverter is used to control the real and reactive power at the connection point. The control input of the chopper is used to control DC bus voltage, since the voltage of the DC bus must be constant for correct system performances. The control system is ordered by the following steps according to the rules of the multi-level representation.

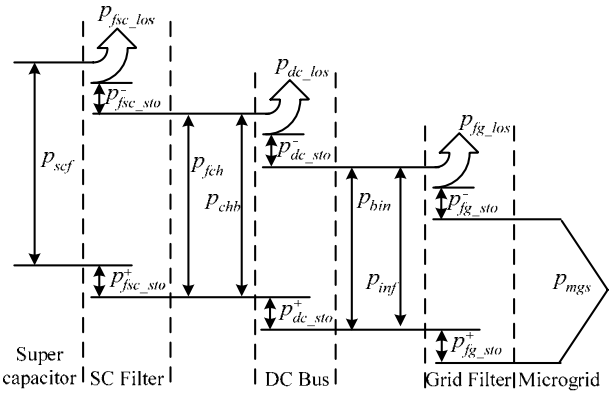

Figure F-2: Power flow from the SC to the microgrid

Table F-1: Equations of the Power calculation interface.

Intermediary powers	Storage powers	Losses
$Int1: p_{scf} = v_{sc} i_{sc}$	$Int3: p_{fsc\_sto} = v_{fsc\_l} i_{sc}$	$Int2: p_{fsc\_los} = R_{fsc} i_{sc}^2$
$Int4: p_{fch} = v_{chp} i_{sc}$	$Int7: p_{dc\_sto} = v_{dc} i_{dc\_c}$	$Int6: p_{dc\_los} = v_{dc}^2 / R_{dc}$
$Int5: p_{chb} = v_{dc} i_{chp}$	$Int11: p_{fg\_sto} = \left(C_{23} \cdot \underline{v}_{fg\_l}\right)^T \cdot \left(C_{23} \cdot \underline{i}_{mg}\right)$	$Int10: p_{fg\_los} = R_{fg} \left(C_{23} \cdot \underline{i}_{mg}\right)^T \cdot \left(C_{23} \cdot \underline{i}_{mg}\right)$
$Int8: p_{bin} = v_{dc} i_{inv}$	Where $C_{23} = \begin{bmatrix} 1 & 0 \\ 0 & 1 \\ -1 & -1 \end{bmatrix}$ is the calculation matrix from two line currents to three line currents.	
$Int9: p_{inf} = \underline{u}_{inv}^T \underline{i}_{mg}$		
$Int12: p_{mgs} = \underline{u}_{mg}^T \underline{i}_{mg}$		

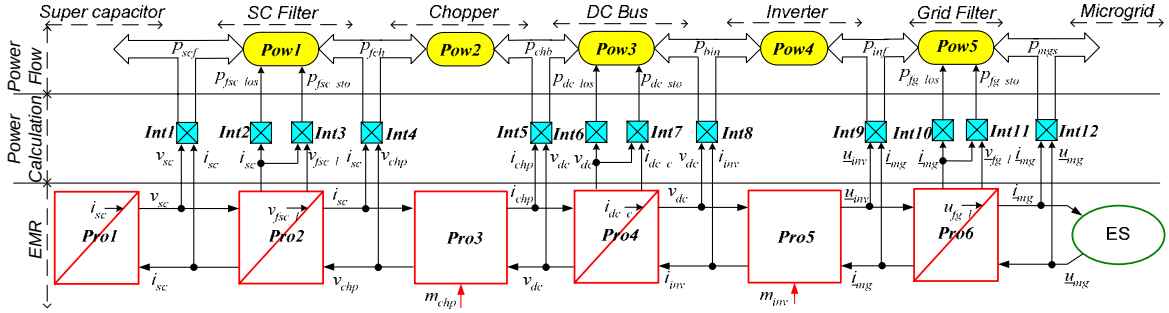

Figure F-3: Multi-level representation of the modeling for a Super Capacitor Bank

Step 4: Mark the stationary quantities and the non-measurable quantities in the EMR level

The SC terminal voltage v_{sc} changes very slowly thanks to a great quantity of stored energy. The DC bus voltage v_{dc} has also a slow dynamic, since it has to be controlled as constant in order to ensure the inverter function. At the ac side, the principal component of all quantities (voltages and currents) is 50 Hz. By modeling them into a 50 Hz rotational Park form, they become stationary. Moreover if their magnitudes are constant, they can be considered constant as $\underline{u}_{mg}$ for the microgrid voltages. In the multi-level representation, the stationary quantities are visualized by the thick solid lines (Fig.F-5).

The voltages v_{chp} and $\underline{u}_{inv}$ and the currents i_{chp} and i_{inv} are difficult to measure since they are modulated by the converters. These non-measurable quantities are visualized by the thick dashed lines (Fig.F-5).

Step 5: Apply the 'pass' rule and the 'block' rule

This step is necessary to fix the electrical chains.

When a macro bloc in the *Power Calculation* level has a stationary quantity input in the *EMR* level, it can be used to serve as a possible passage bloc between the EMR level and the Power Flow level. In this condition, this type of macro blocs is colored in the dark blue color. Such as *Int1* is colored in the dark blue for v_{sc}, *Int5*, *Int6*, *Int7* and *Int8* for v_{dc}, *Int12* for $\underline{u}_{mg}$.

When a non-measurable quantity in the *EMR* level is used as an input of the macro bloc for the storage element, it is impossible to design the control strategy by the inversion of another chain of this macro bloc without estimator or a corrector which rejects the disturbances. Some symbols × are added to present the block in the control part. Such as in *Pro2*, the chain $v_{sc} \rightarrow i_{sc}$ is blocked by the modulation quantity v_{chp}, in *Pro4*, the chain $i_{chp} \rightarrow v_{dc}$

is blocked by the modulation quantity i_{inv}, the chain $i_{inv} \rightarrow v_{dc}$ is blocked by the modulation quantity i_{chp}; in *Pro6*, the chain $\underline{u}_{mg} \rightarrow \underline{i}_{mg}$ is blocked by the modulation quantity $\underline{u}_{inv}$ (Fig.F-5).

Step 6: Fix the electrical chains

The multi-level representation helps us to find the electrical chain in the power model level in order to design the control system.

The first electrical chain is used to control the real and reactive power at the connection point to the microgrid by the modulation functions of the inverter. The path from the control input of the inverter to the powers injected to the microgrid is obvious (Fig.F-5):
$m_{inv}(Pro5) \rightarrow \underline{u}_{inv}(Pro6) \rightarrow \underline{i}_{mg}(Int12) \rightarrow p_{mgs}$ and q_{mgs}

The second electrical chain is used to control the DC bus voltage v_{dc} by the modulation function m_{chp}. Since v_{dc} is a stationary quantity which is suitable for the processes of division in the control system (F-28), the first step of this electrical chain is $m_{chp}(Pro3) \rightarrow v_{chp}$ (Fig.F-5). Now the arrow is pointed to the left side of the chopper, but the destination v_{dc} is at its right side. The power flow level is used to establish the relation between v_{chp} and v_{dc}. At the left side of the chopper, there is only one bloc *Int1* for the passage. So the electrical chain is drawn from v_{chp} to i_{sc} in order to reach *Int1*. Since both external currents (i_{chp} and i_{inv}) of the DC bus are modulation quantities, the end of the electrical chain in the power flow level is fixed on the DC bus storage power p_{dc_sto}. Finally the equations *Int7* and *Pro4* are used to reach the DC bus voltage from p_{dc_sto}. The second electrical chain is (Fig.F-5):
$m_{chp}(Pro3) \rightarrow v_{chp}(Pro2) \rightarrow i_{sc}(Int1) \rightarrow p_{scf}(Pow1) \rightarrow p_{fch}$
$(Pow2) \rightarrow p_{chb}(Pow3) \rightarrow p_{dc\_sto}(Int7) \rightarrow i_{dc\_c}(Pro4) \rightarrow v_{dc}$

Step 7: Control the fast dynamic quantities by the inversion of EMR

The control system of fast dynamic quantities is obtained by using inversion rules of equations from the *EMR* modeling level (Fig.F-5). Hence a grid current controller (macro bloc '*Pro6c*' in the Fig.F-5) is required to enslave grid currents to prescribed reference ($\underline{i}_{mg\_ref}$). Two controllers ('*Pro3c*' and '*Pro5c*') are used for power electronic converters. A voltage controller ('*Pro4c*') is used to set the DC bus voltage reference and a current controller ('*Pro2c*') sets the super capacitor current reference (Fig.F-5). The following sections give the details of each macro control bloc in the '*Control of Dynamic Quantities*' level ('*ProXc*') in the Fig.F-5.

1) Grid connection controller ('*Pro6c*')

A Park transform is used with a synchronization with the first line voltage. In this frame, filter equations are written as:

$$\begin{cases} \dfrac{di_{mgd}}{dt} = \dfrac{1}{L_{fg}}\left(v_{invd} - v_{mgd} - R_{fg} i_{mgd} - L_{fg}\omega_s i_{mgq}\right) \\ \dfrac{di_{mgq}}{dt} = \dfrac{1}{L_{fg}}\left(v_{invq} - v_{mgq} - R_{fg} i_{mgq} + L_{fg}\omega_s i_{mgd}\right) \end{cases} \quad \text{(F-23)}$$

The control of these current is obtained by a compensation of grid voltages, a current decoupling and a closed loop control (Fig.F-4).

2) Inverter controller ('*Pro5c*')

Phase-to-phase voltages are obtained by inversion of the equation (F-13):

$$\begin{cases} u_{inv13\_ref} = v_{inv1\_ref} - v_{inv3\_ref} \\ u_{inv23\_ref} = v_{inv2\_ref} - v_{inv3\_ref} \end{cases} \quad \text{(F-24)}$$

Modulation functions are calculated by inversion of (F-11):

$$m_{inv1\_ref} = \frac{u_{inv13\_ref}}{\hat{v}_{dc}}, \quad m_{inv2\_ref} = \frac{u_{inv23\_ref}}{\hat{v}_{dc}} \quad \text{(F-25)}$$

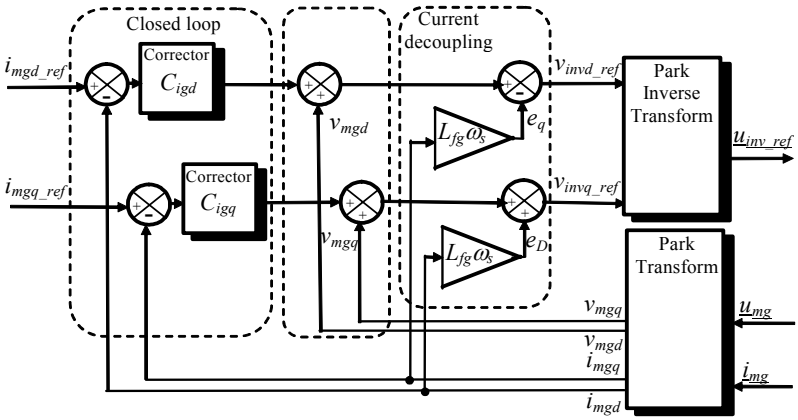

Figure F-4: Grid connection controller (macro bloc '*Pro6c*')

A vector is defined as: $\underline{m}_{inv\_ref} = [m_{inv1\_ref}, m_{inv2\_ref}]^T$. Hence current references can be assumed equal to grid currents.

3) DC bus voltage controller ('*Pro4c*')

The DC bus voltage is controlled by the current i_{dc_c} (Fig.F-1).

$$i_{dc\_c\_reg} = K_{dc\_p}(v_{dc\_ref} - \hat{v}_{dc}) \quad \text{(F-26)}$$

where K_{dc_p} is the proportional parameter of the corrector for the DC bus voltage control.

4) SC current controller ('*Pro2c*')

A control loop of the SC current generates the voltage reference of the chopper (v_{chp_reg}) as:

$$v_{chp\_reg} = \hat{v}_{sc} - K_{fsc\_p}(i_{sc\_reg} - \hat{i}_{sc}) \quad \text{(F-27)}$$

where K_{fsc_p} is the proportional parameter of the corrector for the super capacitor current control.

5) Chopper controller ('*Pro3c*')

The modulation function of the chopper m_{chp_ref} is calculated with the DC bus voltage measurement:

$$m_{chp\_ref} = \frac{v_{chp\_reg}}{\hat{v}_{dc}} \quad \text{(F-28)}$$

Step 8: Power calculation control

The *Power Calculation Control* level is designed by the inversion or the estimation of the *Power Calculation* level.

$$Int1c: \; i_{sc\_reg} = \frac{p_{scf\_reg}}{\hat{v}_{sc}} \quad \text{(F-29)}$$

$$Int7e: \; p_{dc\_sto\_reg} = v_{dc} i_{dc\_c\_reg} \quad \text{(F-30)}$$

The grid current references are deduced (*Int12c*) from the equation *Int12* for the real power (Table F-1) and the following equation for the reactive power:

$$Q_{mgs} = \frac{1}{\sqrt{3}}((2u_{mg23} - u_{mg13})i_{mg1} - (2u_{mg13} - u_{mg23})i_{mg2}) \quad \text{(F-31)}$$

$$Int12c: \begin{cases} i_{mg1\_ref} = \dfrac{(2u_{mg13} - u_{mg23})p_{mgs\_ref} + \sqrt{3}u_{mg23}q_{mgs\_ref}}{2u_{mg13}^{\ 2} - 2u_{mg13}u_{mg23} + 2u_{mg23}^{\ 2}} \\ i_{mg2\_ref} = \dfrac{(2u_{mg23} - u_{mg13})p_{mgs\_ref} - \sqrt{3}u_{mg13}q_{mgs\_ref}}{2u_{mg13}^{\ 2} - 2u_{mg13}u_{mg23} + 2u_{mg23}^{\ 2}} \end{cases} \quad \text{(F-32)}$$

Step 9: Power flow control

The power flow control is obtained by model inversion of the *Power Flow* level with anticipation of calculated filter losses ($\tilde{p}_{fsc\_los}$ and $\tilde{p}_{fg\_los}$) (Table F-1). The exchanged powers with the filters (p_{fsc_sto} and p_{fg_sto}) and the losses in the DC bus (p_{dc_los}) are slight enough to be neglected.

$$Pow1c: \ p_{scf\_reg} = p_{fch\_reg} + \tilde{p}_{fsc\_los} \quad \text{(F-33)}$$

$$Pow2c: \ p_{fch\_reg} = p_{chb\_reg} \quad \text{(F-34)}$$

$$Pow3c: \ p_{chb\_reg} = p_{bin\_reg} + p_{dc\_sto\_reg} \quad \text{(F-35)}$$

$$Pow4c: \ p_{bin\_reg} = p_{inf\_reg} \quad \text{(F-36)}$$

$$Pow5c: \ p_{inf\_reg} = p_{mgs\_ref} + \tilde{p}_{fg\_los} \quad \text{(F-37)}$$

Storage level protection

The terminal voltage of the super capacitor represents its energy storage level. For security reasons, it should be between the maximal allowed value and 50% of this value for an efficiency reason.

In order to limit the terminal voltage of the SC, an additional control function has to be used (macro bloc '*SLP*' in the *Power Supervision* level of the Fig.F-5).

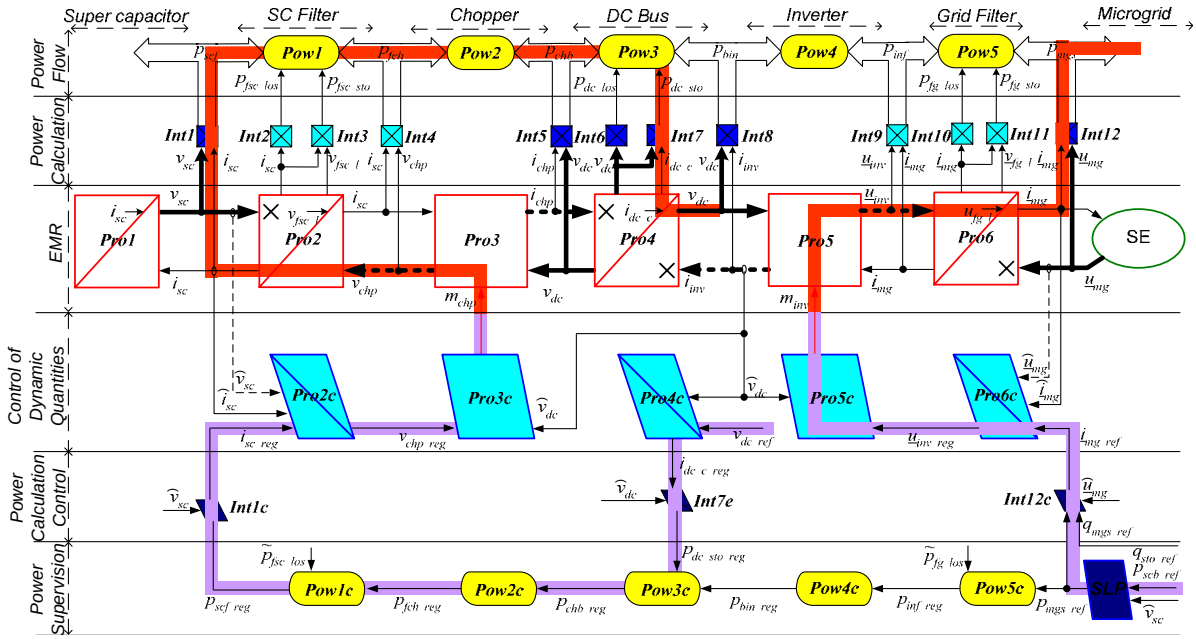

Figure F-5: Control system of the Super Capacitor Bank

Appendix

Appendix G: Hardware In-the-Loop (HIL) Simulation

Presentation

Hardware-In-the-Loop (HIL) simulation has been intensively used for controller assessment for a long time [Bou 08]. The aerospace industry has used this technique since flight control systems is a safety-critical aspect. This methodology yields exhaustive testing of a control system to prevent costly and damageable failures. From 90's, many groups in automotive industry have employed HIL simulation for testing embedded electronic control units. This methodology avoids intense and complex integration tests on the actual vehicle. The development time is reduced and a high quality assurance is obtained. HIL simulation is nowadays more and more used to develop new components and actuators in many fields, such as vehicle component evaluation, assessment of drive controls, power electronics and electric grid, servo control and robotics, railway traction systems for trains and subways, education applications.

In industrial applications, software simulation is always an essential preliminary step to test the required performances of the drive and its control by using simple models of the power system. HIL simulations are sometimes used for validation tests before implementation on actual processes. On the contrary of software simulation, HIL simulation uses one or several actual devices and the other parts of the process are simulated in a controller board or in parallel computers. HIL simulation enables to check availability and reliability of drives (machines, power electronics and control) before their insertion on a whole system. Moreover, many implementation constraints are taken into account such as sensor accuracy, sampling period, modulation frequency, active limitations and so on. More specifically, electrical generators of wind energy conversion systems can be tested by using HIL simulation, and some small-rate power systems can be used to validate control algorithms and Maximum Power Point Tracking strategies before implementation on a full-rate power system. Power propulsion systems for electric vehicles and hybrid electric vehicle can also be tested by HIL simulation, and actual drives can be tested before integration on the vehicle chassis.

An electrical drive can be decomposed into several subsystems (Fig.G-1): the process control, the power electronics set, the electrical machine and the mechanical load to move (the mechanical power train of a vehicle for example). Power devices are connected according to the action and reaction principle. A controller board contains the process control and yields the switching orders of the power electronics converter. Measurements of all power parts are inputs for this controller board. In some cases, several controller boards are used. In other case analog devices as FPGA are used to control the faster dynamics and to achieve high-frequency modulations of power electronics.

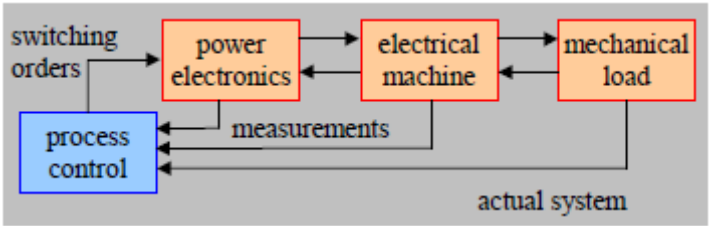

Figure G-1: Subsystems of an electric drive

Limitation of software simulation

The first step of the study is the simulation of the whole system including its control. All parts are simulated in the same simulation environment (software). In order to reduce the computation time, simple models and other simplifications are considered. For instance, the sampling period of the control is often neglected. For these reasons, simulation is not always accurate enough to enable a direct real-time implementation of the control. Before implementation on the actual system, different validations have to be made. HIL simulation could be a very useful intermediary step. One of the simulated parts can be replaced by its hardware device. By this way, the real constraints of this hardware subsystem are taken into account in the simulation loop. Three kinds of HIL simulation can be considered.

Signal level HIL simulation

In the first case, only the controller board (which contains the process control) is tested (Fig.G-2). The other parts (power electronics, machine and mechanical load) are simulated in real-time. The simulation system must manage inputs and outputs of the controller board under test. A second controller board is thus used to simulate in real-time the power parts of the system. A specific signal conditioning is required to impose the same inputs and outputs as imposed by the power parts. This method can be called "signal level HIL simulation" because only signals are used at the interface between the system under test and the simulation environment. This kind of HIL has been very often employed in aerospace and automotive applications for assessment of controller boards.

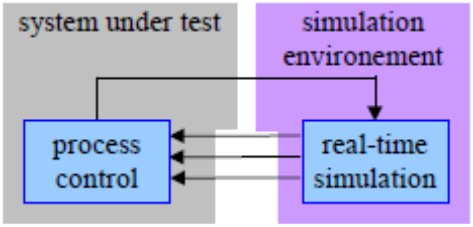

Figure G-2: Signal level HIL simulation

Power level HIL simulation

In the second case, the actual controller board and the power electronics converter are evaluated. The other parts (electrical machine and mechanical load) are simulated. The simulation system must impose inputs and outputs for the power electronics and the controller board under test. The simulation environment is generally composed of a second power electronics set (electric load) and a second controller board (real-time simulation) (Fig.G-3). This method can be called "power level HIL simulation". Indeed the interface between the system under test and the simulation environment require signal and power variables.

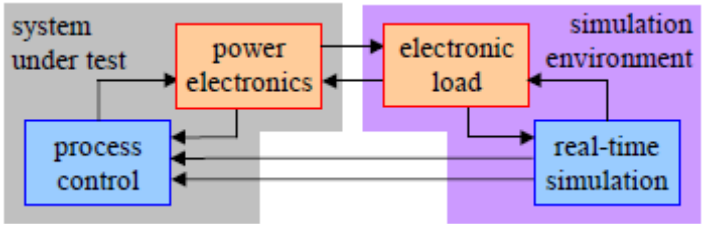

Figure G-3: Power level HIL simulation

Mechanical level HIL simulation

In the last case, the whole drive (control, power electronics and electric machine) is tested and the mechanical part is simulated. The simulation system must impose mechanical inputs

and outputs to the electrical machine under test. Moreover, measurements on the mechanical part have to be sent to the controller board under test. Another electrical machine (load machine) is often used as controlled mechanical load. It is supplied by a second power electronics set (load supply). A second controller board (real-time simulation) is required to control the load machine and to send fictitious mechanical "measurements" to the controller board under test (Fig.G-4). This method can be called “mechanical level HIL simulation”. Indeed the interface between the system under test and the simulation environment corresponds to mechanical variables.

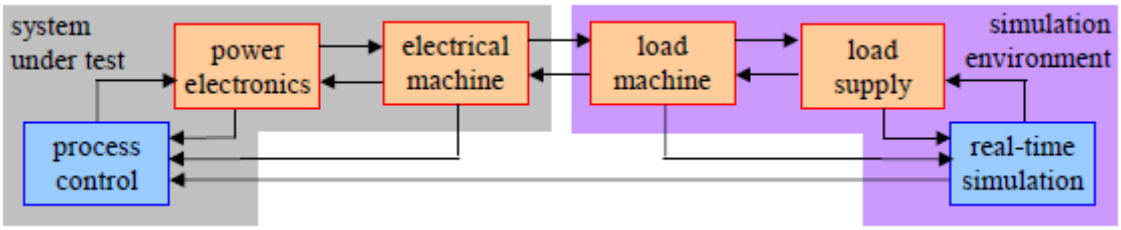

Figure G-4: Mechanical level HIL simulation

Appendix H: Ancillary Services in the context of Microgrid

H.1. Fundamental recalls

In order to present the necessary and possible ancillary services in the context of microgrid, some fundamental principles of grid management systems and classical practices should be recalled to highlight studied problems.

Isochronous Speed Control Mode

Isolated power systems and industrial microgrids are relatively small power systems. They are usually powered by a single AC generator, which is driven by a gas turbine or a diesel engine generator. The frequency of the generator is directly proportional to the speed of the rotating electrical field. Hence the power management relies on a simple Isochronous Speed Mode Control. It uses the physical principle of grid connected synchronous machine stator, which induces the exact synchronization of the machine speed with the grid frequency. A controller operating in the Isochronous Speed Control Mode maintains the turbine at a constant speed. Hence the energy being admitted to the prime mover is regulated in response to changes in load, which would tend to cause changes in the speed. Any increase in load would tend to cause the speed to decrease, but energy is quickly admitted to the prime mover to maintain the speed at the set point. Any decrease in load would tend to cause the speed to increase, but energy is quickly reduced to the prime mover to maintain the speed at the set point.

To increase the total generated power, multiple machines can be connected in parallel. In this case, if all prime movers operate in Isochronous Speed Mode, they will "fight" to control the frequency and result in wild oscillations of the grid frequency. So only one machine can have its governor operating in Isochronous Speed Mode for a stable grid frequency control, all others should work in "Droop Speed Control Mode" or "Fixed Power Control Mode".

Droop Speed Control Mode

In Droop Speed Control Mode, the turbine speed is controlled as a function (the droop characteristic) of turbine load. It refers to the fact that the energy being admitted to the prime mover of the AC generator is being controlled in response to the difference between the grid frequency setpoint and the actual grid frequency. To increase the power output of the generator, the controller increases the speed setpoint of the prime mover, but since the speed cannot change (it is fixed by the frequency of the grid to which the generator is connected) this frequency difference is used to increase the energy being admitted to the prime mover. So, the actual speed is being "allowed" to "droop" below its setpoint.

Fixed Power Control Mode

Nowadays, many small distributed generators (in particular the renewable energy based generators) are integrated in parallel with the grid. A Fixed Power Control Mode can be adopted for them to generate a fixed amount of active and reactive power, because they are not obliged to participate in frequency or voltage regulation until now. Moreover, for renewable energy based generators, the power reference is adapted according to the meteorological conditions in order to generate the maximum power, which is intermittent and

fluctuant. In consequence frequency or voltage regulation is reported to large AC generators in the grid. This can be the case if our studied microgrid is connected to a distribution network.

However, with a large-scale development of distributed renewable energy generators, their generation flexibility should be improved to avoid damaging the stability of the electrical grid. As the conventional turbine-based generators, they should be able to supply a smooth and controllable power in order to provide ancillary services to the electrical grid.

Ancillary services and active generators

An active generator is considered as a generator who participates to the management of the grid. Modern high speed micro-turbines and major of distributed generators are grid-connected with power electronic converters and so no physical relations exist between the rotor of the machine and the grid frequency. Moreover the large scale development of PV generators as well as technological evolution of backup power systems (like super-capacitors and fuel cells) makes appear power plants without any electrical rotating machine. Therefore, ancillary services can be provided only with improved control functions of the power converters (grid inverter for example). Some example features are listed as below:

- Reactive power supply/compensation;
- Harmonics supply/compensation;
- Peak shaving of the energy consumption;
- Improvement of the local power quality;
- Uninterruptible power supply for dedicated loads;
- Feed-in of renewable energies with lowest cost and highest efficiency;
- etc.

In order to perform all these ancillary services, including the frequency and voltage regulation, the distributed power generator must be able to supply corresponding active and reactive power references.

H.2. Ancillary services for the microgrid

The task of a grid supervision is to manage the power and the energy between sources and loads. Then the active and reactive power must be shared among the distributed generators. The originality of a microgrid is that it is a small grid and then a communication network can exists between generators, some dispatchable loads and the microgrid supervision. Active and reactive power references and also other appropriate control signals must be assigned to the distributed generators, storage units and controllable loads. Two implementations of microgrid supervisions exist for distributed generators [Kat 08] [Ped 08]:

- ***Control by sensing electrical quantities***: This method is achieved by using the knowledge of physical quantities at the Point of Common Connection (PCC) [Las 02] [Kat 06] and a droop characteristic control;
- ***Control by signal communication***: This method uses a communication bus to exchange information and control signals [Dim 05] [Bar 05] [Gaz 06] [Deg 06] [Dim-07].

Control by sensing electrical quantities

In Europe, electrical networks have been developed after the Second World War. At this time, communication infrastructures were limited. Coordination of all generators has been implemented through the measurement of two grid physical dynamic quantities: the frequency

and the RMS value of the microgrid voltage [Las 02] [Kat 06]. With this information, a droop characteristic control performs the coordination of Local Controllers (of generators) with a frequency-active power droop characteristic and/or voltage-reactive power droop characteristic. For example, when the frequency decreases the characteristic modifies the power reference in order to increase the generated active power. A local supervision of internal power and energy flows is therefore required as previously detailed "Power dispatching strategy" for the wind/super-capacitors hybrid power system (Fig.II-46) and the active wind generator (Fig.V-14). A droop controller can be easily embedded in the local control system to set active and reactive power references for the active generator.

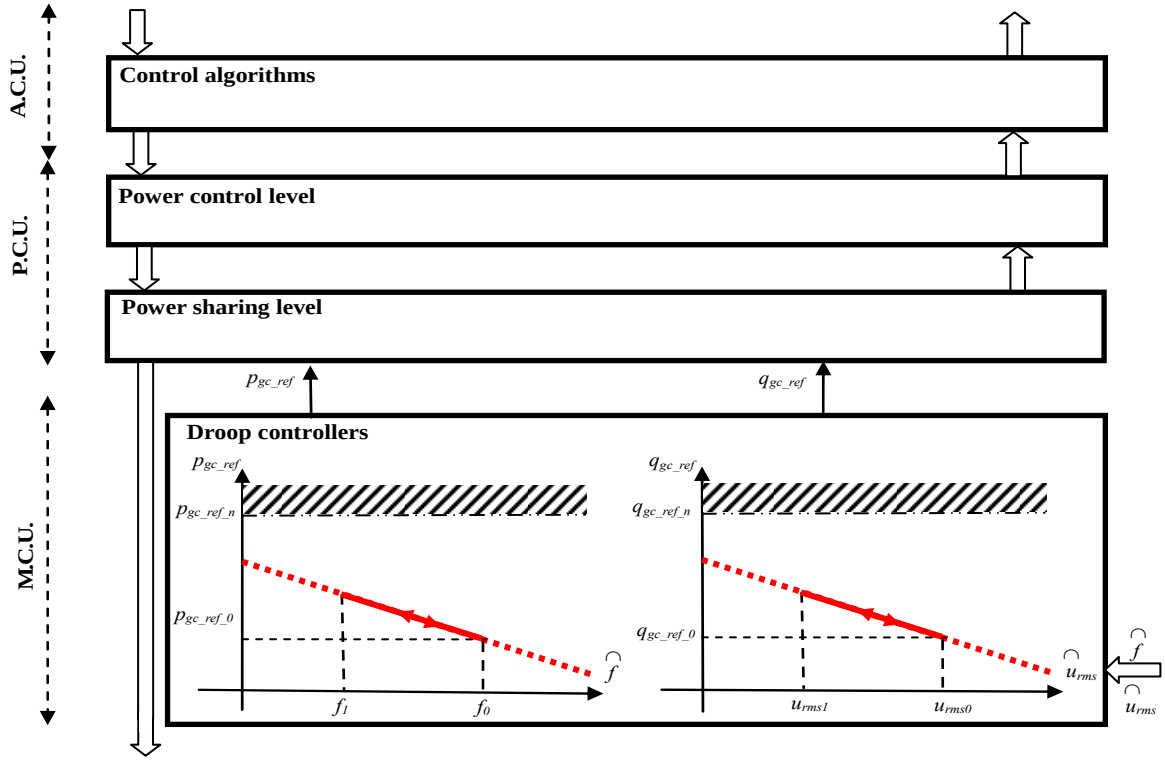

Figure H-1: Droop controllers for the "Power dispatching strategy".

The main advantage of this method is its simple hardware implementations, since the development of a communication network and a central supervision are not necessary. Moreover, this local implementation enables a very fast response and then a good adequacy for frequency control and RMS voltage regulation. This organization works in an autonomous way and sometimes called "non interactive" since it is not coordinated with a higher control center. The main disadvantage is the fact that an optimization function of the microgrid can not be designed with accuracy, since no sufficient information is known from operating points of other generators.

Control by signal communication

Control by signal communication enables information exchange and includes three categories of controllers (Fig.H-2) [Kat 08]:

- Distribution Network Controller (DNC);
- Microgrid Central Controller (MCC);
- Local Controllers (LCs), which are associated with each Active Generator (AG) or loads.

The DNC is intended for an area in which more than one microgrid exists. It does not

belong to the microgrid but is the delegate of the distribution network. The main interface between the DNC and the microgrid is the MCC. The MCC assumes different roles ranging from the maximization of the microgrid value to the coordination of LCs.

The LC controls the DER units and the controllable loads.

In a centralized operation, each LC receives set points from the corresponding MCC [Deg 06]. We have designed several control systems in Chap.II and Chap.V for our active generator. Then it must implement the received set points and send to the MCC some information about their operating point (Fig.H-2).

In a decentralized operation, each LC makes decisions locally (Fig.H-3). It relies on the results of negotiations between agents of every LC functions (multi-agent systems) [Dim 05] [Dim 07].

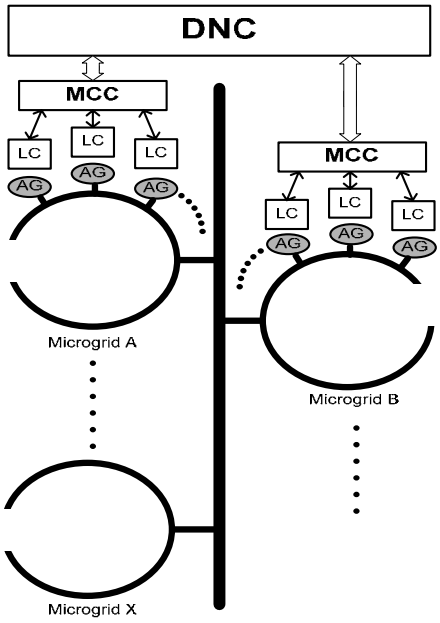

Figure H-2: Centralized operation for microgrid supervisory control

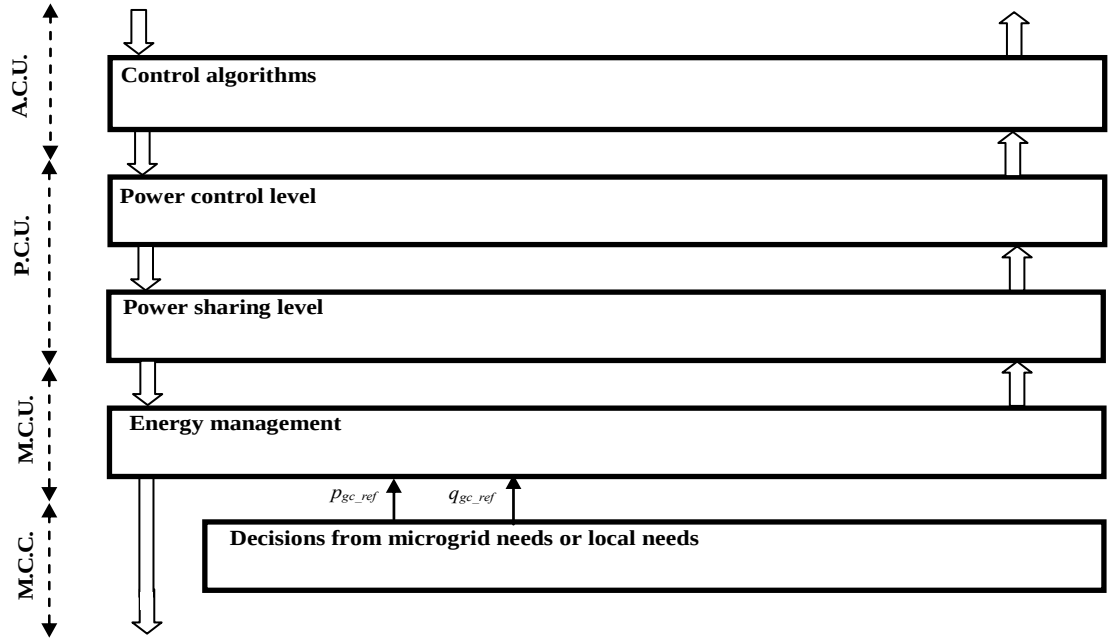

Figure H-3: Decentralized operation for the "Power dispatching strategy".

Appendix I: Technical Data of the Used Super-capacitors

MC BMOD Energy Series 48v BOOSTCAP® Ultracapacitor Modules

Series: BMOD Energy
48 Volt Module

- Low Internal Resistance
- High Energy Availability
- Low Time Constant

Features:

- 48.6V Operating Voltage
- Over 1M duty cycles
- Low internal resistance
- High energy density
- Individually balanced cells
- Mountable option included
- Module-to-module balancing
- Voltage and temperature sensor output included

Applications:

- Industrial
- UPS
- Power Quality
- Telecommunication
- Renewable energy

Overview:

The Energy-type ultracapacitor product line gives industrial customers a much wider range of choices to meet their energy storage and power delivery requirements. The modules are specifically engineered to provide cost-effective solutions for UPS, telecommunications and other lighter duty industrial electronics applications.

In addition to meeting or exceeding demanding industrial application requirements for both watt-hours of energy storage and watts of power delivery per kilogram, all of these products will perform reliably for more than one million discharge-recharge cycles.

The proprietary architecture and material science on which BOOSTCAP® products are based enable continued leadership in controlling costs, flexibility in product offerings and allow application specific performance tailoring.

The cells used in the modules operate at 2.7 volts, enabling them to store more energy and deliver more power per unit volume than any other commercially available ultracapacitor.

*Beginning January 1, 2007, the BMOD0145 will be replaced by the BMOD0165.
We will not be accepting orders after November 15, 2006 for BMOD0145 modules.
Please contact Maxwell Technologies for more information.

› Series Specifications:

Item	Performance	
Operating Temperature Range	-40 °C to +65 °C	
Storage Temperature Range	-40 °C to +70 °C	
Rated Voltage	48.6 V DC	
Capacitance Tolerance	+20%	
Resistance Tolerance	Max.	
Temperature Characteristics	Capacitance Change	Within ± 5% of initial measured value at 25 °C (at -40 °C)
	Internal Resistance	Within 150% of initial measured value at 25 °C (at -40 °C)
Endurance	After 1500 hours application of rated voltage at 65 °C	
	Capacitance Change	Within 20% of initial specified value
	Internal Resistance	Within 60% of initial specified value
Shelf Life	After 1500 hours storage at 65 °C without load shall meet specification for endurance	
Life Test	After 10 years at rated voltage and 25 °C	
	Capacitance Change	Within 30% of initial specified value
	Internal Resistance	Within 150% of initial specified value
Cycle Test	Capacitors cycled between specified voltage and half rated voltage under constant current at 25 °C (1 million)	
	Capacitance Change	Within 30% of initial specified value
	Internal Resistance	Within 150% of initial specified value

› Product Specifications:

Maxwell Part No.	Capacitance (F)	ESR, DC (mohm)	ESR, 1khz (mohm)	Ic (mA)
BMOD0083 E048	80	16.0	12.8	3.0
BMOD0110 E048	110	12.0	9.6	4.2
BMOD0145 E048*	145	11.0	9.0	5.2
BMOD0165 E048	165	7.6	6.3	5.2

*Beginning January 1, 2007, the BMOD0145 will be replaced by the BMOD0165.
We will not be accepting orders after November 15, 2006 for BMOD0145 modules.
Please contact Maxwell Technologies for more information.

› Product Properties:

Maxwell Part No.	Rth (C/W)	Isc (A)	Emax (Wh/kg)	Pmax (W/kg)	Pd (W/kg)
BMOD0083 E048	0.39	3,900	2.48	4,100	1,600
BMOD0110 E048	0.33	4,300	2.91	4,900	1,900
BMOD0145 E048*	0.27	4,800	3.52	4,800	1,900
BMOD0165 E048	0.25	4,800	3.81	6,600	2,600

› Dimensions:

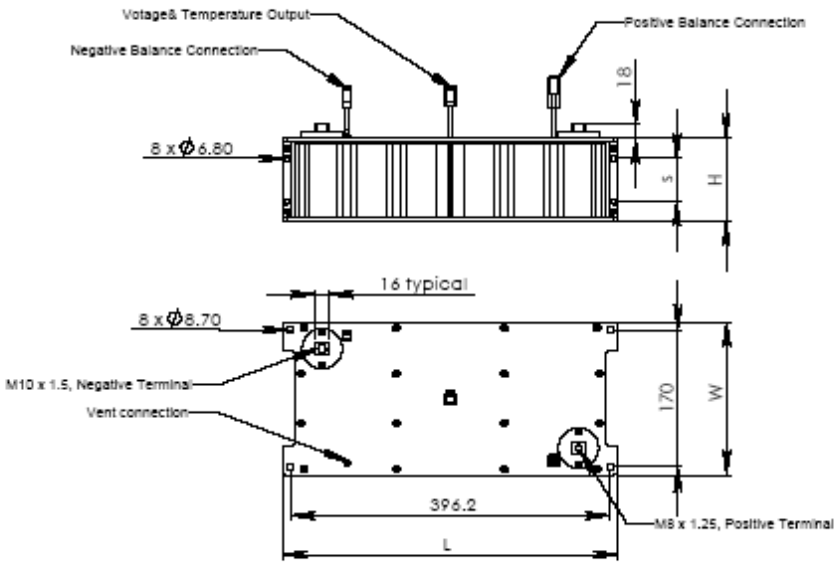

Part Number	Vol (l)	Mass (kg)	Size (mm)			
			L (+/- 0.5)	W (+/- 0.5)	H (+/- 0.5)	s (+/- 0.5)
BMOD0083 E048	8.5	11.0	416	190	108	53.7
BMOD0110 E048	9.8	12.4	416	190	124	70.7
BMOD0145 E048	12.6	13.5	416	190	160	89.4
BMOD0165 E048	12.6	14.2	416	190	160	89.4

Product dimensions and specifications may change without notice. Please contact Maxwell Technologies directly for any technical specifications critical to application.

› Markings: Modules are marked with the following information

Rated capacitance, rated voltage, product number, name of manufacturer, positive and negative terminal, warning marking, serial #

› Mounting Recommendations:

Modules can be secured at 8 locations, 4 front face and/or 4 bottom face, at provided holes for M8 bolts. Follow user manual instructions for terminal, balance and output connections.

Patent Pending

Worldwide Headquarters
MAXWELL TECHNOLOGIES
9244 Balboa Avenue • San Diego, 92123 CA, USA
PHONE: +(1) 858 503 3300
FAX: +(1) 858 503 3301
EMAIL: info@maxwell.com

European Office
MAXWELL TECHNOLOGIES SA
CH-1728 Rossens • Switzerland
PHONE: +41 (0) 26 411 85 00
FAX: +41 (0) 26 411 85 05
EMAIL: info@maxwell.com

www.maxwell.com

Additional Technical Information:

Capacitance and ESR, DC measured per document 1007239

I_C = Leakage current after 72 hours, 25°C Isc = short circuit current (maximum peak current)

R_{th} = Thermal resistance

$$E_{max} = \frac{½\ CV^2}{3600 \times mass} \qquad P_{max} = \frac{\frac{V^2}{4R\ (1khz)}}{mass} \qquad P_d = \frac{\frac{0.12V^2}{R\ (DC)}}{mass}$$

Disclaimer of Warranty/Limitation of Liability

for Uses in Life Support Devices or Critical Systems

Maxwell Technologies, Inc. and its Affiliates ("Maxwell") provide no warranties of any kind either express or implied, including (without limitation) the implied warranties of merchantability and fitness, for uses of its products as components in life support devices or critical systems.

"Life support devices" are devices or systems, which (a) are intended for surgical implant into a living body, or (b) support or sustain life, and whose failure to perform when properly used in accordance with the instructions provided in the labeling can be reasonably expected to result in bodily injury to the user. An example of a life support device includes, but is not limited to, a heart pacemaker.

A "critical system" is any system whose failure to perform can affect the safety or effectiveness of a higher level system, or cause bodily or property injury by loss of control of the higher level device or system. An example of a critical system includes, but is not limited to, aircraft avionics.

Maxwell will not be liable to you for any loss or damages, either actual or consequential, indirect, punitive, special, or incidental, arising out of or relating to these terms.

Patent Pending

Worldwide Headquarters
MAXWELL TECHNOLOGIES
9244 Balboa Avenue • San Diego, 92123 CA, USA
PHONE: +(1) 858 503 3300
FAX: +(1) 858 503 3301
EMAIL: info@maxwell.com

European Office
MAXWELL TECHNOLOGIES SA
CH-1728 Rossens • Switzerland
PHONE: +41 (0) 26 411 85 00
FAX: +41 (0) 26 411 85 05
EMAIL: info@maxwell.com

www.maxwell.com

Bibliography

Bibliography:

A:

[Abb 05] C. Abbey, G. Joos, "Energy Management Strategies for Optimization of Energy Storage in Wind Power Hybrid System", IEEE 36th Power Electronics Specialists Conference, PESC'05, pp.2066-2072, June 2005.

[Abb 07] C. Abbey, G. Joos, "Supercapacitor energy storage for wind energy applications", IEEE Transaction on Industry Application, vol.43, no.3, May/June 2007.

[Ack 01] Ackerman, T, Andersson, G and Söder, L. Distributed Generation: A Definition, Electric Power System Research, vol.57, 2001, pp.195-204.

[Ahm 06] N.A. Ahmed, M. Miyatake, "A Stand-Alone Hybrid Generation System Combining Solar Photovoltaic and Wind Turbine with Simple Maximum Power Point Tracking Control", 5th International Power Electronics and Motion Control Conference, IPEMC'06, vol.1, pp.1-7, Aug. 2006.

[Amp 95] J. Amphlett, et al, "Performance modeling of the Ballard Mark IV solid polymer electrolyte fuel cell", Journal of Electrochemical Society, 142(1), 9-15.

[Ast 08] S. Astier, et al "A review on existing modelling methodologies for PEM fuel cell systems", 2008 Conference of Fundamentals & Developments of Fuel Cells (FDFC 2008), Nancy, France, 10-12 December 2008, CD-ROM.

[Ath 04] K. Athanasas, I. Dear, "Validation of complex vehicle systems of prototype vehicle", *IEEE trans. on Vehicular Technology*, Vol. 53, no. 6, November 2004, pp. 1835-1846.

[Aya 07] M.Y. Ayad et al, "Voltage regulated hybrid DC power source using supercapacitors as energy storage device", Elsevier, Energy Conversion and Management, vol.48, Jul.2007, pp.2196-2202.

B:

[Bar 05] M. Barnes, A. Dimeas, A. Engler, C. Fitzer, N. Hatziargyriou, C. Jones, S. Papathanassiou, M. Vandenbergh, "MicroGrid laboratory facilities", 2005 IEEE International Conference on Future Power Systems, Wind Engineering, 16-18 Nov. 2005.

[Bar 06] P. J. Barrre, A. Bouscayrol, P. Delarue, E. Dumetz, F. Giraud, J. P. Hautier, X. Kestelyn, B. Lemaire-Semail, E. Semail, "Inversion-based control of electromechanical systems using causal graphical descriptions", IEEE-IECON'06, Paris, November 2006, CD ROM.

[Bas 06] J. Bastien, C. Handler, "Hydrogen production from renewable energy sources", 2006 IEEE EIC Climate Change Technology, pp. 1-9, 10-12 May 2006.

[Bec 06] M. Becherif, M.Y. Ayad, A. Miraoui, "Modeling and passivity-based control of hybrid sources: fuel cells and super-capacitors", Industry Application Conference, IEEE-IAS'06, pp.1134-1139.

[Bec 08] M. Beccali, S. Brunone, M. Cellura, V. Franzitta, "Energy. Economic and environmental analysis on RET-hydrogen systems in residential buildings", International Journal of Renewable Energy, vol. 33, 2008, pp.366-382.

[Bla 06] F. Blaabjerg, R. Teodorescu, M. Liserre, A.V. Timbus, "Overview of Control and Grid Synchronization for Distributed Power Generation Systems," IEEE Trans. Ind. Electron., vol.53, iss.5, pp. 398-1409, Oct. 2006.

[Bos 07] T. Bossmann, A. Bouscayrol, P. Barrade, S.Lemoufouet, A. Rufer, "Energetic Macroscopic Representation of a hybrid storage system based on supercapacitors and compressed air", IEEE ISIE 2007, pp. 2691-2696, 4-7 June 2007.

[Bou 00] A. Bouscayrol, B. Davat, B. de Fornel, B. Francois, J. P. Hautier, F.Meibody-Tabar, M. Pietrzak-David, "Multimachine Multi-converter System: application for electromechanical drives", European Physics Journal - Applied Physics, vol. 10, no. 2, pp. 131-147, May 2000.

[Bou 02] A. Bouscayrol, Ph. Delarue, "Simplifications of the maximum control structure of a wind energy conversion system with an induction generator", International Journal of Renewable Energy Engineering, vol.4, no.2, pp. 479-485, Aug. 2002.

[Bou 05a] A. Bouscayrol, P. Delarue, X. Guillaud, "Power strategies for Maximum Control Structure of a wind energy conversion system with a synchronous machine", Renewable Energy, vol. 30, pp. 2273-2288, May 2005.

[Bou 05b] A. Bouscayrol, X. Guillaud, P. Delarue, "Hardware-in-the-loop simulation of a wind energy conversion system using Energetic Macroscopic Representation", *IEEE-IECON'05*, Raleigh (USA), November 2005.

[Bou 06a] A. Bouscayrol, M. Pietrzak-David, P. Delarue, R. Pena-Eguiluz, P. E. Vidal, X. Kestelyn, "Weighted control of traction drives with parallel connected AC machines", IEEE ton Industrial Electronics, vol. 53, no. 6, pp. 1799-1806, December 2006.

[Bou 06b] A. Bouscayrol, W. Lhomme, P. Delarue, B. Lemaire-Semail, S. Aksas, "Hardware-in-the-loop simulation of electric vehicle traction systems using EMR", *IEEE-IECON'06*, Paris, November 2006.

[Bou 07] O. Bouhali, "Contribution des convertisseurs multi-niveaux au raccordement de la production d'origine éolienne sur un réseau électrique", PhD. Thesis, Ecole centrale de Lille in France and Ecole Nationale Polytechnique in Algérie, 2007.

[Bou 07] A. Bouscayrol, A. Bruyère, P. Delarue, F. Giraud, B. Lemaire-Semail, Y. Le Menach, W. Lhomme, and F. Locment, "Teaching drive control using Energetic Macroscopic Representation - initiation level", EPE 2007, Aalborg (Denmark), September 2007, CD-ROM.

C:

[Cet 07] Societe CETH, "Electrolyseur à membrane échangeuse de proton (PEM) Genhy 100® : Notice d'utilisation" Genhysoft® Version1.1e du 30/10/2007.

[Cet 08] http://www.ceth.fr/

[Che 03] Z. Chen,; Y. Hu, "A hybrid generation system using variable speed wind turbines and diesel units", The 29th Annual Conference of the IEEE Industrial Electronics Society, IEEE IECON'03, vol.3, pp.2729-2734, Nov. 2003.

[Chr 07] D. Chrenko, M.-C. Pera, D. Hissel, "Fuel Cell System Modeling and Control with Energetic Macroscopic Representation", IEEE ISIE 2007, pp.169 – 174, 4-7 June 2007.

[Cor 04] J. M. Correa, F. A. Farret, L. N. Canha, and M. G. Simoes, "An electrochemical-based fuel cell model suitable for electrical engineering automation approach", IEEE Trans. Ind. Electron, vol. 51, no. 5, pp. 1103–1112, Oct. 2004.

[Cor 05] P. Corbo, F. E. Corcione, F. Migliardini, and O. Veneri, "Experimental study of a fuel cell power train for road transport application", J. Power Sources, vol. 145, no. 2, pp. 610–619, Aug. 2005.

D:

[Dav 09] B. Davat, et al "A Fuel cell based hybrid systems", the 8th Internation Symposium on Advanced Electromechenical Motion Systems (ELECTROMOTION'09), Lille, France, 1-3 July 2009, CD-ROM.

[Deg 06] Ph. Degobert, S. Kreuawan, X. Guillaud, "Micro-grid powered by photovoltaic and micro turbine", International Conference on Renewable Energy and Power Quality (ICREPQ'06), Palma de Mallorca, Spain, April 5-7, 2006.

[Del 03] P. Delarue, A. Bouscayrol, E. Semail, "Generic control method of multileg voltage-source-converters for fast practical implementation", IEEE ton Power Electronics, vol. 18, no. 2, pp.517-526, March 2003.

[Dim 05] A.L. Dimeas, N.D. Hatziargyriou, "Operation of a multi-agent system for microgrid control", IEEE Trans. on Power Systems, vol. 20, No. 3, pp. 1447-1457, August 2005.

[Dim-07] A.L. Dimeas, N.D. Hatziargyriou, "Agent based control for microgrids", IEEE Power Engineering Society General Meeting, Tampa, USA, June 2007.

[Dir 01] Directive 2001/77/EC of the European Parliament and of the Council of 27 September 2001 on the promotion of electricity produced from renewable energy sources in the internal electricity market, Official Journal of the European Communities, L 283/33.

[Dis 01] Dispower, "Fuel cell/Electrolyzer combinations for long-term storage", Dispower project report, task 1.5.b, 2001.

E :

[Eur 09] http://www.eurobserv-er.org/

[Ewe 05] EWEA, Oct. 2005, Online Documentation. [Online]. Available: http://www.iea-pvps.org.

F:

[Fer 74] R. Fernandes, "Hydrogen cycle peak-shaving for electric utilities", 9th Intersociety Energy Conversion Engineering Conference, 1974.

[Fra 99] B. François, J.P. Hautier, "Pulse Position and Pulse Width Modulation of Electrical Power Conversions: Application to a Three-Phase Voltage-Fed Inverter", 3rd International Symposium on Advanced Electromechanical Motion Systems: ELECTROMOTION 1999, vol.2, pp.653-658, Patras, Greece, July 8-9,1999

[Fra 02] B. François, F. Gillon, P. Brochet, "Power monitoring of an induction motor with an integrated flywheel", ICEM, Bruges, Belgium, 3-2002.

[Fra 04] B. François, D. Hissel, M.T. Iqbal, "Dynamic Modelling of a Fuel Cell and Wind Turbine DC-Linked Power System", ELECTRIMACS 2005, April 17-20, 2005, Hammamet, Tunisia, CD, 4-2005

[Fra 05] B.François, C. Saudemont, B. Robyns, "Feedback loop control strategies with a resonant controller for ac voltage control of a grid-connected decentralized generator", EPE'05, Dresden, Sep., 2005.

[Fra 08] B. François, P. Degobert, B. Robyns, "*SUPER*vision *ENER*gétique de centrales dispersées de production multi source permettant la fourniture de services "système" au sein d'un micro réseau : *SUPERENER*", ANR Project report, Dec. 2008.

G:

[Gab 06] O. Gabriel, C. Saudemont, B. Robyns, M. M. Radulescu, "Control and performance evaluation of a flywheel energy-storage system associated to a variable-speed wind generator", IEEE transaction on Industrial Electronics, vol.53, no.4, Aug. 2006.

[Gaz 06] H. Gaztanaga Arantzamendi, "Etude de structures d'intégration des systèmes de génération décentralisée : Application aux microréseaux", Thèse de doctorat, l'Institut Nationale Polytechnique de Grenoble, le 15 décembre 2006.

[Glo 05] Global Environment Fund, Center for Smart Energy, "The Emerging Smart Grid: Investment and Entrepreneurial Potential in the Electric Power Grid of the Future", October 2005. http://www.globalenvironmentfund.com/GEF%20white%20paper_Electric%20Power%20Grid.pdf

[Gui 00] X. Guillaud, P. Degobert, J.P. Hautier, "Modeling Control and Causality : The Causal Ordering Graph," 16th IMACS Control Engineering, Lausanne 2000, CD ROM.

[Gui 03] X. Guillaud, B. Francois, "A causal method for the modelling of static converter and the control design: Application to a Voltage Source Converter," EPE 2003, September 2003, CD, Toulouse, France.

[Gra 07] F.Grasser,; A.C. Rufer, "An Analytical, Control-Oriented State Space Model for a PEM Fuel Cell System", *Power Conversion Conference*, PCC'07, pp.441-447,April 2007 Nagoya.

[Gre 72] D. Gregory, "A hydrogen-energy system", Report for American Gas Association, Cat. No. L21173, August 1972.

[Gre 73] D. Gregory, "A hydrogen economy", Scientific America, vol.228, No.1, 1973, pp.13-21.

[Gro 45] W. Grove, "On the gas voltaic battery - voltaic action of phosphorus, sulphur and hydrocarbons," *Phil. Transactions*, vol. 1, p. 351, 1845.

H:

[Haj 07] A. hajizadeh, M.A. Golkar, "Intelligent power management strategy of hybrid distributed generation system", Elsesvier, Electrical Power and Energy System, 2007, pp.783-795.

[Han 96] H. Hanselmann, "Hardware-in-the-loop simulation testing and its integration into a CACSD toolset", *IEEE-CCS'96*, Dearborn, Sept. 1996.

[Har 04] K. Haraldsson and K. Wipke. "Evaluating PEM fuel cell system models," *Journal of Power Sources*, vol. 126, pp. 88-97, February 2004.

[Hau 96] J. P. Hautier, J. Faucher, "The Causal Ordering Graph", *Bulletin de l'Union des Physiciens*, (text in French), vol. 90, juin 1996, pp. 167-189.

[Hau 99] J.P.Hautier, J.P.Caron, "Convertisseur statiques, methodologie causale de modelisation et de commande", *Editions Tecnip*, 1999.

[Hau 04] J. P. Hautier, P. J. Barre, "The causal ordering graph – A tool for modelling and control law synthesis", *Studies in Informatics and Control Journal*, vol. 13, no. 4, December 2004, pp. 265-283.

[His 08] D. Hissel, M. Péra, A. Bouscayrol, D. Chrenko, "Représentation énergétique macroscopique d'une pile à combustible", Revue Internationale de Génie Électrique, vol.11/4-5, pp. 603-623, 2008.

[Hoo 03] G. Hoogers, ed., *Fuel Cell Technology Handbook*. CRC Press, 2003.

I:

[Iea 05] IEA-PVPS, Cumulative Installed PV Power, Oct. 2005. [Online]. Available: http://www.iea-pvps.org.

[Iwa 94] I. Iwasaki, H. A. Simon, "Causality and model abstraction", *Artificial Intelligence*, Elsevier, vol. 67, 1994, pp. 143-194.

J:

[Jou 03] A. Von Jouanne, I. Husain, A. Wallace, and A. Yokochi, "Innovative hydrogen/fuel cell electric vehicle infrastructure based on renewable energy sources," in *Proc. 38th IEEE Industry Applications Conf.*, 2003, vol. 2, pp. 12–16.

K:

[Kat 06] F. Katiraei, M.R. Iravani, "Power management strategies for a microgrid with multiple distributed generation units", IEEE Trans. on Power Systems, vol. 21, No. 4, pp. 1821-1831, November 2006.

[Kat 08] F. Katiraei, M.R. Iravani, H. Gaztanaga, A.L. Dimeas, "Microgrids Management", IEEE Power and Energy Magazine, vol. 6, pp. 54-65, May/June 2008.

[Kin 78] W. Kincaide, "Alkaline electrolysis: past, present and future", Hydrogen for energy distribution, Institute of Gas Technology, 1978.

[Koj 04] H. M. Kojabadi, L. Chang, T. Boutot, "Development of a novel wind turbine simulator for wind energy conversion systems using an inverter controlled induction motor", *IEEE trans. on Energy Conversion*, vol. 19, no. 3, pp. 547-552, September 2004.

[Kon 75] A. Konopka, J.K.D. Wiliamson, "Hydrogen production by electrolysis: present and future", 10th Intersociety Energy Conversion Engineering Conference, IEEE Cat. No. 75CHO 983-7 TAB, 1975.

[Kot 03] R. Kottenstette, J. Cotrell, "Hydrogen storage in wind turbine towers", NREL, Golden, CO, www.nrel.gov/docs/fy03osti/34656.pdf, September 2003.

[Kot 08] B. Kroposki, J. Levene, K. Harrison, "Electrolysis: information and opportunities for electric power utilities", American national renewable energy laboratory technical report (NREL/TP-581-40605), Sep. 2006.

L:

[Lab 98] F.Labrique, H.Buyse, G.Séguier, R.Bausiere, "Les convertisseurs de l'electronique de puissance, Commande et comportement dynamique", Tome5, Technique et Documentation – Lavoisier, 1998.

[Lar 00] J. Larminie, A. Dicks, "Fuel Cell System Explained", Wiley, West Sussex, England, 2000.

[Las 02] R. Lasseter, A. Akhil, C. Marnay, J. Stephens, J. Dagle, R. Guttromson, et al., "Integration of distributed energy resources – The MicroGrid concept", CERTS MicroGrid Review, April 2002.

[Leb 07] M. Lebbal, T. Zhou, S. Lecoeuche, B. François, "Dynamically electrical modelling of electrolyser and hydrogen production regulation", The 2nd International Hydrogen Energy Congress and Exhibition (IHEC'07), Istanbul, Turkey, 13-15 July 2007, CD-ROM.

[Lec 04] L. Leclercq, "Apport du stockage inertial associé à des éoliennes dans un réseau électrique en vue d'assurer des services systèmes", university of Lille in France, 2004.

[Lho 05a] W. Lhomme, P. Delarue, P. Barrade, A. Bouscayrol "Maximum Control Structure of a Series Hybrid Electric Vehicle using Supercapacitors", EVS'21, Monaco, April 2005.

[Lho 05b] W. Lhomme, P. Delarue, P. Barrade, A. Bouscayrol, A. Rufer, "Design and Control of a supercapacitor storage system for traction applications", 2005 IEE Industry Applications Conference, vol.3, pp.2013-2020, Oct.2005.

[Li 08a] P. Li, P. Dégobert, B. Robyns, B. François, "Implementation of interactivity across a resilient microgrid for power supply and exchange with an active distribution network", CIRED Seminar 2008: SmartGrids for Distribution, Frankfurt, June 2008, CD-ROM.

[Li 08b] P. Li, B. Francois, P. Degobert, B. Robyns, "Multi-level representation for control design of a super capacitor storage system for a microgrid connected application", ICREPQ'08, Santander, 12-14 mars 2008, 3-2008, CD-ROM.

[Li 08c] C.H. Li et al, "Dynamic modelling and sizing optimization of stand-alone photovoltaic power systems using hybrid energy storage technology", International Journal of Renewable Energy, accepted of publication in 2008.

[Li 09] P. Li, "Formalisme pour la Supervision des Systèmes Hybrides Multi-Sources de Générateurs d'Energie Répartie : Application à la Gestion d'un Micro Réseau", PhD thesis, L2EP, Ecole Centrale de Lille, France, June 2009.

[Lot 74] M. Lotker, "Hydrogen for the electric utilities – long range possibilities", 9th Intersociety Energy Conversion Engineering Conference, 1974.

[Lu 07] B. Lu, X. Wu, H. Figueroa, A. Monti, "A low cost real-time hardware in-the-loop testing approach of power electronics control", *IEEE trans. on Industrial Electronics*, vol. 52, no. 3, April 2007, pp. 919-931.

M:

[Mac 97] D. Maclay, "Simulation gets into the loop", *IEE Review*, May 1997, pp.109-112.

[Mar 05] J.N. Marie-Francoise, H.Gualous, R. Outbib, A.Berthon, "42V power net with supercapacitor and battery for automotive applications", Elsevier, Journal of Power Sources, vol.143, 2005, pp.275-283.

[Maz 03] Mazza, Patrick, "The Smart Energy Network: Electricity's Third Great Revolution", 2003. http://climatesolutions.org/pubs/pdfs/SmartEnergy.pdf

[Mor 06] J. Moreno, M.E.Ortuzar, J.W.Dixon, "Energy-management system for a hybrid electric vehicle, using ultracapacitors and neural networks", IEEE transactions on Industrial Electronics, vol.53, no.2, Apr. 2006, pp.614-623.

O:

[Ona 06] O.C. Onar, M. Uzunoglu, M.S. Alam, "Dynamic modeling design and simulation of a wind/fuel cell/ultra-capacitor-based hybrid power generation system", International Journal of Power Sources, vol.161, iss.1, Oct. 2006, pp.707-722.

P:

[Pay 61] H. Paynter, "Analysis and design of engineering systems", *MIT Press*, 1961.

[Pay 07] A. Payman, S. Perfederici, F. meibody-Tabar, "Implementation of a flatness based control for a fuel cell-ultracapacitor hybrid system", Power Electronics Specialists Conference, IEEE-PESC'07, June 2007.

[Ped 08] M.A. Pedrasa, "Overview of microgrid management and control", Internet document, www.ceem.unsw.edu.au/content/userDocs/OverviewofMicrogrid-ManagementandControl.pdf, September, 2008.

[Pri 02] http://www.princeton.edu/~chm333/2002/spring/FuelCells/images/pem_fuelcell.GIF

[Puk 04] J. T. Pukrushpan, A.G. Stefanopoulou, and H. Peng, "Controlling fuel cell breathing", IEEE Control Syst. Mag., vol. 24, no. 2, pp. 30–46, Apr. 2004.

R:

[Rab 02] C. A. Rabbath, M. Abdoune, J. Belanger, K. Butts, "Simulating hybrid dynamic systems", *IEEE Robotics & Automation Magazine*, Vol. 9, no. 2, June 2002, pp. 39 – 47.

[Rob 01] B. Robyns, M. Nasser, F. Berthereau, F. Labrique, "Equivalent continuous dynamic model of a variable speed wind generator" ELECTROMOTION 2001, vol.8, n°.4, pp. 202-208, dec. 2001.

[Rob 02] B. Robyns, Y. Pankow, L. Leclercq, B. Francois, "Equivalent continuous dynamic model of renewable energy system", ELECTRIMACS 2002, CD-ROM, 18-21 Aout 202, Montreal, Canada.

[Rod 05] P. Rodatz, G. Paganelli, A. Sciarretta, and L. Guzzella, "Optimal power management of an experimental fuel cell/supercapacitor-powered hybrid vehicle", Control Eng. Practice, vol. 13, no. 1, pp. 41–53, Jan. 2005.

[Rub 97] Z. Rubin, S. Munns, J. Moskowa, "The development of vehicular powertrain system modeling methodologies: philosophy and implementation", *System Automotive Engineering*, paper 971089, 1997.

S:

[Sau 05] C. Saudemont, G. Cimuca, B. Robyns, M.M. Radulescu, "Grid Connected or Stand-Alone Real-Time Variable Speed Wind Generator Emulator Associated to a Flywheel Energy Storage System", EPE 2005, Vol. CD-ROM, 9-2005

[Sch 03] Scheepers, M J J. and Wals, A F, SUSTELNET, Policy and Regulatory Roadmaps for the Integration of Distributed Generation and the Development of Sustainable Electricity Networks, New Approach in Electricity Network Regulation, An Issue on Effective Integration of Distributed Generation in Electricity Supply Systems, ECN-C-03-107, Sep. 2003 (http://www.ecn.nl/library/reports/index.html).

[Sch 05] M. E. Schenck, J. S. Lai, and K. Stanton, "Fuel cell and power conditioning system interactions", Proc. 20th Annu. IEEE Appl. Power Electron. Conf. Expo. (APEC), vol. 1, Austin, TX, Mar. 6–10, 2005, pp. 114–120.

[Spa 03] M.R. Von Spakovsky, D. Rancruel, D. Nelson, S.K. Mazumder, R. Burra, K. Acharya, C. Haynes, and R. Williams, "Investigation of system and component performance and interaction issues for solidoxide fuel cell based auxiliary power units responding to changes in application load", in *Proc. IEEE Industrial Electronics Society Conf. (IECON '03)*, vol. 2, pp. 1574–1579, 2003.

[Ste 06] H. Li, M. Steurer, S. Woodruff, K. L. Shi, D. Zhang, "Development of a unified design, test, and research platform for wind energy systems based on hardware-in-the-loop real time simulation", *IEEE trans. on Industrial Electronics*, vol. 53, no. 4, June 2006, pp. 1144-1151.

[Sur 04] B. Suresh, S. Schlag, Y. Inogucji, "Chemical economics handbook marketing research report", SRI Consulting, 2004.

T:

[Ter 99] P. Terwiesch, T. Keller, E. Scheiben, "Rail vehicle control system integration testing using digital hardware-in-the-loop simulation", *IEEE trans. on Control System Tech.*, vol. 7, no. 3, May 99, pp. 352-362.

[Tho 05] P. Thounthong, S. Rael, and B. Davat, "Utilizing fuel cell and supercapacitors for automotive hybrid electrical system", in Proc. 20th Annu. IEEE Appl. Power Electron. Conf. Expo. (APEC), vol. 1, Austin, TX, Mar. 6–10, 2005, pp. 90–96.

[Tho 06] P. Thounthong, S. Raël, and B. Davat, "Test of a PEM fuel cell with low voltage static converter", J. Power Sources. [Online]. 153(1), pp. 145–150, Jan. 2006.

[Tho 07] P. Thounthong, S. Raël, and B. Davat, "Control strategy of fuel cell and supercapacitors association for distributed generation system", IEEE Trans. Ind. Electron., vol.54, iss.6, Dec.2007 pp.3225–3233.

[Tho 09] P. Thounthong, S. Rael, B. Davat, "Energy management of fuel cell/battery/supercapacitor hybrid power source for vehicle applications", Elsevier, Journal of Power Source, to be published.

[Tsi 05] A. Tsikalakis, N. Hatziargyriou, "Economic Scheduling Functions of a Microgrid using a Central Controller and applying different Market and Demand Side Options", CIGRE Symposium, Athens, 13-16 April 2005.

U:

[Ull 98] O. Ulleberg, "Stand alone power system for the future: optimal design, operation and control of solar-hydrogn energy systems", Ph.D. dissertation, Norwegian University of Science and Technology, Trondheim, Dec. 1998.

V:

[Vah 04] A. Vahidi, A. G. Stefanopoulou, and H. Peng, "Model predictive control for starvation prevention in a hybrid fuel cell system", in Proc. 2004 Amer. Control Conf., vol. 1, Boston, MA, Jun. 30–Jul. 2, 2004, pp. 834–839.

[Van 05] Van Werven, M J N, and Scheepers, M J J. DISPOWER, The Changing Role of Energy Suppliers and Distribution System Operators in the Deployment of Distributed Generation in Liberalised Electricity Markets, Report ECN-C—05- 048, June 2005 (http://www.ecn.nl/library/reports/index.html).

[Ver 01] J. Verne, "The Mysterious Island (1874) – A new translation: translated by Jordan Stump", Modern Library, 2001.

W:

[Wen 91] H. Went, B. Roland, "Hydrogen production by water electrolysis", Kerntechnik 56 (1991) N°1.

[Wil 00] Willis, H L and Scott, W G. Distributed Power Generation, Planning and Evaluation, Marcel Dekker Inc, 2000, ISBN 0-8247-0336-7.

Y:

[Yu 04] X. Yu, K. Strunz, "Combined long-term and short-term access storage for sustainable energy system", 2004 IEEE Power Engineering Society General Meeting, vol.2 pp.1946-1951, 10 June 2004.

Z:

[Zho 07] T. Zhou and B. Francois, "Modeling and control design of hydrogen production process by using a causal ordering graph for wind energy conversion System", IEEE ISIE'07, CD ROM, Vigo, Spain, 4 - 7 june 2007.

[Zho 08] T. Zhou, D. Lu, H. Fakham, B. Francois, "Power flow control in different time scales for a wind/hydrogen/super-capacitors based active hybrid power system," EPE-PEMC'08, Poznan, Sep, 2008, CD-ROM.

[Zho 09a] T. Zhou, P. Li, B. François, "Power Management Strategies of a DC-Coupled Hybrid Power System for Microgrid Operations", accepted to the 13th International European Power Electronics Conference and Exhibition (EPE2009).

[Zho 09b] T. Zhou, B. Francois, "Modeling and control design of hydrogen production process for an active hydrogen/wind hybrid power system", International Journal of Hydrogen Energy, vol.34, iss.1, Jan. 2009, pp. 21-30

[Zho 09c] T. Zhou, B. Francois, "Real-Time Emulation of a Hydrogen Production Process for assessment of an Active Wind Energy Conversion System", IEEE Transactions on Industrial Electronics, vol.56, iss.3, March 2009 pp:737–746.

[Zou 07] E.I. Zoulias, N. Lymberopoulos, "Techno-economic analysis of the integration of hydrogen energy technologies in renewable energy-based stand-alone power systems", International Journal of Renewable Energy, 2007; 32:680-696.

[Zub 00] L. Zubieta, R. Bonert, "Characterization of double-layer capacitors for power electronics appications", IEEE transaction on Industry Applications, vol.36, iss.1, pp. 199-205, Jan-Feb 2000.

Curriculum Vitae

Curriculum Vitae (english version)

Name : **Tao ZHOU**
Nationality : Chinese
Address : 18, Rue de la Cité, 59800, Lille
Tel : +33 (0)6 37 20 27 45
Email : taozhou123@hotmail.com
Personal page : http://l2ep.univ-lille1.fr/index.php?page=annuaire&c1=43&c=002

Educations

Since 09/2007 *Lille, France*	**PhD Degree Candidate** in Electrical Engineering in the Laboratoire d'Electrotechnique et d'Electronique de puissance (L2EP) at l'Ecole Centrale de Lille. Subject: « Control and energy management of a hybrid active wind generator including energy storage system with super-capacitors and hydrogen technologies for Microgrid Application ».
09/2004 – 06/2006 *Chengdu, Chine*	**Master Degree** in Power Electronics and Electrical Drive in the SouthWest JiaoTong University (SWJTU) in Chengdu. Subject: « Digital control of high-frequency power electronic converters ».
09/2002 – 06/2004 *Lyon, France*	**Master Degree** in General Engineering at l'Ecole Centrale de Lyon, participation in a student exchange program « double master degrees » between Chine and France.
09/2000 – 06/2004	**Bachelor Degree** in Electronic Information in the SouthWest JiaoTong University

Professional Experience

Since 09/2007 *Lille, Franc*	**Assistant teacher** on « Industrial Electricity », « Electro-technology » et « Power Electronics » at l'Ecole Centrale de Lille.
Since 09/2006 *Lille, France*	**Research Project** (ANR-SUPERENER): « System Control and Energy management of a renewable energy generation based hybrid power system in a Microgrid » in the Laboratoire d'Electrotechnique et d'Electronique de puissance de Lille (L2EP).
09/2004 – 05/2006 *Chengdu, Chine*	**Research Projects** in the laboratory of power electronics in SouthWest JiaoTong University (SWJTU) in Chengdu.
07/2005 – 08/2005 *Chengdu, Chine*	**Internship** in GROUPAMA Chengdu Branch. Subject: Organization and communication**.**
06/2004 – 08/2004 *Tokyo, Japon*	**Internship** in DIESEL UNITED. Subject: Quality assurance of the production.
08/2003 *Annemasse, France*	**Internship** in SICPA in Annemasse, Subject: Production conditioning.

Linguistic Competences and Computer Skills

Languages

- ***English***: ***Fluent*** - Since 1990.Many written and oral experiences in works and travels.
- ***French***: ***Fluent*** - Since 2002.Many interpretation experiences in scientific and commercial meetings.
- ***Japanese*** ***Advanced*** - Since 2005. 3-month internship and life in Japan with everyday communication.
- ***Chinese*** ***Mother tongue***. Born and grown-up in North China, with good accent in Mandarin.

Computer skills

- ***Program***: C et C++
- ***HTML***: Creation of an internet site for a study project while studying in l'Ecole Centrale de Lyon.
- ***Office*** Microsoft Office et Microsoft Project.
- ***Simulation*** Matlab, Simulink, PSpice, Psim

Interests and Hobbies

Ski, tennis, cycling, swimming, cinema, music, widely reading, musical theater, GO and basketball :

Since 01/2007	The French basketball regional league "Excellence Région (Nord – Pas de Calais)", with the basketball club of Villeneuve d'Ascq (ESBVA).
11/2003	The 3rd International university tournament in Milan with the basketball team of l'Ecole Centrale de Lyon.
2000 – 2002	The Chinese University Basketball Association « CUBA » with the basketball team of the SouthWest Jiaotong University, represent la province de Sichuan.

Publications

Type : International Journal

[J1] **Tao ZHOU**, Bruno FRANCOIS, "***Modeling and Control Design of Hydrogen Production Process for an Active Hydrogen/Wind Hybrid Power System***", International Journal on Hydrogen Energy, vol.34, pp.21-30, 2009. **(SCI; Impact factor: 2.725 in 2007)**

[J2] **Tao ZHOU**, Bruno FRANCOIS, Mohamed hadi LEBBAL, Stéphane LECOUECHE, "***Real-Time Emulation of a Hydrogen Production Process for assessment of an Active Wind Energy Conversion System*** ", IEEE Transaction on Industrial Electronics, vol.56, iss.3, pp.737-746, 2009. **(SCI; Impact factor: 2.216 in 2007)**

Type : International Conference

[C1] **Tao ZHOU**, Peng LI, Bruno FRANCOIS, "***Power Management Strategies of a DC-Coupled Hybrid Power System for Microgrid Operations***", accepted to the 13th International European Power Electronics Conference and Exhibition (EPE2009). **(EI)**

[C2] B. DAVAT, S. ASTIER, T. AZIB, O. BETHOUX, D. CANDUSSO, G. COQUERY, A. DE BERNARDINIS, F. DRUART, B. FRANÇOIS, M. GARCIA ARREGUI, F. HAREL, M. HINAJE, D. HISSEL, J-P. MARTIN, M-C. PÉRA, S. PIERFEDERICI, S. RAËL, D. RIU, S. SAILLER, Y. BULTEL, T. CREUZET, C. TURPIN, **T. ZHOU**, "***Fuel cell based hybrid systems***", accepted the 8th International Symposium on Advanced Electromechanical Motion Systems, Lille, France, 1-3 July 2009.

[C3] S. ASTIER, L. BOULON, A. BOUSCAYROL, Y. BULTEL, D. CANDUSSO, S. CAUX, S. CHUPIN, T. COLINART, G. COQUERY, B. DAVAT, A. DE BERNARDINIS, J. DESEURE, S. DIDIERJEAN, J. DILLET, F. DRUART, M. FADEL, G. FONTES, B. FRANCOIS, J.C. GRANDIDIER, F. HAREL, M. HILAIRET, M. HINAJE, S. JEMEI1, O. LOTTIN, L. MADIER, G. MARANZANA, S. MARTEMANIOV, D. NGUYEN, R. ORTEGA, R. OUTBIB, M.C. PERA, S. RAEL, N. RETIERE, D. RIU, S. SAILLER, R. TALJ, **T. ZHOU**, "***A review on existing modelling methodologies for PEM fuel cell systems*** ", 2008 Conference of Fundamentals & Developments of Fuel Cells (FDFC 2008), Nancy, France, 10-12 December 2008.

[C4] **Tao ZHOU**, Di LU, Hicham FAKHAM, Bruno FRANCOIS, "***Power flow control in different time scales for a hybrid power system based on wind generator, hydrogen and super-capacitors***", 13th International Power Electronics and Motion Control Conference, EPE-PEMC 2008, Poznan, 1-3 September 2008. **(EI: 084811743999)**

[C5] Di LU, **Tao ZHOU**, Hicham FAKHAM, Bruno FRANCOIS, "***Design of a power management system for a PV station including various storage technologies***", 13th International Power Electronics and Motion Control Conference, EPE-PEMC 2008, Poznan, 1-3 September 2008, 9-2008. **(EI: 084811743990)**

[C6] Mohamed LABBAL, **Tao ZHOU**, Stephane LECOEUCHE, Bruno FRANCOIS, "***Dynamically electrical modelling of electrolyser and hydrogen production regulation***", The 2nd International Hydrogen Energy Congress and Exhibition (IHEC'07), Istanbul, Turkey, 13-15 July 2007.

[C7] **Tao ZHOU**, Bruno FRANCOIS, M LEBBAL, S LECOEUCHE, "***Modelling and Control Design of Hydrogen Production Process by Using a Causal Ordering Graph for Wind Energy Conversion System***", IEEE International Symposium on Industrial Electronics, ISIE'2007, Vigo, Spain, 4-7 June 2007. **(EI: 083511489316)**

[C8] Mingzhi HE, Jianping XU, **Tao ZHOU**, "***Digital Proportional-Feed-Forward (PFF) Control of Switching DC-DC Converters***", The 4th Power Conversion Conference (PCC'07), Nagoya, Japon, 2-7 April, 2007. **(EI Inspec: 9702343)**

[C9] **Tao ZHOU**, Jianping XU, Bruno FRANCOIS, "***Analog-to-digital converter architectures for digital controller of high-frequency power converters***", The 32nd Annual Conference of the IEEE Industrial Electronics Society (IECON'06), Paris, France, 7-10 November 2006. **(EI: 083611514864)**

[C10]**Tao ZHOU**, Jianping XU, "***ADC architecture with direct binary output for digital controllers of high-frequency SMPS***", The 5th CES/IEEE International Power Electronics and Motion Control Conference (IPEMC'06), Shanghai, China, 14-16 August 2006. **(EI: 082511328310)**

[C11]**Tao ZHOU**, Jianping XU, "***Flash ADC with large conversion range for digital controller of high-frequency power converter***", The 4th IEEE International Conference on Communications, Circuits and Systems (ICCCAS'06), Guilin, China, 25-28 June 2006. **(EI: 081011132227)**

Type : Other publication

[O1]**Tao ZHOU**, "***Retour sur les promesses de la Chine – Progrès du développement durable en Chine***", Technica - La revue des ingénieurs de Centrale Lyon, N°. 570, pages. 14-15, ISBN. 0184-4067, 3-2009.

Curriculum Vitae (version française)

Prénom et Nom : **Tao ZHOU**
Genre : M
Adresse 18, Rue de la Cité, 59800, Lille
Tel : 06 37 20 27 45
Email: taozhou123@hotmail.com
Page personnel : http://l2ep.univ-lille1.fr/index.php?page=annuaire&c1=43&c=002

Educations

Depuis 09/2007 (Lille, France). **Préparation du Diplôme Doctorat** en Génie Electrique dans le Laboratoire d'Electrotechnique et d'Electronique de puissance (L2EP) à l'Ecole Centrale de Lille. Sujet de thèse : « Commande et Supervision Energétique d'un Générateur Hybride Actif Eolien incluant du Stockage sous forme d'Hydrogène et des Super-Condensateurs pour l'Intégration dans le Système Electrique d'un Micro Réseau ».

09/2004 – 06/2006 (Chengdu, Chine) **Master Recherche** en Electronique de Puissance à l'Université de JiaoTong du Sud-Ouest. Sujet du mémoire : «Commande numérique d'un convertisseur électronique de puissance a haute fréquence ».

Obtention du diplôme de Master en juin 2006.

09/2002 – 06/2004 Lyon, France **Ingénieur Généraliste** à l'Ecole Centrale de Lyon.

Obtention du diplôme d'ingénieur en 2006.

09/2000 – 06/2004 Chengdu, Chine **Licences** en Télécommunications à l'Université de JiaoTong du Sud-Ouest. Obtention des prix de première classe trois fois avec des très bons résultats scolaire. Obtention du diplôme en 2004.

Expériences Professionnelles

Depuis 09/2007 Lille, Franc **Enseignement vacataire** en Travaux Pratiques : « Electricité Industrielle », « Electrotechnique » et « Electronique de Puissance »

Dès 09/2006 Lille, France **Projet de recherche** (ANR-SUPERENER) sur la supervision énergétique d'une centrale multi source à base d'énergies renouvelables dans le Laboratoire d'Electrotechnique et d'Electronique de puissance de Lille (L2EP).

09/2004 – 05/2006 Chengdu, Chine **Plusieurs projets de recherche** dans le laboratoire d'électronique de puissance à l'Université de JiaoTong du Sud-Ouest.

07/2005 – 08/2005 Chengdu, Chine **Stage professionnel** à **GROUPAMA**, filiale de Chengdu.

Sujet du stage : Organisation et communication**.**

06/2004 – 08/2004 Aioi, Japon **Stage d'application** à **DIESEL UNITED**.

Sujet de stage : Assurer la qualité de production.

Compétences linguistiques et informatiques

Langues

- ***Anglais***: ***Courant***-Depuis 1990. Beaucoup d'occasion de pratiquer pendant le travail et les voyages.
- ***Français***: ***Courant***-Depuis 2002. Beaucoup d'expérience d'interprète de haut niveau pour le consulat français à Chengdu, pour des conférences scientifique et des communications commerciales.
- ***Japonais*** ***Avancé***-Depuis 2005. 3 mois d'expériences de vie et de stage au Japon.
- ***Chinois*** ***Langue Maternelle***. Bon accent en Mandarin.

Informatique

- ***Program***: C et C++
- ***HTML***: Création d'un site web pour le projet d'étude à l'ECL.
- ***Bureautique***: Microsoft Office et Microsoft Project.
- ***Simulation***: Matlab/Simulink, PSpice, Psim

Centres d'intérêts

Ski, tennis, bicyclette, natation, cinéma, musique, lecture extensive, spectacle musical, GO, et basket :

Depuis 01/2007 Championnat Excellence Région (Nord – Pas de Calais) avec le club de ESBVA

11/2003 Le 3ème Tournoi d'Universités Internationales à Milan avec l'Ecole Centrale de Lyon.

2000 – 2001 Championnat Universitaire Chinois « CUBA » (Chinese University Basketball Association) avec Southwest Jiaotong University , représentant la province Sichuan.

Publications

Type : Revue Internationale

[J1] **Tao ZHOU**, Bruno FRANCOIS, "***Modeling and Control Design of Hydrogen Production Process for an Active Hydrogen/Wind Hybrid Power System***", International Journal on Hydrogen Energy, vol.34, pp.21-30, 2009. **(SCI; Impact factor: 2.725 en 2007)**

[J2] **Tao ZHOU**, Bruno FRANCOIS, Mohamed hadi LEBBAL, Stéphane LECOUECHE, "***Real-Time Emulation of a Hydrogen Production Process for assessment of an Active Wind Energy Conversion System*** ", IEEE Transaction on Industrial Electronics, vol.56, iss.3, pp.737-746, 2009. **(SCI; Impact factor: 2.216 en 2007)**

Type : Conférence Internationale

[C1] **Tao ZHOU**, Peng LI, Bruno FRANCOIS, "***Power Management Strategies of a DC-Coupled Hybrid Power System for Microgrid Operations***", accepted to the 13th International European Power Electronics Conference and Exhibition (EPE2009). **(EI)**

[C2] B. DAVAT, S. ASTIER, T. AZIB, O. BETHOUX, D. CANDUSSO, G. COQUERY, A. DE BERNARDINIS, F. DRUART, B. FRANÇOIS, M. GARCIA ARREGUI, F. HAREL, M. HINAJE, D. HISSEL, J-P. MARTIN, M-C. PÉRA, S. PIERFEDERICI, S. RAËL, D. RIU, S. SAILLER, Y. BULTEL, T. CREUZET, C. TURPIN, **T. ZHOU**, "***Fuel cell based hybrid systems***", accepted the 8th International Symposium on Advanced Electromechanical Motion Systems, Lille, France, 1-3 July 2009.

[C3] S. ASTIER, L. BOULON, A. BOUSCAYROL, Y. BULTEL, D. CANDUSSO, S. CAUX, S. CHUPIN, T. COLINART, G. COQUERY, B. DAVAT, A. DE BERNARDINIS, J. DESEURE, S. DIDIERJEAN, J. DILLET, F. DRUART, M. FADEL, G. FONTES, B. FRANCOIS, J.C. GRANDIDIER, F. HAREL, M. HILAIRET, M. HINAJE, S. JEMEI1, O. LOTTIN, L. MADIER, G. MARANZANA, S. MARTEMANIOV, D. NGUYEN, R. ORTEGA, R. OUTBIB, M.C. PERA, S. RAEL, N. RETIERE, D. RIU, S. SAILLER, R. TALJ, **T. ZHOU**, "***A review on existing modelling methodologies for PEM fuel cell systems*** ", 2008 Conference of Fundamentals & Developments of Fuel Cells (FDFC 2008), Nancy, France, 10-12 December 2008.

[C4] **Tao ZHOU**, Di LU, Hicham FAKHAM, Bruno FRANCOIS, "***Power flow control in different time scales for a hybrid power system based on wind generator, hydrogen and super-capacitors***", 13th International Power Electronics and Motion Control Conference, EPE-PEMC 2008, Poznan, 1-3 September 2008. **(EI: 084811743999)**

[C5] Di LU, **Tao ZHOU**, Hicham FAKHAM, Bruno FRANCOIS, "***Design of a power management system for a PV station including various storage technologies***", 13th International Power Electronics and Motion Control Conference, EPE-PEMC 2008, Poznan, 1-3 September 2008, 9-2008. **(EI: 084811743990)**

[C6] Mohamed LABBAL, **Tao ZHOU**, Stephane LECOEUCHE, Bruno FRANCOIS, "***Dynamically electrical modelling of electrolyser and hydrogen production regulation***", The 2nd International Hydrogen Energy Congress and Exhibition (IHEC'07), Istanbul, Turkey, 13-15 July 2007.

[C7] **Tao ZHOU**, Bruno FRANCOIS, M LEBBAL, S LECOEUCHE, "***Modelling and Control Design of Hydrogen Production Process by Using a Causal Ordering Graph for Wind Energy Conversion System***", IEEE International Symposium on Industrial Electronics, ISIE'2007, Vigo, Spain, 4-7 June 2007. **(EI: 083511489316)**

[C8] Mingzhi HE, Jianping XU, **Tao ZHOU**, "***Digital Proportional-Feed-Forward (PFF) Control of Switching DC-DC Converters***", The 4th Power Conversion Conference (PCC'07), Nagoya, Japon, 2-7 April, 2007. **(EI Inspec: 9702343)**

[C9] **Tao ZHOU**, Jianping XU, Bruno FRANCOIS, "***Analog-to-digital converter architectures for digital controller of high-frequency power converters***", The 32nd Annual Conference of the IEEE Industrial Electronics Society (IECON'06), Paris, France, 7-10 November 2006. **(EI: 083611514864)**

[C10]**Tao ZHOU**, Jianping XU, "***ADC architecture with direct binary output for digital controllers of high-frequency SMPS***", The 5th CES/IEEE International Power Electronics and Motion Control Conference (IPEMC'06), Shanghai, China, 14-16 August 2006. **(EI: 082511328310)**

[C11]**Tao ZHOU**, Jianping XU, "***Flash ADC with large conversion range for digital controller of high-frequency power converter***", The 4th IEEE International Conference on Communications, Circuits and Systems (ICCCAS'06), Guilin, China, 25-28 June 2006. **(EI: 081011132227)**

Type : Autre publication

[O1]**Tao ZHOU**, "***Retour sur les promesses de la Chine – Progrès du développement durable en Chine***", Technica - La revue des ingénieurs de Centrale Lyon, N°. 570, pages. 14-15, ISBN. 0184-4067, 3-2009.

Résumé en Français

Résumé Etendu en Français

De plus en plus de générateurs décentralisés sont intégrés dans le réseau électrique. Par conséquent, de nouvelles structures de réseau électrique sont envisagées pour les accueillir. Le micro réseau en fait partie. L'avantages des micro-réseaux consistent à:

- regrouper les producteurs dispersés et les consommateurs locaux pour minimisation des pertes dues au transport de l'électricité;
- avoir la possibilité de cogénération pour augmenter le rendement global lors de la génération des énergies;
- faciliter l'utilisation des moyens de communication pour optimiser la production électrique et renforcer la qualité et la fiabilité du système électrique.

Aujourd'hui, il est préférable d'intégrer des énergies renouvelables dans le micro-réseau pour réduire l'émission de CO_2 et la consommation des combustibles fossiles. Mais, les sources d'énergies renouvelables sont souvent très intermittentes et fluctuantes. Donc la production à base d'énergies renouvelables est généralement difficile à prévoir. Par contre, la qualité de puissance du réseau électrique est très importante. L'adéquation entre la production des énergies renouvelables et la consommation électrique devient très difficile. Afin de pouvoir augmenter la pénétration des énergies renouvelables dans le réseau électrique, nous devons faire participer la production des énergies renouvelables à la gestion du réseau. C'est le principe du générateur actif.

Le sujet de cette thèse est de transformer un générateur à base d'énergie renouvelable en générateur actif en utilisant des systèmes de stockage d'énergie. Un système hybride multi-source est étudié dans la thèse. Il consiste en un générateur éolien (comme source d'énergie primaire), des super-condensateurs (comme système de stockage à dynamique rapide), des piles à combustible et des électrolyseurs (comme système de stockage a long-terme sous forme d'hydrogène). Ils sont tous connectés à un bus continu commun et un onduleur est utilisé pour la connexion au réseau.

L'objectif de cette thèse est de concevoir le système de commande, y compris les stratégies de supervision énergétique, pour réaliser un générateur actif éolien. Il doit pouvoir fonctionner comme un générateur classique pour pouvoir générer des puissances lisses et contrôlables. Par conséquent, il est capable des fournir des services au système électrique du micro-réseau.

L'introduction du contexte de la thèse est présentée au chapitre I. Et puis la présentation des travaux de la thèse est divisée en quatre chapitres :

Au Chapitre II, l'étude d'un système de génération éolienne est présentée. La modélisation du système et la conception de la commande sont détaillées. Afin de résoudre le problème de la fluctuation de la puissance éolienne, un système de stockage à dynamique rapide par super-condensateur (Annexe I) est ajouté. Les stratégies de supervision des puissances sont proposées pour la coordination des sources différentes dans ce système hybride. Les puissances envoyées au réseau sont bien lissées, mais le fonctionnement ne peut pas être garanti pour long-terme à cause du manque du stockage d'énergie en grande quantité. Il s'agit

du système de stockage à long-terme par hydrogène (incluant les piles à combustible et les électrolyseurs), qui est présenté dans les chapitres suivants.

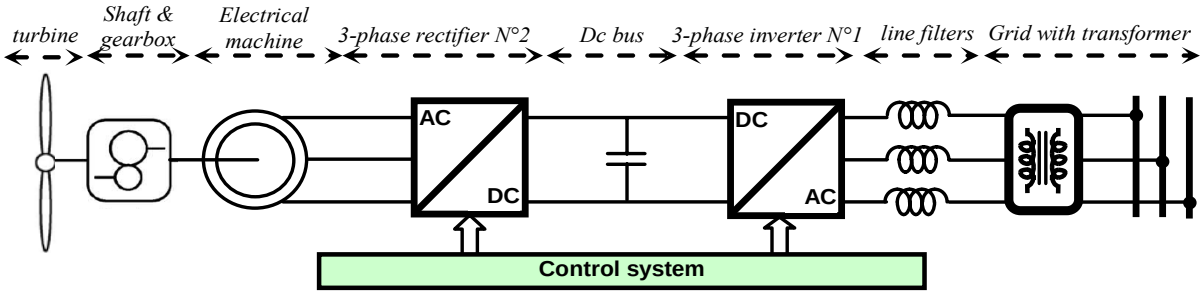

Générateur éolien à vitesse variable

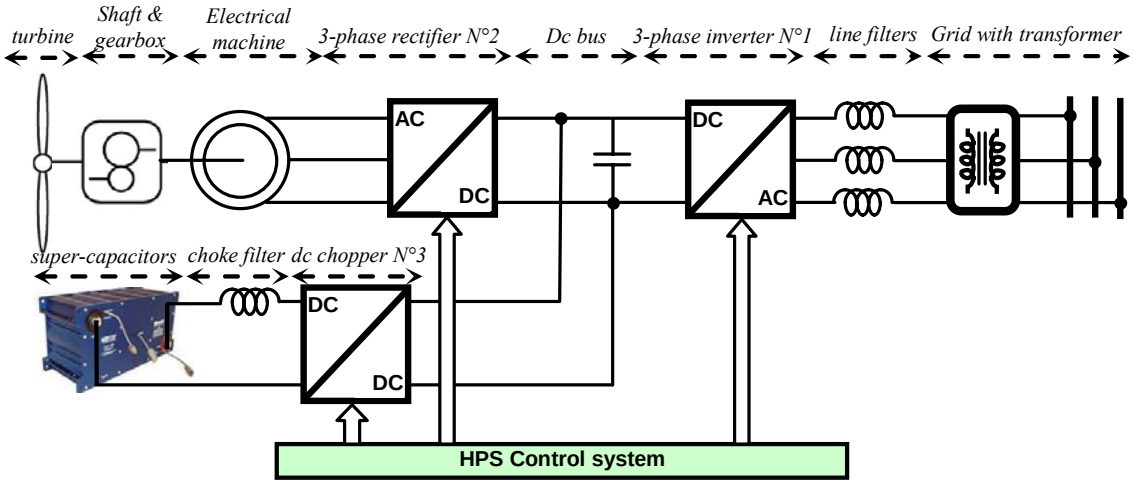

Centrale hybride à base d'énergie éolienne et de super-condensateurs

Au Chapitre III et au Chapitre IV, les études sur un système de pile à combustible et un système d'électrolyseur sont présentées. La modélisation et la commande sont étudiées et validé par des essais expérimentaux sur les systèmes commercialisés (Ballard Nexa 1200W pour la pile a combustible et CETH GENHY 500W pour l'électrolyseur). Afin de rendre la plateforme expérimentale plus flexible, des émulateurs sont réalisés pour la pile à combustible et l'électrolyseur en implémentant les modèles validés sur la carte numérique de commande (DSpace 1102). Ils peuvent fournir les mêmes comportements électriques. Cela nous permet ensuite de tester les stratégies de supervision des puissances au sein du générateur actif éolien, qui sont présenté dans le chapitre suivant.

Système de pile à combustible étudié
(BALLARD NEXA 1200W)

Système d'électrolyseur étudié
(CETH GENHY 500W)

Au Chapitre V, les études du générateur actif éolien sont présentées. La modélisation et la commande du système entier sont présentées. Les stratégies de supervision énergétique sont proposées suivant les caractéristiques de chaque source d'énergie. Elles sont expérimentalement implémentées dans une autre carte numérique de commande (DSpace 1103), et leurs performances sont comparées par rapport à la régulation de la tension du bus continu et au control des puissances transitées au réseau. Les stratégies de gestion énergétique sont également conçues avec la définition des différents modes de fonctionnement pour maintenir les niveaux de stockage dans leurs zones normales.

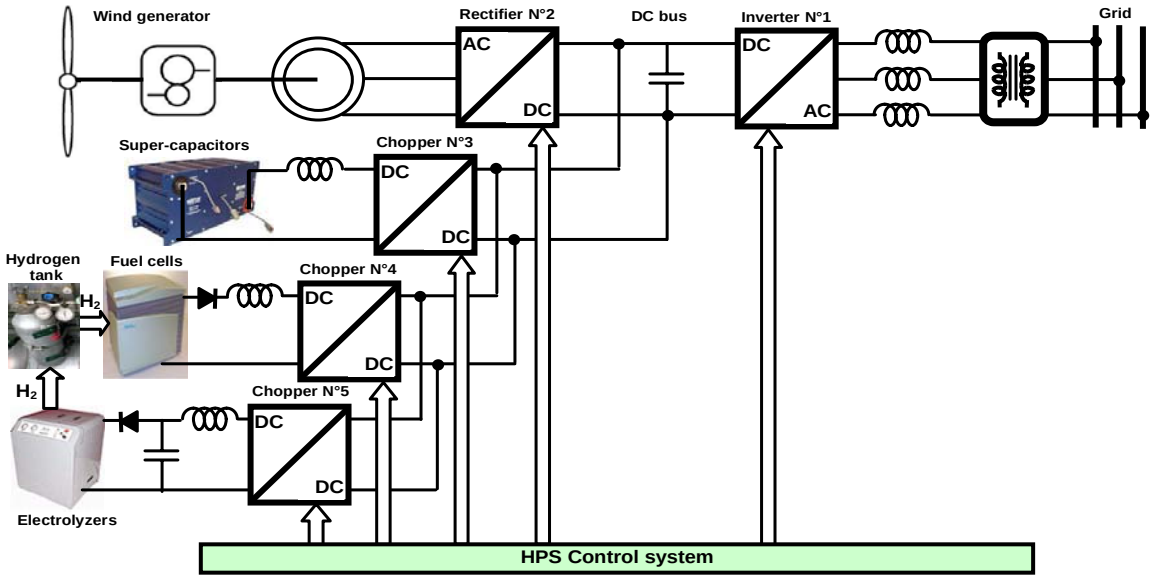

Générateur active éolien incluant le système de stockage sous forme d'hydrogène et des super-condensateurs

Les conclusions et les perspectives de cette thèse sont finalement présentées au Chapitre VI.

Les contributions scientifiques principales de cette thèse sont les suivantes :

- l'utilisation et l'adaptation des formalismes dans la modélisation des systèmes complexes et la conception de commande;
- la conception et la réalisation expérimentale des émulateurs pour réduire le temps et le cout du développement de la plateforme expérimentale.
- la proposition et la validation de deux stratégies de gestion des puissances pour la régulation du bus continu et le contrôle des puissances transitées au réseau ;
- la proposition des stratégies de supervision énergétique avec la définition des modes de fonctionnement pour le générateur actif éolien afin d'assurer une disponibilité énergétique.

Moyennant adaptation, ces contributions peuvent être utilisées aussi pour d'autres centrales hybrides contenant une source d'énergie renouvelable, un système de stockage à dynamique rapide et un système de stockage à long-terme.

Abstract:

A hybrid power system is studied in this thesis for the distributed generation, which is based on renewable energy resources and energy storage systems in microgrid applications. It consists of a wind generator as primary energy source, super-capacitors as fast-dynamic storage system, fuel cells and electrolyzers as long-term storage system in hydrogen. They are all connected to a common DC bus and an inverter is used for the connection of the whole system to the grid. In this thesis, we have presented the system modeling, the control design including the power balancing and energy management strategies. This hybrid power system can finally supply controllable smooth powers as most conventional power plants. The performances have been tested in numerical simulations and also on an experimental test bench. As result, it is able to provide ancillary services to the microgrid.

The main scientific contributions of this thesis are: the use and the adaptation of the graphical tools for the modeling of complex systems and their design; the design and the experimental implementation of real-time emulators in order to reduce the time and the cost of an experimental platform; the proposition and the validation of two power balancing strategies for the DC-bus voltage regulation and the grid power control and, finally, the proposition of energy management strategies for the active wind generator to ensure the energy availability.

Keywords : hybrid power system, active generator, wind generator, fuel cell, electrolyzer, super-capacitor, hydrogen, energy management.

Résumé :

Un système hybride multi-source est étudié dans cette thèse pour la génération dispersée basée sur des sources d'énergie renouvelable et des systèmes de stockage d'énergie. Il comprend un générateur éolien comme source d'énergie primaire, des super-condensateurs comme système de stockage à dynamique rapide, des piles à combustible et des électrolyseurs comme système de stockage sur le long terme sous forme d'hydrogène. Ils sont tous connectés à un bus continu commun et un onduleur est utilisé pour la connexion du système entier au réseau. Dans ce mémoire, nous avons présenté la modélisation du système, la conception du contrôle y compris des stratégies de répartition des flux de puissance et la gestion énergétique. Cette centrale hybride peut finalement générer des puissances lissées et contrôlables comme la plupart des générateurs classiques. Les performances ont été testées en simulation numérique et aussi sur un prototype expérimental.

Les contributions scientifiques principales de cette thèse sont les suivantes : l'utilisation et l'adaptation des formalismes pour la modélisation des systèmes complexes et la conception de leur commande; la conception et la réalisation expérimentale des émulateurs pour réduire le temps et le coût du développement du prototype expérimental; la proposition et la validation de deux stratégies de gestion des puissances pour la régulation du bus continu et le contrôle des puissances transitées au réseau et, enfin, la proposition de stratégies de supervision énergétique avec la définition des modes de fonctionnement pour le générateur actif éolien afin d'assurer une disponibilité énergétique.

Mots clés : Centrale hybride, générateur actif, générateur éolien, pile à combustible, électrolyseur, super-condensateur, hydrogène, supervision énergétique.